Monitoring and Modeling Subgrade Soil Moisture for Pavement Design and Rehabilitation in Idaho

Phase III: Data Collection and Analysis

Final Report

Submitted to

Idaho Transportation Department
P. O. Box 7129
Boise, Idaho 83707-1129

By

Fouad Bayomy
Professor of Civil Engineering and Principal Investigator
and
Hassan Salem
Research Assistant

Center for Transportation Infrastructure, CTI
National Institute for Advanced Transportation Technology, NIATT
University of Idaho

ITD Project SPR 0010 (025) 124
UI-NIATT Project KLK459

Final Report
July 2004
(Revised and re-submitted May 2005)

PREFACE

This is the final report of the ITD project entitled **"Monitoring and Modeling Subgrade Soil Moisture for Pavement Design and Rehabilitation in Idaho"**. The report focuses on phase 3 of the project, which relates to data collection and analysis, but it also encompasses the findings of various phases of the project.

Phase 1 was dedicated to the development of scope of work and feasibility study. It was performed under ITD Agreement FC# 96-48, and UI-NIATT project FMK428. Report of phase 1 was completed in July 1996. Phase 2 was dedicated to sites' installation and development of data collection protocols. It was performed under ITD project SPR 0010 (020) 124, Agreement FC# 97-30 and UI-NIATT project FMK173. Report of Phase 2 was completed in June 2002. Phase 3 of the project was dedicated to Data Collection and Analysis under the ITD research project number SPR-0010(025) 124, Agreement FC# 00-103, and UI-NIATT project KLK459.

Research teams for the three phases are:

Phase 1 (FMK428), 1996:
Dr. James Hardcastle (PI)
Dr. Fouad Bayomy (Co PI)
ITD research coordinator: Mr. Robert Smith, PE

Phase 2 (FMK173), 1997-2001
Dr. Fouad Bayomy (PI)
Dr. James Hardcastle (Co-PI)
ITD research coordinator: Mr. Robert Smith, PE

Phase 3 (KLK459), 2000-2004
Dr. Fouad Bayomy (PI)
Mr. Hassan Salem, Graduate Research Assistant
ITD research coordinators: Mr. Robert Smith, PE, and Mr. Mike Santi, PE

It is noted that overlap existed between phases 2 and 3. The overlap was necessary to complete the installation activities, and yet to proceed with the data collection for the sites that were already installed. For instance, changes in the installation at all sites by replacing all cable concrete vaults at ground level by elevated metal cable boxes were conducted during phase 3 contract. In addition, one of sites (at Weiser) was installed during Phase 3 even though it was part of phase 2 activities. The ITD research coordinator authorized these changes. Thus, the information in this report includes not only the work performed under the phase 3 contract (KLK459) but also includes the necessary relevant information of the work done under the phase 2 contract (FMK173), which related to the site installation and data collection process.

ABSTRACT

Environmental changes have a direct impact on the structural capacity of the pavement, and consequently its performance. While the subgrade soil and the unbound materials are sensitive to moisture variation, the Asphalt Concrete (AC) layers are more sensitive to temperature variations. Quantifying the effect of these two environmental factors, moisture and temperature, is necessary for incorporation in the pavement design process.

The main goal of this research was to quantify the variation of subgrade moisture and asphalt surface temperature at various sites in Idaho and determine their effects on the structural capacity of the pavement layers, and hence determine their influence on the pavement performance. In addition, the impact of the existence of a rockcap base layer on the moisture regime in the subgrade and its effect on the overall pavement structural capacity was to be evaluated.

The research methodology included instrumentation of several pavement sites in northern region (Pack River, Worley, Moscow and Lewiston) and in southern region at Weiser. The Moscow and Weiser sites included adjacent sections of rockcap and aggregate bases to compare the effectiveness of these two types of base materials. Instrumentation sensors used were similar to those used in the FHWA Long Term Pavement Performance (LTPP) Seasonal Monitoring Program (SMP). Time domain reflectometry (TDR) probes were installed to measure volumetric moisture content, MRC thermistors were used to measure temperature at various depths, and ABF resistivity probes were installed to determine frost conditions. Piezometers were also installed to monitor ground water level (GWL) at the instrumented sites. Structural capacity was evaluated using Falling Weight Deflectometer (FWD). The moisture, temperature, resistivity and the GWL data were collected on a monthly basis for almost three years. However, the FWD data, which was collected by the ITD materials, was performed approximately once a year along with the ITD normal FWD testing schedule. This resulted in a great shortcoming in monitoring the seasonal variation of

the pavement structural capacity at the instrumented sites. Therefore, the research relied on the LTPP-SMP database to acquire seasonal FWD data for many sites across the country.

Moisture and temperature data at the instrumented Idaho sites were analyzed to determine the seasonal variability of these two parameters. Historical climatic data were also obtained from weather stations, and augmented with the moisture and temperature data to develop seasonal timing at the various sites. The resistivity data, however, were found erratic and were not considered in any part of the analysis.

Data acquired from the LTPP-SMP database were analyzed to develop correlation models that quantify the variation of the resilient modulus of unbound materials and relate it to moisture variation. Similarly, correlation models to relate the modulus of asphalt concrete layers to the temperature variation were also developed. The developed models showed dependency of the modulus on many other factors such as material type, mix design, climatic region, and other design related parameters. The developed models were then checked using the collected data at the specific sites instrumented in Idaho. Then the models were incorporated in a mechanistic-empirical pavement design process to quantify the effect of the seasonal variation on pavement performance.

Results of the mechanistic analysis, which incorporated the developed models, indicated that the incorporation of the seasonal variation in pavement design process leads to the prediction of significantly shorter pavement service life. This finding is critical to pavement designers, since the lack of consideration of such seasonal variations could result in a premature failure.

To determine the rockcap base layer effectiveness, moisture data at the Moscow and Weiser sites were analyzed. Results showed conflicting trends. In Moscow site, the subgrade experienced more moisture under the rockcap base while the opposite was observed in Weiser. It is believed that the extension of the rockcap layer to the open side ditches, as in Weiser site, allows the surface water to drain away relieving the subgrade from the excess moisture. On the other hand, where the rockcap is enclosed, as in Moscow site, the water in rockcap is entrapped and it drains downward causing the subgrade moisture to increase. However, the mechanistic analysis performed at these two sites, showed that the section with rockcap layer was consistently stronger than the section with aggregate base, even though the subgrade moisture content under rockcap layer was greater. The predicted rutting life, for the pavement section with rockcap layer, was about 5 times greater than the other section with aggregate base. Thus, the presence of rockcap base was always effective in increasing the pavement structural capacity and increasing the fatigue and rutting service lives.

To facilitate the use of the research results, the developed models were applied to the specific conditions tested at the instrumented sites, and moduli seasonal adjustment factors (SAF) were calculated. Algorithm and Tables for these factors at the different regions were developed and provided in this report.

ACKNOWLEDGMENTS

This research was funded under the SPR Project 124 and managed under UI-NIATT contract KLK459. The authors would like to acknowledge the Idaho Transportation Department (ITD) and the Federal Highway Administration (FHWA) for funding this research. Many individuals from ITD and from UI have provided technical support in various phases of the project. While it is hard to mention all these people, the authors would like to present their deep appreciation to all personnel who were involved at various phases. Mr. Robert Smith, ITD research supervisor, coordinated the research from ITD side and has been a solid supporter of this work all over the years. Mr. Mike Santi, Pavement engineer at ITD facilitated data collection and FWD testing. Dr. James Hardcastle, Professor Emeritus, initiated and led the field installation phase of this project while under FMK173 contract. Many people participated in the field data collection and presentation activities including Todd Kimsey, Gregg Woods, Gary Haderlie, Christina Ryan, Mostafa Abu-Hashema, Marwan Mossaad and Mike Gibson. Their efforts are greatly appreciated. This project constituted the main research of the co-author Mr. Hassan Salem, PhD student at UI. The authors would like to acknowledge the constructive comments and feedback provided by Dr. Sunil Sharma and Dr. Thomas Weaver, Professors of Civil Engineering, and Dr. Ismail Genc, Professor of Economics and Statistics who served on the PhD committee of Mr. Salem. Their comments were incorporated in this report. And, at last but not least, the authors would like to thank Ms. Melissa Lines for her efforts in editing the manuscript of this report.

TABLE OF CONTENTS

LIST OF TABLES

LIST OF FIGURES

NOTATIONS

Roman Symbols		**Dimension**
AV	Air voids in the asphalt mix	%
BSG	Bulk specific gravity of asphalt mix	-
D_{60}	The soil particle size diameter for 60% passing	L
DDi	Insitu dry density of subgrade soil	M/L^2
E	Modulus of Elasticity	F/L^2
F	Force	F
F	% age passing # 200 sieve	%
Grade	Asphalt binder grade	-
H	Height	L
L	Length	L
Lat	Latitude	Deg
LI	Liquidity index of soil	%
LL	Liquid limit of soil	%
M	Mass	M
M_r	Modulus of resilience	F/L^2
N_f	Allowable number of load repetitions	-
PI	Plasticity index	%
PL	Plastic limit	%
S	Degree of saturation	%
SAF_{ac}	Seasonal adjustment factor for AC layer	-
SAF_s	Seasonal adjustment factor for subgrade soil	-
Strs	Overburden stress	F/L^2
T	Temperature	T
T_{ac}	Asphalt pavement temperature	T
T_{air}	Air temperature	T

T_r	Temperature ratio	-
Ts	Asphalt surface temperature	T
VMC	Volumetric moisture content	%
W	Gravimetric water content	%
W_r	Moisture ratio	-
Z	Depth	L

Greek Symbols		**Dimension**
ε	Strain	-
ε_c	Compressive strain	-
ε_t	Tensile strain	-
γ_d	Dry unit weight	F/L^3
θ	Volumetric moisture content	%
θ_{sat}	Saturated volumetric moisture content	%
ρ	Density	M/L^3
σ_c	Confining stress	F/L^2

Abbreviations

AC	Asphalt concrete
AI	Asphalt Institute
Class	AASHTO soil classification
EICM	Enhanced integrated climatic model
FHWA	Federal Highway Administration
LTPP	Long term pavement performance
SMP	Seasonal monitoring program
SWCC	Soil water characteristic curve
TDR	Time domain reflectometry

1. INTRODUCTION

This project was initiated a few years ago, with the overall objective to quantify the environmental impacts on pavement performance and to include its effects in the design process for new and rehabilitated pavements. Two main factors were considered in the evaluation of environmental impacts: temperature as a major factor that affects the asphalt materials, and moisture as the major factor that affects the unbound materials such as the subgrade soils and untreated aggregate bases. The execution of the project idea and plans were developed over three phases:

Phase 1 of the project consisted of developing a scope of work and identifying types of instrumentation and the pavement sites to be installed in the state of Idaho. The research plan, developed during Phase I which is documented by Hardcastle and Bayomy (1996), led to the development of Phase 2.

Phase 2 involved the installation of the pavement sites that were identified in Phase 1 and establishing the data collection procedures and protocols. An interim report by Bayomy and Hardcastle (2002) was prepared which documented the installation process at all sites. It also described the data collection procedures and presented some of the data collected at various sites as pilot data presentation and analysis.

Phase 3 focused on data collection and analysis.

It is important to clarify that some of phase 2 activities overlapped with some of phase 3 tasks. For example, the installation of one of the sites (Weiser) under phase 2 contract was actually installed during the time period of Phase 3. In addition, changes in the installation at all sites, for example, replacing all cable housing cabinets from concrete boxes at ground level with elevated metal boxes, as will be described later, were conducted also during phase 3. The overlap was necessary in order to complete the installation activities while proceeding with the data collection for the sites that were already installed. The ITD research coordinator authorized these changes on behalf of the project committee. Thus, this report covers not only the work performed under the Phase 3 contract (project KLK459) but also includes the necessary background information on work done under the phase 2 contract (project FMK173). Detailed report on phase 2 work was prepared by Bayomy and Hardcastle (2002).

The organization of this report includes nine chapters and several Appendices. The appendices are provided only on electronic format in the enclosed CD with this document. Following is a brief description of the report contents.

Chapter 1 provides background about the project development and describes the overall project objectives. It also establishes the research methodology and sets the limitations of this research effort.

Chapter 2 presents a literature review describing in relation to the impacts of environmental changes on the pavement design process for both new and rehabilitated pavements.

Chapter 3 describes the experiment design, including site installation and data collection activities. In addition, the selected sites from the Federal Highway Administration Long Term Pavement Performance (LTPP) database are identified. The LTPP data was used to complement the data collected at the Idaho sites so that appropriate models could be developed.

Chapter 4 presents, interprets, and analyzes the data collected at Idaho sites.

Chapter 5 focuses on the analysis of data (from both Idaho sites and the LTPP database) to evaluate the effects of subgrade moisture variation on the subgrade structure capacity, as represented by the subgrade soil modulus of resilience.

Chapter 6 focuses on the data analysis with respect to the effects of temperature on pavement layers moduli.

Chapter 7 presents the validation of the developed models and an independent analysis of the Enhanced Climatic Model (EICM) using the data collected at Idaho sites.

Chapter 8 describes the implementation of the research findings with respect to moisture and temperature effects. It describes the development of seasonal shift functions that enable the design engineer to include environmental changes in the pavement design process.

Chapter 9 summarizes the research conclusions and recommendations for applying its findings.

The Appendices are provided in electronic format on a CD that should be attached to this report. They include Excel files for the raw data at the Idaho sites and the data obtained from the LTPP database. They also include the original tables and data analysis Excel sheets as well as the SAS output files. Site installation photos are also provided on the CD.

1.1 BACKGROUND

Previous research projects conducted at the University of Idaho by Bayomy and Shah (1993) recommended the use of the Falling Weight Deflectometer (FWD) to evaluate the pavement structure conditions, and provided initial values of subgrade soil resilient modulus for various climatic regions and soil types across the state that were suggested by Hardcastle (1992). In 1996, Bayomy et. al. developed a mechanistic-empirical (M-E) overlay design system that incorporated the recommendations of the 1993 work by Bayomy and the 1992 work by Hardcastle. The M-E overlay design system was implemented in DOS-based software called FLEXOLAY (Bayomy, et. al, 1996). Shortly after Microsoft released its Windows Version of the Visual Basic compiler, the FLEXOLAY program was modified to a Windows-based version called WINFLEX (Bayomy, et al., 1997). The WINFLEX software allowed the incorporation of environmental database for the six climatic regions in the state of Idaho as was suggested and mapped by Hardcastle (1992). Al-Kandari (1994) developed seasonal shift factors (SAF's) for various zones in the state. However, the SAF's developed by Al-Kandari, which were later used in the WINFLEX software, were based on published literature and theoretical work rather than actual measurements in the state of Idaho. Therefore, a need arose to establish realistic seasonal shift factors that are applicable to the soil types and environmental conditions in the state of Idaho. The seasonal shift factors are key inputs in a comprehensive mechanistic-based pavement design system such as the Idaho WINFLEX overlay design program or the AASHTO M-E design guide.

To address the environmental impacts at a national level, the Federal Highway Administration (FHWA) launched the Seasonal Monitoring Program (SMP) as a major component of the Long-Term Pavement Performance (LTPP) research program (Rada, et. al., 1994). Typical instrumentations at a LTPP-SMP site included time domain reflectometry (TDR) moisture sensors, a piezometer for determining ground water table level, temperature sensors, and resistivity sensors for frost depth measurements. Some LTPP sites included dedicated weather stations to collect extensive weather information. However, for sites where weather stations were not installed, LTPP created virtual weather stations by interpolating information from near by actual weather stations. In addition to the climatic and environmental data, FWD testing, surface distress evaluation, pavement surface profile and roughness measurements were performed quarterly at all LTPP-SMP sites.

The LTPP-SMP research program, being a national level program, included about 60 sites representing various climatic regions, pavement types, and subgrade conditions. Idaho had its share by one site that was installed near Idaho Falls (LTPP site No. 16-1010). While the data collected at the Idaho Falls LTPP site was extensive, its use in Idaho is limited in the sense that it surely did not represent the varied climatic regions in the state. The lack of other SMP sites in other climatic regions in Idaho supported the decision to install several other pavement sites, in a manner similar to the LTPP research plans. Therefore, this research project zooms on the state of Idaho and focuses on flexible pavements because they represent the majority of the Idaho state highways.

1.2 OBJECTIVES

The overall objective of this project is to assess the environmental changes and their effects on the pavement design process, especially for the design of rehabilitated pavements in Idaho. A secondary objective of this project is to investigate the effectiveness of placing a rockcap layer under the pavement surface and determine how it impacts the moisture regime under the pavement. This secondary objective was added since the use of a rockcap base layer is commonly practiced in the state of Idaho, and no sites in the LTPP research program included rockcap bases.

As mentioned previously, the project was conducted over three phases to address the stated overall project objective. Throughout this study, several specific objectives were developed and guided the research work. They can be summarized below:

- Study the effect of moisture variation, including frost conditions if they exist, in the pavement unbound layers on the structural capacity of these layers, as represented by the layer moduli. Specific attention was to be paid to pavements with rockcap base layers since it is commonly used in Idaho.
- Study the effect of temperature variation in the pavement asphalt layers and how it affects the moduli values of the asphalt layers.
- Establish seasonal shift factors that can reflect the variation of the temperature, moisture and frost conditions for use in the mechanistic-based design process.
- Assess the effects of the variation of these environmental parameters on the pavement performance

To achieve the goals of the project, several work tasks were identified for the three phases of the project:

Phase 1 was dedicated to developing the scope of work, in which instrumentations and pavement site locations were identified.

Phase 2 of the project was dedicated to site installation and initial data collection. The specific activities in Phase 2 included:

1. Procurement, testing and calibration of instrumentation.
2. Basic soil testing for classification purposes.
3. Instrumentation of the selected sites.
4. Initial data collection to identify possible problems and to refine the data collection scheme.

Phase 3 of the project was dedicated to data collection and analysis. The activities of Phase 3 included:

1. Data collection at all Idaho sites on an approximately monthly basis. For the Moscow site, a more frequent collection schedule was used in order to study the sensitivity of the pavement's moisture and temperature to the weather variations.
2. Identify and obtain pertinent data from the LTPP database to allow for the development of the moduli shift functions for unbound as well as the asphalt bound layers.
3. Develop the seasonal shift functions for both asphalt bound and unbound pavement layers.
4. Validate and check the applicability of the enhanced integrated climatic model (EICM) developed by the FHWA to predict moisture and temperature variation at the selected Idaho sites.
5. Assess the impacts of environmental changes in pavement layers on its performance be means of mechanistic analyses.
6. Develop an implementation plan of the research findings in Idaho.

1.3 RESEARCH APPROACH

The methodology adopted for the sites instrumentation was to employ the same technologies used in the LTPP seasonal monitoring program, SMP. Similar to the LTPP-SMP research experiment, three types of data were to be collected during this project: moisture profile under the pavement using TDR probes, temperature profile under the pavement using thermistor probes, and frost condition using resistivity probes. Basic information on the pavement sections where the probes were installed was also collected. This includes material types, layer thicknesses and traffic information as available from the planning division at ITD. In addition, piezometers were installed to determine the level of the ground water table at the selected sites. Moisture, temperature and resistivity data were collected on a monthly basis, to reflect the seasonal variations over the entire year. For some sites, the data collection activity continued over a three-year period. Similar to the LTPP, measurement of pavement surface conditions as well as structural capacity using Falling Weight Deflectometer (FWD) was also planned. The FWD data was to be collected by ITD crews. Pavement condition data proved to be insignificant though, since most of the sites were newly constructed pavements where changes in pavement surface conditions were not noticeable over the project period.

1.4 LIMITATIONS

As mentioned above, the FWD testing was to be performed by ITD crews. The ITD planned to conduct the testing at the sites along with their annual testing plan. There were no resources available to conduct, for instance, Falling Weight Deflectometer (FWD) testing during all seasons, as was done in the LTPP Seasonal Monitoring Program (SMP). This presented a major limitation to this study, in the sense that there was no structural support testing performed simultaneously with the environmental data collection (moisture, temperature, and frost conditions). Therefore, the annual FWD testing that was done at Idaho sites was considered only to assess the existing structure capacity of the selected pavement sites at an initial period and monitor any changes that could have occurred on an annual basis rather than seasonal basis. Consequently, the researchers relied on the LTPP-SMP database for the moduli-temperature or moduli-moisture data needed to develop the seasonal shift functions that enabled seasonal performance analysis. FWD data from Idaho sites were to be used for check and validation of the developed models from the national database.

Another limitation was the unavailability of weather stations at Idaho sites. However, for the Moscow site, the weather station at the University of Idaho was used to obtain climatic data for the Moscow area. For other sites, climatic data have been obtained from virtual weather stations by interpolating the data from three nearby weather stations, as was done in the LTPP-SMP program.

2. ENVIRONMENTAL IMPACTS ON PAVEMENT PEFORMANCE: A REVIEW

It is well known that environmental changes are the major factor in pavement deterioration. The effect of seasonal variation on pavement performance is generally considered to be very important. While the modulus of the Asphalt Concrete (AC) layers is more sensitive to the temperature variation, the modulus of unbound materials is sensitive to the variation of moisture content. These two environmental factors, temperature and moisture content, must be incorporated in the design process of flexible pavements particularly in seasonal frost areas where pavements are likely to heave during winter and then lose part of their bearing capacity during spring thaw. White and Corre (1990), Berg (1988) and Jano and Berg (1990) concluded that the latter problem is the prominent seasonal phenomena leading to pavement deterioration. As a matter of fact, White and Coree (1990) reported that 60% of the failures during the AASHTO road test occurred during spring. By focusing on the bearing capacity loss during spring thaw in their design procedures, many road administrations support this opinion. The bearing capacity is currently represented by the soil resilient modulus. One of the major differences between the AASHTO1986 Guide and previous interim guides was the adoption of resilient modulus as the preferred parameter for characterizing the quality of subgrade support. The AASHTO Guide also emphasized the need to account for temporal variations in the resilient modulus. The Guide includes a procedure for developing a weighted subgrade resilient modulus for design.

This chapter presents a review of the literature on pavement distresses associated with environmental changes. As the resilient modulus is the main property representing the bearing capacity of the pavement layer, this chapter focuses on reviewing the resilient modulus of unbound materials and the models used for calculating it, for both fine and coarse soils. The chapter also presents the temperature effects on the asphalt concrete (AC) layer modulus, the AC temperature prediction models and how to calculate seasonal adjustment factors (SAF) for different pavement layers. Also reviewed are the climatic models used to predict the effect of environmental changes on pavement layers.

2.1 PAVEMENT DISTRESSES ASSOCIATED WITH ENVIRONMENTAL CHANGES

Depending on the severity of the climatic conditions, it is believed that distresses induced and progressed during winter might have an important contribution to the overall deterioration of the pavement. Unlike the spring thaw-related distresses, which are controlled by the combined action of traffic and climate, winter distresses are primarily associated with climatic factors.

In an attempt to quantify the relative contribution of each season to the overall deterioration of pavements, data gathered at six instrumented test sections were studied and analyzed by Dore and Savard (1998). Three years of data were available for those sections. For the purpose of the study, three seasons were considered. Winter season is defined as the period of time between the beginning of the freezing and the beginning of the thawing of the pavement granular layers. The period included between the beginning of the thawing of the granular base and two weeks after complete thawing is referred to as the spring season. The remainder of the year, referred to as the summer-fall season, is the period when there is no frost action in the pavement structure and subgrade soil. In the context of the two test sites, winter is approximately 110 days long, spring is 60 days and the summer-fall season last about 195 days. Only the extent of the cracks was considered in the study. In most cases, the cracks were of low severity.

2.1.1 Transverse Cracking

A study by Zubeck and Vinson (1996) demonstrated that transverse cracks typically occur as the result of the thermal contraction of the surfacing layer. When the horizontal stresses induced by thermal contraction exceed the tensile strength of the surfacing layer, a crack, which is typically perpendicular to the longitudinal axis of the road, will occur. It is generally accepted that thermally induced cracks appear when temperatures are the lowest, in the middle of winter.

Dore and Savard (1998) reported that 65.5% of the damage occurred during winter while 25.5% occurred during spring and 9% during summer-fall. The observations were consistent with the expectations except for the relatively large cracking rate during spring and summer-fall. They added that the progression of transverse cracking during these periods is mainly associated with deterioration of existing cracks (occurrence of secondary cracks) under traffic action.

2.1.2 Longitudinal Cracking

Longitudinal cracks occur as a result of the transverse differential heave phenomenon. Because of the insulating action of the snow accumulated on the pavement shoulder, frost tends to penetrate deeper in the center of the road. Consequently, frost heave is greater at the center of the road than at the pavement edge. The resulting distortion induces horizontal stresses in the surface layer and when the strength of the material is exceeded, a longitudinal crack occurs. These cracks often occur at weak spots of the surface layers such as paving joints or segregation zones. It is expected that most cracks will be initiated at the end of winter when surface heaving is maximum.

This expectation was supported by the observations taken by Dore and Savard (1998) on six test sections. They found that longitudinal cracks have an average progression rate 1.3 times faster in the winter than in the spring and 4.5 times faster in the winter than in the summer-fall period. Overall, 55% of the damage occurs during winter compared to 23% during spring and 22% during summer. The relatively high damage level observed during spring and summer suggests that differential frost heave is not the sole mechanism involved in the initiation of longitudinal cracks. It is believed that the stress induced by heavy loads circulating near the existing cracks is responsible for most of the additional non-winter crack propagation. This is probably more critical in early spring when frost heave is still important and the weakened road base allows high deflections inducing additional stresses in the surfacing layer.

2.1.3 Fatigue Cracking

Fatigue cracking is the result of repeated tensile stresses induced at the bottom of the surfacing layer bending under circulating heavy loads. Fatigue cracking can take the shape of wheel path longitudinal cracks or alligator cracks. It is generally expected that most of the fatigue cracking in seasonal frost areas will occur during spring when the deflections are the highest and when the asphalt layer is still cold, causing the material to be more brittle.

The rate of progression of fatigue cracking observed on the six test sites by Dore and Savard (1998) tend to support the general understanding of the problem. As a matter of fact, fatigue cracking seems to evolve 1.6 times faster in the spring than in the winter and 15 times faster in the spring than in the summer. However, because of the longer winter season, most of the damage (49%) occurred during that season. 42% of the damage occurred during spring and 9% during summer and fall. Further investigation indicated that increases in the extent of fatigue cracking during winter can be directly associated with partial thawing of the pavement base. Finally, it was concluded that most of the damage occurred during partial thawing periods or during spring.

2.1.4 Roughness & Rutting

Roughness: Pavement roughness is the result of vertical differences between the ideal surface profile and the actual surface profile. Typical roughness indices are measurements of the perception of the road user traveling on the distorted surface. Because frost heave is rarely uniform, roughness can increase drastically during winter. Dynamic loads circulating on distorted pavements during spring can also contribute to the deterioration of the surface profile and the increase of roughness.

Rutting: The rut depth was defined as the maximum vertical distance between the measured profile and a 1.8 m straight edge. There are three major causes of pavement rutting. The first one is associated with the low stability of some asphalt mixtures at high temperatures, referred to stability ruts. They were characterized by narrow longitudinal deformations often separated by humps resulting from the lateral displacement of the material under the wheel load. This type of rut typically occurs during hot summer months when the material stability is the lowest. The second type of rut, referred to as structural ruts, were the result of permanent deformation occurring in the pavement granular layers and in the subgrade soil. They were characterized by wide wheel track deformations, which were then essentially in depression. The structural ruts were likely to evolve rapidly during spring when the pavement structure is weakened by the excessive moisture released from the thawing soils and, to a lesser extent, during hot summer months when stresses are transmitted more directly to the granular layers and the subgrade soils through the softened asphalt layer. The third type of ruts is the result of the wear action of studded tires on the pavement surface.

2.1.5 Summary

After three years of performance monitoring on two test sites with three seasonal frost cycles, Dore and Savard (1998) drew the following conclusions:

Deteriorations such as roughness and rutting in the outer wheel-path are temporary effects, which are essentially recovered after spring thaw. There seems, however, to be residual effects that contribute to the long-term deterioration of the pavement. Deterioration such as cracking has progression rates that vary depending on the season. They are permanent deteriorations that are generally not recovered between seasonal cycles.

Most of the deterioration experienced by the test sections occurred during winter. Around 55% of the pavement damage by cracking occurred during winter. Some of the winter damage is associated with partial thawing periods.

Transverse cracking, longitudinal cracking and winter roughness are related to environmental factors. There are, however, indications that traffic is playing an aggravating role in the development of these forms of deterioration. Fatigue cracking and rutting are associated with heavy loads circulating on the pavement. In this case, the deterioration process is aggravated by environmental factors.

2.2 SEASONAL EFFECTS ON THE RESILIENT MODULUS OF UNBOUND MATERIALS

To study the seasonal effects on the resilient modulus of unbound material one needs to know the factors that affect the resilient modulus of such material. In other words, the models used to predict the resilient modulus of unbound materials should be reviewed. Lab test results reported in the literature showed that the resilient modulus of all classes of unsaturated granular materials decreases to some extent with the increase in moisture content.

Edris and Lytton (1977) suggested that resilient modulus differences due to variations in water content are significant only when water contents are greater than the optimum compaction water content minus two percent.

Hardcastle (1992) reported that the magnitude of the increases in compacted subgrade materials depends on the composition and amount of silt and clay-sized particles in the soil as well as the water content range considered.

Temperature also has significant effects on the soil resilient modulus. The penetration of freezing temperatures into moist pavement subgrade soils can cause more severe effects than the effects of any of the water content changes likely to occur as a result of seasonal variations in precipitation.

This section presents a review of the most popular models used to predict the resilient modulus of unbound materials. It also discusses the effect of seasonal effects (including moisture and temperature) on the resilient modulus of such material.

2.2.1 Models for Estimating the Resilient Modulus of Unbound Materials

2.2.1.1 Stress-Dependent Models

Coarse Grained Soils

Many different relationships have been proposed to express the stress-dependency of the resilient modulus of soils and granular materials. One of the most widely utilized relationships for granular materials including sands and unbound aggregate base materials is the one proposed by Seed et al. (1967) as follows:

$$M_r = K_1\ \theta^{K2} \tag{2.1}$$

Where Mr is the resilient modulus in units of psi for the material subject to a bulk stress θ. The bulk stress θ is the sum of the principal stresses ($\theta = \sigma_1 + \sigma_2 + \sigma_3$). In repeated load triaxial compression tests, θ is the sum of the deviator stress and three times the confining stress ($\theta = \sigma_d + 3\ \sigma_3$). The constants K_1 and K_2 are material properties determined from data obtained in a laboratory test procedure such as AASHTO T-274 (1982).

Fine Grained Soils

Seed and Lee (1962) proposed that the resilient modulus could be related only to the deviator stress as follows:

$$M_r = K\ (\sigma_d)^{\ n} \tag{2.2}$$

Bilinear models have also been proposed for the stress dependency of resilient modulus of cohesive or fined-grained soils. Thompson and Robnett (1979) developed the widely accepted bilinear model, illustrated in Figure 2.1, which require four material constants. With this model the resilient modulus is related to stress state by two linear equations. At deviator stresses less than the "breakpoint" deviator stress, the resilient modulus is given by:

$$M_R = M_{Ri} + (\sigma_{di} - \sigma_d)\ K_3 \tag{2.3}$$

where M_R is the resilient modulus at a given deviator stress, M_{Ri} is the experimentally determined resilient modulus at the breakpoint of the nonlinear relationships, σ_{di} is the deviator stress at the breakpoint and K_3 is the negative slope of the resilient modulus-deviator stress relationship at deviator stresses less than the breakpoint stress, σ_{di}.. At deviator stresses greater than breakpoint deviator stress the resilient modulus is given by the equation:

$$M_R = M_{Ri} - (\sigma_{di} - \sigma_d)\, K_4 \qquad (2.4)$$

where the terms are as defined above and K_4 is slope of the modulus-deviator stress line for deviator stresses greater than the breakpoint deviator stress.

Thompson and Robnett (1979) applied the bilinear model to a large number of repeated-load compression tests in which unsaturated specimens were tested in an unconfined condition, in which the confining stress on the specimens was equal to zero and the bulk stress θ was equal to the deviator stress. Based on the results of these tests, Thompson and Robnett concluded that for many fine-grained compacted unsaturated (cohesive) soils, the deviator stress at the breakpoint of the bilinear relationship is about 6 psi (41.4 kPa).

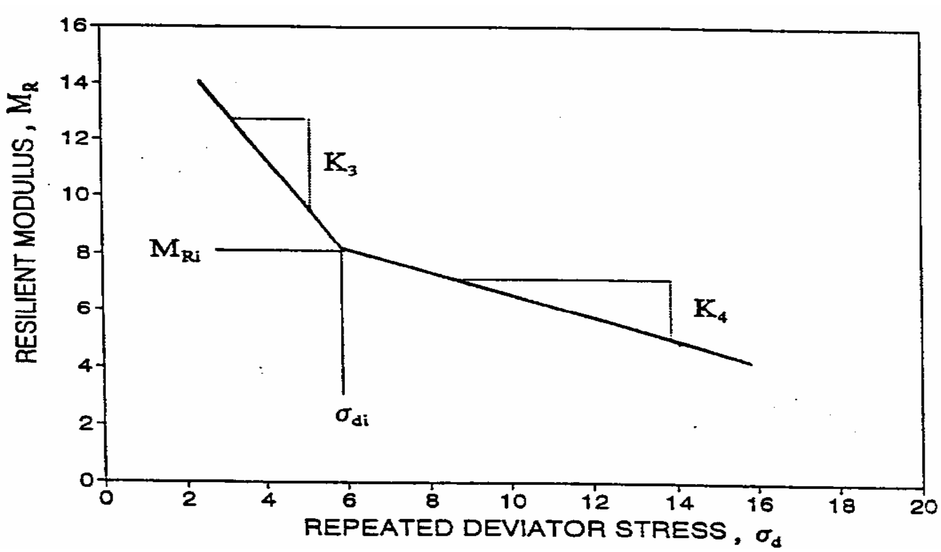

Figure 2.1 Bilinear Resilient Modulus- Deviator Stress Model (Thompson and Robnett, 1979)

2.2.1.2 Regression Models

Coarse Grained Soils

Different investigators have developed relationships between specific material properties and resilient modulus. Using a database of 250 tests on both coarse and fine-grained soils, Carmichael and Stuart (1985) related the resilient modulus (in ksi) to the soil class, bulk stress and water content of granular soils as follow:

$$\text{Log}\,(M_r) = 0.523 - 0.0225\,w + 0.544\,\log\theta + 0.173\,SM + 0.197GR \qquad (2.5)$$

where w is the water content in percent and θ is bulk stress in psi. SM is a "silt factor" which is equal to one for soils classified as SM and zero for all others. GR is a "gravel factor" which is equal to one for soils classified as GM, GW, GC or GP and zero for all others.

Fine Grained Soils

Thompson and Robnett (1979) conducted an extensive testing program on 50 fine-grained surface Illinois soils to test the effect of a number of factors on the resilient modulus. They found that the break point resilient modulus, M_{Ri}, in the bilinear model was significantly correlated with liquid limit, plasticity index, AASHTO classification group index, silt content, clay content, specific gravity and organic carbon content. They observed that in unconfined repeated-load triaxial compression tests, the breakpoint modulus, M_{Ri} was typically about 6 psi. The values of the slope coefficients, K_3 and K_4, in the bilinear stress-dependent model also showed little variability for the Illinois soils.

The results of the regression analysis relating resilient modulus to soil compositional parameters performed by Thompson and Robnett for soils compacted to T-99 maximum dry unit weight at optimum water content showed that the best correlation relationship obtained for the breakpoint modulus, M_{Ri}, of the 50 soils was as follows:

$$M_{Ri} = 6.37 + 0.034C + 0.450\,PI - 1.64\,OC - 0.0038\,S_i - 0.244GI \qquad (2.6)$$

where M_{Ri} is the breakpoint resilient modulus in ksi, C is clay content in percent, PI is plasticity index in percent, OC is organic carbon in percent (by weight), S_i is silt content in percent and GI is the AASHTO classification Group Index, a dimensionless whole number. This regression equation has a correlation coefficient(R) of 0.796 and a standard error of 2.18 ksi. Thompson and Robnett found that the soil properties contributing to lower the breakpoint modulus were the low clay content, low plasticity (liquid limit and plasticity index), low silt content, low group index, low specific gravity and high organic carbon content.

Using the same database as Thompson and Robnett, Thompson and LaGrow (1980) simplified the regression relation for M_{Ri} of fine-grained Illinois soils at T-99 maximum dry unit weight and optimum water content into the following equation:

$$M_{Ri} = 4.46 + 0.098C + 0.119\,PI \qquad (2.7)$$

The terms in Equation 2.7 are as defined before for Equation 2.6.

Carmichael and Stuart (1985) presented correlations relating resilient modulus to fine-grained soil composition parameters. Using a database representing over 250 soils (fine and coarse) and 3,300 modulus test data points, they developed the following relationship:

$$M_r = 37.431 - 0.4566\,PI - 0.6179\,w - 0.1424\,F + 0.1791CS - 0.3248\,\sigma_d$$

$$+ 36.422CH + 17.097\,MH \qquad (2.8)$$

where M_r is resilient modulus in ksi, PI is plasticity index in percent, w is water content in percent, F is percent passing the No. 200 sieve, CS is the confining stress in psi and σ_d is deviator stress in psi. The CH term is a material factor which is equal to one for soils classified as CH and is equal to zero for soils classified as ML, MH, or CL. MH is a material factor equal to one for soils classified as MH and equal to zero for soils classified as ML, CL, or CH. The R^2 for the relationship was 0.759 and the standard error was 5.77 ksi.

Hudson et al. (1994) conducted cyclic triaxial testing to measure the resilient modulus of eight different fine-grained soils representing the subgrade in Tennessee. The statistical analysis of the data revealed the following model having R^2 value of 0.70:

$$\text{Log}(M_r) = 46.93 + 0.0188\,\sigma_d - 0.2222\,\text{Log}(\sigma_d) - 0.0012\,\sigma^2_c + 0.0333\,\gamma_d$$
$$0.0033\,W_d + 0.468\,S - 0.0017\,S^2 - 38.44\,\log(S) + 0.0001\,PL^2$$
$$-\,0.1143\,LI - 0.0278\,LI^2 - 0.0085\,(\text{Class})^2 \qquad (2.9)$$

where,

σ_d	= Deviator stress, psi
σ_c	= Confining pressure, psi
γ_d	= Deviator dry density = deviation from the standard proctor maximum, ± pcf
W_d	= Deviator water content = deviation from the standard optimum, ± %
S	= Degree of saturation, %
PL	= Plastic limit, %
LI	= liquidity index, %
Class	= AASHTO classification, e.g. A-7-6 soil will be 7.6 (the valid range is 4 to 7.6).

2.2.2 Moisture Effects on Unbound Materials

2.2.2.1 Moisture Effects on Coarse-Grained Soils

The moisture sensitivity of coarse-grained materials depends on the amount and nature of its fine fraction. Clean gravels and sands classified GW, GP, SW, and SP are not likely to exhibit moisture sensitivity due to the absence of a sufficient number of the small pores necessary to create significant suction-induced effective stresses even at low moisture contents (Hicks and Monismith, 1971).

Studies of coarse materials containing larger amounts of fines have shown that increasing degrees of saturation above about 80 to 85 percent can have a pronounced effect on resilient modulus. Rada and Witczak (1981) concluded that changes in water content of compacted aggregates and coarse soils could cause modulus decreases of up to 30 ksi (207 MPa).

Several researchers have developed regression relationships between resilient modulus of granular materials and water content. The general regression relationship for granular materials of Carmichael and Stewart (1985) stated previously as Equation 2.8 contains a water content term, which results in a 0.62 ksi (4.3 MPa) decrease in resilient modulus for each one percent increase in water content.

Lary and Mahoney (1984) found regression relationships for resilient moduli of specific northwest aggregate base materials and predominantly coarse subgrade soils. The regression equations for the materials showed that if the initial modulus is on the order of 20 ksi, a one percent increase in moisture content typically results in a resilient modulus decrease from about 0.6 to 1.6 ksi. A reasonable estimate for the influence of water content on reference resilient modulus of coarse soils would be about 0.5 ksi decrease for each one percent water content increase for uniform or well-graded coarse materials containing little or no non-plastic fines (GW, GP, SW, SP) up to about 2.0 ksi per one percent water content increase for sands and gravels containing substantial amounts of plastic fines (GM, GC, SM, SC).

2.2.2.2 Moisture Effects on Fine-Grained Soils

Many researchers have investigated the influence of water content on resilient modulus of fine-grained soils. Seed et al. (1962) studied the influence of "natural" water content on the resilient modulus of the undisturbed samples of the silty clay (CL) AASHTO Road test subgrades soil. Their results showed that for this soil a decrease in water content of only three percent below the T99 optimum resulted in a doubling of the resilient modulus value (from about 5000 psi to about 10,000 psi).

Tests conducted on silty clay (CL) subgrade soil at San Diego County by Jones and Witczak (1977) showed that as its compaction water content was increased from about 11 percent to about 20 percent the resilient modulus varied from almost 40 ksi to a low of about 7.5 ksi.

Figure 2.2 show the influence of compaction water content on the resilient response of two fine-grained Arkansas soils reported by Elliott and Thornton (1988). Both the low plasticity soil in Figure 2.2.A and the highly plastic CH soil in 2.2.B exhibit resilient modulus decreases of roughly 1.1 ksi per each one percent increase in water content.

Hardcastle (1992) reported that most if not all of the differences in resilient moduli of fine-grained soils, which accompany changes in either compaction water content, or post construction changes in in-situ water contents probably occur as a result of the changes in effective confining stresses existing in the material. These changes in effective stresses take place as a result of the changes in soil suction (negative pore water pressures), which usually accompany the change in soil moisture content in unsaturated soils. Therefore, when the moisture content decreases, suction along with effective stress and soil stiffness generally increase until very low moisture contents are reached.

Figure 2.3 shows the regression relationships for the water sensitivity of resilient modulus for fine-grained Illinois subgrade soils and the data on which they are based. The wide dispersion of the data points and the low R^2 value suggest that the regression equations should be limited to providing very approximate estimates only. Using the expression given on the figure and "typical" dry unit weights and specific gravities of solids (105 and 2.70 Ib/ft^3, respectively) the water sensitivity of resilient modulus of fine-grained soils is a 1.9 ksi decrease for each one percent increase in water content. Based on later analysis of essentially the same database, Thompson and LaGrow (1980) suggested that the breakpoint resilient modulus of fine-grained subgrades measured at T-99 maximum dry unit weight and optimum water content be adjusted for moisture contents greater than optimum in accordance with the values listed in Table 2.1.

In more recent studies by Salem et al. (2003), Bayomy et al. (2003) and Salem (2004), regression models were developed to relate the change in subgrade modulus to the change in moisture content for various types of soils. These models were then used to predict the seasonal changes in modulus at Idaho sites using shift functions that adjust the model to the specific site conditions. More details about these studies will be discussed in Chapter 5.

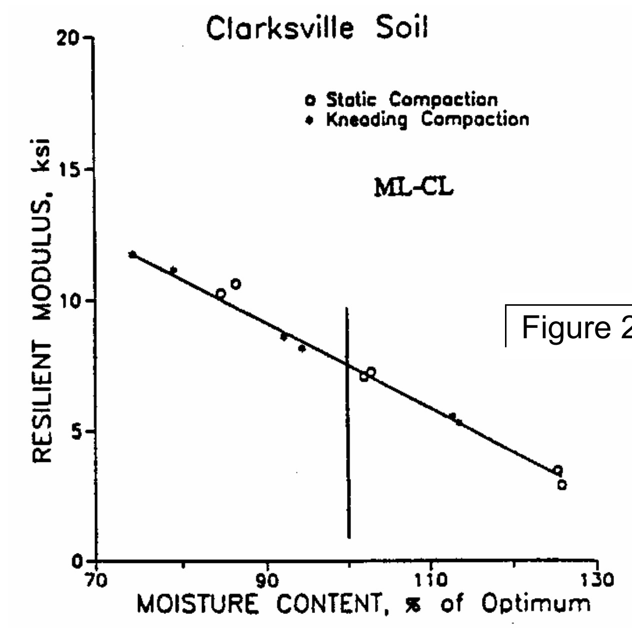

Figure 2.2-A

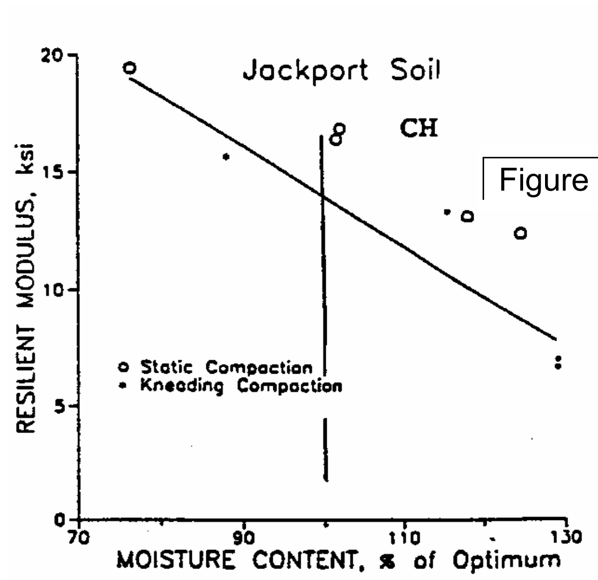

Figure 2.2-B

Figure 2.2 Effect of Compaction Water Content on Resilient Modulus of Fine Grained Soils, A) Low-Plasticity Soil and B) High-Plasticity Soil.

(Elliott and Rhornton, 1988)

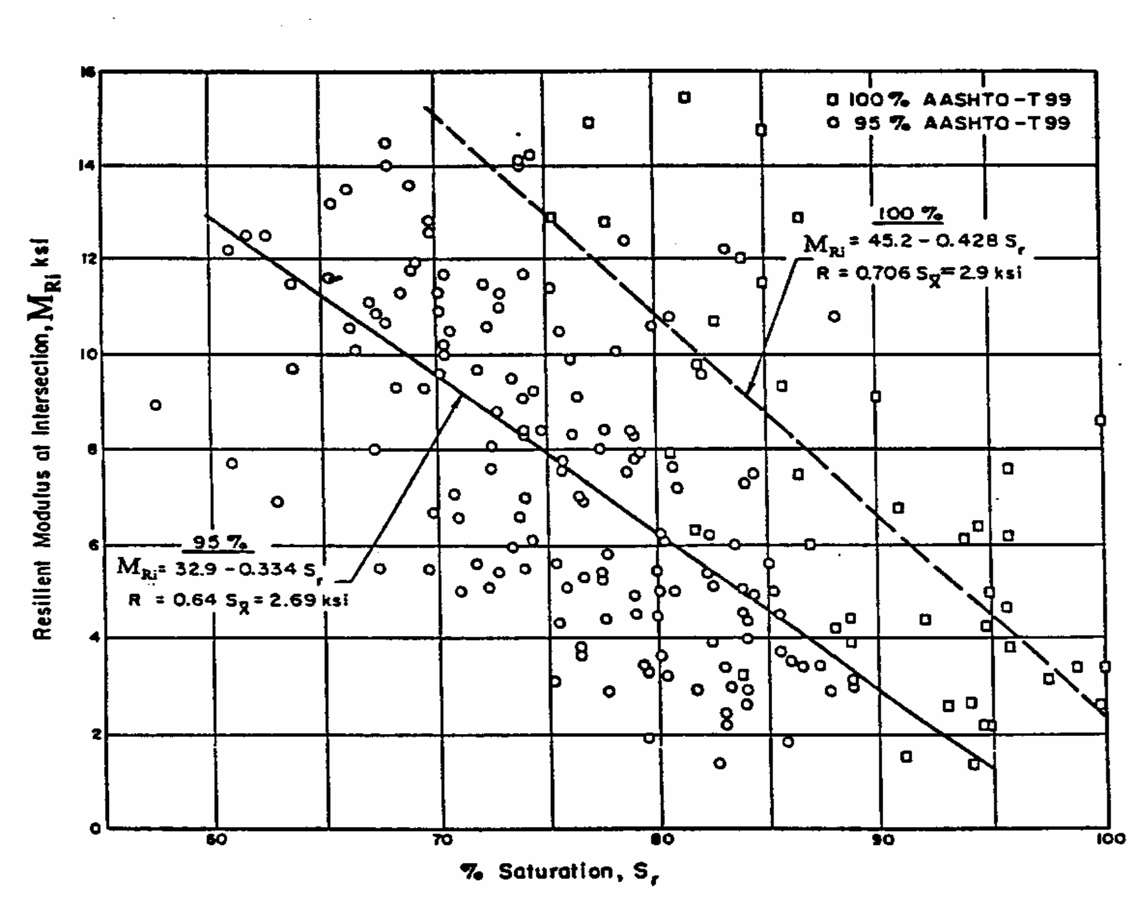

Figure 2.3 Breakpoint Modulus-Saturation Relationship For Fine-Grained Soils (Thompson and Robnett, 1979)

Table 2.1 Moisture Sensitivity Adjustments for Fine-Grained Soils (Thompson and Robnett, 1979)

Soil Textural Class	Possible Unified Soil Classification	Moisture Sensitivity (ksi decrease per percent water content increase)
Clay, Silty clay, Silty clay loam	CH, CL, SC	0.7
Silt loam	ML, SM	1.5
Loam	SM, SC	2.1

2.2.3 Temperature Effects on Soil Resilient Modulus

Temperature has significant effects on the soil resilient modulus. The penetration of freezing temperatures into moist pavement subgrade soils can cause more severe effects than the effects of any of the water content changes likely to occur as a result of seasonal variations in precipitation. Freezing of soil moisture can transform a soft subgrade into a rigid material, at the stress levels existing in pavements. Thawing of the same material can produce a softening effect such that for some time after thawing, the material has a resilient modulus that is only a fraction of its prefreezing value (Hardcastle, 1992).

The variation in resilient modulus of the clay before and after one cycle of freezing and thawing was recorded by Bergen and Monismith (1973). Resilient modulus values of the clay after thawing were reduced to values ranging from 52 to 60 percent of the prefreezing values. The freezing and thawing on a different CH soil (from Tennessee) exhibited resilient modulus decreases of up to 49 percent of the unfrozen value (Thompson and Robnett, 1976).

Freezing increases the resilient modulus of both coarse and fine-grained soils containing moisture. Resilient moduli of six frozen coarse-grained soils and aggregates are shown in Figure 2.4 as a function of temperature (Chamberlain et al., 1989). Similar curves are drawn for fine-grained soils by Chamberlain et al. (1979).

Chamberlain et al. (1979) also investigated freeze-thaw effects on resilient modulus of a low plasticity natural clay subgrade obtained by core sampling. They concluded that the decreases in resilient modulus accompanying freezing and thawing were caused by the increases in water content and decreases in unit weight that occur when soils are frozen with free access to water (open-system freezing). The recovery of the resilient modulus following the thaw induced decreases was attributed to decreasing water content (drying) and increasing dry density.

The effects of one cycle of freezing and thawing on a soil from Idaho classified as sandy silt (ML) exhibits decreases in resilient modulus ranging from 53 to 63 percent of the original values (Hardcastle et al., 1983).

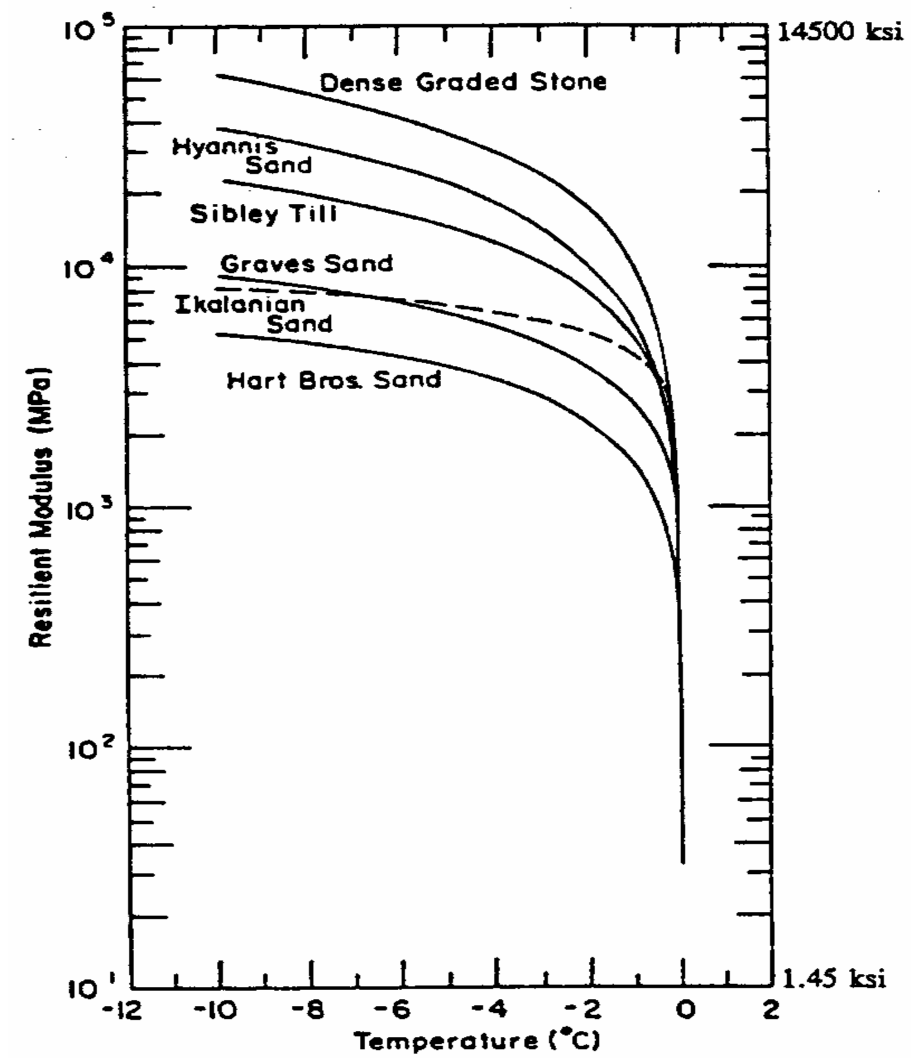

Figure 2.4 Effect of Temperature on Resilient Modulus of Frozen Coarse-Grained Soils (Chamberlain et al., 1989)

2.3 ESTIMATION OF SUBGRADE SOIL MOISTURE CONTENT

Changes in subgrade moisture content are accompanied by changes in subgrade resilient modulus and pavement performance as described before. Methods available to estimate the seasonal fluctuations and long-term changes in subgrade moisture content may include direct measurement and/or theoretical models for soil suction distributions. Relationships between moisture content and soil suction for use in conjunction with the methods for estimating subgrade soil moisture are presented in this section.

2.3.1 Direct Measurement of Subgrade Moisture

Subgrade moisture content near the ground surface depends on a variety of climatic and physical factors including soil type, temperature, precipitation, vegetation, and others. The most reliable method for determining subgrade moisture variations is the direct measurements over an extended time period. Direct measurement of subgrade moisture content is generally the most acceptable method used by the majority of the highway agencies.

Seasonal variations in subgrade soil water contents in Pennsylvania are shown in Figure 2.5 for pavements not subject to subgrade freezing. Figure 2.5 shows the average seasonal changes in subgrade water content measured over a five-foot depth interval for eight different sites in Pennsylvania during the years 1970 through 1973 (Cumberledge et al., 1974). The figure contains data for sands, silts and clays for a variety of climate conditions and pavement types (flexible and rigid). The figure shows that the more permeable sand soils exhibit the greatest seasonal increase in moisture (three to four percent as for the silty soils). The clay soil exhibited averaged seasonal fluctuations of only one percent. It can be seen also that the duration of the period of the increases was shorter for the more permeable sand soils than for the silts.

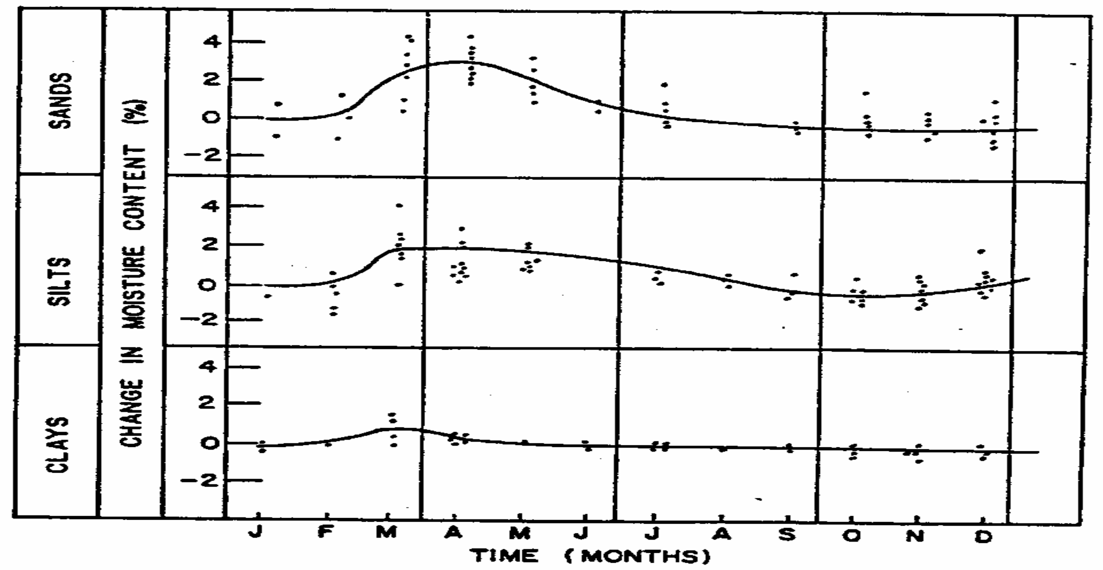

Figure 2.5 Seasonal Subgrade Water Content Changes in Pennsylvania (Cumberledge et al., 1974)

Trends toward long-term equilibrium subgrade soil water contents are illustrated for two Oklahoma pavements in Figure 2.6 and Figure 2.7. The subgrades are clay (CH) and are not located in an area of significant subgrade freezing. The figures are from Marks and Haliburton (1969) who concluded that although both subgrades continue to exhibit seasonal fluctuations in water content, they also trend toward an "equilibrium" value equal to 1.1 to 1.3 times soil's plastic limit. The large seasonal variations of the less impervious pavement of Figure 2.7 were attributed to infiltration whereas the water content changes in the more impervious pavement of Figure 2.6 were attributed to capillarity and seasonal changes in groundwater table elevations.

In regions where adequate surface drainage details have been provided, increases in average annual subgrade water content are attributed primarily to changes in the evapotranspiration regime brought about by the removal of vegetation and placement of the relatively impervious pavement surfacing (Picornell and Rahim, 1991). Although freeze-thaw cycles and uneven distributions of rainfall continue to produce seasonal variations in subgrade water content, measurements of subgrade moisture show that a new average "equilibrium" water content tends to be established within 5 years (Haupt, 1981).

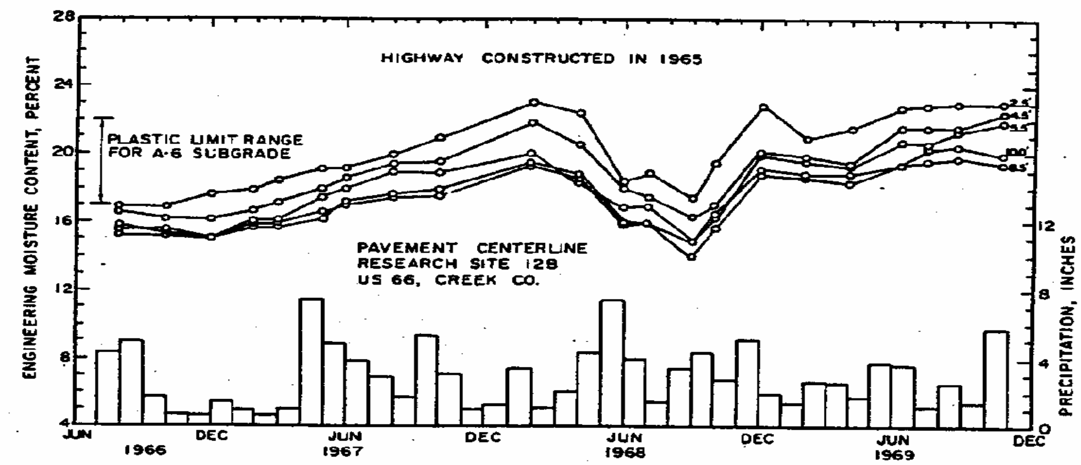

Figure 2.6 Subgrade Water Content Changes Beneath AC Pavement Attributed to Capillarity (Marks and Haliburton ,1969)

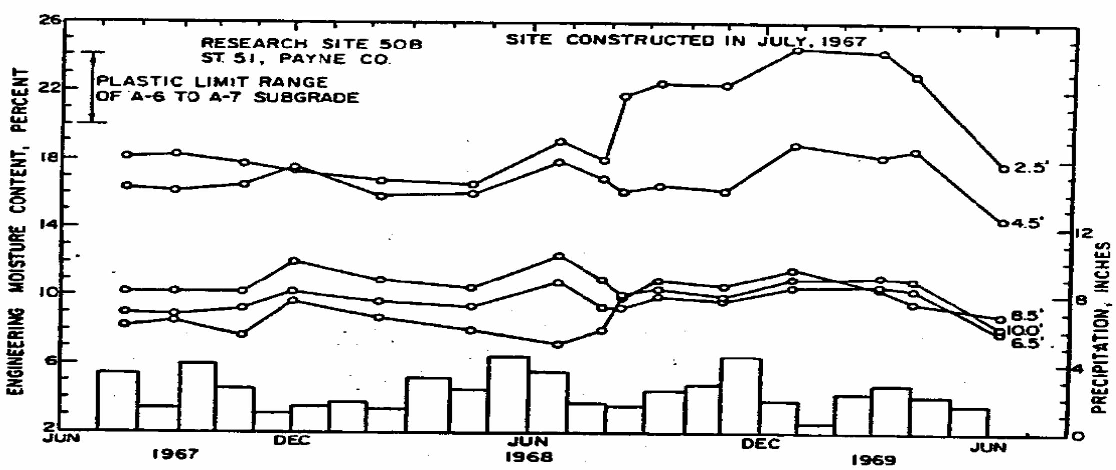

Figure 2.7 Subgrade Water Content Changes Beneath PCC Pavement Attributed to Infiltration (Marks and Haliburton ,1969)

2.3.2 Subgrade Water Content and Soil Water Characteristic Curves

2.3.2.1 Soil Suction

Definition

Suction can be defined as the negative gauge pressure relative to the external gas pressure on the soil water to which a pool of pure water must be subjected in order to be in equilibrium through a semi-permeable membrane with the soil water, i.e., suction $\psi = u_a - u_w$ where U_a is the pore air (gas) pressure and u_w is the pore water pressure. The pore water pressure u_w is always lower than the pore air pressure across a meniscus, that is, in an unsaturated soil. It can be defined also as a measure of a soil's affinity for water or the tendency of a soil to imbibe water (Hardcastle, 2000).

Components of Suction

Matric Suction: It can be defined as the surface tension (capillarity or meniscus) effects, or the adsorption (hydration) of clay minerals (polar H_2O molecules attracted to charged soil particles).

Osmotic (Solute) Suction: Ion concentration differences between the "free" pore water and the adsorbed water in soils with charged particles (that is, fine-grained soils with plasticity)

Total Suction: Sum of matric and osmotic.

Soil suction is usually mainly matric suction and changes in suction are due to changes in matric suction.

Units of Suction

A. Pressures: psi, kPa, atmospheres, bars, etc.

B. Head: cm H_2O or cm Hg

C. pF: $\log_{10}$ (head in cm of H_2O)

The soil suction, which is the negative pore water pressures, at a point can be computed as the unit weight of water multiplied by the height of the point above the groundwater table. Once the suction is known the water content of the soil at the point can be obtained from a moisture characteristic curve (also called a water retention curve) for the soil.

Table 2.2 Common Units of Soil Suction & Corresponding Relative Air Humidity at 20°C (Hardcastle, 2000)

Units of Suction						Relative Humidity, %
pF	cm H20	atm	bar	psi	kPa	
0	1	0.001	0.000981	0.0142	0.0981	100.00
1	10	0.01	0.00981	0.1422	0.981	100.00
2	100	0.10	0.0981	1.422	9.81	99.99
3	1,000	1.0	0.981	14.22	98.1	99.92
4	10,000	10	9.81	142.2	981	99.27
5	100,000	100	98.1	1,422	9,810	93.00
6	1E6	1000	981	14,220	98,100	48.43
7	1E7	10,000	9,810	142,200	981,000	0.07

2.3.2.2 Soil Water Characteristic Curve (SWCC)

The SWCC has been defined as the variation of water storage capacity within the macro and micro pores of a soil, with respect to suction (Fredlund et al., 1995). This relationship is generally plotted as the variation of the water content (gravimetric, volumetric or degree of saturation) with soil suction. The determination of a soil's moisture characteristic curve is a procedure routinely performed in agricultural and soil physics laboratories, commonly with the pressure-plate extraction (drying) procedure (Klute, 1986).

Moisture characteristic curves are plotted in a variety of ways, using a variety of units for suction including all of those listed in Table 2.2. In agricultural applications, water contents in moisture characteristic curves are usually expressed in terms of the volumetric water content or the volume of water per unit total volume of soil. The volumetric water content is related to the gravimetric (engineering) water content as follows:

$$W = \frac{\theta}{G_s(1-n)} = \theta \times \frac{\gamma_w}{\gamma_d} \tag{2.10}$$

where W is the engineering (gravimetric) water content, θ is the volumetric water content, G_s is the specific gravity of the soil solids and n is the porosity of soil, γ_w is the unit weight of water and γ_d is the dry unit weight of soil. All terms in Equation 2.12 are dimensionless ratios. Engineering water content and porosity are commonly stated in percent. The engineering (gravimetric) water content, W, is related to degree of saturation, S_r, as follows:

$$W = (S_r\ n) / [G_s\ (1\text{-}n)] \tag{2.11}$$

where the symbols are as defined above.

To represent the SWCC, several mathematical equations have been proposed. Most of the equations are empirical in nature and are based on the analysis of measured SWCCs. The most popular equations are those of Gardner (1958), shown in Equation (2.12) and Fredlund and Xing (1994) given by Equations (2.13, 2.14).

$$\theta_w = \theta_r + \frac{\theta_s + \theta_r}{1 + \left(\frac{h}{a}\right)^b} \tag{2.12}$$

$$\theta_w = C(h)x\left[\frac{\theta_s}{\left[\ln\left[\exp(1) + \left(\frac{h}{a}\right)^b\right]\right]^c}\right] \tag{2.13}$$

$$C(h) = \left[1 - \frac{\ln\left(1 + \frac{h}{h_r}\right)}{1 + \left(\frac{10^6}{h_r}\right)^b}\right] \tag{2.14}$$

where,

θ_w	= Volumetric water content
θ_s	= Saturated volumetric water content
θ_r	= Residual volumetric water content
h	= Soil matric suction, kPa
h_r	= Soil parameter, function of the suction at which residual water content occurs in kPa.
a	= Soil parameter, function of the air entry value of the soil in kPa.
b	= Soil parameter, function of the rate of water extraction from the soil, once the air entry value has been exceeded.
c	= Soil parameter, function of the residual water content.
C (h)	= Adjustment factor which forces all curves through a suction of 1,000,000 kPa at zero water content.

2.3.2.3 Correlating SWCC Fitting Parameters to Well-Known Soil Properties

In a recent study conducted by Zapata et al. (1999) the fitting parameters of the Fredland and Xing (1994) equation were statistically correlated to well-known soil properties. The soils were divided into two categories: soils having a plasticity index (PI) greater than zero and those having a PI equal to zero. The data assembled for the soils with PI greater than zero included the percentage passing # 200 sieve and the Atterberge limits, particularly the plasticity index. For soils with PI equal to zero (non-plastic soils), the diameter D_{60} was the main soil property used for correlation. For the soils with PI greater than zero, the product of the percentage passing the # 200 sieve, as a decimal, was multiplied by the PI as a percentage, to form the weighted PI. This value was designated as wPI, and used as the main soil property for correlation.

<u>For Soils with PI > 0:</u>

The Fredlund and Xing fitting parameters in Equations 2.13 & 2.14 (parameters a, b, c, and h_r,) were correlated with the new wPI parameter.

The equations found are the following:

$$a = 0.00364(wPI)^{3.35} + 4(wPI) + 11 \tag{2.15}$$

$$b/c = -2.313(wPI)^{0.14} + 5 \tag{2.16}$$

$$c = 0.0514(wPI)^{0.465} + 0.5 \tag{2.17}$$

$$h_r/a = 32.44e^{0.0186(wPI)} \tag{2.18}$$

The wPI parameter in equations 2.15 through 2.18 is defined as:

$$wPI = \text{Passing \#200} \times PI \tag{2.19}$$

where,

Passing #200 = Material passing the #200 U.S. Standard Sieve in decimal
PI = Plasticity Index (%)

In those cases where the saturated volumetric water content, θ_{sat}, is unknown the user can make use of the following correlation:

$$\theta_{sat} = 0.0143 (wPI)^{0.75} + 0.36 \tag{2.20}$$

Although Equation (2.20) produces a more or less unbiased estimate of the $\theta_{sat,}$ Zapata et al. (1999) recommended having direct measurements of density and specific gravity, G_s, so that θ_{sat} can be calculated from direct measurements. Equation (2.21) for estimating G_s, can be used with only small to moderate error when directly measured G_s values are not available:

$$G_s = 0.041 (wPI)^{0.29} + 2.65 \tag{2.21}$$

<u>For Soils with PI = 0</u>

For granular soils with Plasticity Index equal to zero, the parameter used to relate to the SWCC was the Diameter D_{60} from the grain-size distribution (GSD) curve. The correlations found are as follows:

$$a = 0.8627\,(D_{60})^{-0.751} \tag{2.22}$$

$$b' = 7.5 \tag{2.23}$$

$$c = 0.1772\,\mathrm{Ln}\,(D_{60}) + 0.7734 \tag{2.24}$$

$$h_r/a = 1/(D_{60} + 9.7\,e^{-4}) \tag{2.25}$$

where,

D_{60} = Grain diameter corresponding to 60% passing by weight or mass (mm)

b' = Average value of fitting parameter b

Zapata et al. (1999) did not find correlation between the 'b' parameter and D_{60}. Therefore, a constant average b value was suggested. In those cases where the θ_{sat}, is unknown, the following average value was recommended for soils with PI equal to zero:

$$\theta_{sat} = 0.36 \tag{2.26}$$

2.3.2.4 Predicted SWCC Based on D60 and wPI

Zapata et al. (1999) concluded that if a single soil is sent out to a dozen laboratories across the country for SWCC measurement, the results show variability greater than that of the experimental data shown in Figure 2.8, for example. Likewise, if a single laboratory is asked to reproduce the SWCC for a single soil, the variability can typically be as greater as the difference between the wPl = 10 curve and the wPI = 30 curve in Figure 2.8. These observations have led the authors of EICM version 2.6 (Witczak et al., 2000) to conclude that soil suction and SWCCs simply cannot be measured with great precision at the present time. They also added that it is difficult to develop a predictive model for SWCCs that is consistent with all of the SWCCs reported in the literature because of the fairly high probability that any given measured SWCC has significant experimental error associated with it. Therefore, they concluded that the SWCC could probably be estimated from D60 or wPI (Figure 2.8) about as accurately as it can be measured, unless the laboratory or person making the measurement is highly experienced.

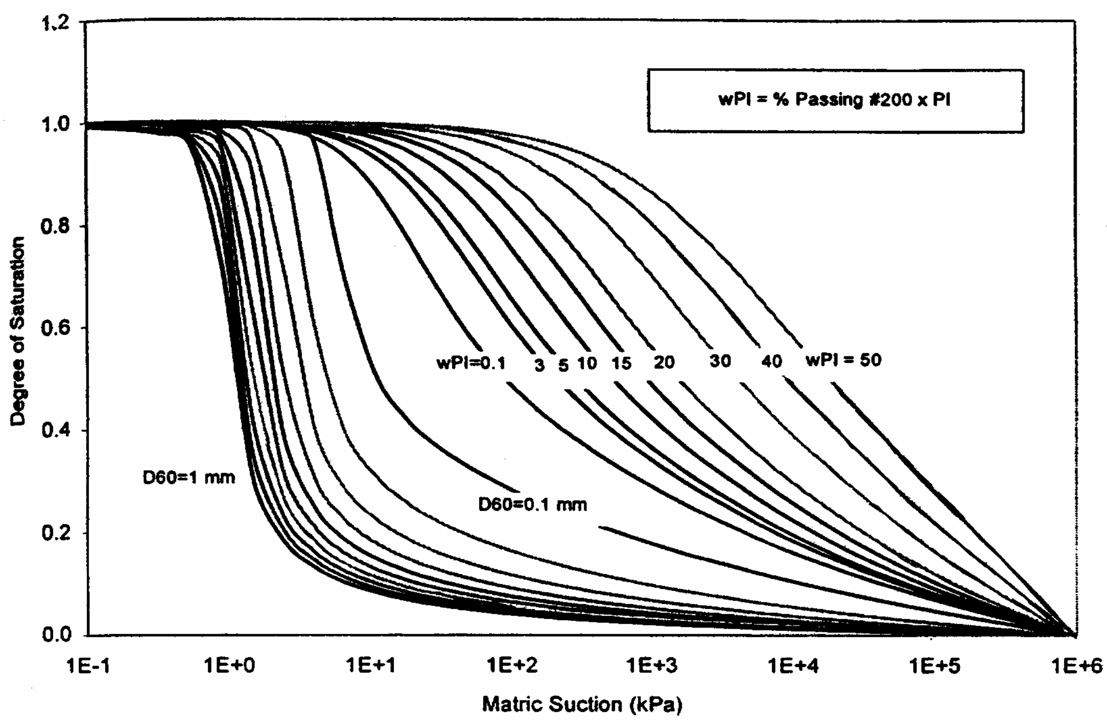

Figure 2.8 Predicted SWCC Based on D60 and wPI (Zapata et al., 1999)

2.4 SEASONAL EFFECTS ON THE AC LAYER MODULUS

The elastic modulus of the asphalt concrete (AC) layer is highly affected by the pavement temperature. Newton's law explains this mechanism through the following equation:

$$\tau = \mu * (\delta\varepsilon / \delta\tau) \tag{2.27}$$

where,

τ = Shearing resistance between the microscopic layers;

μ = Viscosity (a function of temperature)

$\delta\varepsilon / \delta\tau$ = Rate of shear stain.

As temperature changes, the viscosity of the binder material changes (the higher the temperature, the lower is the viscosity) thus changing the shear resistance of the material. The elastic modulus of a material (E) is related to the shear modulus (G) and Poisson's ratio (ν) by the following equation:

$$E = 2(1 + \nu)\, G \qquad (2.28)$$

This mechanism explains why the elastic modulus of asphalt concrete decreases as temperature increases. However, since pavement temperature is related to ambient air temperature, and the latter often follows a sinusoidal pattern throughout the year, Ali (1996) expected that the elastic modulus of the AC layer follow the temperature cycle. This theory was supported by observations made on the seasonal sites included in the analysis (e.g., Sites 48SA and 48SF located at a no-freeze zone in Texas). The sinusoidal function was expressed as:

$$E_1 = A + B \sin (2\pi f T + C) \qquad (2.29)$$

where,

E_1 = AC elastic modulus

A = average value

B = amplitude of the wave (if the dependent variable is constant then B = 0);

T = time of observation (e.g., month of the year 1 to 12)

f = frequency (number of increments per cycle = 1/12 in case of using month increments, and there is one cycle per year)

C = phase angle which controls the starting point on the curve and the peak month(s).

Equation 2.29 indicates that the values of E_1 have a minimum value of (A-B) and a maximum value of (A+B). Figure 2.9 shows a sinusoidal curve fitted to average monthly values of back-calculated AC layer elastic modulus in MPa, taken at seasonal site. The figure shows the values of constants A, B and f pertinent to the given site. The model was found to fit the data points very well (R^2 = 94%). Ali (1996) concluded that, in general, depending on site location (i.e. southern or northern hemisphere and latitude), AC material characteristics and meteorological variables, the values of A, B, C and f will change to reflect the average value of E_l, the magnitude of change, phase angle and cycle frequency respectively.

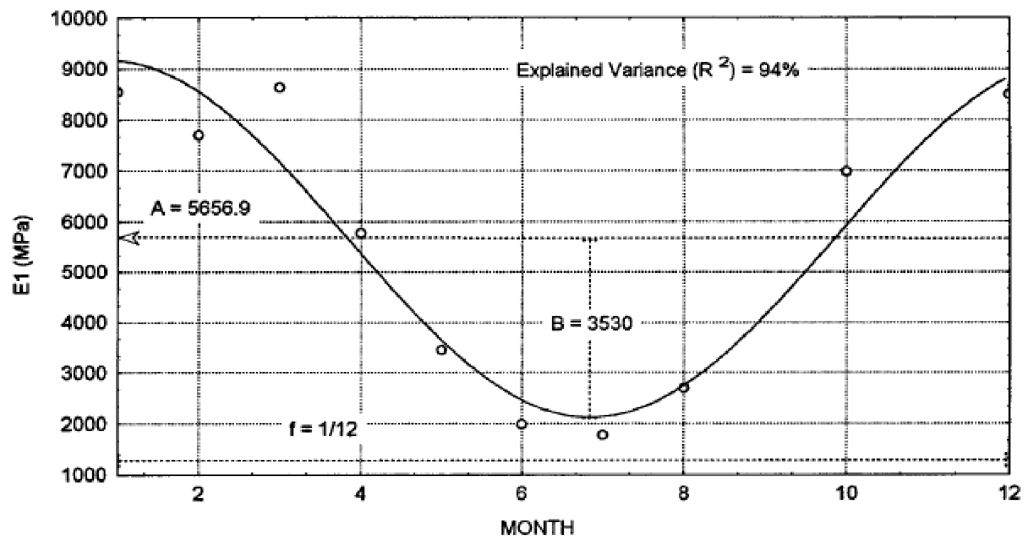

Figure 2.9 Sinusoidal Curve Fitted to Average Monthly Values of Backcalculated AC Layer Modulus (Ali, 1996).

Von Quintus and Simpson (2002) illustrated examples of the monthly variation of the computed elastic moduli for some selected LTPP test sections. As shown in Figure 2.10, the modulus of the asphalt concrete layer increases for the winter months and decreases for the summer months.

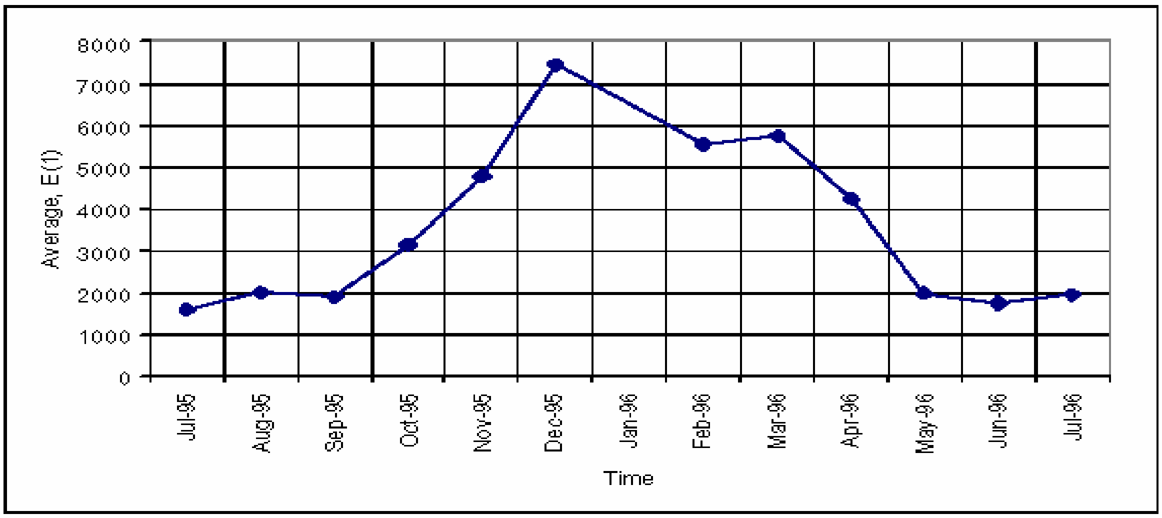

Figure 2.10 Monthly Variation of AC Layer Modulus for Site 04-1024 (Von Quintus and Simpson, 2002).

Zuo at al (2002) used hourly pavement temperature data from an instrumented pavement site in Tennessee, to examine the effects of temperature averaging on predicted pavement life. They assumed a typical full-depth asphalt pavement section supported by subgrade soils of different strength. They found, for their assumed section, that the pavement life could be overestimated by 50 to 75 percent if the temperatures are aggregated into monthly averages. The authors also showed that even hourly average temperatures could produce errors if the hourly distribution of truck traffic was not taken into account.

2.4.1 Relating Temperature Variation to AC Layer Modulus

Using initial LTPP lab data, Rada et al. (1991) developed the SHRP's equation to predict the modulus of asphalt concrete from its material characteristics and testing conditions (loading time and temperature). It could be estimated by:

$$\log_{10}[E_{ac}] = 0.553833 + 0.28829 * P_{200} * f^{-0.17033} - 0.03476 * V_a + 0.070377 * \eta_{70,10^6}$$

$$+ 0.000005 * \left[t_p^{(1.3+0.498251*\log(f))} * P_{ac}^{0.5}\right] - 0.00189 * \left[t_b^{(1.3+0.49825*\log(f))} * P_{ac}^{0.5} * f^{-1.1}\right]$$

$$+ 0.931757 * f^{-0.02774} \tag{2.30}$$

where,

E_{ac} = AC modulus, x 10^5

V_a = Percent air voids in mix

f = Test frequency

t_p = Mid depth AC layer temperature (F)

P_{200} = Percent Aggregate weight passing # 200 sieve

$\eta_{70,10^6}$ = Asphalt viscosity at 70 F

P_{ac} = Percent asphalt content by volume of mix

As it appears from the SHRP equation, the most sensitive variable is temperature. To avoid the use of this cumbersome equation, a graphical representation of this equation was prepared by Bayomy et al. (1993) for average conventional asphalt mixes. This presentation is a relationship between the modulus values against the temperature. To adjust for a modulus value determined at a certain temperature, the modulus value is plotted on the graph against the temperature (SHRP's equation). Then a parallel curve is drawn to the mix characteristic curve. The new parallel curve is the temperature-adjusting curve for the pavement layer. Figure 2.11 shows a schematic of the shifting procedure. From Figure 2.11 the slope of the SHRP's equation is equal to 0.12692. The intercept, F_{cept}, of the new curve can be determined by the following equation:

$$F_{cept} = (E_{test})^{0.35} + Slope * T_{test} \tag{2.31}$$

Then, the asphalt modulus at any season can be determined by using the following equation:

$$E_{season} = (F_{cept} - Slope * M_p)^{\frac{1}{0.35}} \tag{2.32}$$

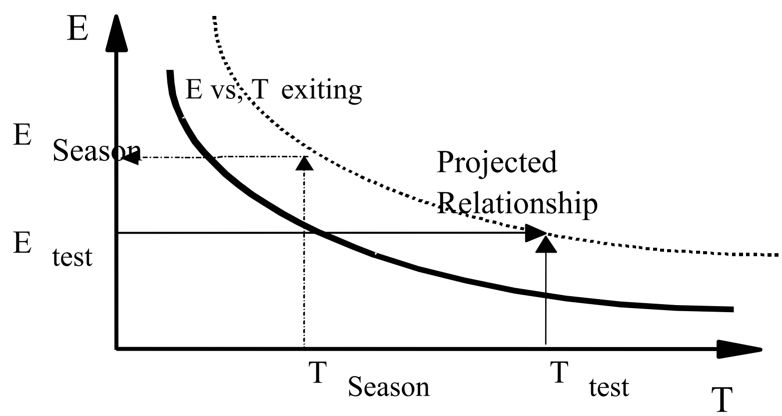

Figure 2.11 Schematic of the Modulus-Temperature Adjustment (Bayomy et al., 1993)

Based on data collected at LTPP site (48-1077) at located at Texas, Ali and Lopez (1996) found that the AC elastic modulus could be well correlated (R^2= 0.72) to the AC layer temperature with this model:

$$E = e^{9.372 - 0.0361 * T} \tag{2.33}$$

where,

E = The AC elastic modulus in MPa.

T = The pavement temperature in ^oC at depth 25 mm from the surface.

Figure 2.12 shows the application of the model on the collected data. The intercorrelations between temperatures at various depths were very high. This suggested that in constructing a model to predict the value of AC modulus, only one measure of temperature should be included in the model. There is no need to include more than one temperature measure since there exists a large degree of redundancy between temperature measures. The authors found that the coefficient of determination (R^2) reduced to 0.63 and 0.66 when using the pavement temperatures at depths 69 mm and 112 mm from the AC layer, respectively. They also found that when using the asphalt surface temperature the coefficient of determination was 0.63.

Similar regression models to relate the AC modulus to the mid-depth pavement temperature for four Tennessee sites were developed by Marshal et al. (2001). The coefficients of determination ranged from 0.87 to 0.98, suggesting excellent correlations at all four sites.

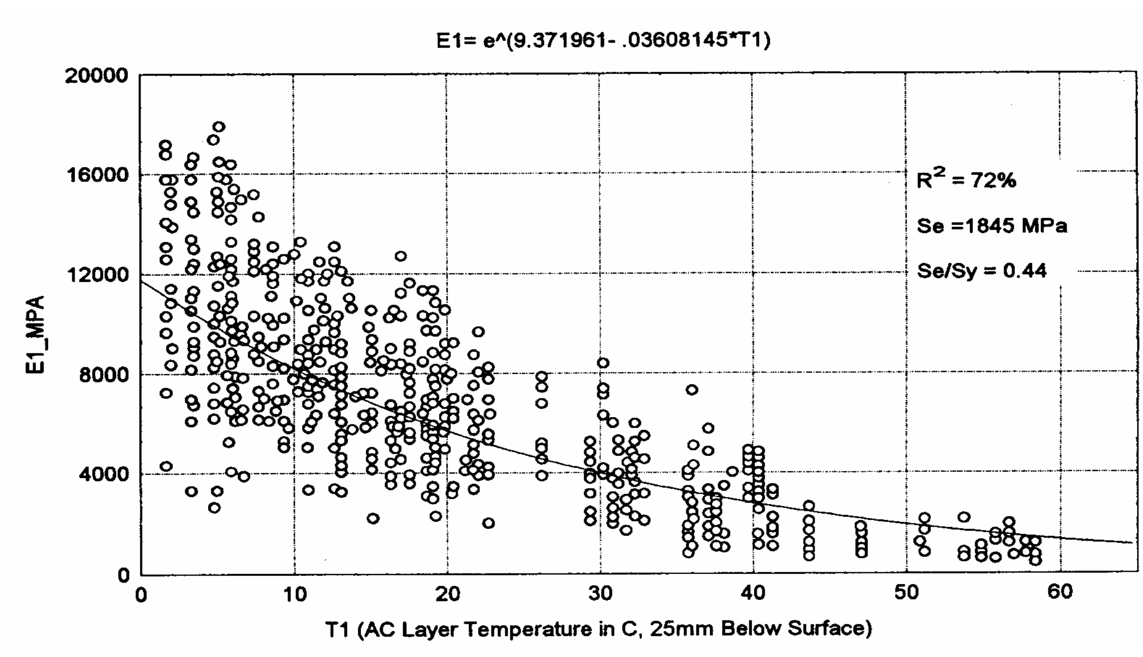

Figure 2.12 Exponential Model of the Asphalt Concrete Modulus and Temperature (Ali and Lopez, 1996)

Von Quintus and Simpson (2002), graphically illustrated examples of the computed elastic moduli for the asphalt concrete surface layer as a function of mid-depth temperature. The modulus of the asphalt concrete layer increased with decreasing temperatures. However, there were some cases where there were inconsistent changes in modulus with temperature. Some of these test sections were identified as having potential stripping in the HMA layer or were found to have extreme variations in the underlying support layers.

From the flexible pavement sites in the LTPP SMP, Drumm and Meier (2003) developed site-specific models of asphalt modulus as a function of internal temperature, surface temperature, and air temperature. The internal temperature produced the best correlation, but the surface temperature produced a model that was almost as good. The air temperature produced the worst correlation because it fails to capture the significant heating affects of solar radiation. The authors commented that, ideally, the solar radiation would be incorporated into the model as an additional variable, but solar radiation was not included in the SMP instrumentation plan.

Salem and Bayomy (2004) used multiple regression techniques to relate the variation in the AC layer modulus to the variation in pavement temperature for both freezing and nonfreezing zones. They developed two regression models, for both zones, to predict the AC modulus from the pavement temperature and the AC layer properties. The layer properties included in their model are the AC layer thickness, mix specific gravity, mix void ratio and asphalt binder grade. They also developed a model for determining the AC modulus seasonal adjustment factor. More details about this study will be discussed later in Chapter 6.

2.4.2 Pavement Temperature Prediction Models

Many regression models were developed to predict the AC layer temperature from the air temperature. Some of these models are old and cannot be applied to various site locations with accuracy. Others are quite accurate but they require many input data parameters that may not be available to the ordinary practitioner. This section reviews the most popular models developed to predict the AC pavement temperature.

2.4.2.1 Asphalt Institute Model

The Asphalt Institute (AI) model (1982) relates the mean pavement temperature, T_p to the mean monthly air temperature, T_a by the equation:

$$T_p = T_a\left(1 + \frac{1}{z+4}\right) - \frac{34}{z+4} + 6 \qquad (2.34)$$

where,

T_p = Mean pavement temperature at depth Z, ^{O}C

T_a = Mean monthly air temperature, ^{O}C

Z = Depth from surface, mm

2.4.2.2 BELLS Equations

A series of pavement temperature prediction models have been developed using data from the LTPP-SMP (Stubstad et al 1994, Stubstad et al 1998 & Lukanen et al 2000), named BELLS after the first letters of the authors' names. The primary model predicted the pavement temperature at various depths using the AC layer thickness, 5-day mean air temperatures, infrared surface temperature reading, and time of day. Because defective infrared surface temperature probes were used during data collection, the first BELLS equation is only valid for a temperature range of 15^{o}C – 25^{o}C. A second model, BELLS2, was developed using corrected infrared surface temperature data. To decrease the amount of data required to use the model, the 5-day mean air temperature was replaced by the average of the previous day's high and low air temperatures. As a consequence of the LTPP testing protocol under which the temperature data were obtained, the pavement surface was shaded for an average of 6 min prior to temperature sampling, so the BELLS2 model was based on biased surface temperatures. A third model, BELLS3, was therefore developed for use during routine Falling Weight Deflectometer (FWD) testing when the pavement surface is typically shaded for less than a minute. The BELLS3 equation, for use during routine testing is:

$$T_p = 0.95+ 0.892 * IR + \{\log (d)-1.25\} * [-0.448 * IR + 0.621*(1\text{-}day+ 1.83 *\sin (hr18-15.5)] + 0.042 * IR \sin (hr18-13.5) \qquad (2.35)$$

where,

T_p	= Pavement Temperature at depth d, ^{O}C
IR	= Infrared surface temperature, ^{O}C
Log	= Base 10 logarithm
d	= Depth at which temperature is to be predicted, mm (greater than zero)
1-day	= Average air temperature the day before testing
hr18	= Time of day on a 24-hr clock system, but calculated using an 18-hr AC temperature rise-and-fall time cycle

When using the sin (hr18 – 15.5), use the decimal form for the time. For example, if the time is 13:15, then in decimal form, 13.25-15.5 = -2.25; -2.25/18= -0.125; -0.125x2″= -0.785 radians; sin (-0.785) = -0.707 and the same is in sin (hr18 – 13.5).

The main disadvantage of this model is that it requires many input parameters that may be available only for researchers, not for practitioners.

2.4.2.3 The IPAT (Idaho Pavement Temperature) Model

Based on LTPP data and temperature data collected at the state of Idaho, Abo-Hashema and Bayomy (2002) used regression analysis to relate the asphalt pavement temperate to the air temperature. The regression analysis led to the following equation:

$$T_p = 1.5932 * T_a * Z^{-0.1261} + 0.2041 * T_m * Z^{0.0806} + 5.3109^{-0.0314} \qquad (2.36)$$

where,

T_p = Pavement temperature at depth Z, ^oC;

T_a = Air temperature, ^oC;

T_m = Thermal history, which is defined as the average air temperature calculated during the 24 hours preceding the time at which the pavement is tested, ^oC;

Z = Depth from surface, mm (must be greater than zero)

This equation represents the new Idaho Pavement Temperature (IPAT) model. The R^2 of the regression equation is 0.955 and the standard error of estimate (SEE) is 1.85 ^oC. Since the data used in this analysis were for mid-depth pavement temperature. Equation 2.36 is not valid for Z =0, which means that it cannot be used to predict the pavement surface temperature (i.e. at Z =0).

Abo-Hashema and Bayomy compared their model (IPAT model) to the BELLS3 model, and the Asphalt Institute (AI) model. The statistical analysis indicated that the correlation coefficients for the IPAT, the BELLS, and the AI models were 0.971, 0.985, and 0.96 respectively, with SEE 1.85^{o}C, 4.5^{o}C, and 2.2^{o}C respectively.

2.4.2.4 LTPP High & Low Pavement Temperature Models

The LTPP models are empirical models developed from LTPP seasonal monitoring by Mohseni & Symons (1998). These models relate pavement temperatures (low and high) to air temperature, latitude, and depth.

<u>High Pavement Temperature Model</u>

$$T_{pav} = 54.32 + 0.78\ T_{air} - 0.0025\ Lat^2 - 15.14\ \log_{10}(H+25) + z\ (9 + 0.61\ S_{air}^2)^{0.5} \quad (2.37)$$

where,

T_{pav} = High AC pavement temperature below surface, ^{o} C

T_{air} = High air temperature, ^{o} C

Lat = Latitude of the section, degrees

H = Depth to surface, mm

S_{air} = Standard deviation of the high 7day mean air temperature, ^{o} C

z = Standard normal distribution table, z = 2.055 for 98% reliability

The R^2 value of that model is 0.76 and SEE is 3.0 based on 309 data points.

<u>Low Pavement Temperature Model</u>

$$T_{pav} = -1.56 + 0.72\ T_{air} - 0.004\ Lat^2 + 6.26\ \log_{10}(H+25) - z\ (4.4 + 0.52\ S_{air}^2)^{0.5} \quad (2.38)$$

where,

T_{pav} = Low AC pavement temperature below surface, ^{o} C

T_{air} = Low air temperature, ^{o} C

Lat = Latitude of the section, degrees

H = Depth to surface, mm

S_{air} = Standard deviation of the mean low air temperature, ^{o} C

z = Standard normal dist. table, z = 2.055 for 98% reliability

The R^2 value of that model is 0.96 and SEE is 2.1 based on 411 data points.

2.5 INTEGRATED CLIMATIC MODEL

Recent studies have shown that important climatic factors such as temperature, rainfall, wind speed and solar radiation could be modeled for design purposes by using a combination of deterministic and stochastic analytical methods. These techniques provided the input into climatic-materials-structural-infiltration-drainage-frost penetration-frost heave and thaw weakening models that resulted in meaningful simulations of the behavior of pavement materials and of subgrade conditions or characteristics over several years of operation. The integrated model developed under contract to Federal Highway Administration, by Lytton et al. (1989); upgraded by Larson and Dempsey (1997), has been designed to perform these tasks. The model, shown in Figure 2.13, is composed of four major components. They are the Precipitation (PRECIP) Model, the Infiltration and Drainage (ID) Model, the Climatic-Material-Structural Model (CMS) Model and the CRREL (The U.S. Army Cold Regions Research and Engineering Laboratory) Model for Frost Heave-Thaw Settlement.

2.5.1 Precipitation Model

The Precipitation Model, developed by Liang and Lytton (1989), is a mathematical model that uses a deterministic algorithm that is applicable wherever rainfall amounts and patterns are required for pavement engineering design. The procedure uses average climatic data and mathematical concepts to simulate rainfall patterns that are considered acceptable for design purposes. Using simulated rainfall data ensures that rainfall during the design period will be equal to or greater than the long-term climatic average. Actual precipitation data can cause an unconservative prediction of drainage behavior. This occurs when the amount of precipitation in the design period is considerably below the long-term average. Use of actual precipitation data, though, is recommended when modeling extreme rainfall events. Also, actual precipitation data should be used when comparing modeled data to actual pavement performance data over a given time period.

This module of the ICM provides the amount of rain and the day on which rainfall occurs, which is in turn a required input to the Infiltration and Drainage Model. These data were used along with the drainage analysis to compute the probabilities of wet and dry days, wet and dry base courses and the probability of developing base course moduli associated with different degrees of saturation.

Output data from the Precipitation Model is computed for each month of the design period. It consists of the amount of rainfall, the day on which it occurs, the number of thunderstorms and some statistical analysis.

2.5.2 Infiltration and Drainage Model

The Infiltration and Drainage Model (ID), developed by Liu and Lytton (1985), performs several tasks in evaluating the effect of precipitation on a pavement profile. These tasks include drainage analysis, infiltration analysis and pavement design evaluation. The ID model uses a numerical technique to compute the degree of drainage versus time of an initially saturated granular base course with lateral drainage overlying a permeable or impermeable subgrade. This analysis assumes that the base course is a free draining material. The pavement evaluation module of the ID model uses an empirical procedure to evaluate the relative adequacy of the base course design in terms of the amount of time that is required to reach a critical degree of saturation. The more rapidly the base course can drain, the more effective it will be as a load carrying member of the pavement structure under wet conditions.

The infiltration module of the ID Model includes the previously described analysis along with the probabilistic analysis of rainfall amounts and patterns derived from the Precipitation Model or from actual rainfall amounts. The ID model then conducts a rainfall analysis to calculate the probability of wet and dry days. The ID model uses this analysis to model the infiltration of water through cracks in the pavement and calculates the probability of having a wet or dry pavement profile.

The output of ID model includes the degree of saturation of the base course, the degree of drainage over consecutive dry days and the probability of a dry/wet base course.

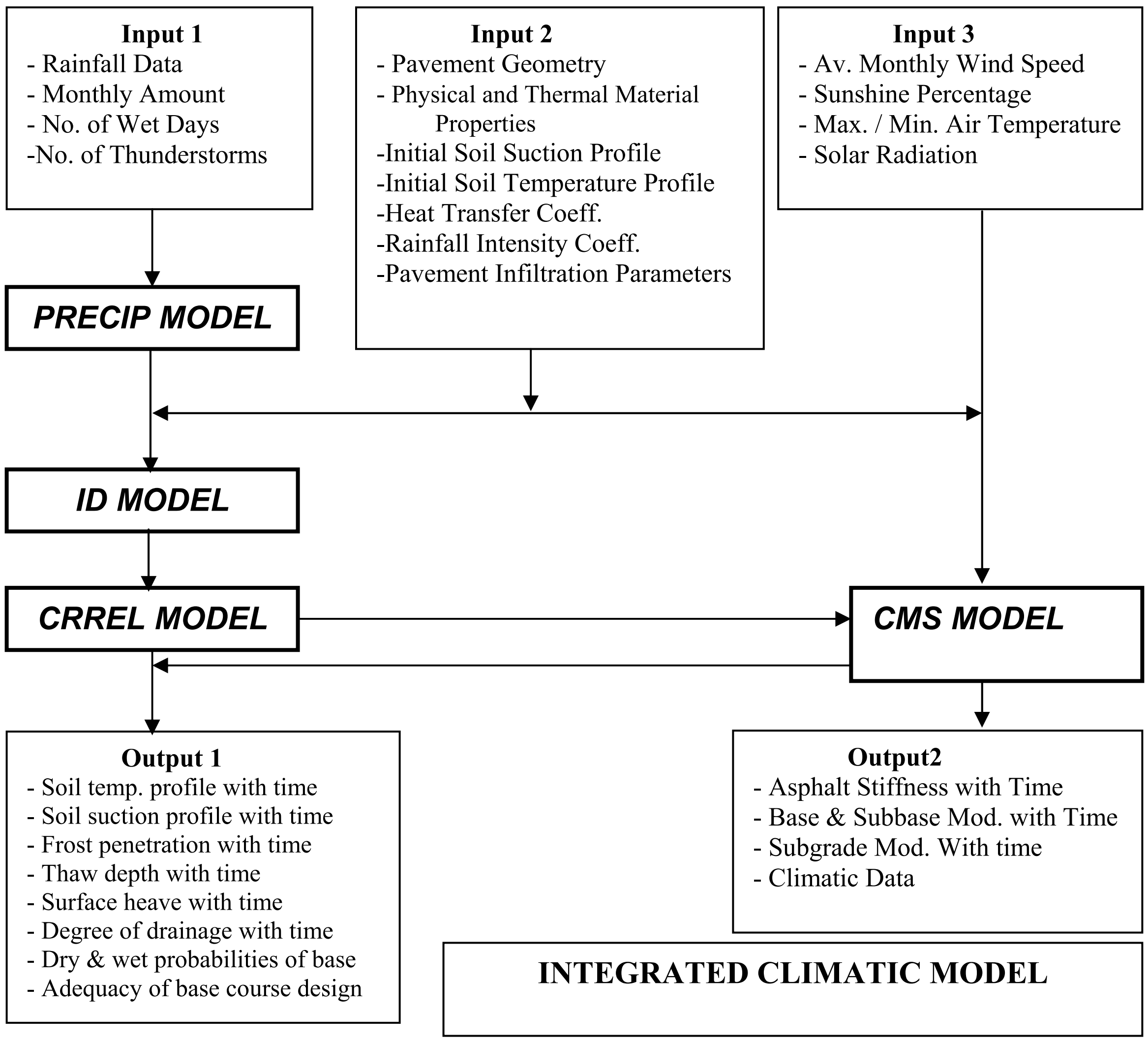

Figure 2.13 Integrated Climatic Model (Lytton et al., 1990)

2.5.3 Climatic-Materials-Structures Model

Temperatures throughout the pavement structure are dominated by atmospheric conditions at the surface. While it is easy to monitor air temperatures, there is not a direct correspondence between air temperatures and surface temperatures. The Climatic-Materials-Structures Model (CMS), developed by Dempsey et al. (1985), generates the heat flux at the surface, which then establishes the temperature profile through the pavement layers.

The CMS model was used to determine the temperature distribution in the pavement layers. The value for the temperature at the bottom of the pavement layer is given to the Frost Heave and Thaw Settlement Model for the soil temperature predictions. The model considers radiation, convection, conduction, and the effects of latent heat. It does not consider transpiration, condensation, evaporation, or sublimation. These latter effects were ignored because of the uncertainty in their calculations and because their omission does not create significant errors in the heat balance at the surface of the pavement. Heat fluxes caused by precipitation and moisture infiltration were also neglected.

2.5.4 Frost Heave and Thaw Settlement Model

The United States Army Cold Regions Research and Engineering Laboratory (CRREL) Frost Heave and Thaw Settlement Model, developed by Guyman et al (1986), is a mathematical model of coupled heat and moisture flow in soils. The phase change of water to ice is computed using the CRREL model and therefore is capable of providing a measure of frost heave. The CRREL Model uses the temperature profile through the pavement layers as established by the CMS Model to compute changes in the soil temperature profile, and thus frost penetration and thaw settlement. The soil suction profile as it varies with time is also determined. The freezing zone may range in thickness from a few millimeters to many meters, and wherever it occurs it controls the movement of moisture due to ice segregating and partially blocking the pores in the soil against moisture movement. The nature of this blockage is handled by reducing the unsaturated hydraulic conductivity (permeability).

2.5.5 Enhanced Integrated Climatic Model (EICM) for 2002 Guide

For the development of AASHTO2002, some modifications by Witczak et al (2000) were made to EICM. Such modifications include: the incorporation of an algorithm capable of predicting the soil-water characteristic curve (SWCC) based on soil index properties, the addition of an algorithm for the prediction of unsaturated hydraulic conductivity based on SWCC; and the development of sets of default soil parameters based on AASHTO soil classification system.

2.5.5.1 Main Modifications Made on EICM Versions

ICM Version 2.0, and prior versions required that the user specify the Gardner's pore pressure coefficients for each unbound pavement layer, along with the lower boundary suction, and an initial pore pressure profile. The program documentation provides recommended default values (as a function of material type) for the Gardner's coefficients, and recommends that the lower boundary suction and initial pore pressure profile be estimated from the depth of the water table. With Version 2.1, entry of the Gardner's coefficients was made optional. Also, the initial moisture content profile, and the depth to the water table replaced the initial pore pressure and lower boundary suction inputs. Results obtained using version 2.1 without entry of the Gardner's coefficients were significantly better than those obtained using assumed values for the Gardner's coefficients with version 2.0. For this reason, user-supplied Gardner coefficients were not used with version 2.1 (Witczak et al., 2000).

The EICM Version 2.1 makes use of the equation proposed by Gardner (1958). This equation has three fitting parameters: θ_r, a, and b (See Equation 2.12). Also, in the EICM version 2.1 and prior versions only two of the three Gardner equation parameters were treated as variables, with the third, the residual volumetric water content (θ_r) taken to be zero. An equation with two parameters has shown, in many cases, to misrepresent the SWCC due to excessive constraints to the relationship (Witczak et al., 2000). With version 2.6, the Fredland and Xing equation (1994) was applied with its coefficient correlated to well-known soil properties such as D60 and wPI as previously mentioned by Zapata et al. (1999). The

Gardner parameters are still available for those who prefer to work with them or have old input files.

2.5.5.2 Definitions and Important Relations Used with EICM 2.6

<u>Initial Volumetric Water Content</u>: The initial water content (θ_o) is the water content at the start of the program or that at the first day of the analysis. If a value is specified, the entire layer will be set to that water content.

<u>Equilibrium Volumetric Water Content:</u> The equilibrium volumetric water content (θ_{eq}) is strongly tied to the SWCC of the soil. It is therefore recommended that the user perform measurements of water content for each layer in the pavement profile. Care should be taken to enter the equilibrium volumetric water content, θ_{eq}, rather than the equilibrium gravimetric water content, ω_{eq}. If ω_{eq} is available, the volumetric water content can be calculated using the following equation:

$$\theta_{eq} = \omega_{eq} (\rho_{dry} / \rho_{water}) \tag{2.39}$$

where,

θ_{eq} = Equilibrium volumetric water content

ω_{eq} = Equilibrium gravimetric water content

ρ_{dry} = Dry density

ρ_{water} = Density of water (1 gm/cm^3)

<u>The saturated volumetric water content</u>: It is also called porosity (θ_{sat}), and can be determined by:

$$\theta_{sat} = 0.0143 (wPI)^{0.75} + 0.36 \tag{2.40}$$

wPI = Passing # 200 x PI

where,

Passing # 200 = Material passing #200 U.S. standard sieve expressed as a decimal

PI = Plasticity index (%)

The saturated hydraulic conductivity: The saturated hydraulic conductivity (K_{sat}) can be calculated by:

$$K_{sat} = 76639\,(\theta_{\mathbf{sat}} - \theta_{33kPa})^{12.9} + 10^{-12} \qquad (2.41)$$

where,

K_{sat} = Saturated hydraulic conductivity (m/s)

$\theta_{\mathbf{sat}}$ = Saturated volumetric water content = porosity

θ_{33kPa} = Water content at 33 kPa of suction, from the SWCC

Equation 2.41 is now intrinsic to the EICM, version 2.6. When the user does not specify a value for k_{sat}, the EICM calculates it, provided the wPI, D60, or AASHTO classification is input. This information is also needed by the EICM to calculate the SWCC and the θ_{33kPa}.

The soil specific gravity (G_s). This important property is needed, together with the dry density, to determine the $\theta_{\mathbf{sat}}$ for the soil. The following equation can be used to estimate G_s, when wPI is known.

$$G_s = 0.041(\mathrm{wPl})^{0.29} + 2.65 \qquad (2.42)$$

If the dry density is known but G_s and θ_{sat} are unknown, then the best estimate of $\theta_{\mathbf{sat}}$ is obtained by first using Equation 2.42 to calculate G_s. Then the dry density and G_s are used together to calculate porosity = θ_{sat}. This procedure for getting θ_{sat} is superior to the use of Equation 2.40. Thus, Equation 2.40 should be used only when the dry density is not available.

Default Values for the Basic Soil Properties Used with EICM 2.6:

Witczak et al. (2000) proposed the following soil properties default values, shown in Tables 2.11 and 2.12, to be used with EICM Version 2.6 for the adaptation of AASHTO2002:

Table 2.3 Soil Properties Default Values vs. AASHTO Soil Classification System (Witczak et al., 2000)

AASHTO Classification	wPI	D_{60} (mm) (Range)	G_s (Range)	θ_{sat} (Range)	ρ_{dry} (gm/cm3) (Range)
A-1-a	0	3 (D60 > 2)	2.65	0.36	1.70
A-1-b	0	1 (0.45-2)	2.65	0.36	1.70
A-2-4	1.2 (0.2-3.5)		2.69 (2.68 - 2.71)	0.38 (0.36 - 0.40)	1.68 (1.61 -1.72)
A-2-5	2 (0.2-3.5)		2.70 (2.68 - 2.71)	0.38 (0.36 - 0.40)	1.66 (1.61 -1.72)
A-2-6	2.6 (0.55 - 5.25)		2.70 (2.68 -2.72)	0.39 (0.37 - 0.41)	1.65 (1.58 -1.71)
A-2-7	6 (0.75 -15.75)		2.72 (2.69 - 2.74)	0.41 (0.37 - 0.47)	1.59 (1.42 -1.72)
A-3	0	0.18 (0.074 - 0.45)	2.65	0.36	1.70
A-4	4.1 (1.44-10)		2.71 (2.70 - 2.73)	0.40 (0.38 - 0.44)	1.62 (1.51 -1.70)
A-5	6.8 (1.44-10)		2.72 (2.70 - 2.73)	0.42 (0.38 - 0.44)	1.58 (1.51 -1.70)
A-6	8.84 (3.96-15)		2.73 (2.71 - 2.74)	0.43 (0.40 - 0.47)	1.55 (1.44 - 1.64)
A-7-5	25.8 (10.8-45)		2.76 (2.73 - 2.77)	0.52 (0.45 - 0.61)	1.31 (1.07 - 1.54)
A-7-6	15 (5.4-29)		2.74 (2.72 - 2.76)	0.47 (0.41 - 0.54)	1.46 (1.25 -1.63)

Table 2.4 Best Estimated D60 for Base Course Materials (Witczak et al., 2000)

Base Course Material Grading AASHTO M 147 –65 (1990)	Best Estimate D_{60} (mm) (Range)
Grading A	11.5 (5-17.5)
Grading B	11.5 (5-17.5)
Grading C	7 (3.5-11)
Grading D	4 (1.1-7.5)
Grading E	3 (0.5-5)
Grading F	1.4 (0.3-2.5)
Base Course materials with some plasticity, used wP1 = 0.5	

2.5.5.3 Evaluation of EICM Moisture Prediction Capabilities

Richter and Witczak (2001) have discussed the application of data collected at 10 LTPP SMP sites to evaluate the volumetric moisture prediction capabilities of the ICM. The moisture prediction capabilities of the Integrated Climatic Model (ICM) were evaluated by applying the model to predict the subsurface moisture contents for the test sections, and then comparing the results to the data collected at those sites. Several versions of the ICM model were considered in this work. Six of the sites were modeled with Version 2.1 of the ICM. Poor agreement between the model output and the monitored moisture data was observed because several of the key material parameters required by the model are not among the data collected for the test sections used in the evaluation. Based on their findings, Richter and Witczak (2001) concluded that Version 2.6 of the ICM could sometimes provide reasonable estimates of the variation in the in-situ moisture content of unbound pavement materials. The findings for one of the sites suggested that the model might not work well for sites in arid climates; however, they recommended more extensive evaluation to draw definitive conclusions in this regard.

2.6 SUMMARY

The information presented in this chapter could be summarized into the following points:

Based on laboratory testing Carmichael and Stuart (1985) and Hudson et al. (1994) developed regression models to predict the soil resilient modulus from soil properties like plasticity index, water content, percent passing the No. 200 sieve, and the acting stresses. The models of Carmichael and Stuart (1985) showed that only one percent increase in the soil moisture content causes a reduction in its modulus by 0.62 ksi (4.3 MPa) for fine-grained soils, while the corresponding reduction in coarse-grained soils is only 0.0025 ksi (0.017 MPa), which is very minimal, compared to fine grained soils.

Fine-grained soils were found to exhibit more modulus reduction with the increase of water content than the coarse grained soils. All subgrade soils containing water reportedly exhibit modulus increases to at least 100 ksi (68.95 MPa) when cooled to temperatures below freezing. The softening effect of the thaw appears to increase with the amount of water in soil and with the amount and plasticity of fines.

Thaw-induced modulus reductions were greatest for fine-grained soils and increase with plasticity based on a study by conducted by Chamberlain et al. (1979). For practical purposes, Hardcastle (1992) suggested that the resilient moduli of frozen soils might be considered to be independent of soil type

The most reliable method for determining subgrade water content variations is direct measurements made over an extended time period. Cumberledge et al. (1974) showed that the more permeable sand soils exhibit the greatest seasonal increase in moisture (three to four percent) as for silty soils. The clay soil exhibited averaged seasonal fluctuations of only one percent. The duration of the moisture increase period was shorter for more permeable sand soils than for silts.

In a study on subgrade soils beneath both rigid and AC pavement, Halliburton (1970) concluded that although both subgrades continue to exhibit seasonal fluctuations in water content, both also trend toward an "equilibrium" value equal to 1.1 to 1.3 times soil's plastic limit. The large seasonal variations of the less impervious pavement were attributed to infiltration whereas the water content changes in the more impervious pavement were attributed to capillarity and seasonal changes in groundwater table elevations.

The soil moisture content could be estimated from a soil water characteristic curve (SWCC) if the soil suction is known. However, based on a research made by Zapata et al. (1999) the authors of EICM version 2.6 (Witczak et al., 2000) concluded that soil suction and SWCCs simply couldn’t be measured with great precision at the present time. They also added that it is difficult to develop a predictive model for SWCCs that is consistent with all of the SWCCs reported in the literature because of the fairly high probability that any given measured SWCC has significant experimental error associated with it. Therefore, they concluded that the SWCC could probably be estimated from the basic soil properties like D60 or wPI about as accurately as it can be measured, unless the laboratory or person making the measurement is highly experienced.

Ali and Parker (1996) found out that the backcalculated resilient moduli of both subgrade and AC surface could be correlated to the month of the year in a sinusoidal function with reasonable accuracy.

Ali and Lopez (1996) modeled the AC layer modulus to AC temperature at depths 25, 69 and 112 mm from surface for one LTPP site (48-1077). They found that the intercorrelations between temperatures at various depths were very high. This suggested that when constructing a model to predict the value of AC modulus, only one measure of temperature should be included in the model. The authors found that the AC modulus could be related to the pavement temperature at 25mm depth with coefficient of determination (R^2) of 0.72 They found also that R^2 value reduced to 0.63 and 0.66 when using the pavement temperatures at depths 69 mm and 112 mm from the AC layer, respectively. Finally, when using the asphalt surface temperature the coefficient of determination was 0.63.

Von Quintus and Simpson (2002) showed that the modulus of the asphalt concrete layer increases with decreasing temperatures. However, there were some cases where there were inconsistent changes in modulus with temperature. Some of these test sections were identified as having potential stripping in the HMA layer or were found to have extreme variations in the underlying support layers.

Many statistical models were developed to predict the AC layer temperature from the air temperature. Some of these models are old and cannot be applied to sites with different climatic conditions with accuracy, like the asphalt institute (AI) model (1982). Other models are quite accurate but they require many input parameters that may not be available to the ordinary practitioner, such as BELLS models [(Stubstad et al 1994, Stubstad et al 1998 & Lukanen et al 2000)]. A more recent model, called IPAT, was developed by Abo-Hashema and Bayomy (2002). The authors compared their model (IPAT) to BELLS3 and AI models. The statistical analysis indicated that the correlation coefficients for IPAT, BELLS, and AI models are 0.971, 0.985, and 0.96 respectively. Models for predicting the high and low air temperatures were predicted and incorporated in the LTPPBIND, a SUPERPAVE binder selection program Mohseni and Symons (1998).

Several modifications were made through the different versions of the integrated climatic model. The modifications made to water content prediction included in the more recent Enhanced Integrated Climatic Model EICM 2.6 (2000) are:

- Representation of the Soil-Water Characteristic Curve (SWCC) by the Fredlund and Xing equation. The Gardner equation remains available to the EICM user.
- The parameters of the Fredlund and Xing equation (Fredlund and Xing, 1994) were correlated with basic soil index properties: D60 and wPI = Percentage Passing #200 times Plasticity Index (PI).
- Default values for the basic soil index properties needed to determine the SWCC were estimated as a function of the AASHTO soil classification system.
- Default values for the basic soil index properties needed to determine the SWCC were estimated for base course materials designed under AASHTO Designation M 147-65 (1990).
- Algorithms to estimate porosity (saturated volumetric water content), specific gravity and saturated hydraulic conductivity based on wPl were developed.
- Incorporation into the EICM of unsaturated hydraulic conductivity prediction based on the SWCC proposed by Fredlund, et al. (1994).

The volumetric moisture prediction capabilities of the EICM were evaluated in a study by Richter and Witczak (2001). They found poor agreement between the model output and the monitored moisture data observed. Richter and Witczak concluded that Version 2.6 of the ICM could sometimes provide reasonable estimates of the variation in the in-situ moisture content of unbound pavement materials. However, they added that the model might not work well for sites in arid climates and they recommended more extensive evaluation to draw definitive conclusions in this regard.

3. EXPERIMENT DESIGN AND DATA COLLECTION PROTOCOLS

This chapter presents the experiment design, including installation and data collection activities. The chapter describes the locations, instrumentation, and installation at the Idaho sites as well as the characterization tests performed on the subgrade soils and the average climatic data for the different. In addition to data from the Idaho sites, data used from the LTPP database were also identified. The LTPP data were used to complement the data collected at the Idaho sites so that appropriate models could be developed.

3.1 IDAHO SITES

3.1.1 Sites Selection

Five sites were identified for this study including four in north Idaho and one in the southern region. Table 3.1 lists details of all site identifications and Figure 3.1 shows all site locations.

The original plan was to install, if possible, sites where two adjacent pavement sections, one with rockcap and the other with ¾" aggregate base, were available. This was to allow for the comparison of the effectiveness of the rockcap base on the moisture regime under the pavement. It was possible to install two adjacent sites at the Moscow and Weiser locations (sites #2 and #5 in Figure 3.1) only because new construction was available. Site #4 near the Pack River in northern Idaho did not have adjacent sections. However, the installation south of the Pack River (Site #4A) is in a pavement section with a natural gravel aggregate base referred to as "river cap." A river cap base material is river gravel with large aggregate size, 2- 3 in, with high fine content. The rockcap, on the other hand, is crushed material without fine content.

Site #1 (SH-128, Lewiston)

This site is located on the SH-128, known as Down River Road, in Lewiston, Idaho at approximately milepost (MP) 0.3. It is installed in a new diversion, where the pavement is constructed on a granular fill. Only rockcap base exists in this location, and therefore one installation only was made at this site.

Site #2 (SH-8, Moscow)

This site is located on SH-8 (Pullman Moscow Road) at MP 1.06. The pavement section is a new construction on Loess subgrade soil with at least 12" rockcap base. A 100 ft section was constructed with ¾" aggregate base to replace the rockcap. Site #2A was installed in the rockcap section, and Site #2B was in the ¾" aggregate base section. Cable conduits were installed during construction, and no trenches were cut in the pavement. A schematic diagram showing the two installations is presented in Figure 3.2.

Site #3 (US-95, Worley)

This site is located on US-95, MP 400 near Worley. It is installed in an existing new constructed pavement. The entire pavement section was constructed on rock cap base and there was no aggregate base section available. One installation only was made at this site.

Site #4 (US-95, Pack River)

Two installations were made at this location. The first one (Site 4A) was installed south of Pack River at milepost 485.25 on US-95, southbound lane. It is in an existing pavement with gravel aggregate base, known as river cap. There was no rock cap base available in the location. Thus, it substitutes the rock cap section needed in this location. The second installation (Site #4B) was installed about one mile north of # 4A, north of Pack River at MP 486.5 on US-95, southbound lane. The subgrade soil description in this area is lacustrine silt.

Site #5 (US-95, Weiser)

This site is located on US-95 in down town Weiser at the intersection with Park Street. Similar to Site #2, two adjacent installations were made. The pavement section is a new construction with 6" rock cap base. A 100 ft section was constructed with ¾" aggregate base to replace the rock cap. Site #5A was installed in the rock cap section, and Site #5B was in the ¾"aggregate base section. Cable conduits were installed during construction, and no trenches were cut in the pavement.

Table 3.1 Idaho Site Locations and Description

Site	Site #	Location	Description
SH-128, Lewiston	1	Down River road, Lewiston. MP 0.3 in the eastbound lane. Located at 0.3 miles from the Washington state borderline, midway from intersection of SH-12 and Red Wolf crossing bridge.	New pavement on rockcap base
SH-8, Moscow	2A	SH-8 in Moscow, Mile Post 1.05 mile in the westbound lane. Across from TriState store	New pavement on rockcap base
	2B	SH-8 in Moscow, Mile Post 1.07 in the westbound lane. Across from TriState store	New pavement on aggregate base. 100 ft section only.
US-95 at Worley	3	US 95 at Worley, MP 400, southbound Lane	Existing pavement on rockcap base
US-95 at Pack River	4A	US 95 at Colburn, south of Pack River at MP 485.25, southbound lane.	Existing pavement on rivercap base
	4B	US 95 at Colburn, north of Pack River at MP 486.5, southbound lane.	Existing pavement on aggregate base
US-95 at Weiser	5A	US-95 at the intersection of US95 and Park street in down town Weiser. Site 5A is north to 5B in the northbound lane.	New pavement on rockcap base
	5B	US-95 at the Intersection of US95 and Park street in down town Weiser. Site 5B is south to 5A in the northbound lane.	New pavement on ¾" aggregate base

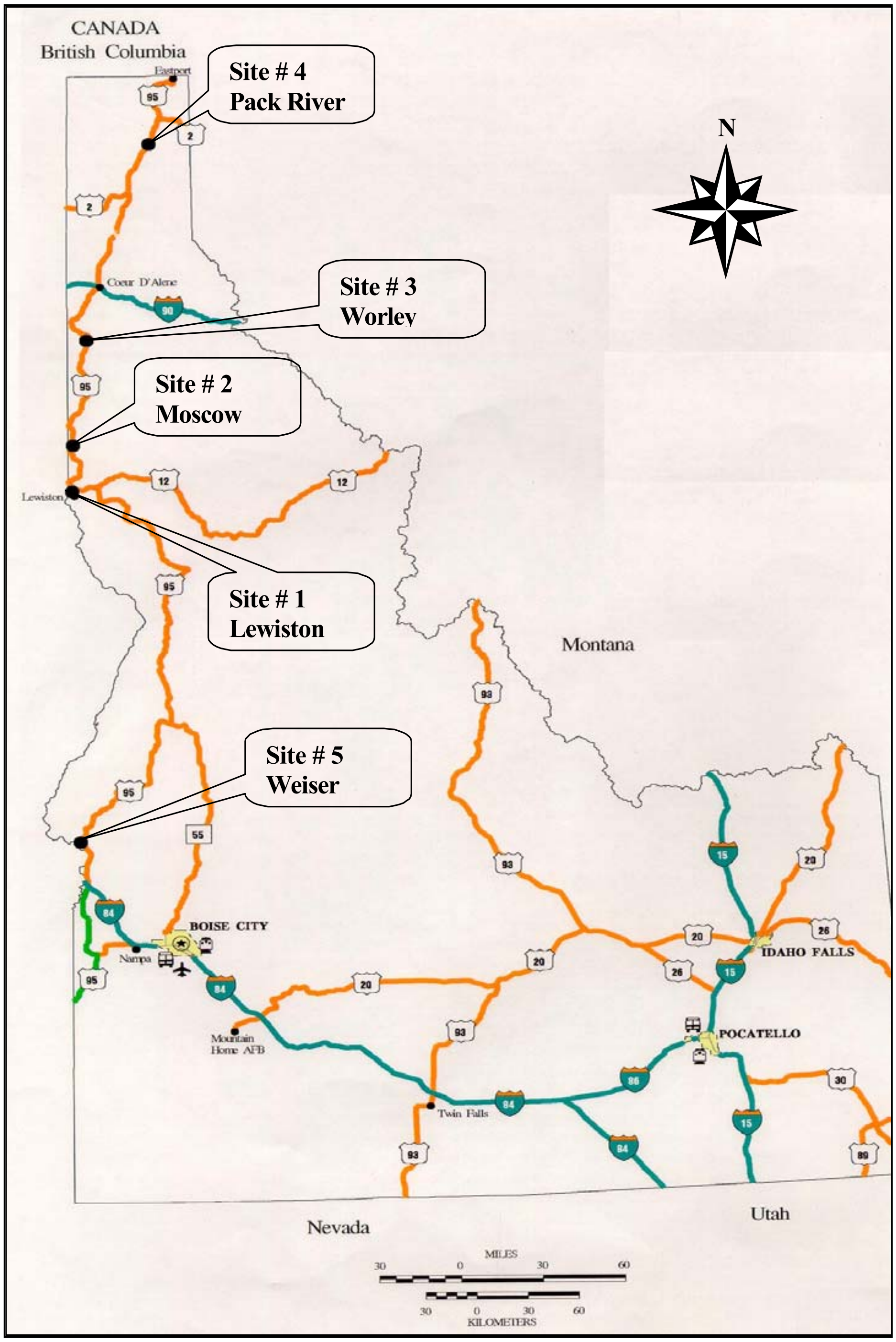

Figure 3.1 Idaho Site Locations (Bayomy and Hardcastle, 2002)

3.1.2 Site Instrumentation

Instrumentation at each site was the same, in that each site instrumentation hole contained three types of probes; a moisture probe (TDR), a temperature sensor (MRC type), and a resistivity sensor, manufactured by ABF Manufacturing, Inc.

Figure 3.2 shows a schematic of the typical probe installation at all sites. The anchored dimensions shown in Figure 3.2 are probe anchors to the pavement surface. All these dimensions are provided in the Installation Info tables in Appendix A for all sites, and summarized in Table 3.2.

All sites have identical instrumentation except for the TDR probes in sites #1 and 2 where they were types K and F. Type K is in the top and F is in the bottom. The main difference between the two types is mainly the length. Type F is longer than type K by about 6 inches. Also, type K integrates the moisture content at 4 different depths 6 inches apart, while type K integrates the moisture content at 5 different depths 6 inches apart. Sites 3, 4 and 5 have one TDR type (F) for the top and bottom. Descriptions of all of the probes can be found in the MP917 manual, provided in Appendix B.

<u>Installation Process</u>

An eight-inch diameter vertical hole was opened in the center of the wheel path by a coring machine and an auger to depth of about 6 ft deep into the subgrade. Materials removed were kept in order and so that it can be placed back in the hole as close to the original condition as possible. Once the hole was prepared, probes were inserted around the hole circumference. Soil samples were taken at various depths to determine the existing moisture content at each depth and to perform the characterization tests for the in-situ soil.

Two TDR probes were installed on top of each other to cover the entire hole depth, with the first segment in the base layer. The MRC temperature and the ABF resistivity sensors were also installed so that the top of the sensor was in the base layer. All dimensions of the installation sites are shown in the SiteInfo tables in Appendix A.

During the installation, soil samples were collected at approximately every foot and the moisture content was determined. Results of the gravimetric moisture content are presented in Appendix A as part of the site installation information. To check equipment operation, preliminary data collection was made upon completion the installation at each site.

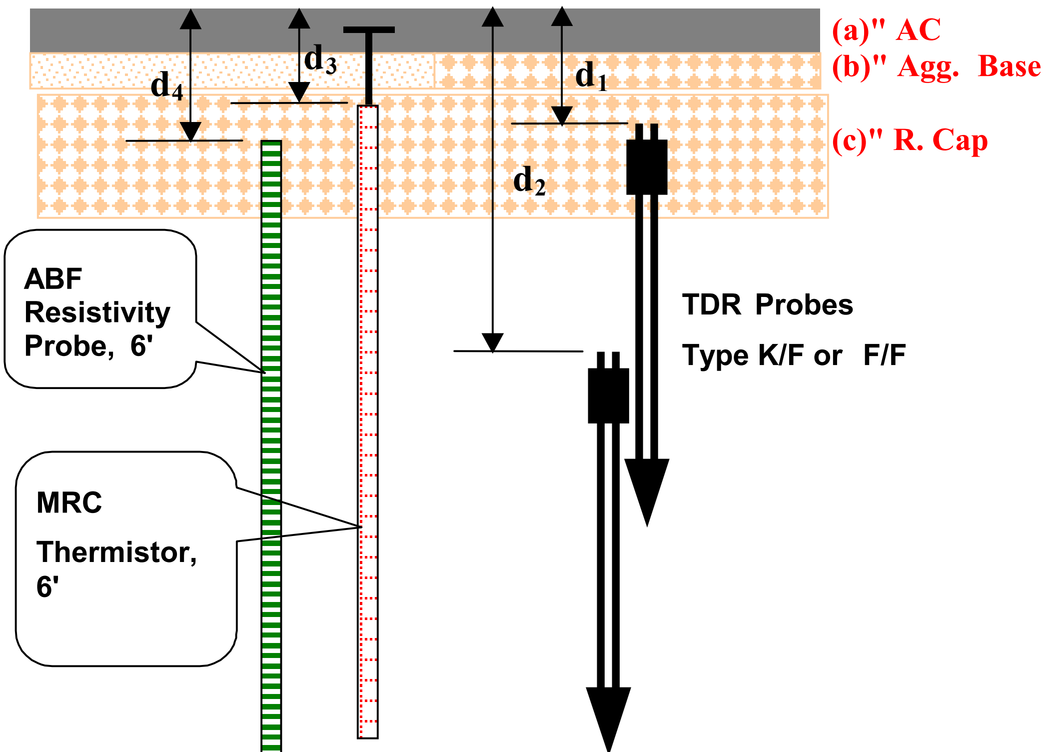

Figure 3.2 Schematic for Probe Installation at All Sites

Table 3.2 Probe Anchors to the Pavement Surface (Inches), for the Different Sites

Site / Layer	Lewiston	Moscow		Worley	Pack River		Weiser	
Site #	1	2A	2B	3	4A (S)	4B (N)	5A	5B
d_1 (in)	16	16	16	12	12	13	7	7
d_2 (in)	47	40	40	46	45	49	42	36
d_3 (in)	23	19	19	21	20	21	12	11
d_4 (in)	23	22	22	23	20	23	12	11

3.1.3 Data Collection Procedures

Four types of data were collected regularly at each site: the volumetric moisture content by the TDR probes, the resistivity data by the ABF probes and the temperature data by the MRC sensors. Also, the ground water table was determined by the atmospheric piezometers. Additional data planned to be collected at the sites included structural capacity data by the FWD testing and the climatic data, which was to be imported from a nearby weather station.

3.1.3.1 Moisture Data

Moisture data included both gravimetric moisture content and volumetric moisture content. Determination of the gravimetric moisture content was only possible at the time of installation. Soil samples were collected and the moisture content was determined by the standard methods. Results of the gravimetric moisture content are presented in the tables in Appendix A.

The volumetric moisture data was collected by the moisture point instrument (MP-917). A detailed description of the instrument and its basic operation are provided in the instrument manual, MP-917 (2004). The Moisture Point technology is based on the Time Domain Reflectometry (TDR). The device measures the volumetric moisture content of the soil system. Moisture data collection at each site followed simple standard procedures. A detailed description of these procedures is presented in the instrumentation manual of the MP-917.

It is worth mentioning that the gravimetric moisture content (W) can be calculated from the volumetric moisture content (θ) using Equation 2.10, Chapter 2.

$$W = \theta \times \frac{\gamma_w}{\gamma_d} \qquad (3.1)$$

3.1.3.2 Ground Water Level

Vertical piezometers were installed at each site near the installation holes. The piezometers were installed in the shoulders, to avoid traffic and pedestrian obstruction. Ground water level was determined by marking a metal measure tape with a water-soluble marker, then inserting the tape to the end of the piezometer. The water level was then indicated by the part of the tape mark that was washed out by the water.

3.1.3.3 Temperature Data

Pavement temperatures were collected from the temperature sensors (MRC type), which were installed at different depths from the pavement surface. The air temperature was also recorded at the same time.

3.1.3.4 Soil Characterization Tests

A set of lab tests was performed on the soil samples taken from each site in order to classify these soils. The tests included the determination of the in-situ moisture content at various depths, sieve analysis and Atterberg limits. The results of the lab tests and soil classifications are included in Table 3.3.

The thickness of the pavement layers was also measured during site instrumentation, and the results for the different sites are also included in Table 3.3.

3.1.3.5 Climatic Data

As stated previously, one of the limitations to this study was the unavailability of weather stations at each site. However, an effort was made to collect the climatic data from the nearby weather stations, as was done in the LTPP-SMP program. The average 30 years climatic data between 1961 and 1990 for the rainfall and temperature were downloaded from the climate database (2002). Table 3.4 shows the locations of the weather stations located near the Idaho sites and the average monthly rainfall and air temperature for each station.

3.1.3.6 FWD Data

To evaluate the pavement structure capacity at the different Idaho sites, the FWD testing was conducted using Dynatest equipment, as shown in Figure A.7, Appendix A. The test was conducted once a year during the summer, for four years (1999, 2000, 2001 and 2002). For each site the test was conducted at five different stations using two different loads (8,000 lb and 12,000 lb). The pavement temperature was recorded during the test and resulting deflection will be used later for backcalculating the pavement layers' moduli.

3.1.3.7 Traffic Data

The traffic data were downloaded from the Idaho Transportation Department (ITD) website (ITD, 2004). The data were used to determine the seasonal variations in the traffic loads to be used in the pavement performance analysis.

Table 3.3 Layers' Thickness & Subgrade Soil Characterization Tests, for Different Sites

Site / Test	Lewiston	Moscow		Worley	Pack River		Weiser	
	1	2A	2B	3	4A (S)	4B (N)	5A	5B
Construction year	97	96	96	96	88	98	99	99
AC surface Thickness, in	6	4.8	4.8	7	6	12	6	6
Agg. Base Thick., in	-	6	27.6	-	-	-	6	12
Rock Cap, Thick., in	20	21.6	0	21	24 (river cap)	Undefined	6	0
Subgrade Type	Granular Fill	CL	CL	Silt & Clayey silt	Lacustrine silt & silty gravel	Lacustrine silt	ML	ML
% Pass # 4	100	100	100	100	100	100	100	100
% Pass # 10	100	100	100	100	88	100	100	100
% Pass # 40	100	100	100	100	65	100	100	100
% Pass # 200	62	98	98	82	29.5	92	70	70
LL, %	25	30.3	30.3	40.2	NP	NP	39.8	39.8
PI, %	NP	8	8	18.4	NP	NP	9.6	9.6
AASHTO Class.	A-4	A-4	A-4	A-6	A-2-4	A-4	A-4	A-4
Unified Classif.	ML	CL	CL	CL	SM	ML	ML	ML

Table 3.4 Average Monthly Rainfall & Temperature for Weather Stations Near Idaho Sites.

Site	Lewiston	Moscow	Worley	P. River	Weiser
Weather St	Lewiston	Moscow	Plummer	Sandpoint	Weiser
Latitude, °N	46.41	46.73	47.31	48.3	44.23
Long., °W	117.03	116.9	116.96	116.5	116.95
Elevation, ft	705	2660	2916	2099	2130
Month	A) Average Monthly Rainfall, mm				
Jan	32.5	78.9	64.5	103.1	37
Feb	22.6	57.6	93.4	84	28.9
Mar	27.6	60.9	96.6	72.3	27.1
Apr	28.7	54.8	21.5	53.8	23.1
May	33.2	56.8	27.1	64	19.5
Jun	31.7	45.2	63.2	57.4	22.3
Jul	17	23.8	9.5	32	5.5
Aug	19.8	29.4	8.3	41.4	11.6
Sep	19.8	32.5	33.1	43.4	14.2
Oct	22.8	46.9	82.6	59.6	18.7
Nov	29.2	83.3	82.7	120.3	42.1
Dec	30.4	76.4	78	119.1	41.1

Month	B) Average Monthly Temperature, °F				
Jan	33.4	28.8	28.6	24.8	25.3
Feb	39.0	34	34	30.4	32.5
Mar	44.1	39.2	39.6	36.7	41.7
Apr	50.5	45.7	46.4	44.6	49.1
May	58.3	52.7	54	52.5	57.6
Jun	66.7	59.5	61.3	59.5	65.7
Jul	73.9	65.5	67.5	64.4	72.1
Aug	73.6	66.2	67.1	63.7	70
Sep	64.0	58.3	58.3	55.2	60.4
Oct	52.2	48.4	47.1	44.4	48.9
Nov	41.2	36.9	36.1	33.8	37.4
Dec	34.3	29.5	29.1	27	27.9

3.2 LTPP SITES

3.2.1 Background

The original Long-Term Pavement Performance (LTPP) program was established by the Strategic Highway Research Program (SHRP) in 1987 to study the long-term performance of the in-service pavements. The original SHRP-LTPP program included two main experiments, the General Pavement Studies (GPS) and the Specific Pavement Studies (SPS). At the conclusion of the SHRP in 1992, the LTPP program continued under the management of the Federal Highway Administration (FHWA).

The FHWA-LTPP program team recognized the need to study the environmental impacts on pavement performance. Consequently, the FHWA-LTPP team launched the Seasonal Monitoring Program (SMP) as an integral part of the LTPP program. The primary objective of the SMP was to study the impacts of temporal variations in pavement response and materials properties due to the separate and combined effects of temperature, moisture and frost/thaw variations. The SMP experiment focused on collecting data that captured the seasonal variations of the pavement material properties along with the associated variations in pavement performance. The factorial design of the SMP experiment included 32 different study factors. Table 3.5-A summarizes the original experiment design of the LTPP-SMP (Rada et al, 1994). The original design included 32 design cells, with three sites to be selected for each flexible pavement cell (cells 1-16) and one site for each rigid pavement cell (cells 17-32). However, due to practical implementation of this huge study program, not all cells were filled with the required number of sites. The real SMP design is shown in Table 3.5-B.

Table 3.5 Experimental Design the LTPP Seasonal Monitoring Program (Rada et al, 1994)

A) LTPP-SMP Original Design

Pavement Type	Subgrade Soil Type	No Freeze Zone		Freeze Zone	
		Dry	Wet	Dry	Wet
Flexible, Thin AC Surface, <127 mm	Fine	1	2	3	4
	Coarse	5	6	7	8
Flexible, Thick AC Surface, >127 mm	Fine	9	10	11	12
	Coarse	13	14	15	16
Rigid –Jointed Plain Concrete, JPC	Fine	17	18	19	20
	Coarse	21	22	23	24
Rigid Jointed Reinforced Concrete, JRC	Fine	25	26	27	28
	Coarse	29	30	31	32

B) LTPP-SMP Real Design

Pavement Type	Subgrade Soil Type	No Freeze Zone		Freeze Zone	
		Dry	Wet	Dry	Wet
Flexible, Thin AC Surface, <127 mm	Fine	0	2	2	1
	Coarse	1	4	3	3
Flexible, Thick AC Surface, >127 mm	Fine	0	4	1	2
	Coarse	3	3	4	7
Rigid –Jointed Plain Concrete, JPC	Fine	1	5	1	3
	Coarse	1	1	1	2
Rigid Jointed Reinforced Concrete, JRC	Fine	0	1	0	3
	Coarse	0	1	0	1

The data collected by the FHWA-LTPP program for the SMP study included, in addition to the basic LTPP data designated for the General Pavement Studies (GPS), data that relate to the seasonal variations of the material properties and the structural capacity of the existing pavements. Most of the LTPP data were released to the public in CD formats via the DataPave software. The latest DataPave software released is version 3.0, which includes the data released in January 2002. It is now available online through http://datapave.com.

In this study, the LTPP-SMP database was used for more extensive FWD data, which was needed for seasonal performance analysis. The LTPP-SMP database was used to develop regression models that relate the pavement layers moduli to the environmental change of subgrade moisture and asphalt pavement temperature.

3.2.2 LTPP Sites Selection

Out of all sites in the LTPP-SMP experiment, about 21 sites were constructed with flexible pavements and 14 sites having sufficient data were considered in this study. An additional site (48-4143), even though it is a rigid pavement, was included in the modulus-moisture analysis because it has a clayey subgrade soil, like most of the soils in the Idaho sites. Table 3.6 shows all the LTPP-SMP sites with flexible pavement and highlights (with an asterisk) the sites that are not included in our study. Out of the fifteen selected sites, some sites were used to study the subgrade modulus variation with moisture content, other sites were used to study the asphalt concrete (AC) modulus variation with temperature, and others were used to predict the asphalt pavement temperature from the air temperature, as shown in Table 3.7. Table 3.7 also shows the site location, latitude, longitude and elevation above the sea level, the type of surface, and the surface thickness for each site.

Table 3.6 LTPP_SMP Sites Locations and Identifications

Sites ID	Exp. No.	State	SHRP Region
Climatic Region: Wet Freeze			
9-1803-1	GPS1	Connecticut (CT)	North Atlantic
23-1026-1	GPS1	Maine (ME)	North Atlantic
24-1634-1	GPS2	Maryland (MD)	North Atlantic
25-1002-1	GPS1	Massachusetts (MA)	North Atlantic
27-1018-1*	GPS1	Minnesota (MN)	North Central
27-6251	GPS1	Minnesota (MN)	North Central
33-1001-1	GPS1	New Hampshire (NH)	North Atlantic
40-4165-1*	GPS2	Oklahoma (OK)	Southern
Climatic Region: Dry Freeze			
16-1010-1	GPS1	Idaho (ID)	Western
30-8129-1	GPS1	Montana (MT)	Western
49-1001-1	GPS1	Utah (UT)	Western
83-1801-1*	GPS1	Manitoba (MB)	North Central
Climatic Region: Wet No Freeze			
13-1005-1	GPS1	Georgia (GA)	Southern
13-1031-1*	GPS1	Georgia (GA)	Southern
28-1016-1	GPS2	Mississippi (MS)	Southern
48-1077-1	GPS1	Texas (TX)	Southern
48-1122-1	GPS1	Texas (TX)	Southern
Climatic Region: Dry No Freeze			
4-1024-1*	GPS1	Arizona (AZ)	Western
4-0113-1*	SPS1	Arizona (AZ)	Western
4-0114-1*	SPS1	Arizona (AZ)	Western
35-1112-1	GPS1	New Mexico (NM)	Southern

* Sites that are NOT included in our study due to the lack of data

Table 3.7 Selected LTPP_SMP Sites & Their Locations

Site	State	Surface Thick. (mm)	Elev. (m)	Lat. (Deg.)	Long. (Deg.)	Soil (Mod.- Mois.)	AC (Mod. - Tempr.)	Tempr. Predic.
North Atlantic								
9-1803	CT	183	50	41.39	72.03		x	
23-1026	ME	163	148	44.57	70.29		x	
24-1634	MD	91	12	38.37	75.26	x		
25-1002	MA	198	27	42.17	72.61		x	
27-6251	MN	188	416	47.46	94.91		x	
33-1001	NH	213	77	43.22	71.51		x	
Western								
16-1010	ID	272	1455	43.68	112.12		x	x
30-8129	MT	76.2	1353	43.31	109.14			x
49-1001	UT	140	1325	37.28	109.58			x
Southern								
13-1005	GA	195.6	138	32.61	83.7	x	x	x
28-1016	MS	200	122	33.06	89.57		x	x
48-1077	TX	129.5	559	34.54	100.4	x	x	x
48-1122	TX	86.4	143	29.24	98.25	x	x	x
48-4143	TX	264	13	30.04	94.37	x		
35-1112	NM	160	1146	32.03	103.5	x	x	x

x Sites donates analysis type where data is used.

3.2.2.1 Selection of Sites for Subgrade Modulus-Moisture Variation

The first step in the selection process was to select sites that have different soil types, particularly the fine-grained soils, which are primarily affected by moisture variation. The second step was to isolate all sites in the freeze zones (wet and dry) from the non-freeze zones, since the frost susceptibility of a soil would certainly influence its modulus change, especially in the transition from the freeze period to the thaw period. It is also recognized that the frost susceptibility issue is another important factor that may influence soil behavior in the freeze and thaw period. In the third step, extensive data mining was performed to gather and consolidate available data in all sites in the no-freeze zones (wet or dry), which have sufficient data to allow development of the desired prediction models.

The extensive analysis revealed six LTPP sites that were appropriate. These six sites are 35-1112, 48-1122, 48-1077, 13-1005, 48-4143 and 24-1634. The subgrade soils of the previous sites are: sand, coarse clayey sand, fine sandy silt, fine sandy clay, clay and silt, respectively. It is important to note that even though the LTPP site number 24-1634 is located in Maryland, which is classified geographically as freeze zone, the climatic data of this site indicated no frost conditions. The authors included the data obtained from this site in their analysis because it was the only site that had fine silt subgrade soil. This type of fine soil is highly affected by the variation in moisture content.

Details for all 6 of the selected sites are shown in Table 3.8. The table shows the site location, minimum average monthly air temperature, subgrade soil type, soil classification, soil sieve analysis, Atterberg limits, dry density and optimum moisture content for each of the soil types in the selected sites. The downloaded data for each site included the backcalculated elastic modulus for both volumetric and gravimetric moisture content of subgrade soil at different time intervals.

The backcalculated subgrade resilient (elastic) modulus was obtained from the LTPP database table (MON_DEF_FLX_BAKCAL_SECT). The gravimetric moisture content was obtained from the table SMP_TDR_AUTO_MOISTURE. These tables are available in the DataPave software. The moisture content of the subgrade is provided in the LTPP database as moisture profile along the subgrade depth. The average moisture content along the depth was considered the corresponding moisture for the backcalculated resilient modulus at a given location. The subgrade soil properties were collected from many tables, since not all the data were available in one table. Tables (SMP_TDR_MOISTURE_SUPPORT) and (INV_SUBGRADE) were used to download most of the data and tables (TST_UG04_SS03) were used to download the Atterberg limits, while table (TST_UG05_SS05) was used to get the dry density and optimum moisture content.

Table 3.8 Selected LTPP Sites and Subgrade Soil Characterizations (After NAVFAC (1986))

LTPP Sites	1	2	3	4	5	6
	48-4143	13-1005	48-1122	24-1634	48-1077	35-1112
Location	Texas	Georgia	Texas	Maryland	Texas	New Mexico
Surface Type	Rigid	Flexible	Flexible	Flexible	Flexible	Flexible
Minimum Monthly Avg. Air Temp, C°	9.7	8.7	9.7	1.7	3.6	5.8
Soil Type as Identified by LTPP	Lean Inorganic Clay	Fine Clayey Sand	Coarse Clayey Sand	Fine Silt	Fine Sandy Silt	Coarse, poorly graded sand
AASHTO Soil Classification	A-7-6	A-6	A-2-6	A-4	A-4	A-3
% Passing # 4	-	-	99	99	94	100
% Passing # 10	-	-	97	98	93	99
% Passing # 40	-	-	75	98	87	94
% Passing # 200	90	38.4	6.5	97.9	51.8	2.7
D60, mm	-	-	0.3	0.012	0.1	0.18
Liquid Limit, %	41	27	26	-	-	-
Plasticity Index, %	23	12	12	NP	NP	NP
Max. Dry Density, gm/cm^3	1.730	2.05	1.858	1.746	1.906	1.698
Optimum Moisture, %	15.0	10.0	8.0	12.0	10.0	12.0
In-Situ Dry Density, gm/cm^3	1.719	1.826	1.850	1.789	1.723	1.641
Overlying Pavement Thickness, cm	51.3	42.7	70	54.4	40	31.2
Overburden Stress, gm/ cm^2	110	88	136	104	84	65

3.2.2.2 Selection of Sites for Asphalt Concrete Modulus-Temperature Variation

To study the AC modulus variation with temperature, all of the selected sites were included in this study except sites 48-4143, which has a rigid pavement and site 24-1634 because it does not have sufficient data. The AC layer modulus was downloaded for the different sites at different time intervals. The AC layer temperature at different depths, the asphalt surface temperature and air temperature were downloaded from different tables. An extensive effort was made to select the temperatures values at the same time intervals at which the FWD test was made in order to measure the AC layer modulus. The average daily air temperature was also downloaded for the same day on which the test was conducted as well as the day before.

Other supporting data describing the properties of the AC layer for the different sites were also downloaded. These data included: the AC layer thickness, the bulk specific gravity (BSG) of the asphalt mix, the maximum specific gravity (MSG) of the asphalt mix, the void ratio in the asphalt mix, the asphalt binder grade, the asphalt binder penetration at 77 ^{o}F, asphalt binder specific gravity, and asphalt binder content.

The AC modulus and mid-depth asphalt temperature were downloaded from the table MON_DEFL_FLX_BAKCAL_SECT. Supporting data for the modulus and the mid-depth AC temperatures were also downloaded from the table MON_DEFL_FLX_BAKCAL_POINT for outside lanes at the nearest locations from the installed AC temperature sensors. The asphalt pavement temperatures at different depths (25 mm from the surface, mid-depth and 25 mm from bottom of the AC layer thickness) were downloaded from the table (MON_DEFL_TEMP_VALUES) every 30 minutes. An effort was made to select the reading at approximately the same time of the FWD test. The exact depths of the thermoster probes were downloaded from the table (MON_DEFL_TEMP_DEPTHS). The asphalt surface temperature and the air temperature recorded during the FWD testing were downloaded from the table (MON_DEFL_LOC_INFO). The average daily air temperature was downloaded from the table (SMP_ATEMP_RAIN_DAY). The asphalt binder grade, penetration and specific gravity were downloaded from the table (INV_PMA_ASPHALT). The bulk specific gravity was downloaded from the table (TST_AC02), the maximum specific gravity was downloaded from the table (TST_AC03), the percentage air voids in the asphalt mix was downloaded from the table (INV_PMA_ORIG_MIX), and the content of the asphalt binder percentage was downloaded from the table (TST_AC04). The different properties of the AC layer for the different sites are shown in Table 3.9.

Table 3.9 Properties of AC Layer for the Different LTPP Sites.

No	LTPP Site	State	AC Layer Thickness (mm)	Bulk Gs of AC Mix (BSG)	Air Voids in AC Mix (%)	AC Binder Grade	Binder Specific Gravity	Binder Content (%)
1	13-1005	GA	195.6	2.341	4.40	AC-30	1.034	4.68
2	28-1016	MS	200	2.359	2.67	AC-30	1.03	4.45
3	48-1077	TX	129.5	2.373	3.05	AC-10	0.985	4.5
4	48-1122	TX	86.4	2.321	3.20	AC-10	0.99	4.61
5	35-1112	NM	160	2.464	4.40	AC-30	1.015	5.05
6	9-1803	CT	183	2.444	5.35	AC-20	1.01	4.3
7	23-1026	ME	163	2.352	3.85	AC-10	1.015	5.1
8	25-1002	MA	198	2.427	6.80	AC-20	1.026	5.5
9	33-1001	NH	213	2.386	5.80	AC-20	1.03	4.7
10	16-1010	ID	272	2.294	5.30	AC-10	1.026	5.2
11	27-6251	MN	188	2.353	5.80	N/A	N/A	4.5
12	30-8129	MT	76	2.324	4.50	AC-10	1.03	5.8
13	49-1001	UT	140	2.350	2.10	AC-10	1.04	5.7

4. ANALYSIS OF COLLECTED DATA AT IDAHO SITES

This chapter presents an analysis of the data collected at the Idaho sites with respect to moisture and temperature variations. It also presents an analysis of the Enhanced Climatic Model (EICM). The objective of this analysis is to verify the EICM applicability and determine whether it could be used to predict the impacts of the environmental changes on pavement layers in Idaho.

4.1 MOISTURE DATA ANALYSIS

4.1.1 Moisture Variation with Time

Moisture content of soils near the ground surface depends on a variety of climatic and physical factors including soil type, temperature, precipitation, vegetation, and others. It is widely known that pavement subgrade soils not only experience temporary (seasonal) changes in moisture content but also undergo changes in their long-term average annual moisture content. In the Idaho study, as well as for the LTPP research program, the variation of subgrade soil moisture was monitored by means of TDR moisture sensors, which measure the volumetric moisture content. Thus, the analysis presented here focuses on the variation of the volumetric moisture content.

The volumetric moisture content was generally recorded at the sites on a monthly basis. Sometimes it was recorded weekly, daily, or twice a day at the Moscow and Lewiston sites in order to capture the moisture changes during the spring season. The average subgrade volumetric moisture contents that were recorded through the length of the bottom TDR sensors are presented in Figure 4.1. The figure shows the variation of subgrade volumetric moisture content versus time for the five Idaho sites: Lewiston, Moscow, Worley, Pack River and Weiser respectively. Almost all of the sites show higher fluctuation in moisture content for the early time period just after site construction, and then the moisture content for most of the sites moves toward long-term equilibrium with little seasonal fluctuation.

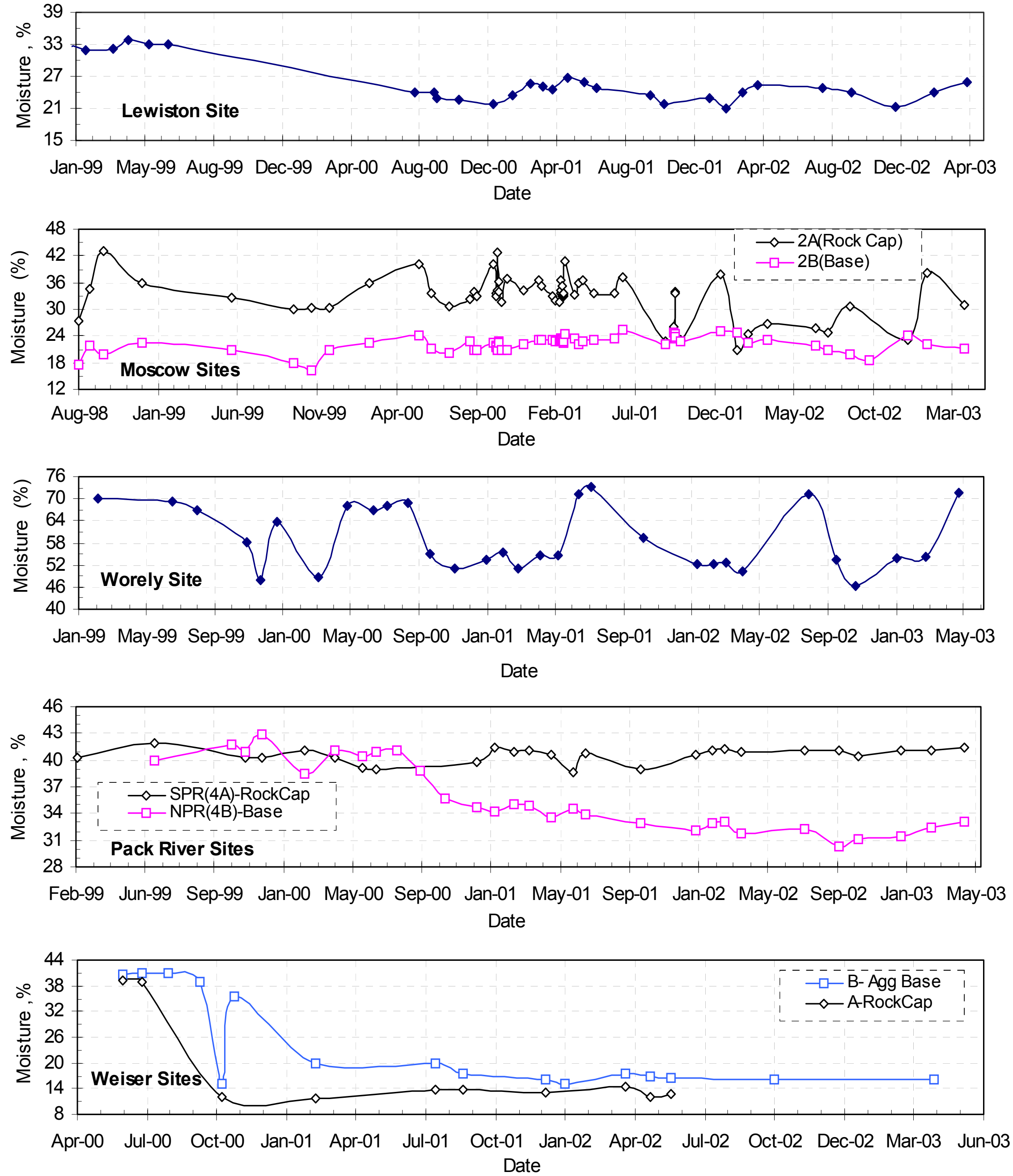

Figure 4.1 Average Subgrade Volumetric Moisture Content with Time for the Different Idaho Sites

The previous observation was also observed by Halliburton (1970) in a similar study on subgrade soils beneath both rigid and AC pavement. He concluded that although both subgrades continue to exhibit seasonal fluctuations in moisture content, both also trend toward an "equilibrium" moisture content value of about 1.1 to 1.3 times soil's plastic limit. Figure 4.1 indicates also that the seasonal fluctuation in moisture content is much higher at the Worley site, while it is much less at the Weiser Site.

Effect of GWL

The ground water level (GWL) was monitored by manual measurements of the water level in the installed piezometers at the each site. The water level could only be measured at two sites, Moscow (2A) and South Pack River (4A). At other sites, piezometers showed dry surface, and no measurements were possible. This concludes that the GWL was deeper than the depth and of the installed piezometers, which indicates the insignificant effect of the GWL on the moisture regime at these sites.

Figure 4.2 shows the seasonal fluctuation in both the GWL and the measured volumetric moisture content, at depth 4.5 ft from the pavement surface, for both the Moscow and Pack River sites. The figure shows that the positive change in the GWL is accompanied by a similar positive change in the moisture content. This observation is noticed for both sites, especially the Moscow site because it has more data points. The increase in moisture content due to the increase in GWL is also supported by the SWCC equations, like the one by Fredlund and Xing (1994), previously stated as Equation 2.13

$$\theta_w = C(h) x \left[\frac{\theta_{sat}}{\left[\ln \left[\exp(1) + \left(\frac{h}{a} \right)^b \right] \right]^c} \right] \qquad (2.13)$$

Through this equation, it could be observed that the volumetric moisture content (θ_w) increases when the matric suction (h) decreases, and vice versa. For a fixed point above the GWL, when the GWL increases the distance to this point from the GWL decreases. This results in decreasing the matric suction. According to Witczak at al (2000), the matric suction can be estimated as D $\gamma_{w,}$ where D is the distance to the GWL.

Figure 4.2 indicates also that the ground water level is much higher during the late winter, spring and early summer seasons, months (February, March, April and May), while the minimum water level is observed during the fall and early winter (August through December).

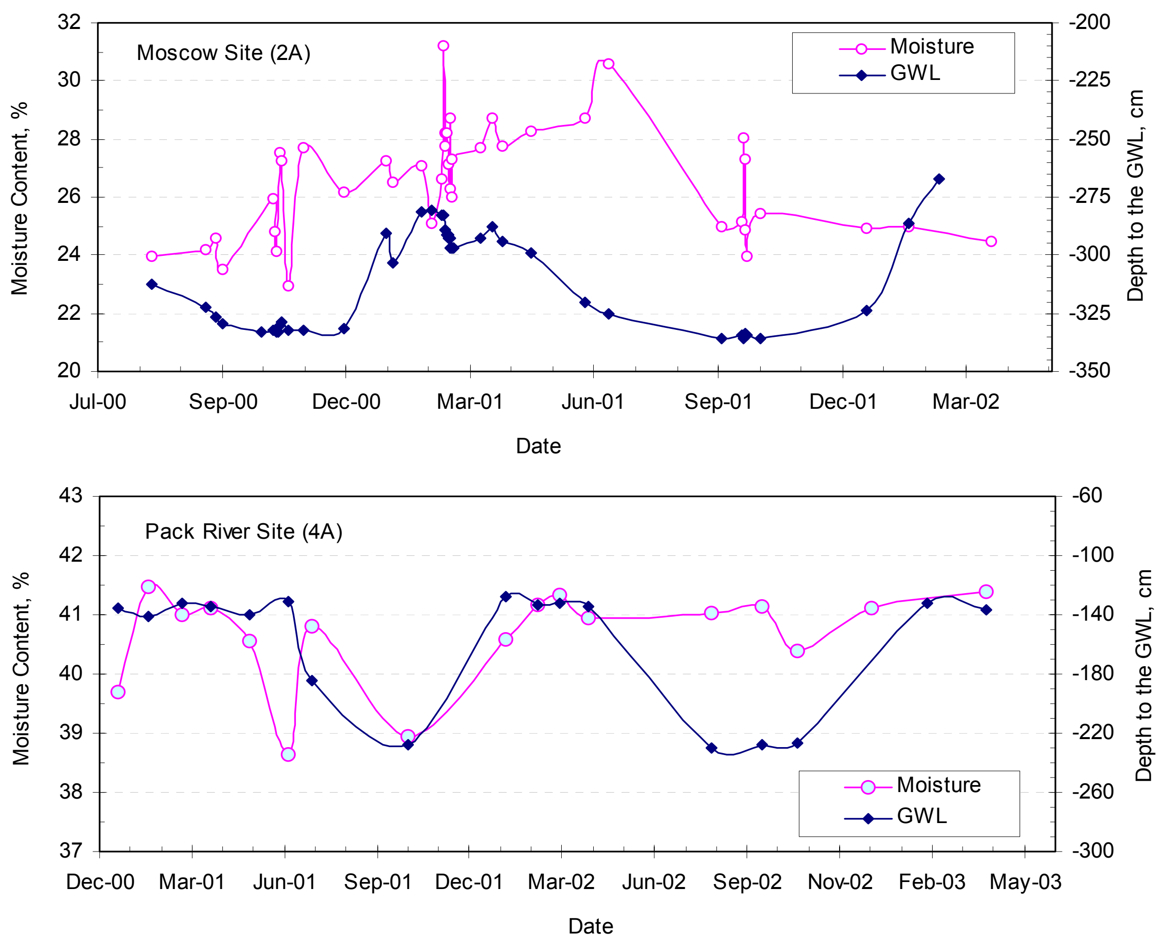

Figure 4.2 Measured Water Content at 4.5ft Depth and the Monitored GWL versus Time

4.1.2 Average Monthly Variation of Moisture and Rainfall

The average monthly moisture content for all sites was calculated and plotted in Figure 4.3. The average monthly rainfall for weather stations nearest to the Idaho sites based on 59 years' record is shown in Figure 4.4. Comparing the two figures, it could be noticed that the Weiser sites have the lowest moisture content and have also the lowest rainfall amounts. On the other hand, the sites having higher moisture contents (Worley and Pack River-A) also have the higher rainfall amounts.

The figures also show that the Worley site has higher moisture content than the Pack River sites, although it has a lower rainfall amount, but that may be due to its soil type. The soil type at the Worley site is clay with relatively high plasticity index (18.4%), while the soil type in Pack River sites are nonplastic silt with silty gravel, as previously presented in Table 3.3. The fine plastic soils usually retain higher moisture content due to the large surface area. The moisture content is also proportional to its plasticity as reported by Halliburton (1970).

Zapata et al. (1999) indicated that the equilibrium moisture content at a given degree of saturation was expected to be proportional to the specific surface area of the soil. The PI is a fair indicator of the surface area. However, a soil with a small percentage of highly active clay would have a high PI but only a moderate surface area. Therefore, the use of the weighed Plasticity Index (wPI) was considered a better indicator of soil particle surface area available for water absorption and retention. Applying this concept on the moisture data from the sites having plastic soils (Worley, Moscow and Weiser), we can find some agreement. The Worley site, having the highest water content, also have the highest wPI of 15.1. On the other hand, the site having the average lowest water content, the Weiser site, also has the lowest wPI of 6.7.

Figure 4.3 shows also that the seasonal variation in moisture content is small for most of the sites (within 2% around the average) except the Moscow-A (+/- 5%) and Worley site (+/- 10% around the average).

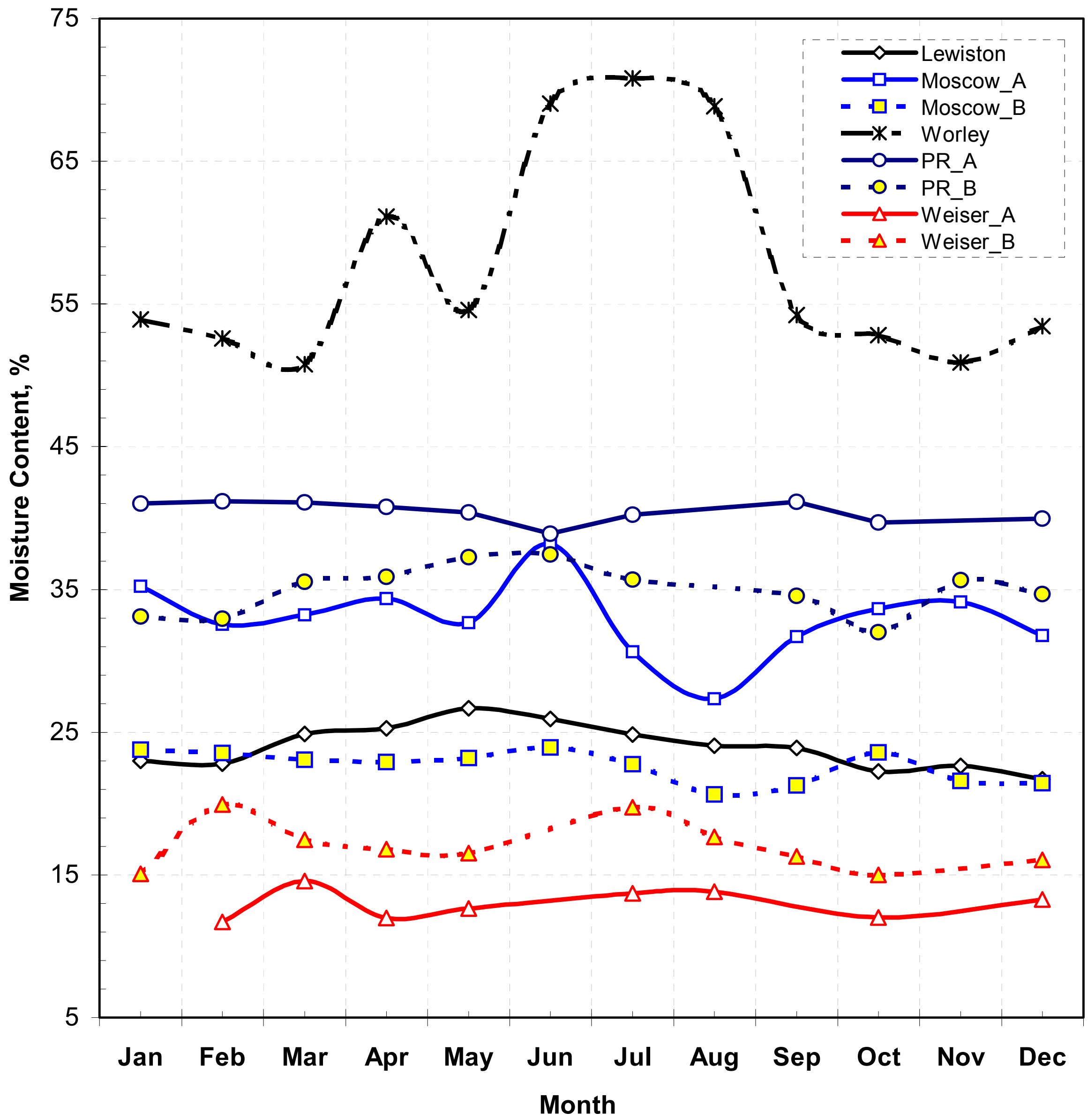

Figure 4.3 Average Monthly Volumetric Moisture Content for Idaho Sites

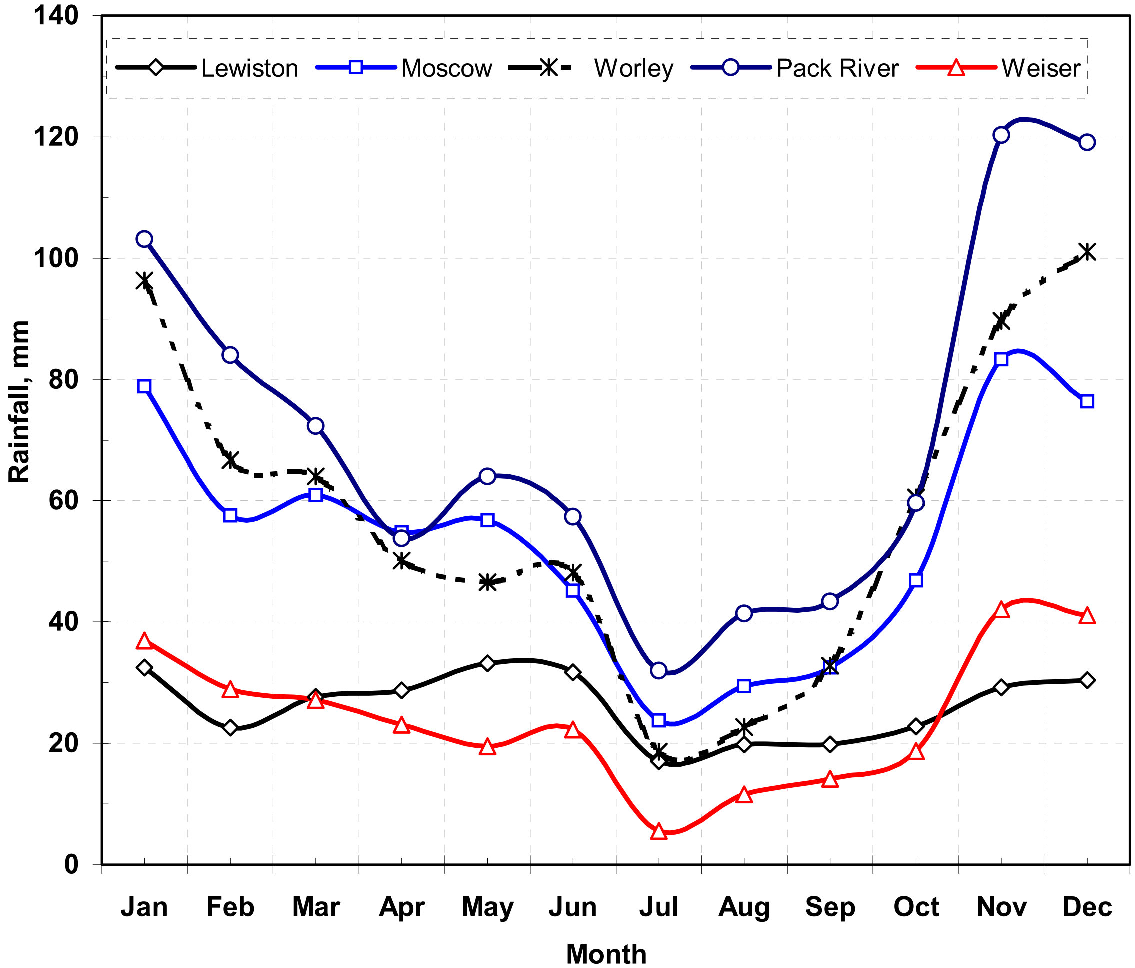

Figure 4.4 Average Monthly Rainfalls for Idaho Sites

The moisture content versus average monthly rainfall for all sites is shown in Figure 4.5 through Figure 4.7. The figures indicate that the moisture content is highly related to the average monthly rainfall amounts in most of the sites (Lewiston, Moscow- A, Moscow -B and Pack River –A). For example, Figure 4.5 shows that the moisture content at the Lewiston site increases when the average rainfall increases. However, when the rainfall drops (during July and August) the moisture content does not drop suddenly, because the soil is fine and has little permeability, but it continues to decrease gradually.

In conclusion, the variation in the subgrade moisture content depends on the rainfall amount, the level of the ground water table and the soil type fine or coarse, plastic or non-plastic. Other factors that may affect the subgrade moisture content could be solar radiation and the topography.

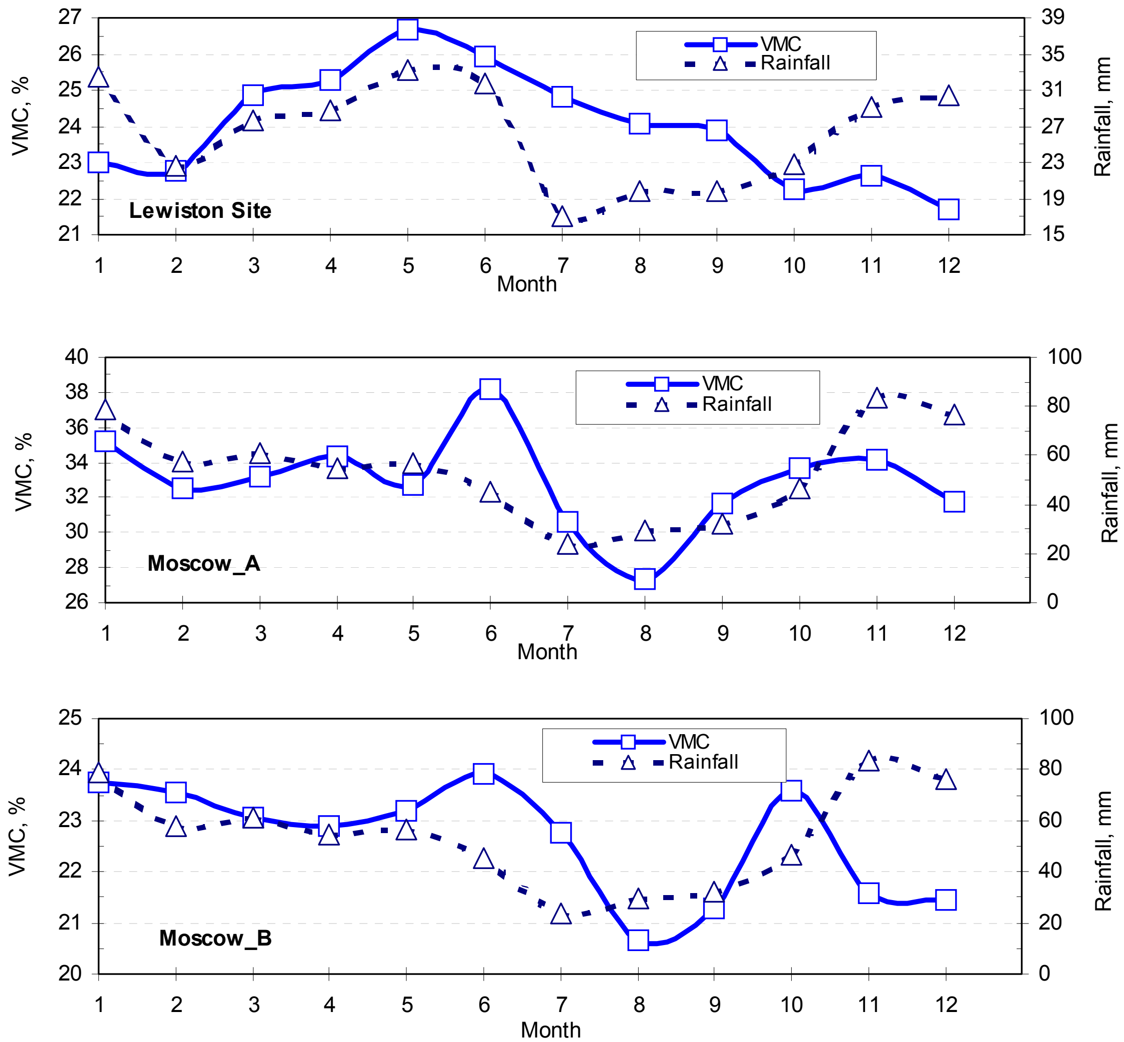

Figure 4.5 Moisture Content versus Rainfall for Lewiston and Moscow Sites

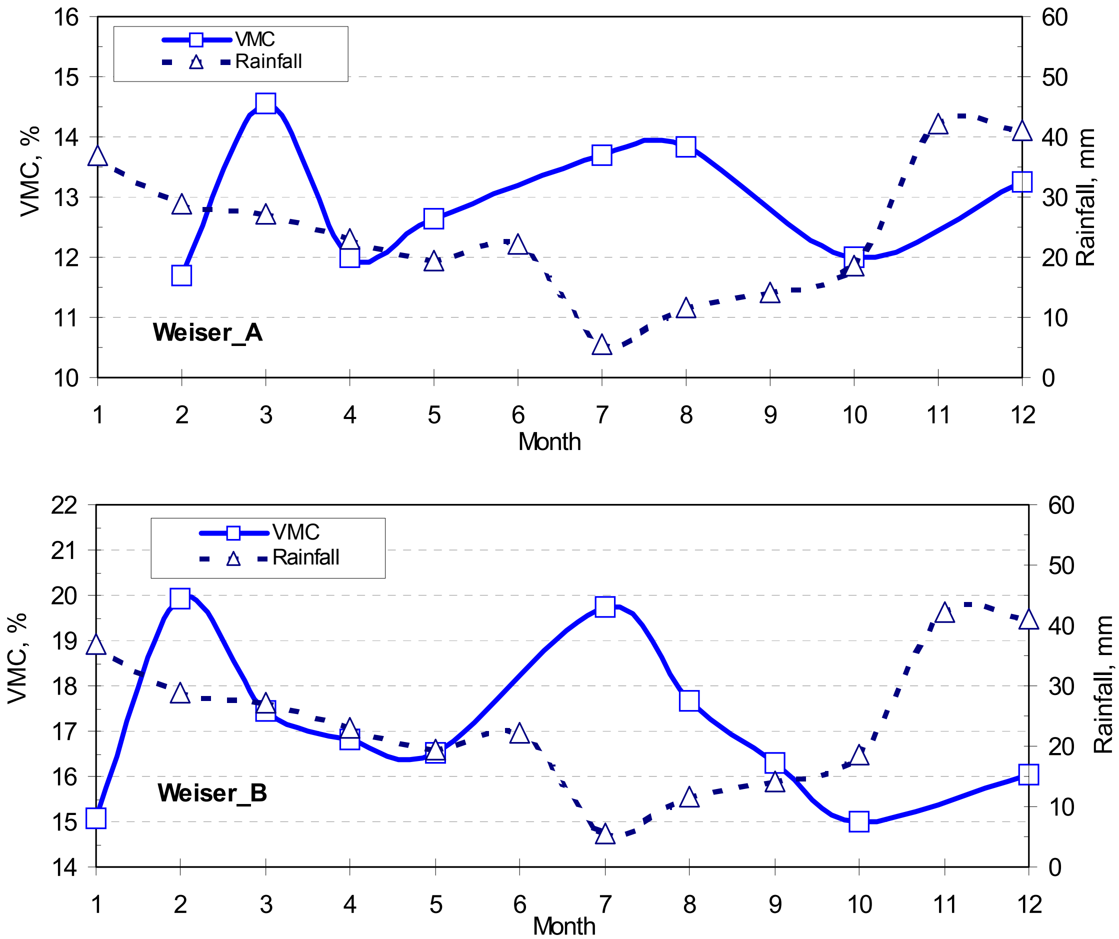

Figure 4.6 Moisture Content versus Rainfall for Weiser Sites

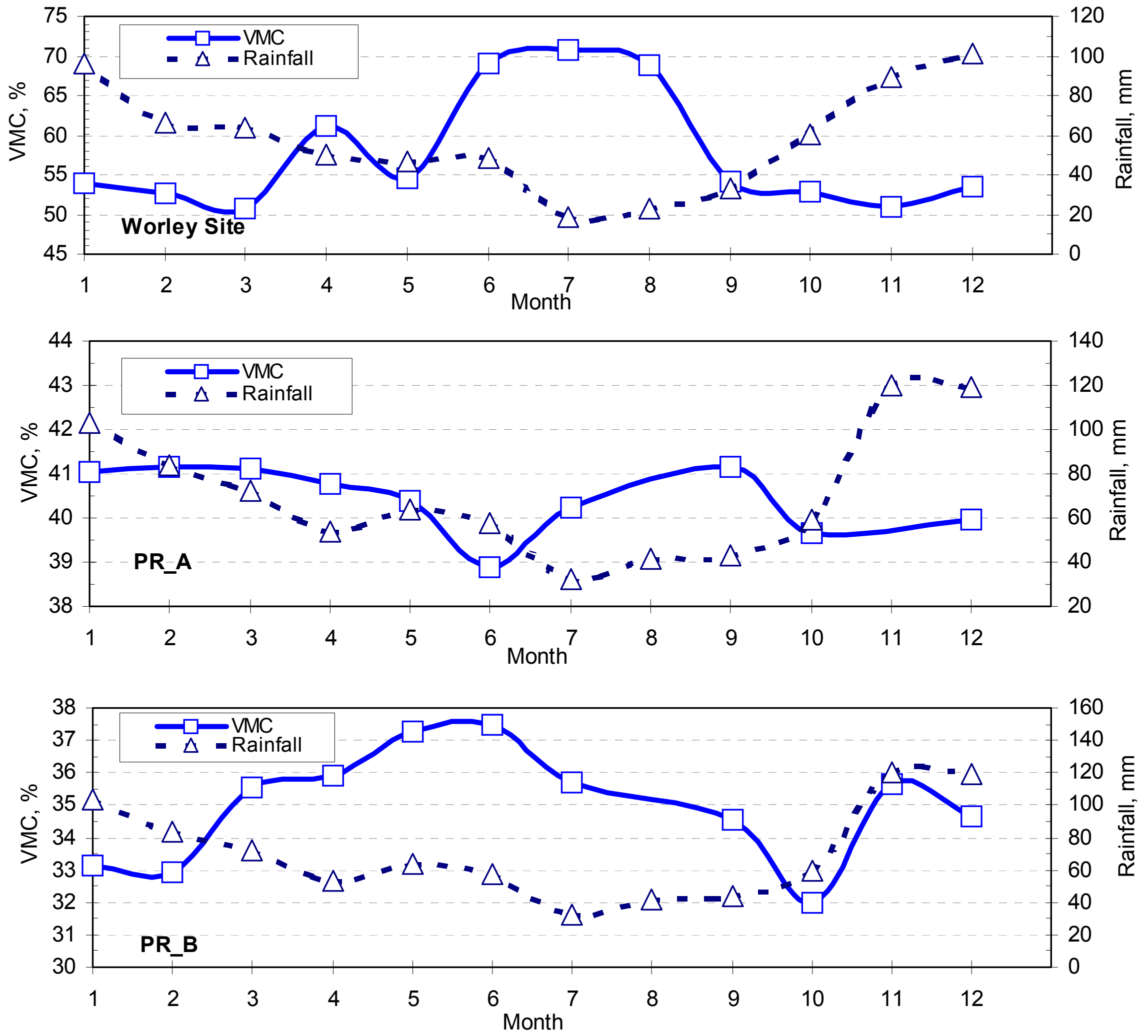

Figure 4.7 Moisture Content versus Rainfall for Worley and Pack River Sites

4.1.3 Impact of Rockcap Base Layer on the Moisture Regime in the Underlying Subgrade

As previously stated, a secondary objective of the moisture measurement in the Idaho sites was to determine the effectiveness of having a rockcap base layer on the moisture regime under pavement. Two sites (Moscow and Weiser) had installations with two identical pavement sections constructed adjacent to each other, with the base layer of one being a rockcap and the other being a ¾" aggregate base. The moisture content data were analyzed for these two sites and Figure 4.8 shows the subgrade moisture content versus time for both the Moscow and Weiser sites. Each of the two figures show two curves; site (A) for subgrade soil moistures under a pavement having a rockcap layer and site (B) for subgrade soil moisture under a pavement having an aggregate base layer. The two figures indicate that the subgrade moisture content under the rockcap base at the Moscow site is higher than the moisture content under the base course. However, the reverse was observed at the Weiser sites. There, the subgrade soil moisture under a base layer was higher than the subgrade soil moisture under a rockcap layer. Also, the two figures indicate that the difference in the subgrade soil moisture under the base and rockcap layers is decreasing with time and it would reach a negligible amount with long-term moisture equilibrium.

It is the researchers' viewpoint that this could have happened due to the fact that the site at Moscow was confined (had no adjacent daylight ditch drain) and the ground water that is coming from rainfall had no exit. On the other hand, the rockcap in Weiser site continued to the shoulder and water in the rockcap had an exit to the adjacent daylight ditch drain. Thus, if the pavement section has a daylight drainage layer (open to a side ditch), the rockcap shows its effectiveness in draining the water out of the system. In a closed system like the one in Moscow, the water may seep vertically and cause an increase in subgrade moisture.

The site in Lewiston (on rockcap) was showing very minor variations. Figure 4.5 showed that the moisture content at both the Lewiston and Moscow site (2A) was highly related to the average rainfall, and may also be related to the presence of the rockcap layer that helps in water seepage through the subgrade layer. However, the contribution of the rockcap (because if its high modulus and no-freeze potential) is very significant. The expected reduction in subgrade modulus, if any, due to moisture increase under the rockcap layer will be superceded by the high modulus of the rockcap. Consequently, reduction of thickness is very likely with pavements with rockcap base. This will be verified later in this report using the results of the FWD tests performed at the Moscow sites, which would show better structural analysis.

It should be noted that the moisture contents presented in Figure 4.8 are the average subgrade moisture contents through the length of the bottom TDR probes. The variability in subgrade moisture content under the rockcap layer in the Moscow site could be attributed to the failure of two of the moisture sensors in the bottom TDR probe after October 2001. Also, for the upper TDR probe, only the upper sensor is located in the base and/or rockcap layer, while the other sensors are located in the subgrade layer just below the base and /or rockcap layer. The average moisture content in the subgrade layer from the upper TDR probe was calculated and is presented in Figure 4.9 for both the Moscow and Weiser sites. The data for the Moscow site shows that the difference in subgrade moisture content under both the rockcap and base layers is very small compared to Figure 4.8.

The subgrade moisture content profiles with depth under rockcap and base layers are presented in Figure 4.10 and Figure 4.11 for both Moscow and Weiser sites, respectively. The figures show the volumetric moisture content versus depth from pavement surface at different months. The figures indicate that there is some significant change in the subgrade moisture under base and rock cap at the shallow depths just below the base or rock cap layer. The subgrade layer starts at depth 2.7 ft from the surface at Moscow site and 1.5 ft at Weiser site. Comparing these numbers with moisture content profiles shown in Figure 4.10 and Figure 4.11, it could be observed that the subgrade moisture content just below the base layer is greater than the moisture content just below the rockcap layer for both sites. At a depth of 4 ft, the subgrade moisture content under rockcap layer becomes greater than the moisture content under base layer for Moscow site, while it is smaller in Weiser site. Finally, at greater depths (6.5 ft at Moscow site and 5.5 ft at Weiser site), there is no significant difference in the subgrade moisture content under both rockcap and base layers.

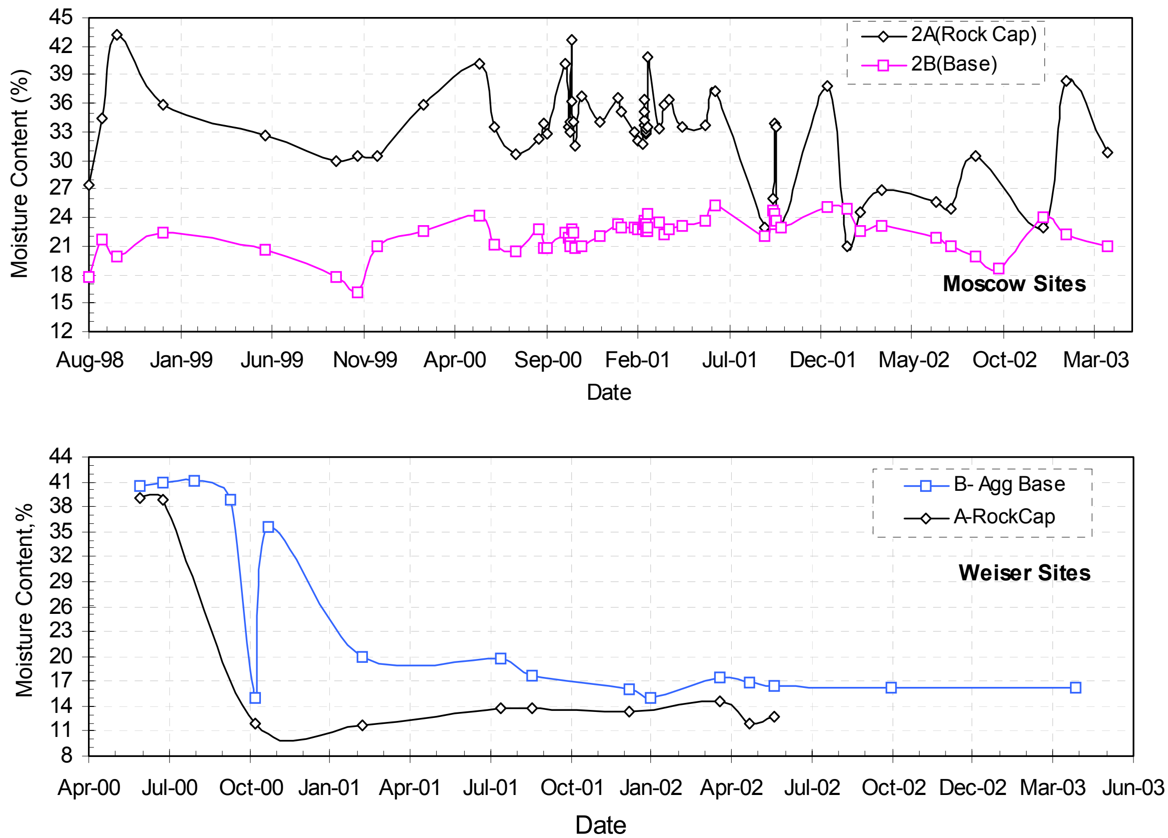

Figure 4.8 Average Subgrade Moisture Content versus Time from the Lower TDR Probe

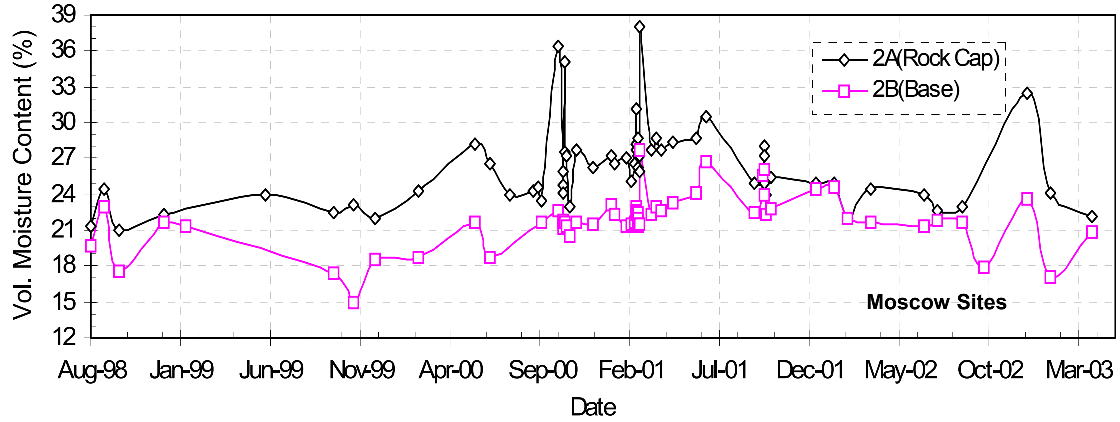

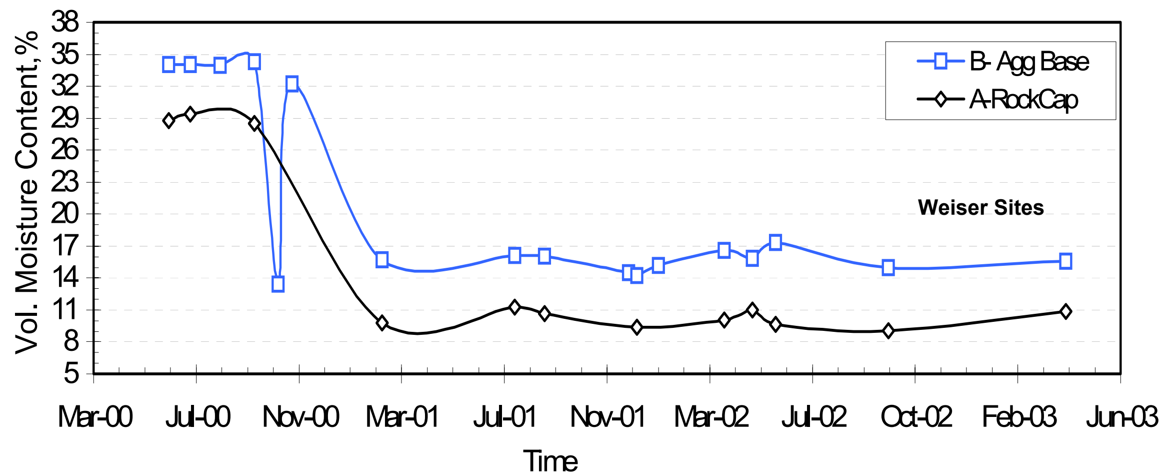

Figure 4.9 Average Subgrade Moisture Content versus Time from the Upper TDR Probe

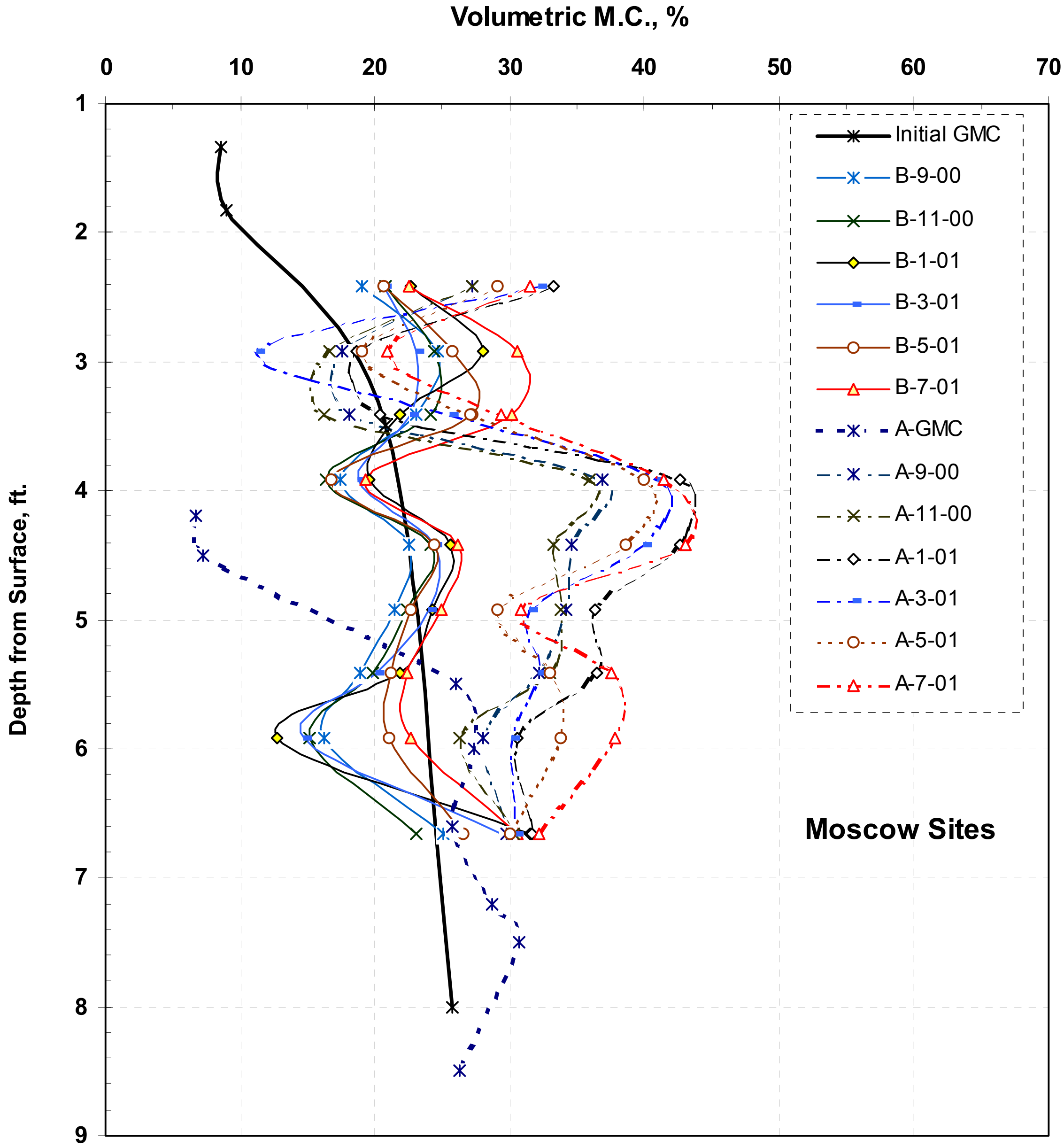

Figure 4.10 Subgrade Moisture Content versus Depth at Different Months for Moscow Sites

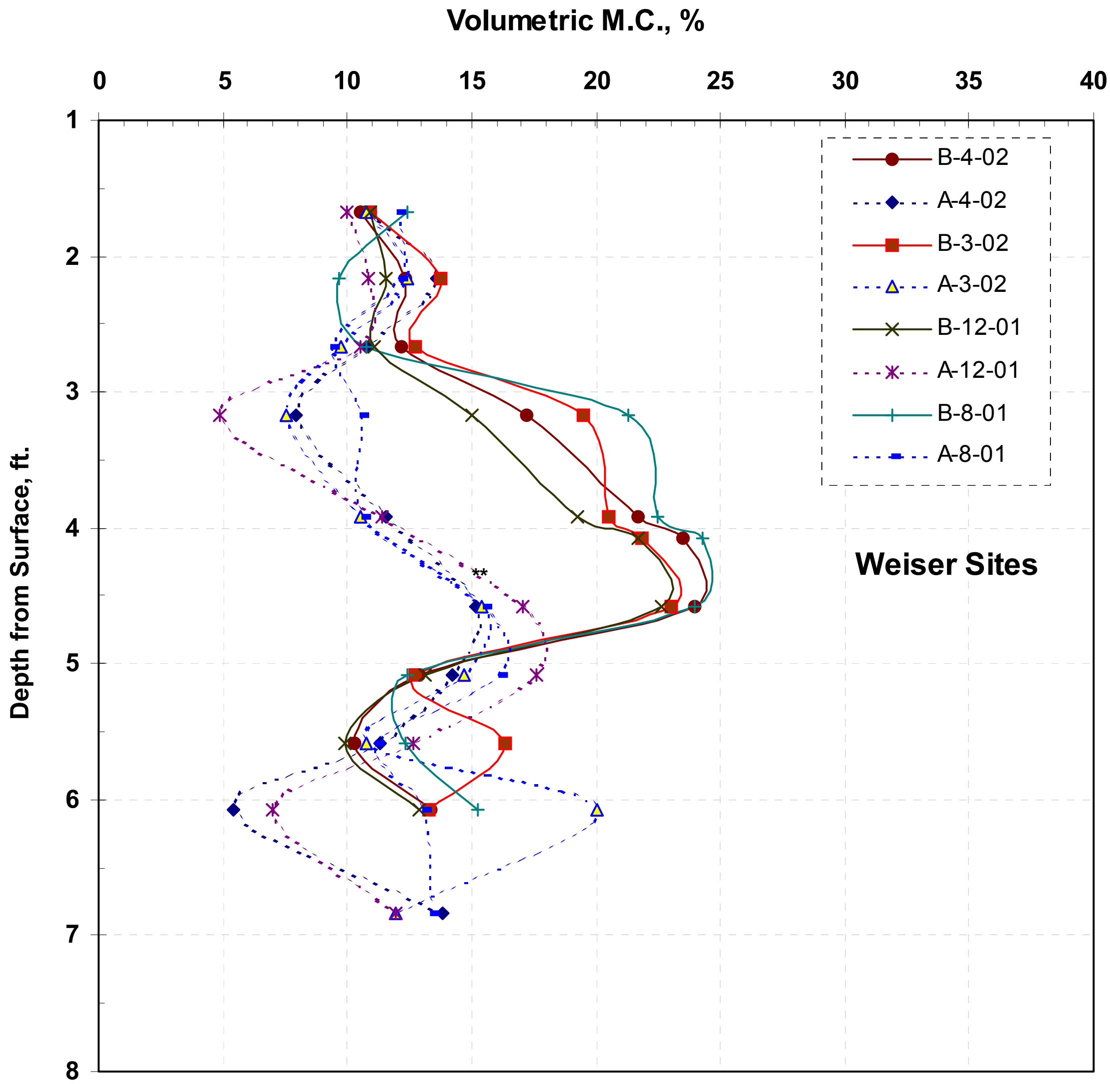

Figure 4.11 Subgrade Moisture Content versus Depth at Different Months for Weiser Sites

4.2 TEMPERATURE DATA ANALYSIS

It is well documented that seasonal variation of pavement temperature greatly affects its modulus. The relationships that govern such variation will be discussed in detail later in this study. In this chapter, the data collected at the Idaho sites are only presented for the purpose of investigating pavement temperature variation with time.

Figure 4.12 through Figure 4.14 show the variation of both air and mid-depth pavement temperatures for Moscow, Worley, Pack River, Lewiston, and Weiser sites respectively. The figures indicate that both temperatures follow a sinusoidal function with time; while the temperature increases during summer months it decreases significantly during winter months. The figures show also that the air temperatures sometimes is less or greater than the pavement temperature depending on the time of the day at which the temperature was recorded. For example, if the temperature is recorded in the morning, the air temperature is expected to be greater than pavement temperature. On the other hand, if the temperature is recorded in the afternoon, the pavement will be heated and the asphalt temperature will certainly exceed the air temperature. Both air and pavement temperature measurements for the Idaho sites will be used later in this study to validate a model for predicting pavement temperature from air temperature.

The average 30-year air temperature versus time for all sites is presented in Figure 4.15. The figure indicates the Lewiston site has the higher average air temperature, while the Pack River sites have the lower average air temperature. This average monthly temperature data, together with the rainfall data, will be used later in this study to specify the seasons and seasonal adjustment factors for each site.

Figure 4.16 and Figure 4.17 show the measured pavement temperatures versus depth at different months for the Moscow and Lewiston sites, respectively. Both figures show that the temperature increases with depth during winter months while it decreases with depth during summer months until it stabilize at the lower depth of about 7 feet. The temperature at the lower depth could be considered constant through the year. This constant value decreases when going upward if the surface temperature is cooler (during winter), while increases if the surface temperature is hotter (Summer).

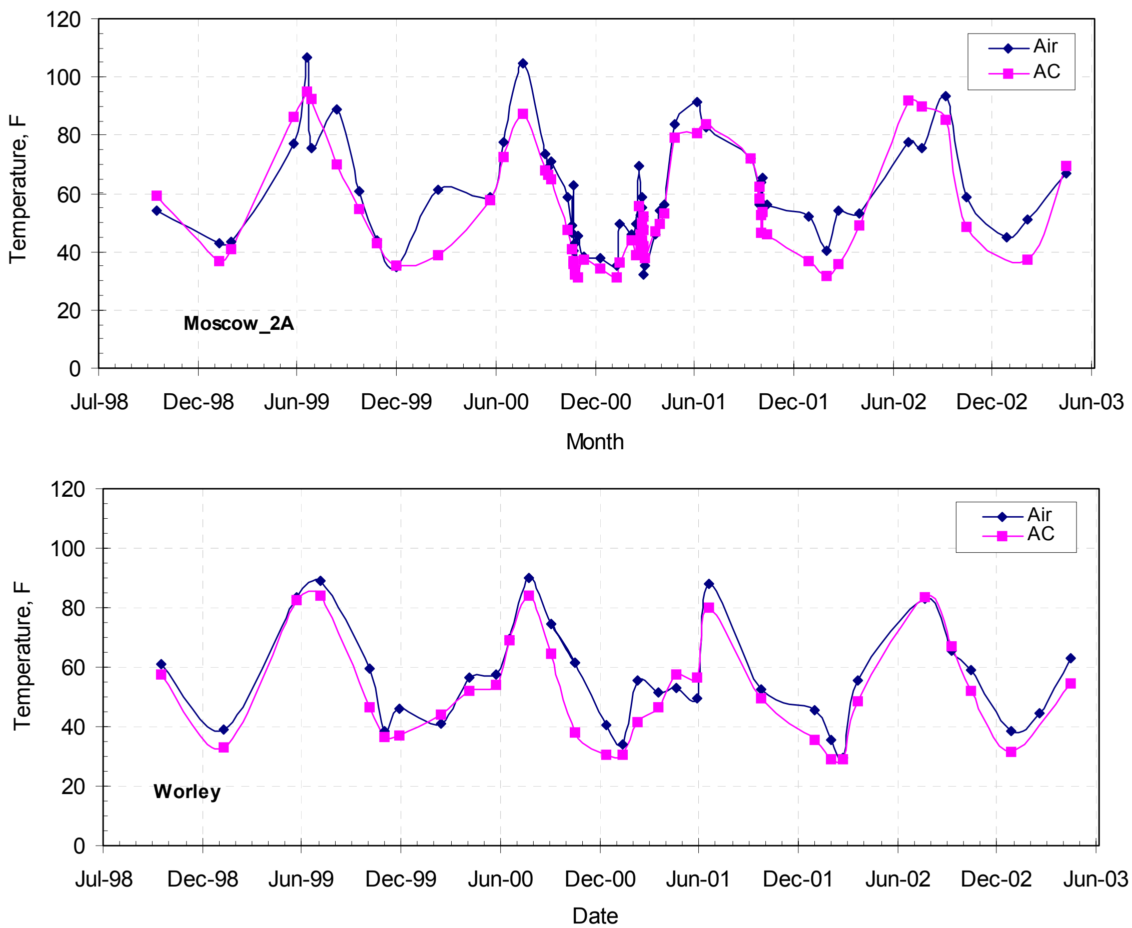

Figure 4.12 Pavement and Air Temperatures versus Time for Moscow and Worley Sites

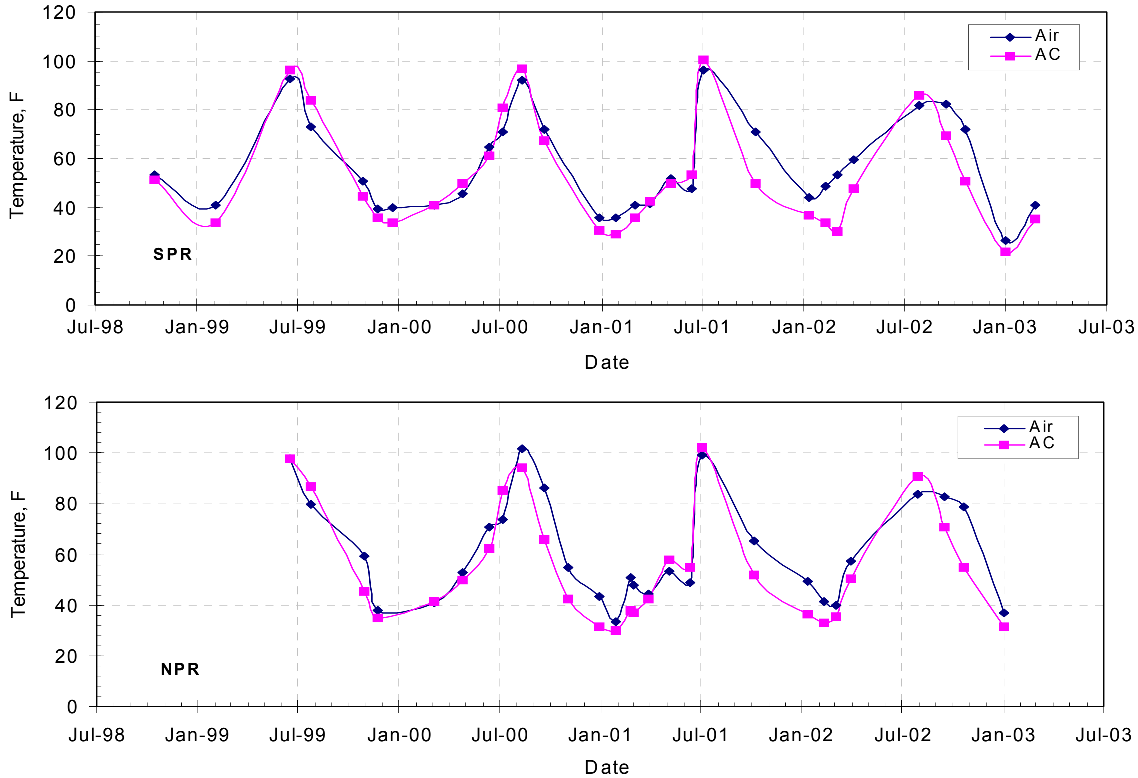

Figure 4.13 Pavement and Air Temperatures versus Time for Pack River Sites

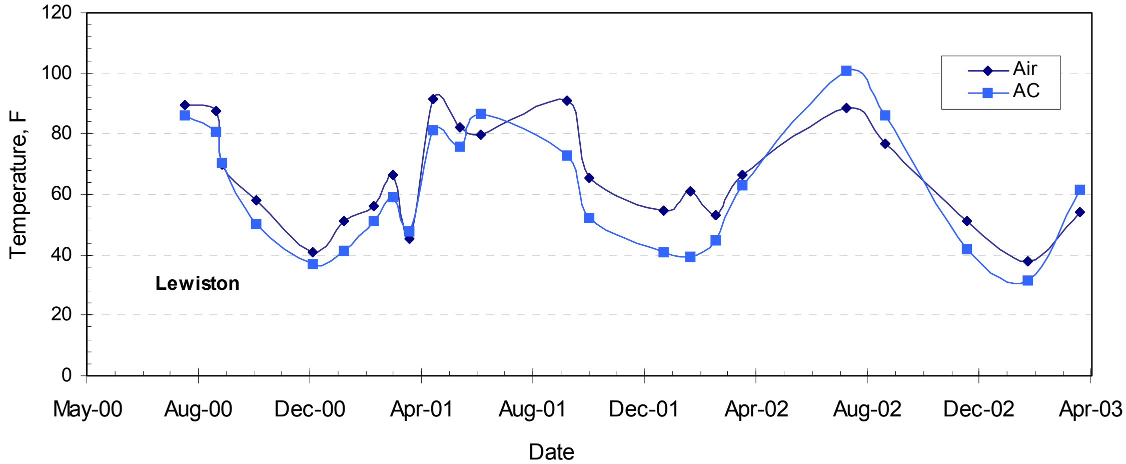

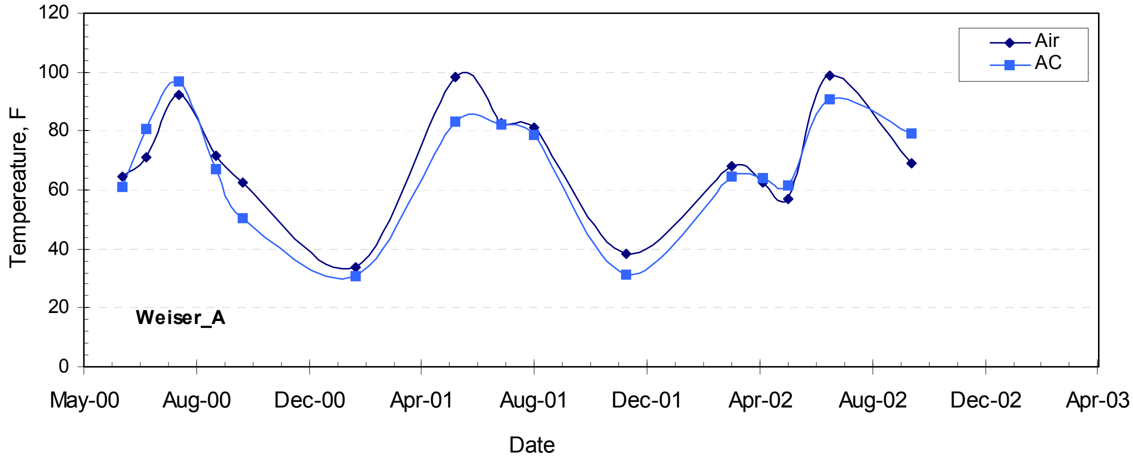

Figure 4.14 Pavement and Air Temperatures versus Time for Lewiston and Weiser Sites

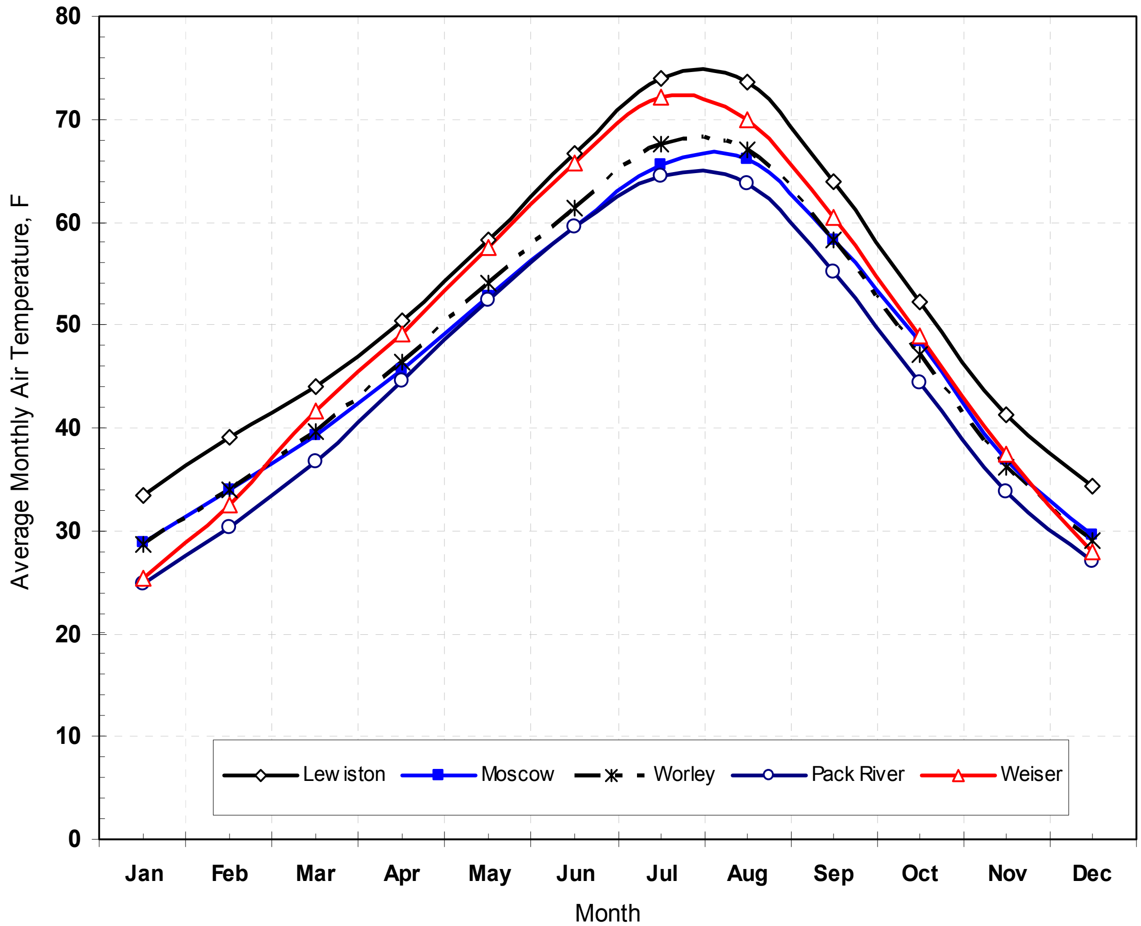

Figure 4.15 Average 30 Year Air Temperatures versus Time for All Sites

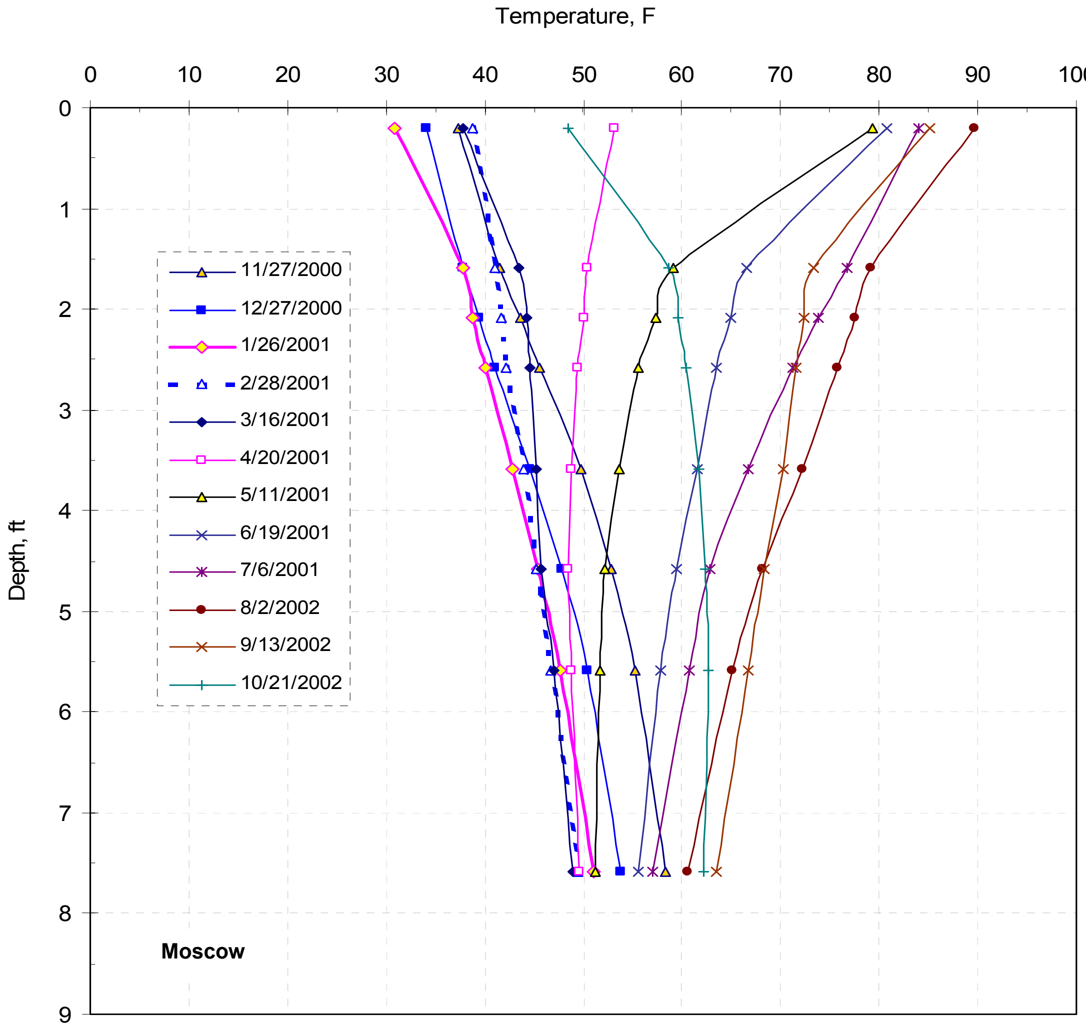

Figure 4.16 Measured Pavement Temperatures versus Depth at Different Months for Moscow Site

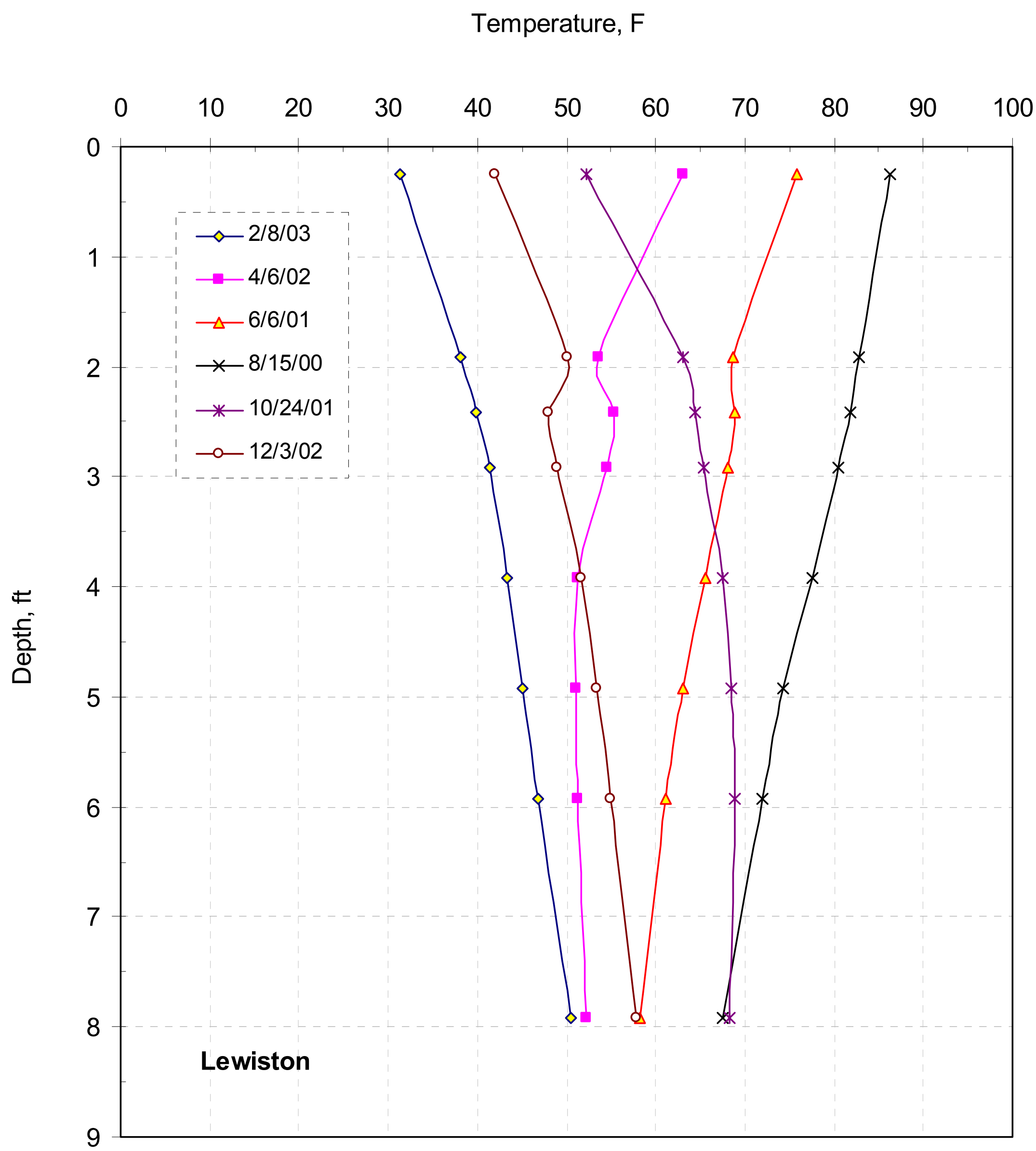

Figure 4.17 Measured Pavement Temperatures versus Depth at Different Months for Lewiston Site

4.3 EICM VALIDATION

This section describes the analysis of the Enhanced Climatic Model (EICM). The purpose of this analysis was to verify the EICM applicability to Idaho sites and determine whether it could be used to predict the impacts of the environmental changes on pavement layers in Idaho.

4.3.1 Input Data to the EICM

The broad categories of input data required by the EICM software are as follows.

- *Initialization data,* which define the analysis period, the geographic location of the site under consideration, and the time increments to be used in the simulation and reporting of the results.

- *Climatic boundary conditions,* including temperature, precipitation, wind speed, percent sunshine and water table depth data. Climatic data provided with the program may be used where site-specific weather data are not available.

- *Thermal properties,* which characterize the tendency of the pavement surface to absorb and emit heat, as well as the temperature range over which freezing and thawing occur.

- *Infiltration and drainage inputs,* which characterize both the extent of cracking in the surface, and the drainage characteristics of the base material and geometry.

- *Asphalt material inputs,* including layer thickness, mix design information, data defining the modulus-temperature relationship, and thermal characteristics.

- *Material properties,* including layer thickness, density, saturated permeability, and other data characterizing the base, subbase, and subgrade layers.

- *Initial profiles,* which characterize the temperature moisture conditions of the pavement on the first day of the simulation period.

The ECIM was employed to predict the subgrade moisture content and pavement temperature for the Moscow (2A), south Pack River (4A) and Lewiston sites. The predicted moisture and temperature data were then compared to the corresponding data collected at those sites. Since the GWL is a major input in the EICM, the Moscow and Pack River sites were selected because they are the only sites that have information about the GWL. For Lewiston site, the GWL is assumed to be approximately 10 ft below the surface, relative to the water level in the adjacent river.

The data used as input to the EICM for Moscow (2A), south Pack River (4A) and Lewiston (1) sites are summarized in Table 4.1. Most of the data required for moisture prediction can be obtained directly from the soil characterization tests and the site properties presented in Table 3.3. In general, when required input data by EICM were not available, default values were used.

Among the EICM input parameters shown in Table 4.1 is the linear length of cracks surveyed in a specified section length and the initial moisture content at the beginning of the analysis period. The crack length would affect the amount of water penetrating to the subgrade soil. Since there are more data points collected at the Moscow site than the other two sites, the Moscow site was considered for three EICM trials for moisture prediction, as shown in Table 4.1. In the first trial the crack length surveyed in a 100 feet long pavement section was assumed to be only 1.0 ft. For the second trail the crack length was assumed to be 100 ft. This was done to check if the crack length would affect the subgrade moisture prediction in the Moscow site. For the third trial, the initial moisture content at the beginning of the analysis period was entered as collected, while for the first two trials it had been left blank for EICM default.

Table 4.1 Input Parameters Used with EICM for Moscow, Pack River and Lewiston

Variable	Moscow (2A)			SPR	Lewiston
	Trail 1	**Trail 2**	**Trail 3**	**(4A)**	**(1)**
Initialization Data					
Year Modeled	2001	2001	2001	2001	2001
First Month	January	January	January	January	January
First Day	1	1	1	1	1
Length of Analysis period, days	365	365	365	365	365
Time increment for outputs, hrs	6	**6**	**6**	1	1
Time increment for calculations, hrs	0.5	**0.5**	**0.5**	0.5	0.5
Latitude	46.73	46.73	46.73	48.3	46.41
Longitude	116.9	116.9	116.9	116.5	117.03
Elevation	2660	2660	2660	2099	705
Climate/ Boundary Conditions					
Temperature and Rainfall	UI-Weather	UI-Weather	UI-Weather	Interpolation	Interpolation
Wind speed	UI-Weather	UI-Weather	UI-Weather	Interpolation	Interpolation
Water Table depths, ft	9.5	**9.5**	**9.5**	4.62	**10**
Thermal Properties					
Surface short wave Absorptivity	0.8	0.8	0.8	0.8	0.8
Time when min Tempr occur	4	4	4	4	4
Time when max Tempr occur	15	15	15	15	15
Upper Temper limit of freezing, F	32	32	32	32	32
Lower Temper limit of freezing, F	30.2	30.2	30.2	30.2	30.2
Infiltration and Drainage					
Linear length of cracks/joints, ft	1	100	100	100	100
Total survey length of cracks, ft	100	**100**	**100**	100	100
Base fines type	Inert filler	Inert filler	**Silt**	Silt	Inert filler
Base, % fines	2.5	2.5	2.5	5	2.5
Base, % gravel	70	70	70	60	70
Base, % Sand	27.5	27.5	27.5	36	27.5
One side base width, ft	25	25	25	15	12
Sloe ratio, %	1.5	1.5	1.5	1.5	1.5
Internal Boundary Conditions	Suction	Suction	Suction	Suction	Suction

Table 4.1 Continued

Variable	Moscow (2A)			SPR (4A)	Lewiston (1)
	Trail 1	Trail 2	Trail 3		
Asphalt Material properties (Layer1)					
Thickness, inch	4.8	4.8	4.8	6	6
No. of elements	3	3	3	2	3
Thermal conductivity, BTU/hr-Ft-0F	0.67	0.67	0.67	0.67	0.67
Heat capacity, BTU/Ft-0F	0.22	0.22	0.22	0.22	0.22
Total unit weight, PCF	148	148	148	148	148
Layer 2					
Layer type	A-1-a	A-1-a	A-1-a	A-1-b	A-1-a
Thickness, inch	27.6	27.6	27.6	24	20
No. of elements	5	5	5	4	5
Porosity	0.25	0.25	0.25	0.25	0.25
Gs	2.65	2.65	2.65	2.66	2.65
Saturated permeability, ft/ hr	1000	1000	1000	100	1000
Dry unit wt, PCF	120	120	120	135	120
P # 4	3	3	3	40	3
PI	0	0	0	1	0
P # 200	0	0	0	2	0
D60, mm	37.5	37.5	37.5	2	37.5
Initial moisture content, %	--	**--**	**21**		**20**
Layer 3					
Layer type	A-4	A-4	A-4	A-2-4	A-4
Thickness, inch	240	240	240	240	240
No. of elements	12	12	12	40	12
Porosity	0.38	0.38	0.38	0.28	0.38
Gs	2.71	2.71	2.71	2.68	2.71
Saturated permeability, ft/ hr	0.0001	0.0001	0.0001	1	0.0001
Dry unit wt, PCF	110	110	110	122	110
P # 4	100	100	100	100	100
PI	8	8	8	0	1
P # 200	98	98	98	29.5	62
D60, mm	0.05	0.05	0.05	0.1	0.05
Initial moisture content, %	-	**---**	**35**		**30**

4.3.2 Moisture Prediction Using EICM

Figure 4.18 show the measured moisture content compared to the EICM predicted one for the Moscow site, at 5.5 ft depth. The figure presents the results of the three trails previously discussed and presented in Table 4.1. The three trials included assuming both a 1ft crack length, a 100 ft crack length and the initial moisture content. The figure shows that the EICM predicted moisture for the three trails are coinciding with each other. This indicates that there is no significant difference in the EICM moisture predicted when changing the crack length and considering the initial moisture content.

The results of Figure 4.18 and Figure 4.19 show very poor correlations between the predicted and measured moisture content at the three sites. The figures indicate also that the EICM overestimate the moisture contents for both Moscow and Lewiston sites while it underestimates the moisture in the Pack River site. The reason for this will be discussed later in this chapter. Furthermore, unlike the collected data, the EICM output does not show seasonal fluctuation in the predicted moisture content at all sites.

Figure 4.21 and Figure 4.21 show the measured versus EICM predicted moisture content profiles for both Moscow and Pack River sites. The difference between the predicted and measured moisture content profiles could be related to the EICM assumptions for moisture prediction, which will be discussed later in this chapter. The figures show also that the EICM assumes that the moisture content is constant below a certain depth, which is close to the GWL. Then, this constant moisture content reduces gradually when going above the GWL, as will be discussed later in this chapter.

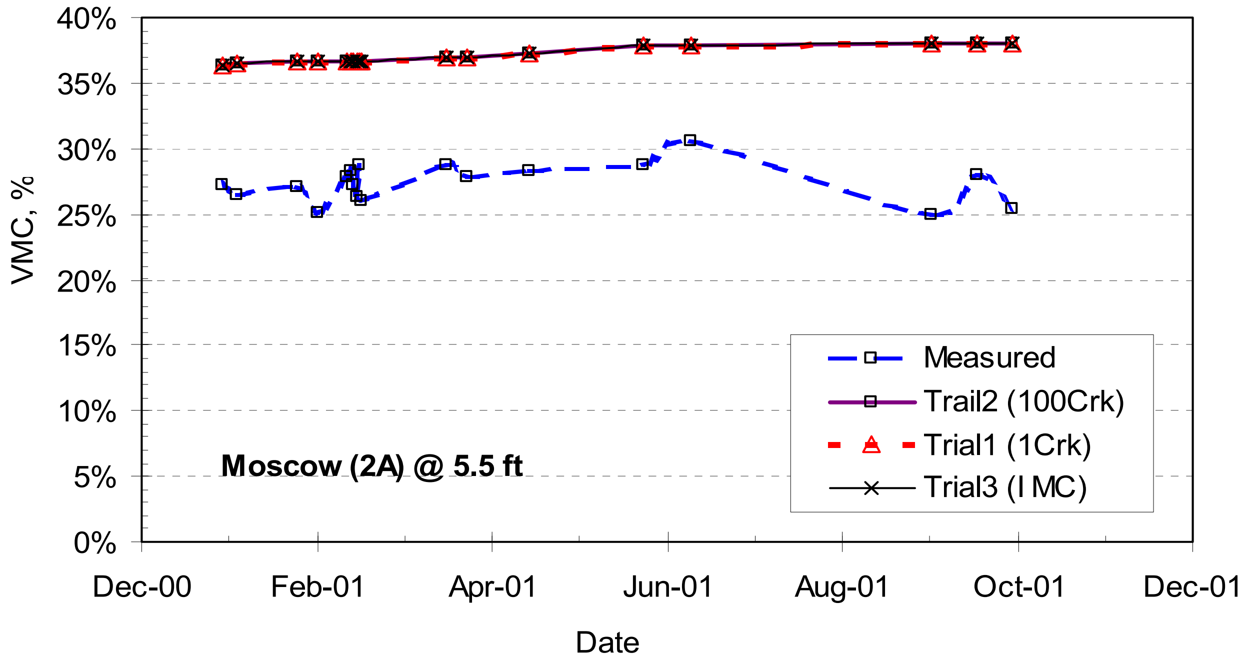

Figure 4.18 Measured vs. EICM Predicted Moisture Contents for Moscow Sites, at 5.5 ft Depth

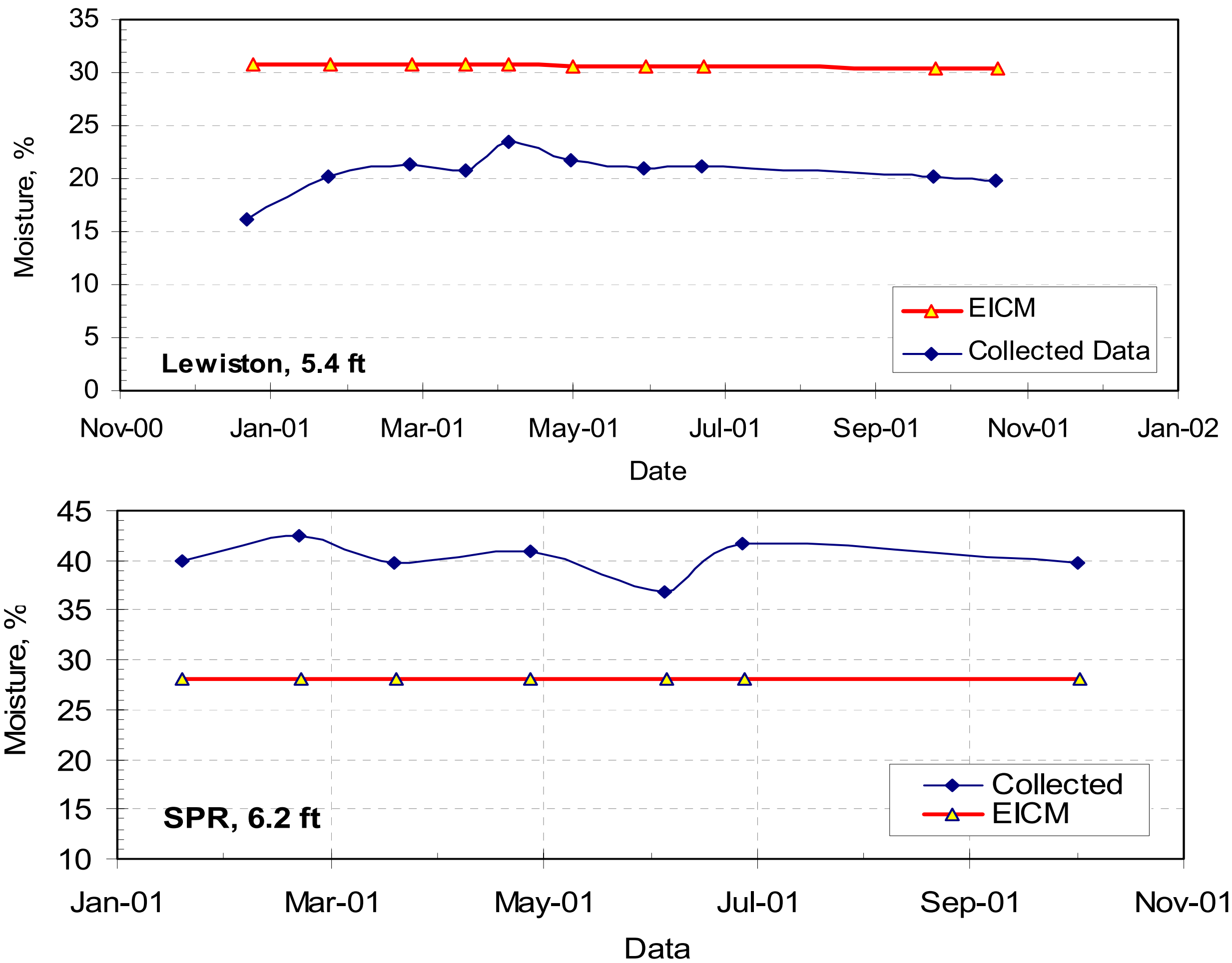

Figure 4.19 Measured vs. EICM Predicted Moisture Contents for Lewiston and SPR Sites

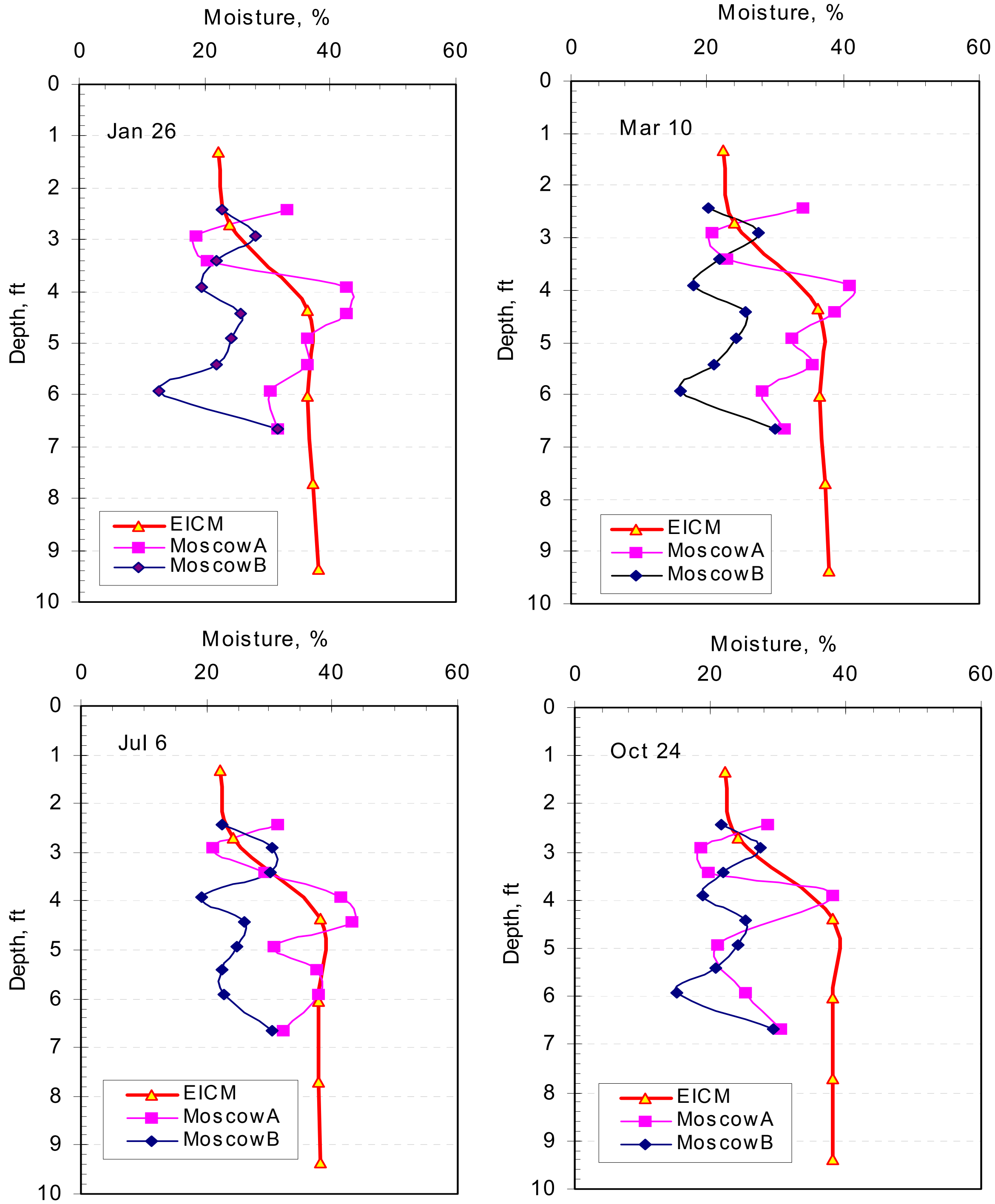

Figure 4.20 Measured vs. EICM Predicted Moisture Profile for Moscow Sites

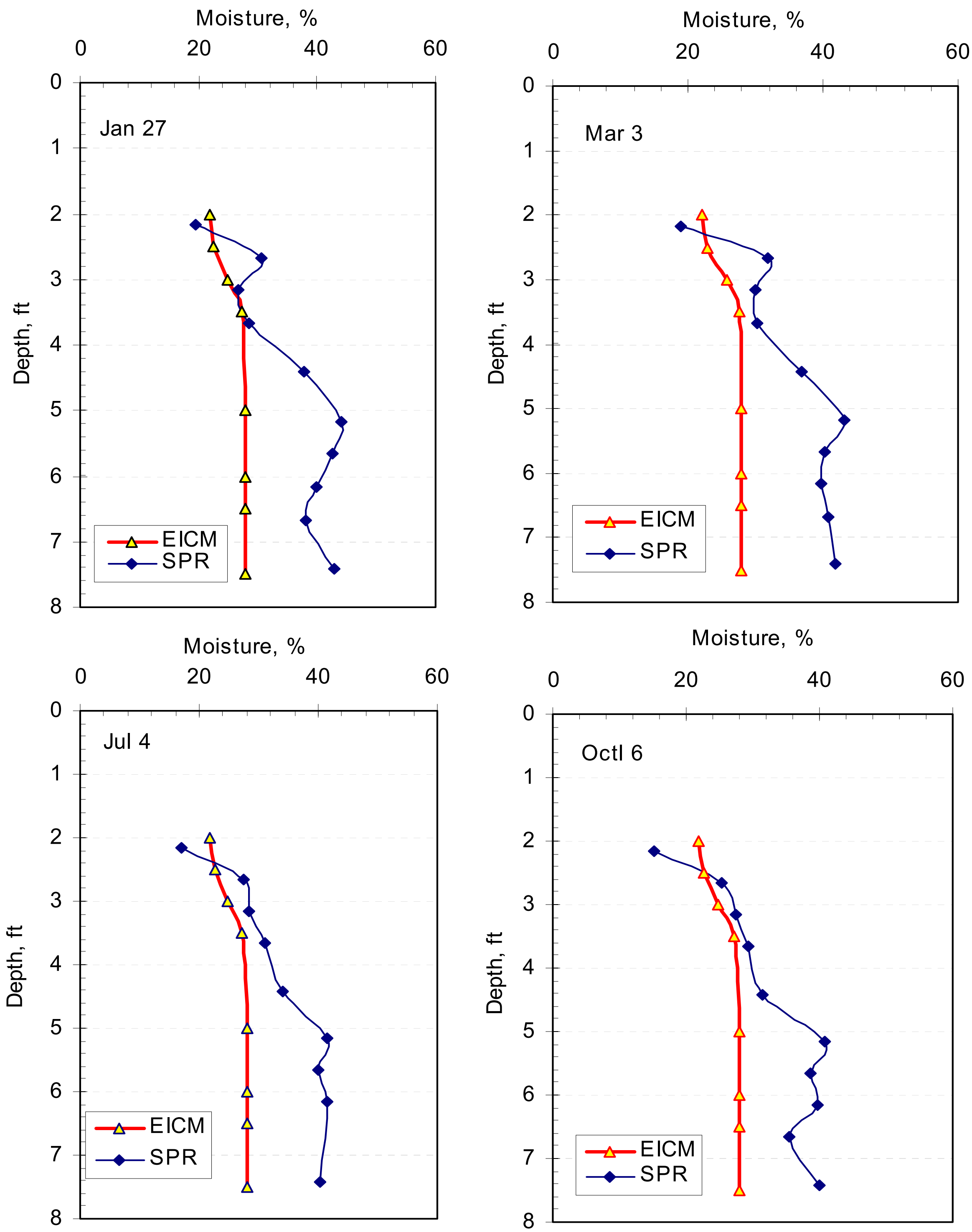

Figure 4.21 Measured vs. EICM Predicted Moisture Profile SPR Site

4.3.2.1 *EICM Moisture Prediction Procedures*

The EICM predicts the moisture content based on the soil water characteristic curve (SWCC). Several mathematical equations have been proposed to represent the SWCC. Most of the equations are empirical in nature and are based on the measured SWCCs. As explained in Chapter 2, the EICM uses the Fredlund and Xing (1994) equation, to predict the volumetric moisture content (θ_w) from the soil matric suction (h) as follows:

$$\theta_w = C(h) x \left[\frac{\theta_{sat}}{\left[\ln \left[\exp(1) + \left(\frac{h}{a} \right)^b \right] \right]^c} \right] \tag{2.13}$$

$$C(h) = \left[1 - \frac{\ln\left(1 + \frac{h}{h_r}\right)}{1 + \left(\frac{10^6}{h_r}\right)^b} \right] \tag{2.14}$$

To predict the volumetric moisture content (θ_w), the soil suction or SWCC should be known. Zapata et al. (1999) found that if a single soil sample were sent out to a dozen laboratories across the country for SWCC measurement, the results would show great variability. Therefore, the authors of EICM version 2.6 (Witczak et al., 2000) concluded that soil suction and SWCCs simply couldn't be measured with great precision at the present time. They also added that it is difficult to develop a predictive model for SWCCs that is consistent with all of the SWCCs reported in the literature because of the fairly high probability that any given measured SWCC has significant experimental error associated with it. Therefore, they concluded that the SWCC could probably be estimated from D60 or wPI about as accurately as it can be measured, unless the laboratory or person making the measurement is highly experienced.

Zapata et al. (1999) statistically correlated the fitting parameters of the previous Fredland and Xing (1994) equation to well-known soil properties (wPI & D60). These fitting parameters were also incorporated into the new version of EICM (Witczak et al., 2000).

To find these fitting parameters, the soils were divided into two categories; soils having a plasticity index (PI) greater than zero and those having a PI equal to zero. The data assembled for the soils with PI greater than zero included the percentage passing #200 sieve and the Atterberg limits, particularly the plasticity index. The reasoning behind this choice, as explained by Zapata et al. (1999) is as follows. The equilibrium at a given degree of saturation was expected to be proportional to the specific surface area of the soil. The PI is a fair indicator of the surface area. However, a soil with a small percentage of highly active clay would have a high PI but only a moderate surface area. Therefore, the use of the weighed PI, wPI, was considered a better indicator of soil particle surface area available for water absorption and retention. The wPI value was used as the main soil property for correlation in plastic soils (PI> 0). For non-plastic soils (PI = zero), the diameter D_{60} was the main soil property used for correlation.

For Plastic Soils (PI > 0):

The Fredlund and Xing fitting parameters in Equations 2.13 & 2.14 (parameters a, b, c, and h_r,) were correlated with the new wPI parameter through the following (Equations 2.15 to 2.19, Chapter 2):

$$wPI = \%Passing\ \#200 \times PI \quad (2.19)$$

$$a = 11 + 4\,(wPI) + 0.00364(wPI)^{3.35} \quad (2.15)$$

$$c = 0.5 + 0.0514\,(wPI)^{0.465} \quad (2.17)$$

$$b/c = 5.0 - 2.313\,(wPI)^{0.14} \quad (2.16)$$

$$h_r/a = 32.44e^{0.0186\,(wPI)} \quad (2.18)$$

The other main parameter in the Fredlund and Xing (1994) equation, which primarily affects the moisture prediction, is the saturated volumetric water content (θ_{sat}). The saturated volumetric water content is also called porosity, which is the ratio between the volume of voids (equals to the water volume, for saturated soil) divided by the total volume. If the saturated volumetric water content is unknown, Zapata et al. (1999) suggested the use of the following correlation:

$$\theta_{sat} = 0.36 + 0.0143\,(wPI)^{0.75} \tag{2.20}$$

<u>For Non-Plastic Soils (PI = 0)</u>

For granular soils with Plasticity Index equal to zero, the parameter used to relate to the SWCC was the Diameter D_{60} from the grain-size distribution (GSD) curve. The correlations found are as follows:

$$a = 0.8627(D_{60})^{-0.751} \tag{2.22}$$

$$b' = 7.5 \tag{2.23}$$

$$c = 0.1772 \,\mathrm{Ln}\,(D_{60}) + 0.7734 \tag{2.24}$$

$$h_r/a = 1/(D_{60} + 9.7\,e^{-4}) \tag{2.25}$$

Zapata et al. (1999) did not find correlation between the 'b' parameter and D_{60}. Therefore, a constant average b value was suggested. In those cases where the θ_{sat}, is unknown, the following average value was recommended for soils with PI equal to zero:

$\theta_{sat} = 0.36$

Finally, to apply Fredlund and Xing (1994) the only unknown left is the matric suction (h). Witczak et al. (2000) reported that the matric suction (u_a - u_w) can be assumed equal ($D\,\gamma_w$), where D is the distance from the GWL. They also added that this assumption is probably fairly accurate in most cases, when the GWL is shallow.

4.3.2.2 *Moisture Content Prediction Based on Soil Suction*

The previous analysis showed that the EICM simply predicts the moisture content based on the saturated volumetric moisture content (θ_{sat}) and soil suction. The soil suction, in turn, depends on the distance from the GWL. Therefore, in order for the EICM to reflect the seasonal variation in moisture content, the seasonal variation in the GWL should be provided.

The previous equation by Fredlund and Xing (1994), Equation 2.13, for moisture content prediction is programmed in a spreadsheet to predict the moisture variations in the Moscow (2A) site. The equation fitting parameters were related to the subgrade soil properties (wPI) according to Zapata et al. (1999), as explained before. The saturated volumetric moisture content (θ_{sat}) is considered 30 %, based on the collected moisture data for the Moscow site at the lowest TDR sensor, Figure 4.10. The distance from the GWL (D) is considered variable based on the measured GWL at various seasons. The soil suction considered equals D $\gamma_{w,}$ based on Witczak et al. (2000).

The output of this analysis is presented in Figure 4.22. The figure indicates that the predicted moisture content shows a little seasonal variation relative to the variation in the GWL. The figure shows also that the predicted moisture content is closer to the measured moisture content. The reason is simply because the actual measured saturated volumetric moisture content (θ_{sat}) was considered, not the EICM default value. The EICM default values for θ_{sat} or porosity are based on the soil type and are presented in Table 4.1 for each sites. These values for Layer 3 are 0.38, 0.38 and 0.28 for Moscow, Lewiston and South Pack river sites respectively. These values are very close to the EICM predicted moisture in Figure 4.18 and Figure 4.19.

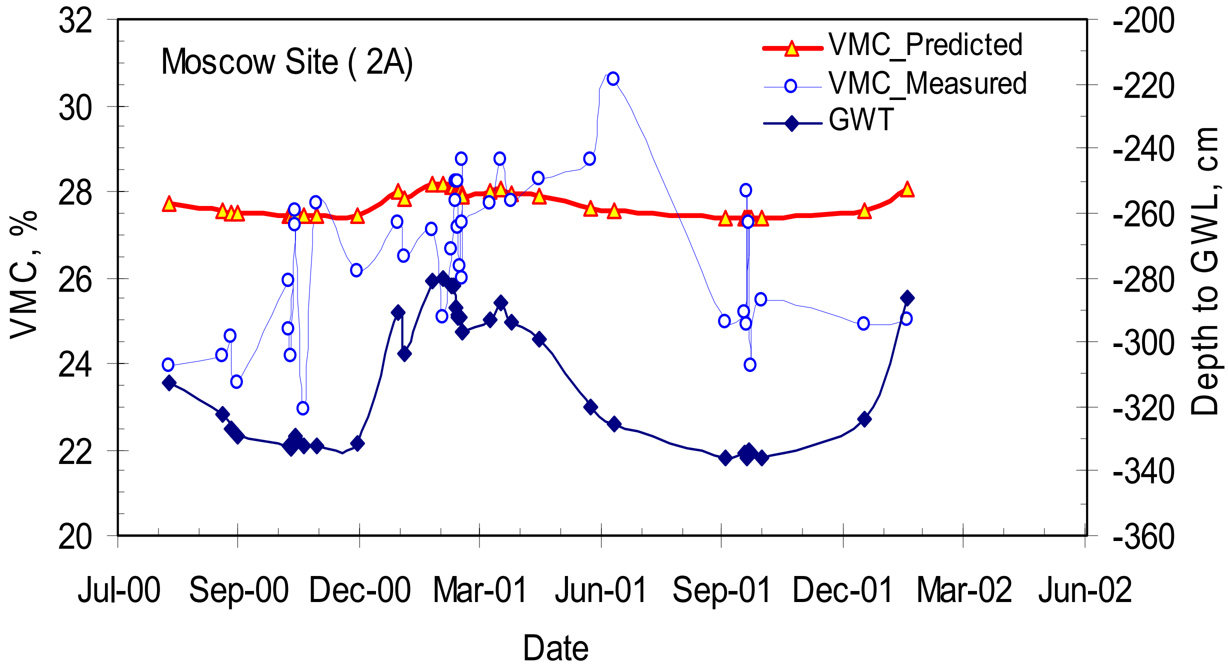

Figure 4.22 Modeling Subgrade Moisture Based on Soil Suction

4.3.2.3 *Explanations for the Disagreement between EICM Predicted and TDR Measured Moisture Content*

There are several possible explanations for disagreement between EICM predicted and TDR measured values of the moisture content as follows:

1- Difficulty in simulating the moisture variations:

Drumm and Meier (2003) demonstrated that the variation of soil moisture is very complicated. That is because of the influence of a number of factors such as soil type, precipitation, location of the GWL, solar radiation, and the topography. The interaction of soil moisture changes between the unsaturated zone and saturated zone, together with precipitation and evaporation, makes the properties of the unsaturated zone very complicated. They also added that, for most cases, it is not appropriate to predict the variation of soil moisture with an analytical model, which can include all the processes like infiltration, drainage, evaporation and heat transfer. Instead, the variation of soil moisture can be obtained from in-situ measurements, and then regression methods are used to find the correlation between the soil moisture variation and environmental factors.

2- Errors in the assumptions of reflecting the environmental conditions:
For developing the EICM, Lytton et al.(1993) proposed the following assumptions in considering the upper boundary conditions for moisture predictions:

- If the surface temperature is below freezing: It is assumed that there is no flow of water into the soil. While this may be a good assumption during freezing period, but it does not take into account the accumulated snow, which will transform into water during the thaw period

- When there are no frozen zones in the soil column: Once more, no flow is assumed to penetrate the upper surface, requiring a zero gradient boundary condition. This assumes that the pavement overlying the subgrade is impervious. While this is a convenient assumption, it is not usually a realistic one.

- If the surface temperature is at the "freezing point depression," temperature or above: Thawing is in process, and a frozen zone exists below the surface. A positive pore water pressure converted into centimeters of water is set as the upper surface boundary condition to simulate the pressure applied to the surface of a subgrade by an overlying pavement.

Furthermore, Drumm and Meier (2003) reported that the ID model, which accounts for the precipitation and infiltration, is not used in the direct calculation of the subgrade moisture. The subgrade moisture is determined only as a function of the distance above the water table.

Thus, the ID model only applies to sites with a high water table. For sites with a low water table, this model would result in unreasonably low and relatively constant moisture content, even if the subgrade were subjected to climatic variations. In addition, for pavement sites with a shallow water table, soil suction may not vary linearly with distance from the water table as calculated from hydrostatic pressure. For example, the existence of a coarse gravel layer right above the water table would provide a capillary break.

3-Errors in the SWCC:
Witczak et al (2000) reported that a substantial error in the position of the SWCC will produce a corresponding error in the predicted moisture content because the EICM simply computes the equilibrium suction as D γ_w, where D is the distance to the GWL, and enters the SWCC with suction to get θ.

4- Error in the matric suction assumption (u_a - u_w = D γ_w):
Witczak et al (2000) also reported this assumption is probably fairly accurate in most cases, when the GWL is shallow. However, some research indicates that the assumption is not good, particularly when the water table is deep.

5- Errors in the TDR values:
The known weak correlations between TDR measured moisture contents and lab measured moisture contents illustrate that the value from any particular TDR probe could be substantially in error.

4.3.3 Temperature Prediction Using EICM

The EICM was employed to predict the AC mid depth temperature and the temperature profile for the Moscow, Pack River and Lewiston sites. The predicted temperature data were compared to the corresponding data collected at those sites. The results, shown in, **Figure 4.23** demonstrate good correlations between the measured and predicted pavement temperatures at both sites. The coefficient of determination between the predicted and measured pavement temperature was found to be 0.85, 0.93 and 0.95 for the Moscow, Pack River and Lewiston sites respectively. Figure 4.24 also shows good correlations between the predicted and measured temperature profiles for the Moscow site.

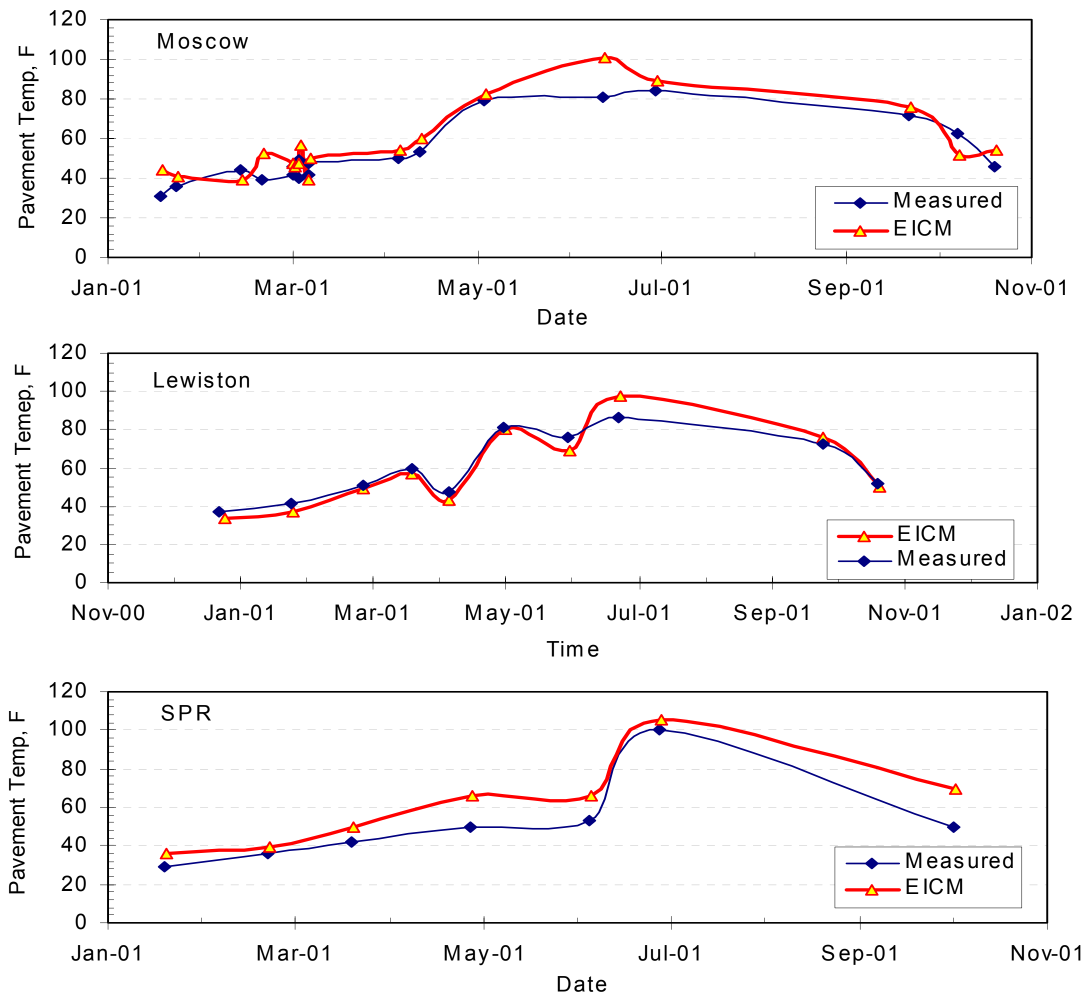

Figure 4.23 Measured and EICM Modeled Pavement Temperature vs. Time

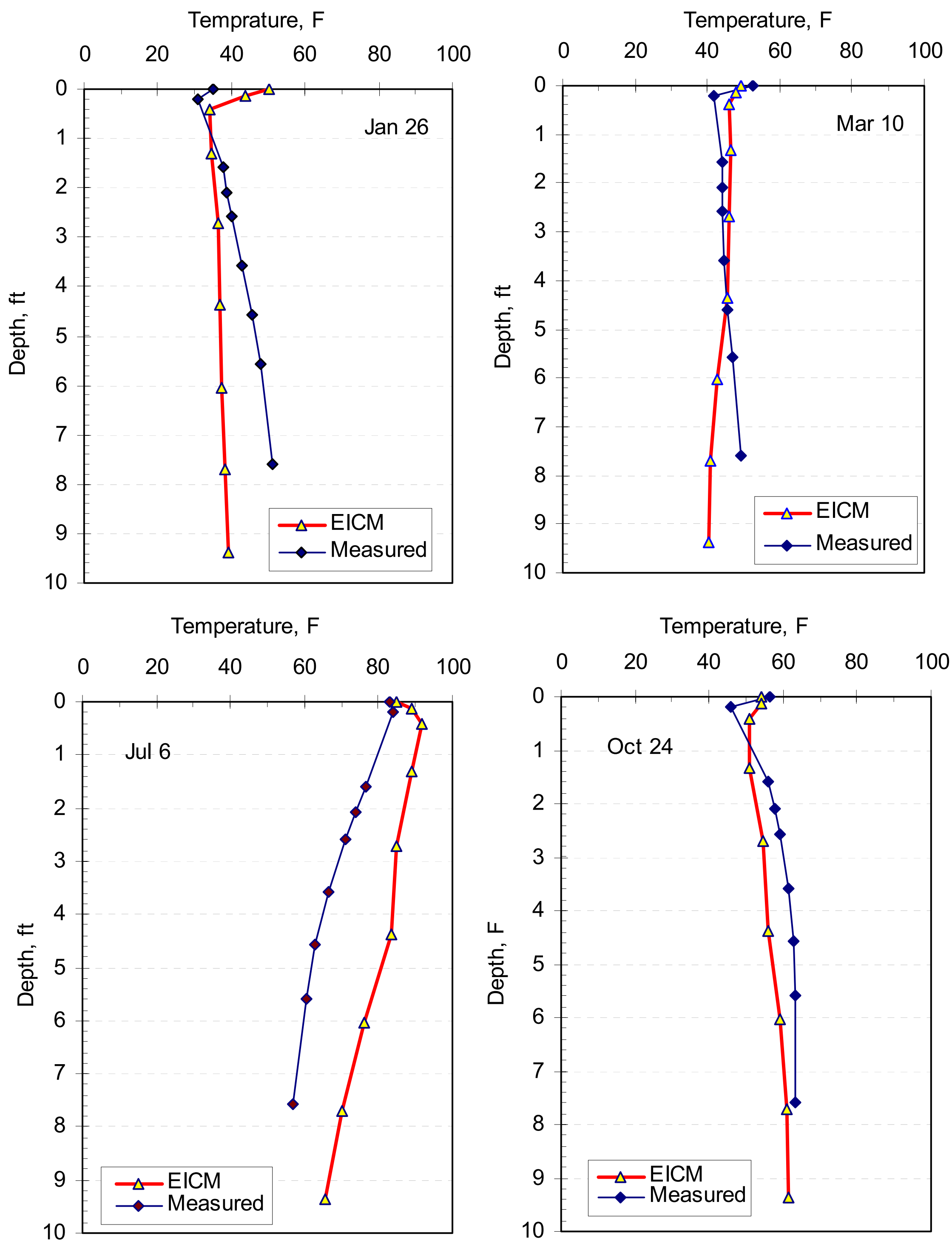

Figure 4.24 Measured versus EICM Modeled Temperature Profile, Moscow Site

4.4 SUMMARY

The findings described in this chapter are summarized in the following points:

- The moisture contents measured at most of the Idaho sites showed long-term equilibrium with little seasonal fluctuation. The seasonal variation ranged from +/- 2 % to about +/- 10% from the average value.
- The seasonal variation in subgrade moisture content could be related to the rainfall amount, the level of the GWL, and soil type (fine or coarse, plastic or non-plastic).
- In order for the rockcap layer to show its effectiveness in draining the water out of the pavement system, it should be connected to a daylight drainage layer (open to a side ditch), as shown in Weiser sites. However, in a closed system like the one in Moscow, the water may seep vertically through the layer voids and cause an increase in subgrade moisture.
- The change in subgrade moisture under base and rock cap is noticed only at shallow depths just below the base or rock cap layer. At deeper depths, there was no significant difference in the moisture content under base and rock cap layers, where the moisture reaches equilibrium.
- The application of the EICM to some of the Idaho sites showed good correlations in temperature predictions while it did not show good correlations between the predicted and measured moisture contents when using the EICM default values.
- The analysis of the EICM moisture prediction showed that the main factors affecting the moisture predictions are the GWL and the saturated volumetric moisture content. The analysis showed also that the crack length in the pavement section, which reflects rainfall amount or seasonal variation, has insignificant effect in moisture prediction in the selected sites. In addition, the analysis showed that the EICM can only predict the seasonal variation in moisture content if the actual seasonal variation in the GWL at each season is known.
- It is recommended that the model be applied to more sites having different types of subgrade soil and variable GWL to support these conclusions.

5. SUBGRADE MODULUS - MOISTURE DATA ANALYSIS FOR LTPP SITES

This chapter addresses the seasonal variation of the subgrade resilient modulus with the change in moisture content at various seasons. The analysis in this chapter is based on data collected at the LTPP sites in the non-freeze zones.

5.1 SELECTED DATA

The research approach described in this chapter was to select LTPP-SMP sites that represent various soil categories and use the backcalculated modulus and gravimetric moisture content data to develop regression models for the modulus-moisture relationships for various soils. Three regression models were developed to relate the variation in modulus with the variation in soil moisture content at various seasons. These models incorporate site conditions like the in-situ dry density and in-situ overburden stress, and soil properties such as soil plasticity index, percent fines as indicated by percent passing sieve 200, and soil particle size for 60% passing, D60. A model for determining the SAF was also developed.

The selected sites were placed in two groups, sites for plastic soils (LTPP sites 48-4143, 13-1005, and 48-1122), and non-plastic subgrade soil (LTPP sites 24-1634, 48-1077 and 35-1112. In the following discussions, the sites will be referred to by their serial numbers (1 through 6), shown in Table 5.1. The data were analyzed to investigate the changes over time (time series analysis), and to develop models for modulus prediction for both types of soil groups. In addition, a generalized model for the seasonal adjustment factor was developed.

Table 5.1 Selected LTPP Sites and Subgrade Soil Characterizations

LTPP Sites	1	2	3	4	5	6
	48-4143	13-1005	48-1122	24-1634	48-1077	35-1112
Location	Texas	Georgia	Texas	Maryland	Texas	New Mexico
Surface Type	Rigid	Flexible	Flexible	Flexible	Flexible	Flexible
Minimum Monthly Avg. Air Temp, C°	9.7	8.7	9.7	1.7	3.6	5.8
Soil Type as Identified by LTPP	Lean Inorganic Clay	Fine Clayey Sand	Coarse Clayey Sand	Fine Silt	Fine Sandy Silt	Coarse, poorly graded sand
AASHTO Soil Classification	A-7-6	A-6	A-2-6	A-4	A-4	A-3
% Passing # 4	-	-	99	99	94	100
% Passing # 10	-	-	97	98	93	99
% Passing # 40	-	-	75	98	87	94
% Passing # 200	90	38.4	6.5	97.9	51.8	2.7
D60, mm	-	-	0.3	0.012	0.1	0.18
Liquid Limit, %	41	27	26	-	-	-
Plasticity Index, %	23	12	12	NP	NP	NP
Max. Dry Density, gm/cm^3	1.730	2.05	1.858	1.746	1.906	1.698
Optimum Moisture, %	15.0	10.0	8.0	12.0	10.0	12.0
In-Situ Dry Density, gm/cm^3	1.719	1.826	1.850	1.789	1.723	1.641
Overlying Pavement Thickness, cm	51.3	42.7	70	54.4	40	31.2
Overburden Stress, gm/ cm^2	110	88	136	104	84	65

5.2 MOISTURE AND MODULUS VARIATION WITH TIME

Time series plots for the relationship between both gravimetric moisture content and subgrade backcalculated modulus for the different sites considered in this study are presented in Figure 5.1. The data indicate that both moisture content and backcalculated elastic modulus have almost a sinusoidal function with time. The data also indicate that the backcalculated elastic modulus could be related to moisture content in an inverse function. It increases when the moisture decreases, and vice versa. This correlates with the data obtained by Ali and Parker (1996).

The same behavior was observed at all sites except site 35-1112, where the modulus showed an increasing function with increasing moisture content. Careful analysis of the data showed that the subgrade soils at that site had recorded field moisture contents that were below the lab optimum moisture content. Since the soil is granular (coarse, poorly graded sand) and is non-plastic, it is most likely that the field condition was on the dry side of the optimum, which may lead to an increase in the modulus with the increase in moisture content until near the optimum.

The results for sites 24-1634 and 13-1005 in Figure 5.1 indicate that the maximum modulus values and minimum moisture values are recorded through the summer season (July and August), while the minimum modulus values and maximum moisture values are recorded through the winter (January and February). Figure 5.2 shows the moisture content and the average monthly rainfall for 3 different sites. The figure indicates that the moisture change is generally associated with the average monthly rainfall.

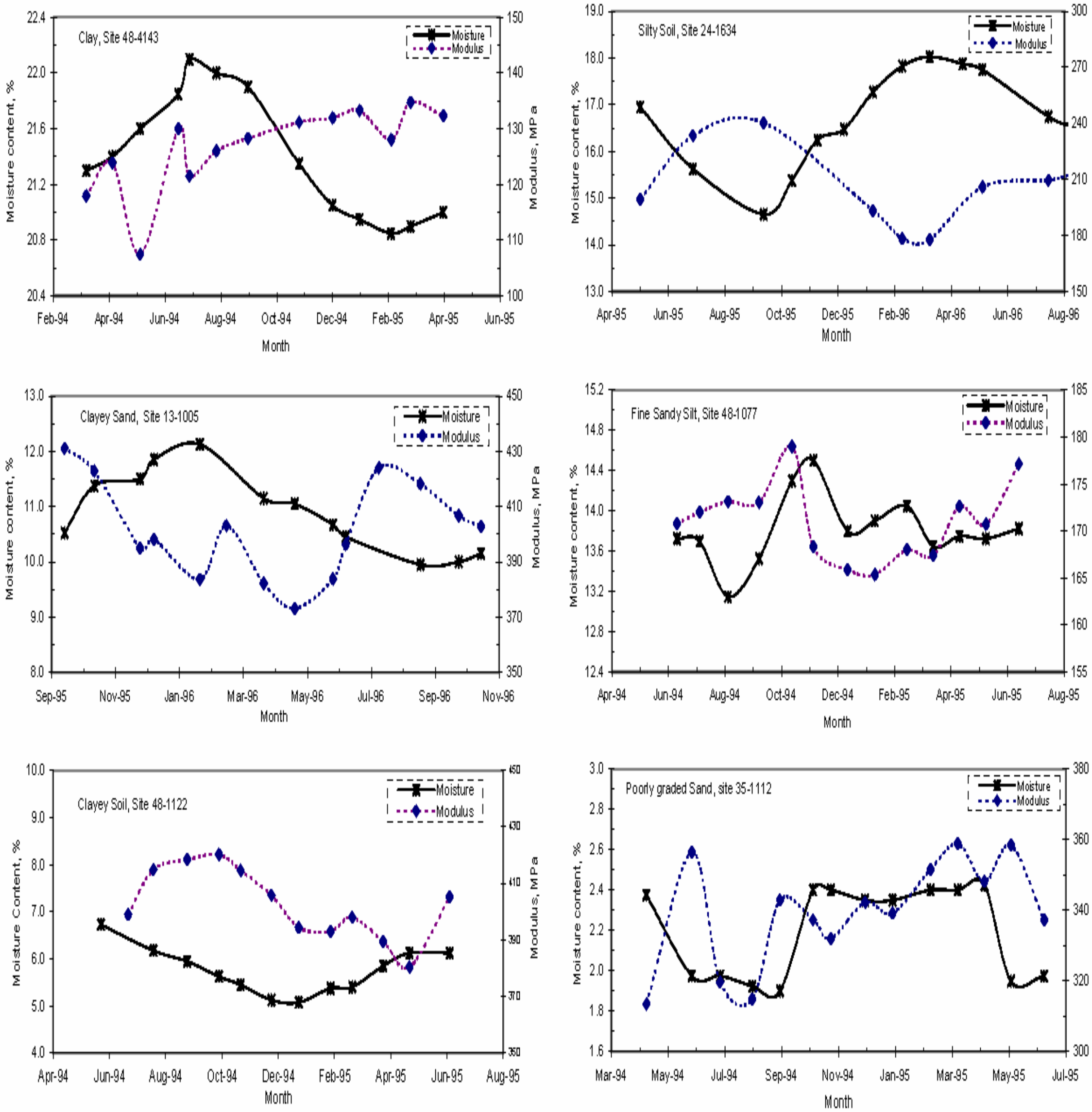

Figure 5.1 Seasonal Variation of Modulus and Moisture for Various Soil Types

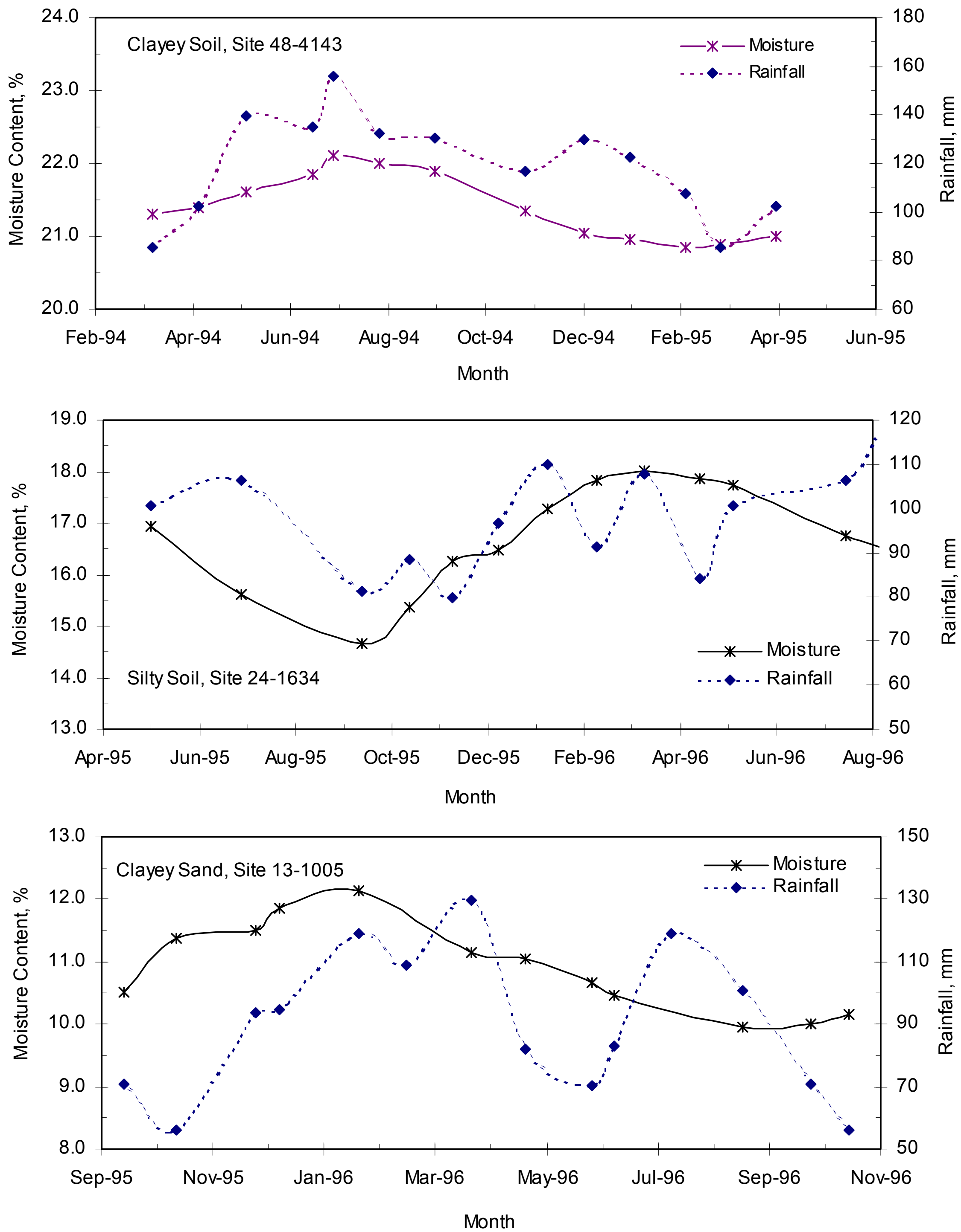

Figure 5.2 Moisture and Rainfall Variation with Seasons

5.3 SUBGRADE MODULUS-MOISTURE RELATIONSHIP

5.3.1 Model Development for Plastic Soils

Previous laboratory studies by Carmichael and Stuart (1985) and Hudson et al. (1994), discussed in Chapter 2, showed that the soil resilient modulus could be related to the moisture content and the soil properties such as soil fine content (F) and the plasticity index (PI). In this study, multiple regression analysis techniques were applied to relate the backcalculated elastic modulus to subgrade moisture content and other soil properties such as Atterberg limits and percentage passing sieve # 200. Data from the first three LTPP sites (48-4143,13-1005 and 48-1122) were used in this analysis. The subgrade soils at these three sites are clay, fine sandy clay and coarse sandy clay, respectively.

SAS software version 8.0 was used to perform the multiple regression analysis to predict the subgrade modulus from moisture content and the previously stated soil properties. The program's output of the regression analysis is shown in Table 5.2. The ANOVA results indicate that the natural logarithm of the backcalculated modulus (E1) could be related only to the logarithm of moisture content (X1), with a function having a coefficient of determination (R^2) value of 0.6981. However, when adding other soil properties like PI and F to the model, a better model having R^2 value of 0.9891 could be achieved. Hence, a regression model in the form of Equation 5.1 was fitted. The results of the regression analysis for the model are also shown in Table 5.2. The results of the statistical test that evaluates the significance of each regression coefficient indicate that all the estimated model parameters are significant (p-value is less than 0.05). Equation 5.1 below represents the final model for this group of soils, based on 183 data points:

$$E1 = 8.82 - 0.673 * X1 - 2.44 * X2 + 0.0084 * F - 0.11 * PI \qquad (5.1)$$

where,

E1 = Natural logarithm of (E)

E = Backcalculated elastic modulus, MPa

X1 = log (moisture content, %)

X2 = 1/ (moisture content, %)

F = Percentage passing sieve # 200, %

PI = Plasticity index, %

The model given by Equation 5.1 takes the general form shown below:

$$\text{Log}(E) = C_o + C_1 * \text{Log}(\text{moisture}) + C_2 * (1/\text{moisture}) \quad (5.2)$$

where,

$$C_o = 8.82 + 0.0084\,F - 0.11\,PI \quad (5.2a)$$

$$C_1 = -0.673 \quad (5.2b)$$

$$C_2 = -2.44 \quad (5.2c)$$

E, F and PI are as described before.

Figure 5.3 shows the model application on the data collected from sites 48-4143,13-1005 and 48-1122, respectively. The three plots in the figure indicate that the model fits the data very well and that the modulus decreases with increasing soil moisture even if the field moisture content is less than the optimum moisture content, as in sites 13-1005 and 48-1122 respectively. This would be acceptable since the subgrade soils at both sites are cohesive soils (sandy clay). Hence, when the moisture content decreases, the soil becomes harder and its modulus increases, and vice versa. It should be noted that this model could be applied only for plastic soils, as there is a term in the model for PI. For non-plastic soils, this model will be modified to account for soil properties other than PI, as is discussed below.

Table 5.2 Regression Analysis Procedures for Plastic Soils Model Development

Dependent Variable: E1

R-Square Selection Method

Number in Model	R-Square	C(p)	BIC	Root MSE	Variables in Model
1	0.9767	176.6577	-844.4975	0.07112	PI
1	0.7840	2926.776	-491.2373	0.21651	F
1	0.6981	4151.479	-437.8291	0.25593	x1
1	0.5068	6880.904	-359.4122	0.32712	x2
2	0.9795	137.8704	-863.9304	0.06683	F PI
2	0.9768	177.2805	-844.1832	0.07120	x2 PI
2	0.9767	178.3979	-843.6575	0.07132	x1 PI
2	0.9022	1241.671	-617.3199	0.14614	x1 x2
3	0.9884	13.2697	-950.0654	0.05045	x1 F PI
3	0.9871	32.4110	-933.3682	0.05329	x2 F PI
3	0.9781	159.8558	-852.5841	0.06930	x1 x2 PI
3	0.9161	1045.302	-641.4009	0.13579	x1 x2 F
4	0.9891	5.0000	-957.7523	0.04902	x1 x2 F PI

Analysis of Variance

Source	DF	Sum of Squares	Mean Square	F Value	Pr > F
Model	4	33.90986	8.47747	3528.46	<.0001
Error	155	0.37240	0.00240		
Corrected Total	159	34.28227			

Root MSE	0.04902	R-Square	0.9891
Dependent Mean	5.70630	Adj R-Sq	0.9889
Coeff Var	0.85899		

Parameter Estimates

Variable	DF	Parameter Estimate	Standard Error	t Value	Pr > |t|	Variance Inflation
Intercept	1	8.81933	0.31794	27.74	<.0001	0
x1	1	-0.67276	0.12405	-5.42	<.0001	301.27894
x2	1	-2.43912	0.76112	-3.20	0.0016	135.24219
F	1	0.00838	0.00066926	12.52	<.0001	32.88774
PI	1	-0.11065	0.00343	-32.28	<.0001	16.50651

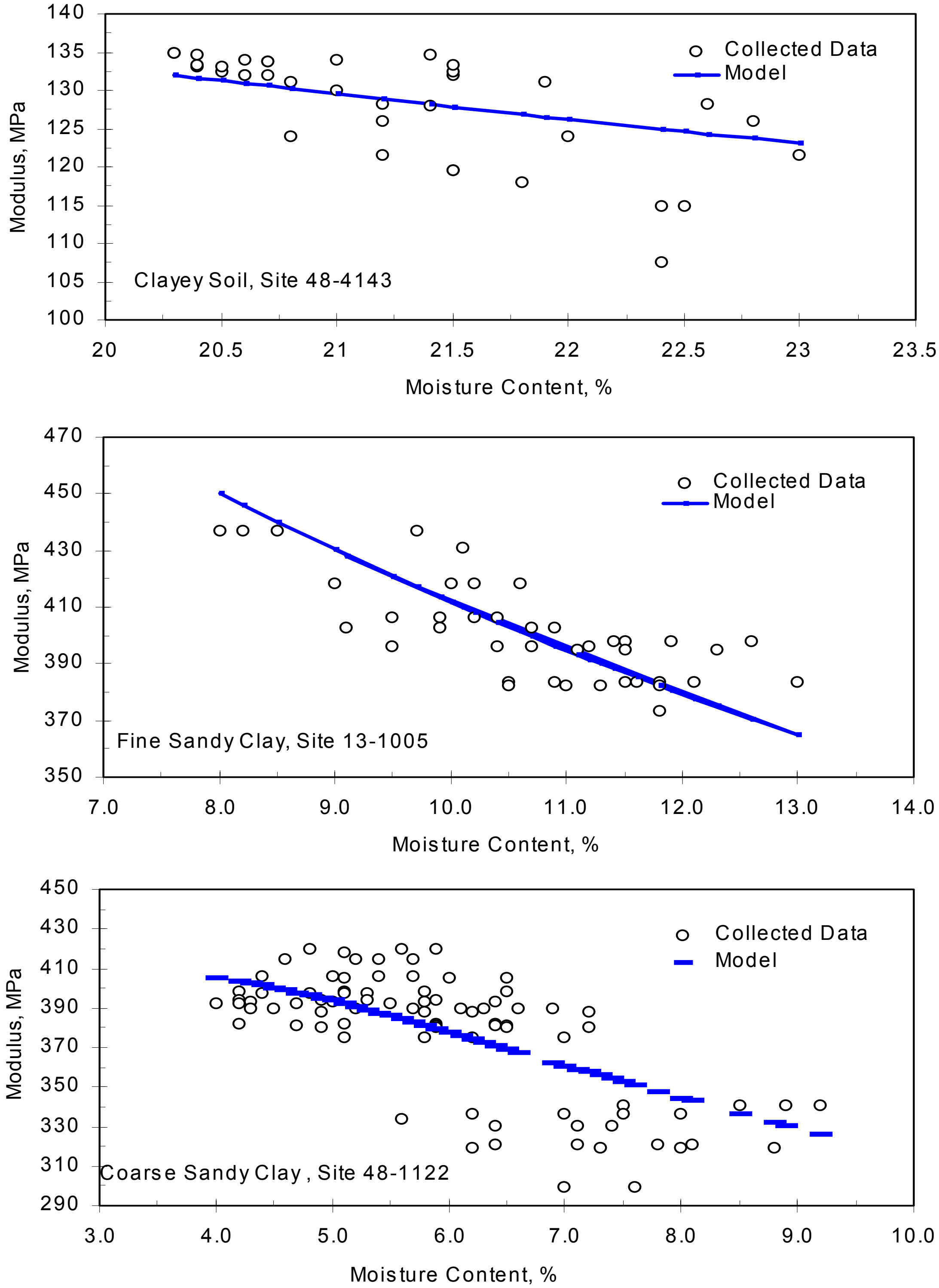

Figure 5.3 Applying the Model to Data from 3 Different Sites Having Plastic Soils

5.3.2 Model Development for Non-Plastic Soils

As was described previously, the model shown in Equation 5.2 could not be applied directly for non-plastic soils (sandy and/or silty soils), since there is a term in the model for PI. However, several trials were made to develop a model that best represents the behavior of non-plastic soils. The PI variable was replaced with the soil parameter D60, which is the soil size for 60% passing. This was selected based on the study by Witczak et al. (2000). Similar to the above analysis on plastic soils, data from sites (24-1634, 48-1077 and 35-1112) with non-plastic materials were used to develop a model in the form:

$$E1 = 24.4035 - 103.9\ D60 - 0.05143\ F1 - 0.06328\ F2 + 1.6205\ D1 + 9.9362\ D2 \qquad (5.3)$$

where,

$$F1 = F * X1 \qquad (5.3a)$$

$$F2 = F * X2 \qquad (5.3b)$$

$$D1 = D60 * X1 \qquad (5.3c)$$

$$D2 = D60 * X2 \qquad (5.3d)$$

D60 = Soil grain size for 60% passing

E1, X1, X2 and F are the same as defined in Equation 5.1.

The results of the multi-regression analysis are presented in Table 5.3. The table indicates that the model has R^2 value of 0.981 and total SSE of 0.276 based on 116 data points. Figure 5.4 shows the predicted outcome versus the data observations at these three sites, which once again verifies the high degree of correlation as represented by the developed regression model. The final model that represents the modulus-moisture relationship for non-plastic soils, based on 135 data points, can thus be written as:

$$\text{Log}(E) = 24.4035 - 103.9\ D60 + X1\ [1.6205\ D60 - 0.05143\ F] + X2\ [9.9362\ D60 - 0.06328\ F] \qquad (5.4)$$

Therefore, the model takes also the same general form of plastic soils, shown in Equation 5.2, where:

Co	= 24.4035	- 103.9 D60	(5.4a)
C1	= 1.6205 D60	- 0.05143 F	(5.4b)
C2	= 9.9362 D60	- 0.06328 F	(5.4c)

Table 5.3 Regression Analysis Procedures for Non-Plastic Soils Model Development

```
                               Dependent Variable: E1
                              R-Square Selection Method
Number in                                              Root
Model  R-Square        C(p)           BIC      MSE   Variables in Model
1      0.6616   1865.793    -370.0824       0.20702   F1
1      0.6496   1936.368    -365.9980       0.21068   D2
1      0.6378   2004.954    -362.1609       0.21418   D60
1      0.6306   2047.401    -359.8477       0.21632   F2
---------------------------------------------------------------------
2      0.9150   385.9621    -529.9672       0.10420   F2 D1
2      0.8489   772.3992    -463.6155       0.13893   F1 D1
2      0.8442   800.1583    -460.0338       0.14110   D60 D1
-----------------------------------------------------------------------
3      0.9394   245.5762    -567.9669       0.08841   F1 D1 D2
3      0.9376   255.8867    -564.7130       0.08968   D60 D1 D2
3      0.9283   310.0575    -548.9654       0.09611   F2 D1 D2
-----------------------------------------------------------------------
4      0.9780    21.5542    -679.3287       0.05347   D60 F1 F2 D2
4      0.9692    73.1114    -642.7080       0.06329   D60 F1 F2 D1
4      0.9459   209.5456    -580.0817       0.08390   F1 F2 D1 D2
------------------------------------------------------------------------
5      0.9810     6.0000    -692.9490       0.04991   D60 F1 F2 D1 D2

                                   Analysis of Variance
                                   Sum of            Mean
Source                   DF       Squares          Square    F Value    Pr > F
Model                     5      14.29001         2.85800    1147.42    <.0001
Error                   111       0.27648         0.00249
Corrected Total         116      14.56649

Root MSE              0.04991    R-Square     0.9810
Dependent Mean        5.49464    Adj R-Sq     0.9802
Coeff Var             0.90830

                                   Parameter Estimates
Parameter      Standard                                Variance
Variable    DF      Estimate          Error    t Value    Pr > |t|      Inflation
Intercept    1      24.40350        1.21481      20.09      <.0001              0
D60          1    -103.88527        7.24603     -14.34      <.0001     7128.32186
F1           1      -0.05143        0.00334     -15.41      <.0001     4144.52754
F2           1      -0.63284        0.04060     -15.59      <.0001      174.50063
D1           1       1.62054        0.38679       4.19      <.0001       61.90521
D2           1       9.93618        1.19521       8.31      <.0001      181.04734
```

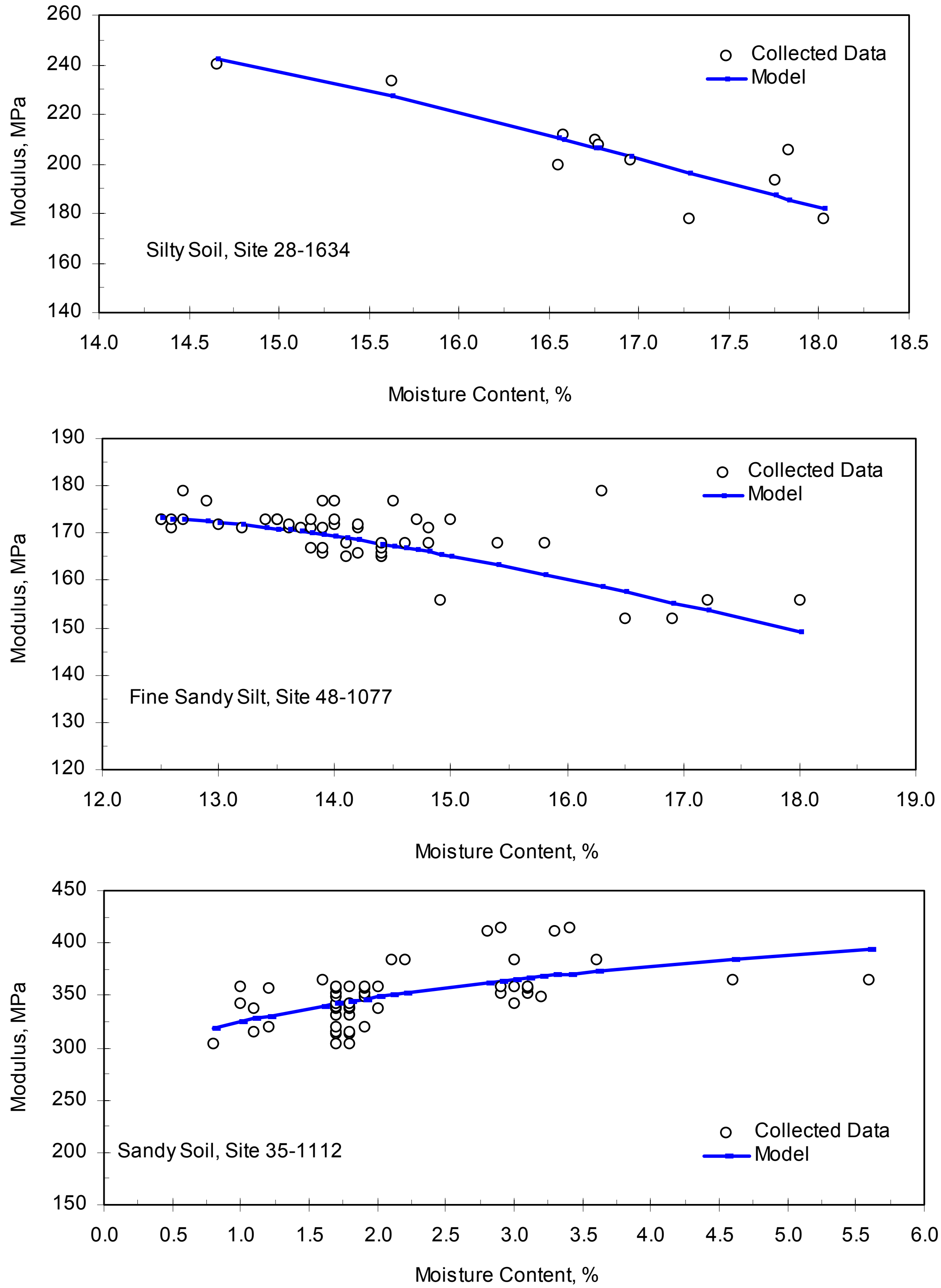

Figure 5.4 Applying the Model to Data from 3 Different Sites Having Non-Plastic Soils

5.3.3 Generalized Model for Both Plastic and Nonplastic Soils

The previous two models predict the soil modulus from the moisture content and basic soil properties like Atterberg limits, D60 and percentage passing sieve # 200, after classifying the soils into plastic and non-plastic soils. Extensive effort was made to develop one model that can predict the subgrade modulus for both soil types. To achieve this purpose, the modulus moisture relationships for the six different sites were plotted on the same graph. The results are shown in Figure 5.4. The figure indicates that the modulus values for all sites follow almost the same pattern of exponential function decreasing with increasing moisture content. The figure indicates also that the coarse grained soils (sand and clayey sand) showed high modulus values and lower moisture contents, while fine grained soils (clay, silt and sandy silt) showed lower modulus values and higher moisture contents (Mois). The average function, for all the 6 sites, that relates the backcalculated modulus in MPa to moisture content in percent is given below:

$$E = 484 \text{ EXP } (- 0.0578 \text{ Mois}) \qquad (5.5)$$

The model given by Equation 5.5 cannot be applied directly to estimate the modulus since it relies only on the moisture content. However, it is very useful to show the trend of the modulus- moisture relationship. The upper and lower lines represent the borders for the modulus moisture relationship. The model shown in Equation 5.5 has R^2 value of 0.714. The reason for the lower R^2 value could be related to including the site (35-1112), which is coarse sand. The modulus values in this site increase with moisture increase because the in-situ moisture content is much smaller than the optimum, as explained before. Therefore, this site was excluded to see its effect on the model. Figure 5.5 shows the average model, upper and lower limits after excluding site 35-1112. The new model is shown in Equation 5.6. The figure indicates that the R^2 value is increased to 0.80.

$$E = 618 \text{ EXP } (- 0.074 \text{ Mois}) \qquad (5.6)$$

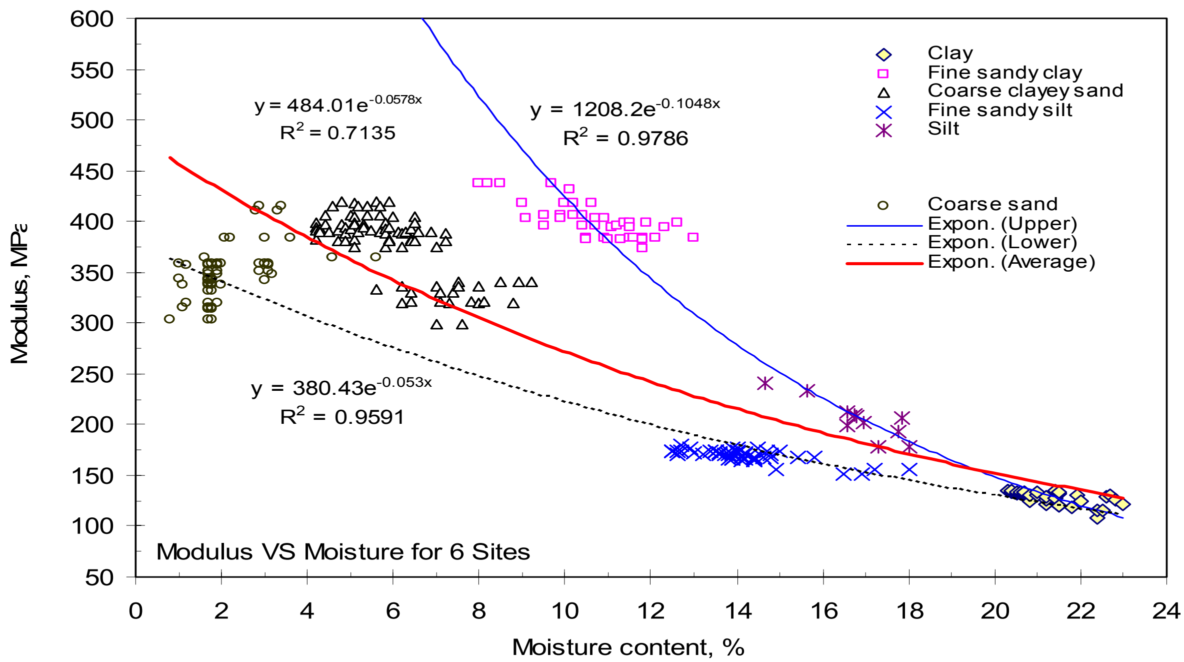

Figure 5.5 Modulus Moisture Relationships for 6 Different Sites

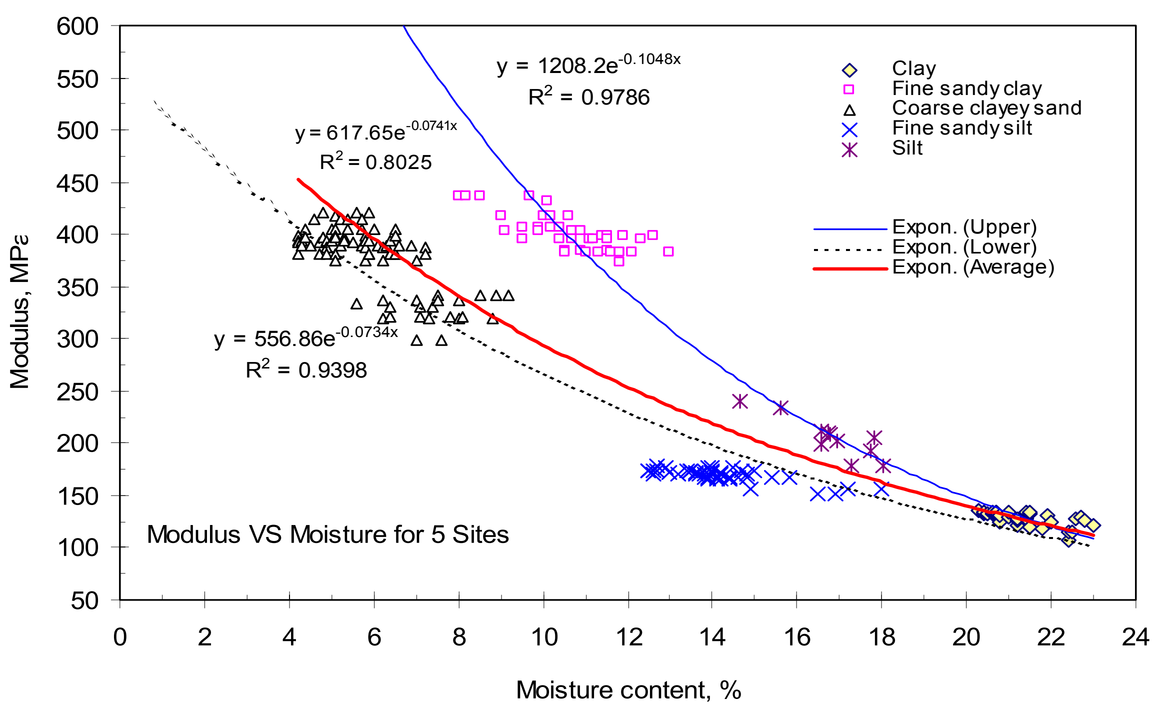

Figure 5.6 Modulus Moisture Relationships for 5 Different Sites

The simple model shown in the previous Equation 5.6 can be used to capture the trend of modulus-moisture relationship. The intercept and exponent may experience little change according to each site condition, but the trend would be the same. The intercept range would be, as shown in the figure, from 557 to 1200 MPa, while the exponent range would be –0.073 to –0.105.

Equations 5.5 and 5.6 present good correlation between the backcalculated modulus and subgrade moisture but they may not be accurately employed to predict the subgrade modulus because some site-specific conditions are not included in the model. Subgrade soil properties like Atterberg limits cannot be included in the model because there are some soils that are non-plastic. D60 also cannot be included since it is not available for all sites. Therefore, extensive data mining was conducted to find the site-specific conditions that may affect the modulus values and can be applied for both plastic and non-plastic soils. The data mining revealed that the in-situ dry density of soil and the overburden stress would affect the soil modulus according to Hudson et al. (1994).

Therefore, multiple regressions using SAS software was employed to predict the soil modulus from the moisture data, in-situ dry density, overburden stress, pavement thickness above subgrade soil and percentage passing sieve number 200. The in-situ dry density was calculated for all sites based on Equation 2.12, as the ratio between the volumetric and gravimetric moisture contents. The regression analysis results are shown in Table 5.4. The table indicates that the model shown below could be achieved based on 277 data points from the six different sites.

$$E1 = -0.8117 - 0.0791\ Mois - 0.0405\ H + 0.0155\ Strs + 4.284\ DDi + 0.0032\ F \quad (5.7)$$

where,

E1	= Natural logarithm of the modulus (E, in MPa)
Mois	= Gravimetric moisture content, %
H	= Pavement thickness above subgrade soil, cm

Strs = Overburden stress, gm/cm^2

DDi = Insitu dry density of subgrade soil, gm/cm^3

F = Percentage passing sieve # 200

Table 5.4 indicates that all variables are significant at a confidence level of more than 95 percent. The model has R^2 of 0.928 and SSE of 3.79. Figure 5.7 shows the model when fitted to the data of the 6 different sites. The figure indicates that the model fits the data, but it is not perfect for all sites. For example, consider site 35-1112, in which its modulus increases with moisture increase as previously explained.

When excluding site 35-1112, which has coarse sand, a better model is achieved as shown in Figure 5.8. The regression analysis outputs of the new model are shown in Table 5.5. The table indicates that the R^2 value for the new model is increased to 0.989 and the SSE reduced to 0.538 while the total data points are 219. The table indicates also that the modulus could be predicted only from the in-situ dry density with R^2 value of 0.90. The new model is given by the following equation.

$$E1= -7.490-0.0407\ Mois - 0.0493\ H + 0.0202\ Strs + 7.761\ DDi + 0.002\ F \qquad (5.8)$$

The measured and predicted moduli for both models were plotted against the equity line (45^o line), and the results are shown in Figure 5.9. The figure indicates that data are well centered around the equity line for both models, while the dispersion of the data is much less for the second model, when excluding the site 35-1112.

Table 5.4 Regression Analysis Procedures for the General Model Based on Data of 6 Sites

Dependent Variable: E1
R-Square Selection Method

Number in Model	R-Square	C(p)	BIC	Root MSE	Variables in Model
1	0.7134	804.6149	-809.0597	0.23340	Mois
1	0.6936	879.1351	-790.6040	0.24133	F
1	0.1489	2929.125	-507.7206	0.40221	DDi
1	0.0379	3347.096	-473.7008	0.42765	H
2	0.8696	218.8995	-1024.8069	0.15774	Mois DDi
2	0.7788	560.4566	-879.8887	0.20542	DDi F
2	0.7535	655.7329	-850.0633	0.21685	Mois H
3	0.9235	17.7391	-1168.6051	0.12099	Mois H DDi
3	0.9212	26.6844	-1160.3328	0.12286	Mois Strs DDi
4	0.9247	15.2985	-1170.8435	0.12027	Mois H DDi F
4	0.9246	15.6778	-1170.4847	0.12035	Mois H Strs DDi
4	0.9218	26.4474	-1160.4901	0.12262	Mois Strs DDi F
5	0.9277	6.0000	-1179.7064	0.11807	Mois H Strs DDi F

Analysis of Variance

Source	DF	Sum of Squares	Mean Square	F Value	Pr > F
Model	5	48.67009	9.73402	698.31	<.0001
Error	272	3.79151	0.01394		
Corrected Total	277	52.46160			

Root MSE	0.11807	R-Square	0.9277
Dependent Mean	5.61441	Adj R-Sq	0.9264
Coeff Var	2.10290		

Parameter Estimates

Variable	DF	Parameter Estimate	Standard Error	t Value	Pr > |t|	Variance Inflation
Intercept	1	-0.81170	0.28376	-2.86	0.0046	0
Mois	1	-0.07909	0.00558	-14.16	<.0001	25.07617
H	1	-0.04048	0.00854	-4.74	<.0001	318.04689
Strs	1	0.01552	0.00462	3.36	0.0009	305.44093
DDi	1	4.28408	0.17360	24.68	<.0001	3.86865
F	1	0.00316	0.00092462	3.42	0.0007	18.12070

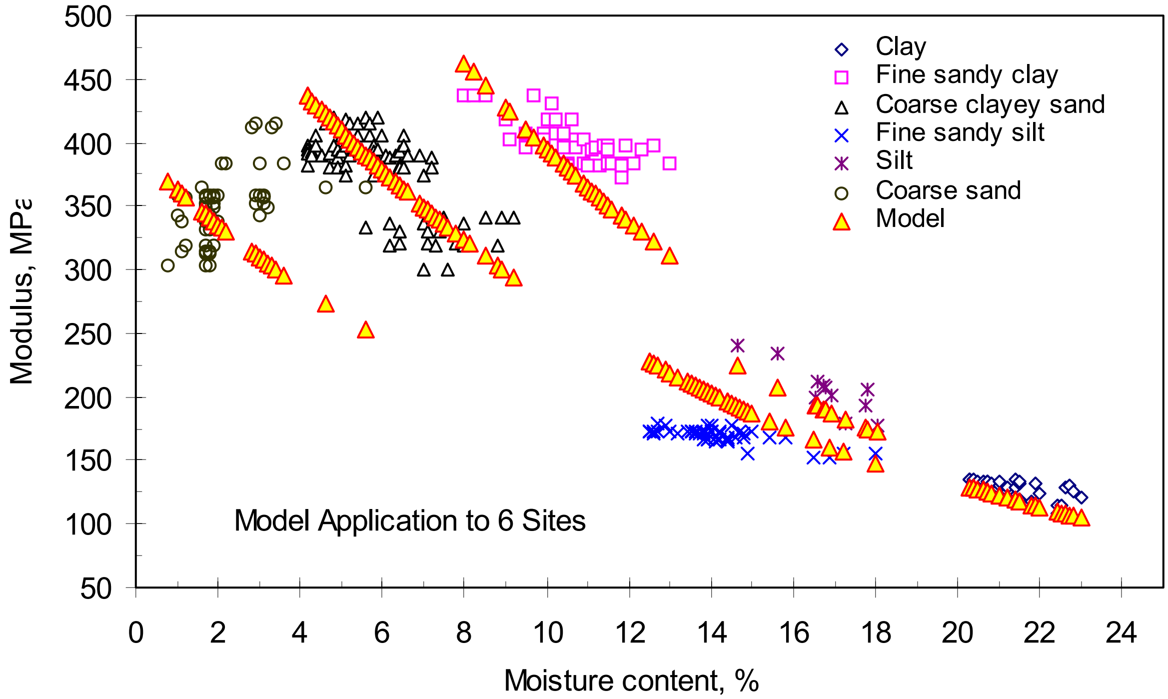

Figure 5.7 Model Application to Data from 6 Different Sites

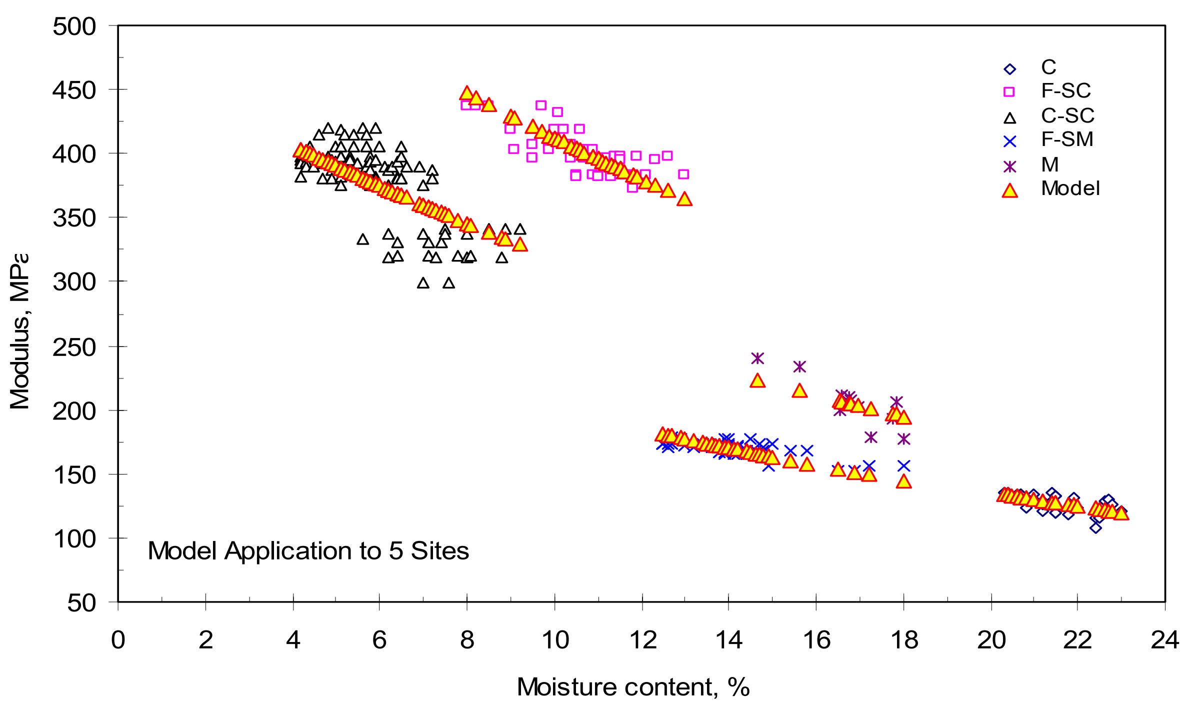

Figure 5.8 Model Application to Data from 5 Different Sites

Table 5.5 Regression Analysis Procedures for the General Model Based on Data from 5 Sites

Dependent Variable: E1
R-Square Selection Method

Number in Model	R-Square	C(p)	BIC	Root MSE	Variables in Model
1	0.9062	1539.346	-858.9458	0.14230	DDi
1	0.7979	3564.183	-690.6948	0.20883	Mois
1	0.6850	5675.789	-593.2244	0.26071	F
1	0.2479	13853.56	-401.8958	0.40288	H
2	0.9638	462.3504	-1066.6921	0.08854	H DDi
2	0.9626	485.7682	-1059.2986	0.09006	Strs DDi
2	0.9241	1204.908	-905.2259	0.12824	Mois DDi
3	0.9832	101.9929	-1231.1222	0.06046	Mois H DDi
3	0.9790	180.1103	-1183.5670	0.06757	Mois Strs DDi
3	0.9787	186.7584	-1179.9596	0.06814	H DDi F
3	0.9765	227.5197	-1159.0541	0.07154	Strs DDi F
4	0.9874	25.9262	-1290.1197	0.05253	Mois H Strs DDi
4	0.9832	103.9533	-1229.7477	0.06060	Mois H DDi F
4	0.9792	179.4209	-1183.9135	0.06749	Mois Strs DDi F
4	0.9791	181.0012	-1183.0493	0.06763	H Strs DDi F
5	0.9886	6.0000	-1308.5601	0.05015	Mois H Strs DDi F

Analysis of Variance

Source	DF	Sum of Squares	Mean Square	F Value	Pr > F
Model	5	46.50612	9.30122	3698.39	<.0001
Error	214	0.53820	0.00251		
Corrected Total	219	47.04431			

Root MSE	0.05015	R-Square	0.9886
Dependent Mean	5.56105	Adj R-Sq	0.9883
Coeff Var	0.90179		

Parameter Estimates

Variable	DF	Parameter Estimate	Standard Error	t Value	Pr > |t|	Variance Inflation
Intercept	1	-7.49004	0.24655	-30.38	<.0001	0
Mois	1	-0.04066	0.00306	-13.30	<.0001	25.31554
H	1	-0.04927	0.00372	-13.24	<.0001	201.12890
Strs	1	0.02015	0.00201	10.00	<.0001	177.79876
DDi	1	7.76095	0.13400	57.92	<.0001	5.35118
F	1	0.00200	0.00042675	4.68	<.0001	16.33225

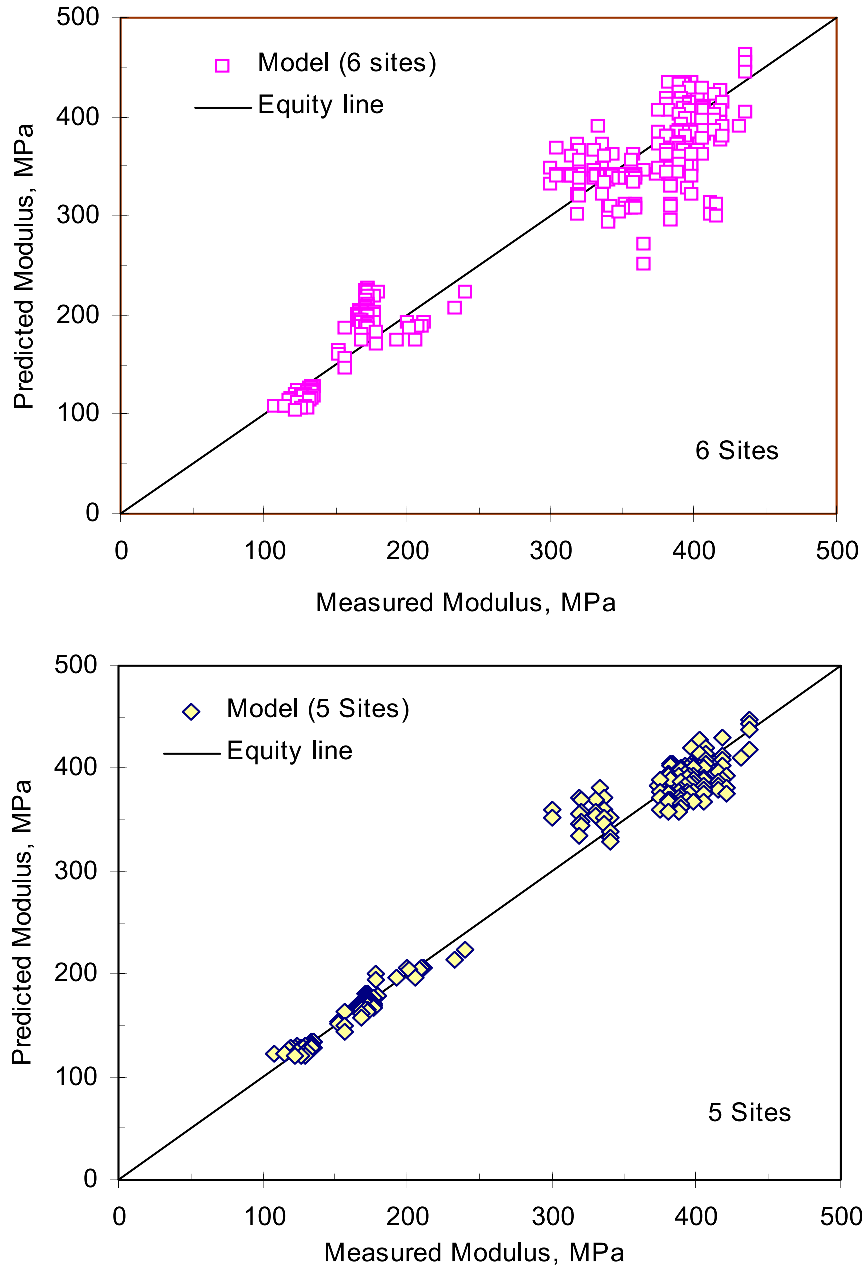

Figure 5.9 Measured vs. Predicted Modulus Values Based on the General Model

5.3.4 Estimating the Subgrade Seasonal Adjustment Factor

The previous analysis allows for prediction of the absolute value of the soil modulus at given moisture contents for the investigated soil types. There is a concern that the developed relationships may be site-specific due to the fact that few sites were identified in the LTPP database. However, the trends of the relationships are likely to be applicable for the soil groups investigated, which may limit the applicability of the developed equations to the soil types investigated.

In order to predict the change in modulus with moisture on a relative basis, an effort was made to develop a shift factor that allows transferring the modulus from one season to another. For this purpose, modulus and moisture data were sorted and analyzed to relate the modulus ratio to the moisture ratio instead of using the absolute values of the modulus and moisture. The modulus ratio was defined to be the modulus at a given season to that of a known reference season, and similarly the moisture ratio is the ratio of the moisture content at the considered season to that of the same reference season.

Based on several statistical trials of various models, an equation was developed in the form:

$$SAF_s = K_1 (W_r)^{k2} \tag{5.9}$$

where,

SAF_s	= Subgrade Seasonal Adjustment Factor for a season, equals to (E_{Season}/ E_{ref})
E_{Season}	= Subgrade modulus at a given season
E_{ref}	= Subgrade modulus at the reference season
W_r	= Moisture ratio, equals to (W_{Season}/ W_{ref})
W_{Season}	= Water content at a given season
W_{ref}	= Water content at the reference season
K_1 and K_2	= Model parameters in which, K_1 depends on reference point, and K_2 represents the sensitivity of modulus change with moisture.

Data for the sites (1 through 5) are listed in Table 5.5, and were used to fit a regression model in the form of Equation 5.9. The results of the regression analysis are shown in Table 5.6. Plots of the data for all soils are shown in Figure 5.10.

The variables in the model shown by Equation 5.9 are dimensionless. Once the user determines the reference modulus and moisture content, Equation 5.9 can be used to determine the modulus at any season by multiplying the reference modulus value by the SAF value of that season. It should to be noted that the parameter K_1 depends on the selected reference point, and the parameter K_2 depends on the soil sensitivity to moisture. The smaller the value of K_2, the more sensitive is the soil to moisture variations. Table 5.6 show that the fine silty soil is the more sensitive to moisture variation and then clay while clayey sand is less sensitive to moisture variations. This would indicate that the seasonal variation in the granular base layers would be minimal.

In this analysis, the author used the lowest moisture content as the reference point, which is generally associated with the highest modulus. Therefore, almost all SAF values, as shown in Figure 5.10, were below 1, and K_1 values were almost equal to 1 for all soils. Practically, the reference modulus and moisture values are the ones determined at the construction stage, which would be the values determined at the optimum moisture content. As such, it is recommended that the user determine two modulus-moisture points in order to determine the K_1 and K_2 parameters.

Table 5.6 Parameters k_1 and k_2 for the SAF Model (Equation 5.9)

Site		Soil Type	K_1	K_2	R^2
1	48-4143	Clay	0.99	-1.07	0.48
2	13-1005	Fine Clayey Sand	0.99	-0.29	0.57
3	48-1122	Coarse Clayey Sand	1.04	-0.35	0.53
4	24-1634	Fine Silt	1.01	-1.32	0.72
5	48-1077	Fine Silty Sand	1.02	-0.35	0.50

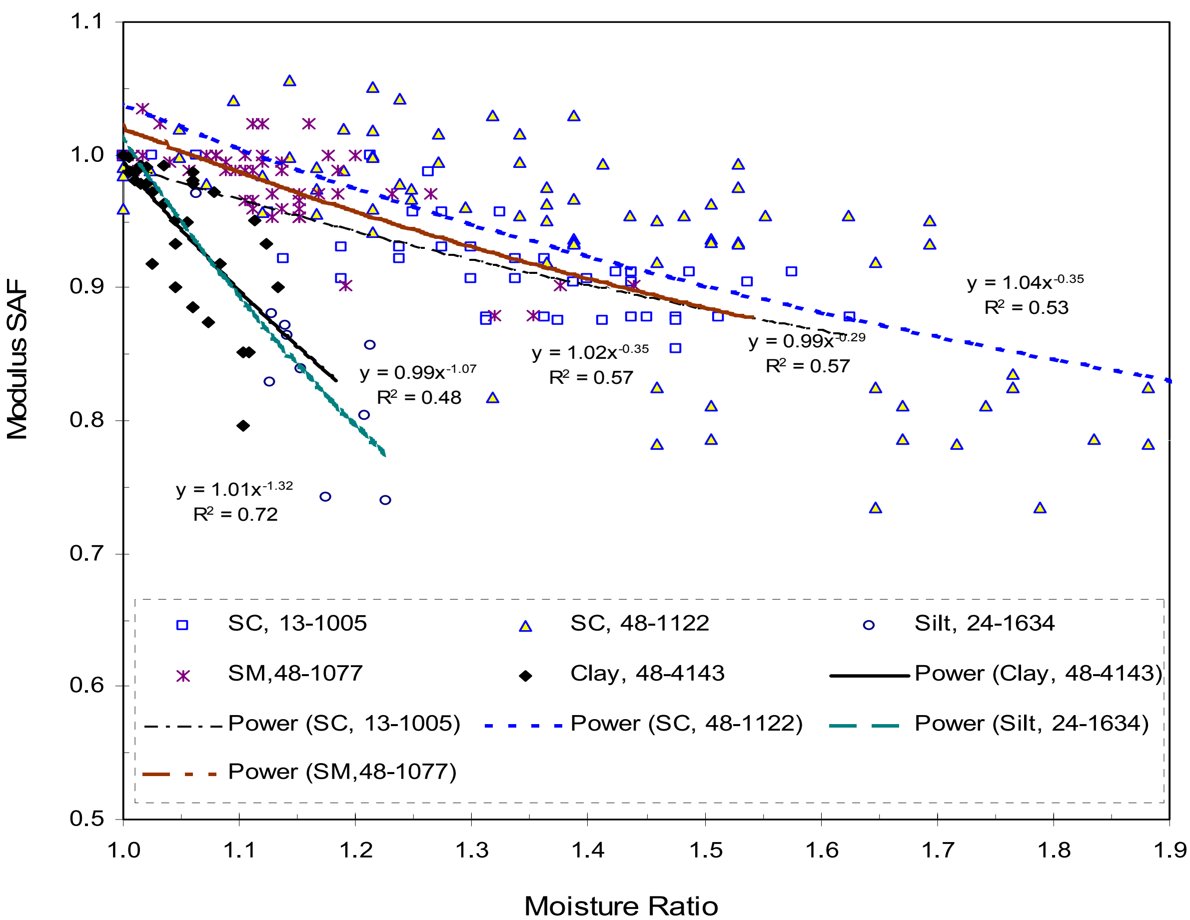

Figure 5.10 Subgrade Modulus Shift Factor versus Moisture Ratio for Different Soil Types

5.4 SUMMARY

The data presented in this chapter were downloaded from the LTPP-SMP database. Based on the analysis described in this chapter, the findings are summarized below:

- The variation of the subgrade modulus and moisture with time followed an inverse function, where the modulus decreased with moisture increase. This result was valid for all soils where the field moisture contents observed were above the optimum. This relationship might change if the field moisture is below optimum. In this case, an increase in the soil moisture may cause an increase in the modulus value as well.

- A relationship between subgrade modulus and the gravimetric moisture content was determined for different soil types. General models relating subgrade modulus to soil moisture and other soil properties were developed and applied for different soil types. The general model present in Equation 5.8 will be validated later in this document using data from the Idaho sites.

- A model for calculating the modulus seasonal adjustment factor (SAF_s) of subgrade soil was developed. The model given by Equation 5.9 adjusts the subgrade modulus from one reference season to another. This allows the determination of subgrade resilient modulus at any season by multiplying the reference value by the SAF for that season. The reference value is the modulus value determined by testing during any selected season (for instance, the summer). The SAF determined here is dependent on the variation in moisture content from one season to another.

- The data presented showed that the more sensitive soils to moisture various was the fine silty soil and then clay while coarser soils, like clayey sand, was less sensitive to moisture variations. This would indicate that the seasonal variation in the granular base layers would be minimal.

6. AC MODULUS - TEMPERATURE DATA ANALYSIS FOR LTPP SITES

This chapter addresses the impacts of temperature variations on the AC layer modulus.

6.1 SELECTED DATA

Data from eleven different LTPP sites were used in the analysis. Five sites from the nonfreezing zones that were included in the subgrade modulus - moisture relationship were also included in this analysis. Another six sites from the freezing zones were also included to determine the difference in the behavior of the freezing and nonfreezing sites, if any. The AC layer properties for the different sites are shown in Table 6.1. These properties include the AC layer thickness, the bulk specific gravity of the AC mix, the percent air voids in the AC mix and the AC binder grade, specific gravity and percentage.

Table 6.1: Properties of AC Layer for the Different LTPP Sites

No	LTPP Site	State	AC Layer Thick. (mm)	Bulk Gs of AC Mix (BSG)	Air Voids in AC Mix (%)	AC binder Grade	Binder Specific Gravity	Binder Content (%)
1	13-1005	GA	195.6	2.341	4.4	AC-30	1.034	4.68
2	28-1016	MS	200	2.359	2.67	AC-30	1.03	4.45
3	48-1077	TX	129.5	2.373	3.05	AC-10	0.985	4.5
4	48-1122	TX	86.4	2.321	3.20	AC-10	0.99	4.61
5	35-1112	NM	160	2.464	4.4	AC-30	1.015	5.05
6	9-1803	CT	183	2.444	5.35	AC-20	1.01	4.3
7	23-1026	ME	163	2.352	3.85	AC-10	1.015	5.1
8	25-1002	MA	198	2.427	6.80	AC-20	1.026	5.5
9	33-1001	NH	213	2.386	5.80	AC-20	1.03	4.7
10	16-1010	ID	272	2.294	5.30	AC-10	1.026	5.2
11	27-6251	MN	188	2.353	5.80	N/A	N/A	4.5
12	30-8129	MT	76	2.324	4.5	AC-10	1.03	5.8
13	49-1001	UT	140	2.350	2.1	AC-10	1.04	5.7

6.2 AC MODULUS & TEMPERATURE VARIATION WITH TIME

The backcalculated modulus and mid-depth pavement temperature were analyzed versus time for each site. Figure 6.1 shows the asphalt concrete (AC) modulus – temperature relationship over time for three different sites from nonfreezing zones. The figures indicate that both modulus and temperature follow a sinusoidal function over time. This finding agrees with the conclusion given by Ali (1996). The figures indicate also that when the temperature increases the modulus decreases and vice versa.

The sinusoidal model proposed by Ali (1996) was used to fit the data for most of the given sites. The model is shown in Equation (6.1).

$$E = a_1 + b_1 * \sin (c_1 * M + d_1) \tag{6.1a}$$

$$T = a_2 + b_2 * \sin (c_2 * M + d_2) \tag{6.1b}$$

where,

E	= AC elastic modulus
T	= AC pavement temperature
M	= Month
a_i, b_i, c_i & d_i	= Model coefficients

The model coefficients a_i, b_i, c_i and d_i were estimated using the SOLVER program for four different sites. The estimated coefficients are presented in Table 6.2. The table indicates that the model coefficients c_i and d_i are almost the same, for both modulus and temperature models, in the four sites. However, the coefficients a_i and b_i differ for each site possibly due to the site climatic conditions and/or the properties of the AC layer. The model was applied to the data from three different sites using the estimated coefficients presented in Table 6.2. The estimated values of the dependent variables (modulus and temperature) are graphically represented in Figure 6.2.

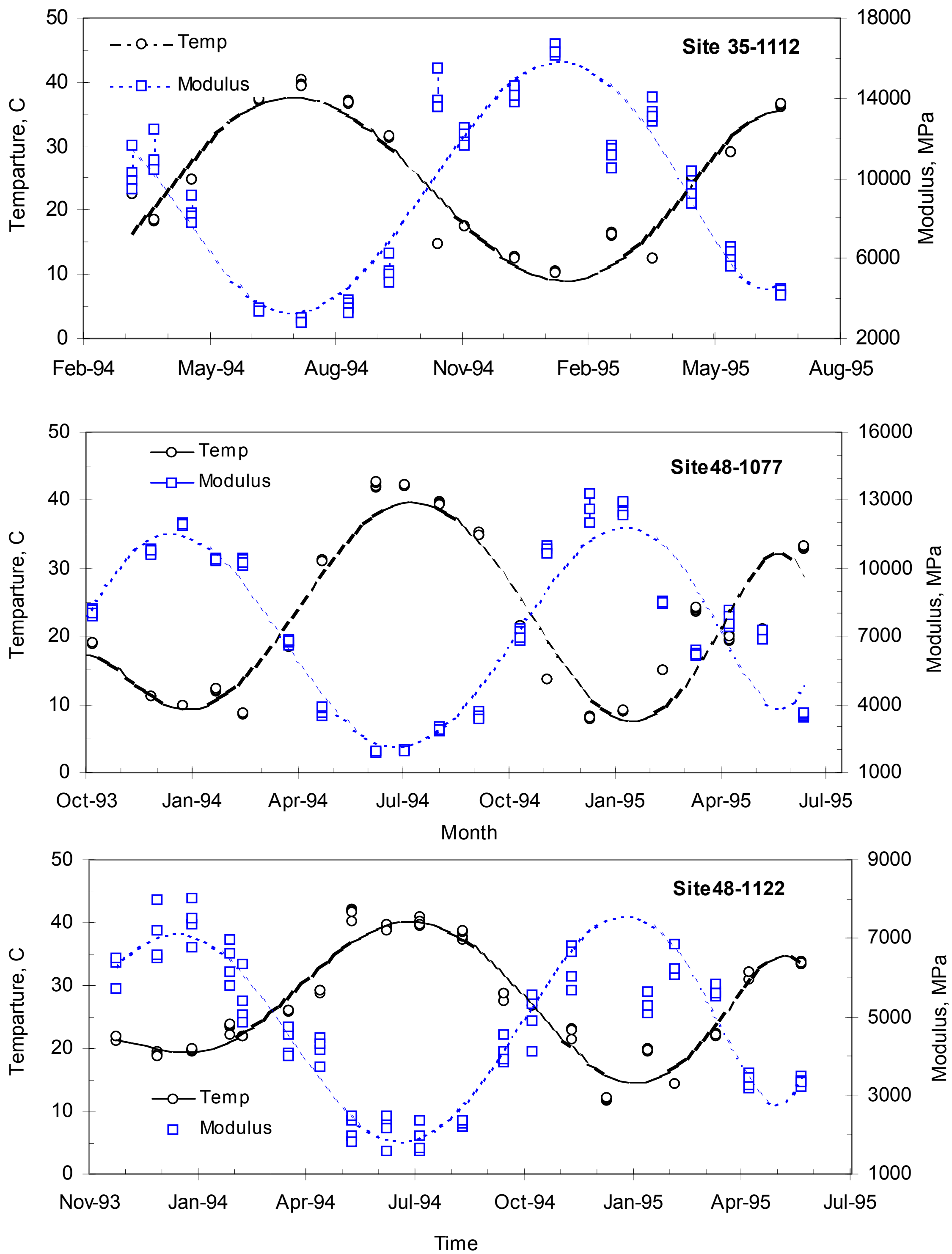

Figure 6.1: AC Layer Elastic Modulus &Pavement Temperature vs. Time

To generalize the previous sinusoidal model, the AC modulus value was replaced by a relative value called AC shift factor (SF), and Equation 6.1 can be rewritten as follows:

$$SF = a_3 + b_3 * \sin (c_3 * M + d_3) \qquad (6.1c)$$

The shift factor mentioned above can be determined according to the following Equation:

$$SF = E_{season} / E_{winter} \qquad (6.2)$$

E_{season} = AC elastic modulus at any season.

E_{winter} = AC elastic modulus during winter.

Table 6.2: Estimated Coefficients for the Sinusoidal Function (Equation 6.1)

Variable	Site	R^2	Estimated Model Coefficients			
			a_i	b_i	c_i	d_i
Modulus	13-1005	0.91	9408.7	-5705.8	6503.5	-491.5
	28-1016	0.85	8790.2	-5108.4	6503.7	-492.4
	48-1077	0.94	8916.7	-6764.2	6503.5	-490.9
	35-1112	0.85	9408.7	-5705.8	6503.5	-491.5
	Average	0.89	9162.7	-6235.0	6503.5	-491.2
Temperature	13-1005	0.92	22.8	-12.5	49.8	14.3
	28-1016	0.89	26.0	-14.7	49.7	15.2
	48-1077	0.92	24.8	-16.7	49.7	14.6
	35-1112	0.87	22.8	-12.5	49.8	14.3
	Average	0.90	23.8	-14.6	49.8	14.4
AC SF	13-1005	0.91	0.63	0.42	0.48	1.43
	28-1016	0.69	0.64	0.37	0.58	0.72
	48-1077	0.94	0.60	0.46	0.41	2.02
	35-1112	0.83	0.65	0.44	0.45	1.50
	Average	0.84	0.63	0.45	0.43	1.76

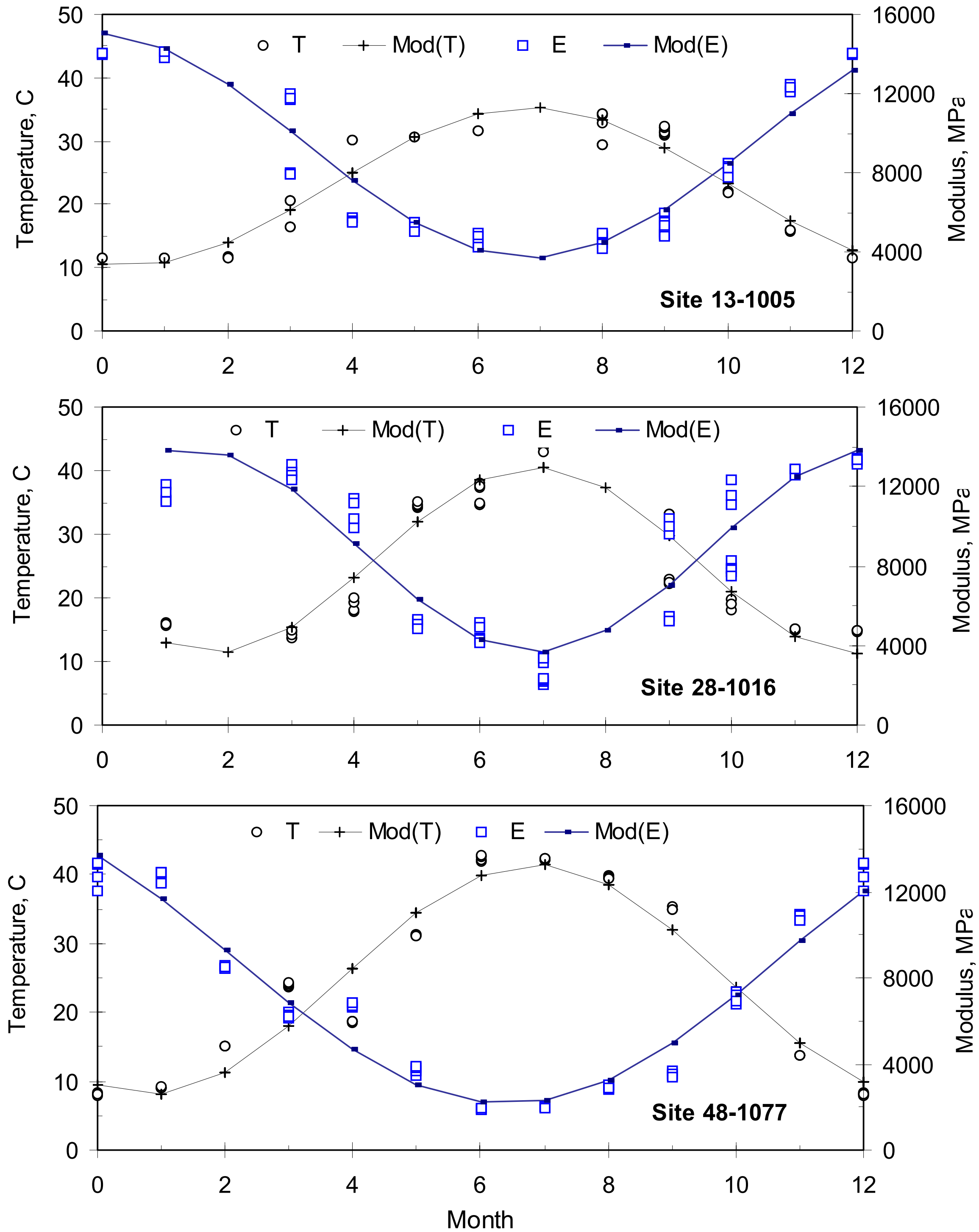

Figure 6.2 : Modeling AC Modulus & Temperature vs. Months

The AC shift factor was calculated for all the sites and the sinusoidal model (Equation 6.1c) was used to fit the data for four of the sites using SOLVER. The estimated model coefficients are shown in the bottom part of Table 6.2, which indicate R^2 range from 0.69 to 0.94. The good R^2 range indicates that the model fits the data very well. The model fitted to the given data from four different sites is presented in Figure 6.3. The figure indicates that there is not great variability between the four sites.

Figure 6.4 shows the average estimated SF fitted to the data from four different sites. This average value could be used as a default values for the AC SAF with good accuracy (R^2 ranges from 0.69 to 0.94) if the information about the AC modulus and temperature values is not available. The figure indicates that the AC modulus during summer drops to about 20% of its winter value, which should be taken into consideration during the design of asphalt pavement.

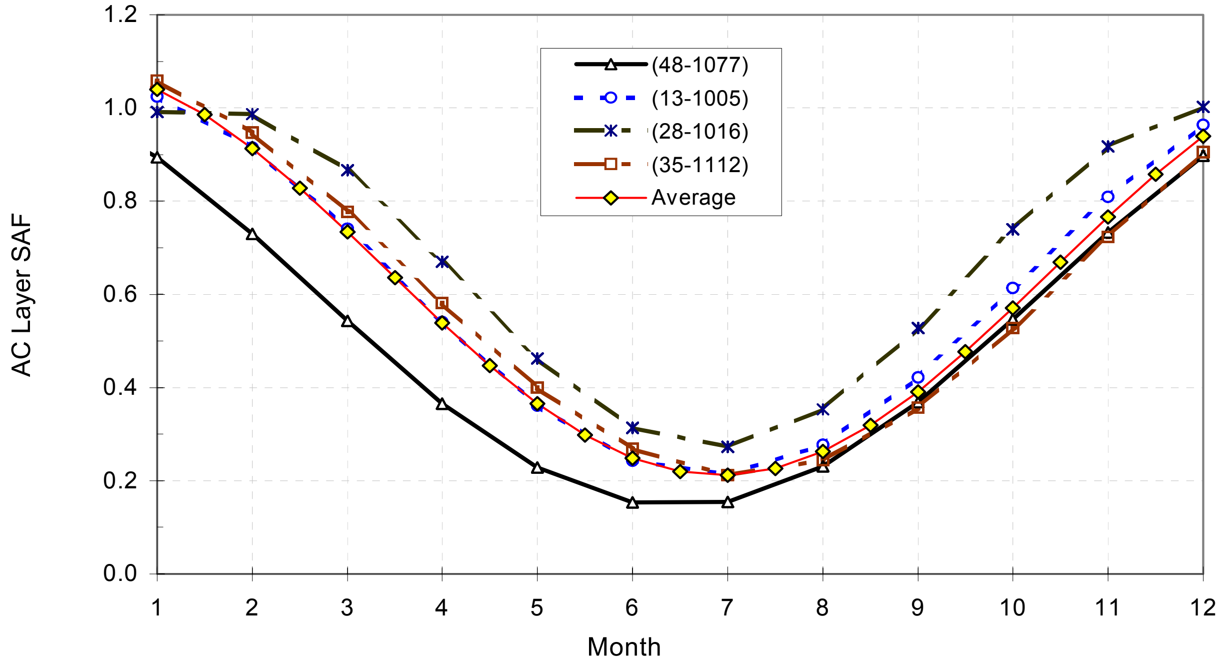

Figure 6.3: AC Layer SF (E_{season}/E_{winter}) vs. Months for Different Sites

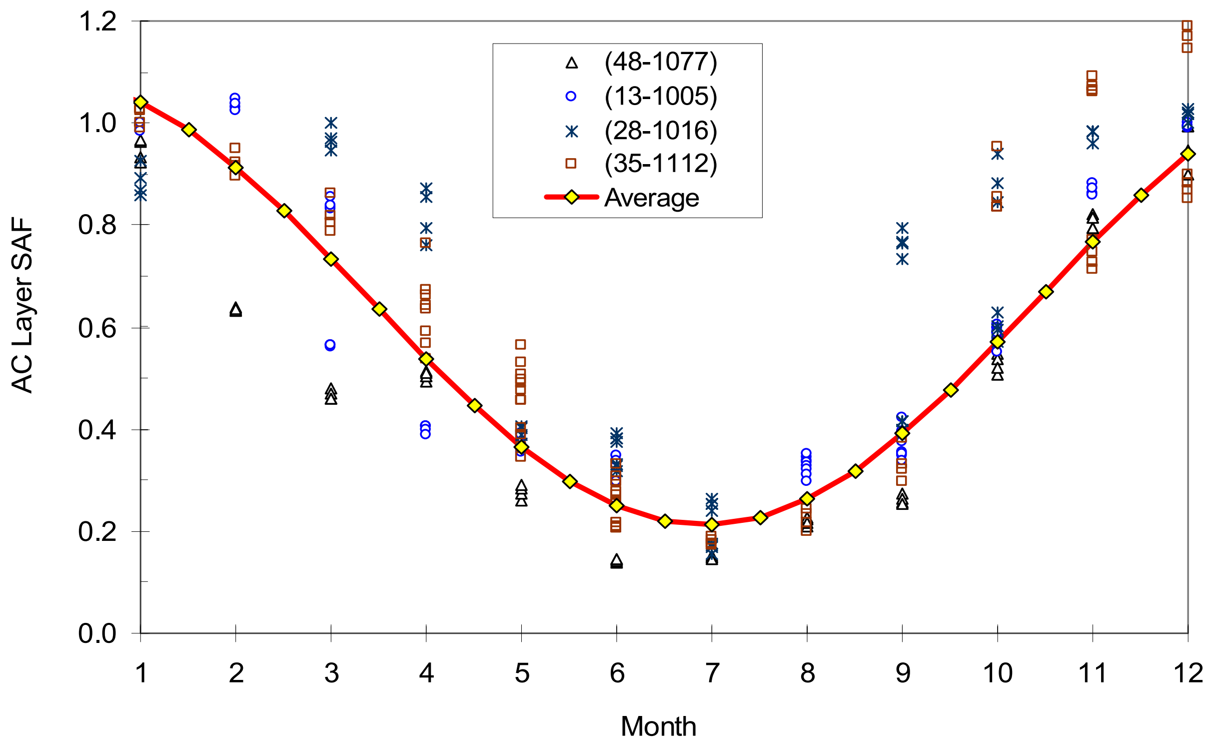

Figure 6.4: Average AC Layer SAF (E_{season}/E_{winter}) vs. Months for Different Sites

6.3 AC MODULUS - TEMPERATURE RELATIONSHIP

6.3.1 Modulus -Temperature Variation with Depth

To develop the modulus-temperature relationship, a preliminary analysis was conducted for three different sites to determine the location (depth) in the pavement where the temperature value best correlates with the AC modulus. Three different pavement temperatures at different depths from the AC surface were considered in addition to the asphalt surface temperature and the air temperature. The three sites included in this analysis are 13-1005, 28-1016 and 35-1112.

Statistical analysis using SAS software was carried out to relate the natural logarithm of the backcalculated AC modulus to the different temperatures. The statistical results of the three sites, based on 149 data points, are presented in Table 6.3. The table indicates that the mid-depth pavement temperature, T2, achieved the highest coefficient of determination (R^2= 0.93) and the least root mean squared errors (root MSE=0.1614). The AC temperatures at the lower depth (25 mm from the bottom, T3) and shallow depth (25 mm from the surface, T1) achieved lower R^2 values (0.91 and 0.88 respectively) while the pavement surface temperature achieved the lowest coefficient of determination (R^2 =0.785), even lower than the air temperature (R^2 =0.86).

Based on this finding, the mid-depth pavement temperature was used in the modulus - temperature analysis for this study. This assessment disagrees with the results of Ali and Lopez (1996) since they used the temperature at 25 mm depth (T1). The main reason for this disagreement may be because they based their analysis on data from only one site. The author believes that the mid-depth asphalt (T2) temperature is the best temperature to represent the pavement rather than T1 or T3 because it represents the AC average temperature value. However, the author agrees with Ali and Lopez (1996) in that there is no need to include more than one temperature measure since there exists a large degree of redundancy between temperature measures. Furthermore, a possible high correlation between various measures of temperature would render results unreliable if used in the same estimation process thanks to the multicollinearity problem. Figure 6.5 through 6.7 show the relationship between the AC modulus and the pavement temperature at various depths. The figures indicate that while the three pavement temperatures look the same at lower temperature, using the temperature at the shallow depth of 25 mm (T1) overestimates the modulus at the higher temperature values where the mid-depth is considered the average value.

Table 6.3: Relating AC Modulus to Temperature at Different Depths

Dependent Variable: E1
R-Square Selection Method

Number in Model	R-Square	Root MSE	Variable
1	0.9306	0.16136	T2
1	0.9079	0.18584	T3
1	0.8850	0.20771	T1
1	0.8597	0.22935	Tair
1	0.7850	0.28396	Ts

E = AC backcalculated modulus, MPa
E1 = log (E)
Tair = Air temperature, C
Ts = AC surface temperature, C
T1 = AC Temperature at 25 mm depth from AC surface, C
T2 = Mid-depth AC temperature, C
T3 = AC temperature at 25 mm from the bottom of the AC Layer, C

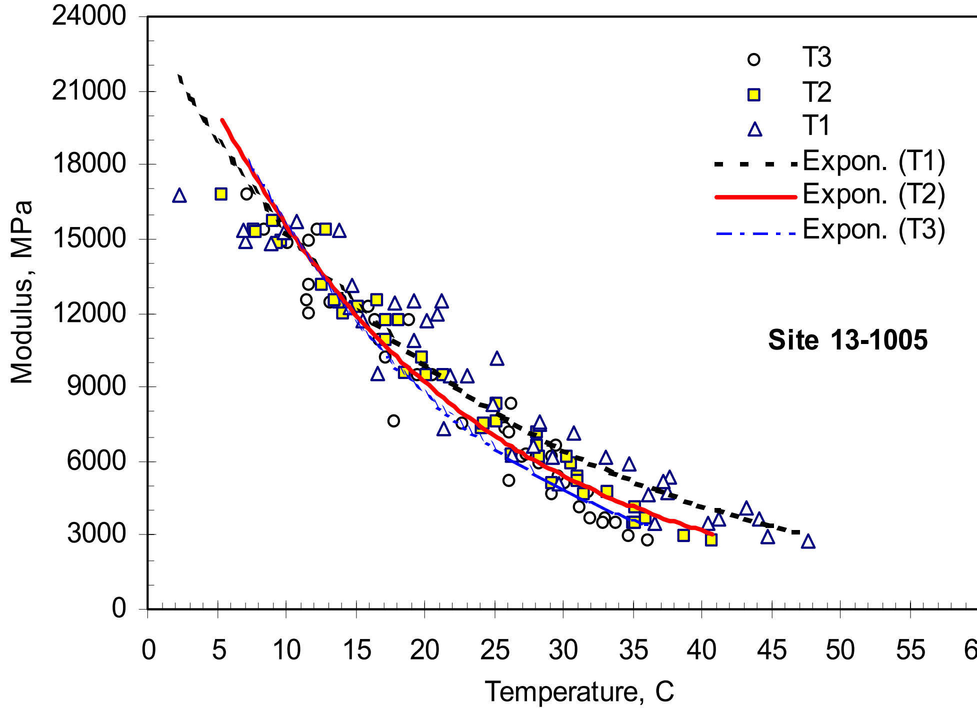

Figure 6.5: AC Modulus versus Temperature at Various Depths for Site13-1005

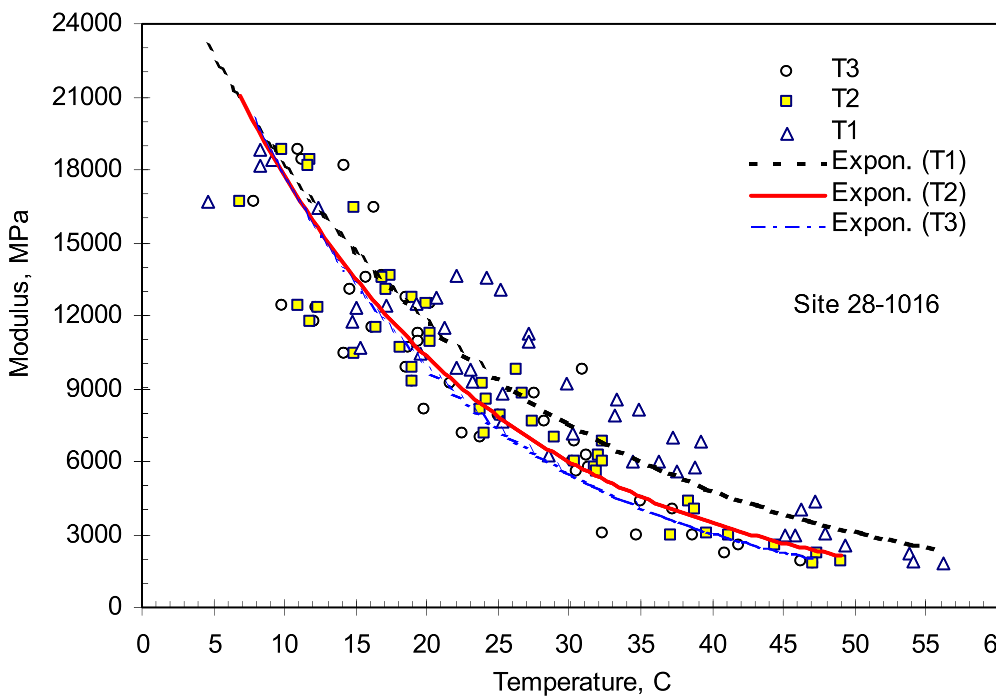

Figure 6.6: AC Modulus versus Temperature at Various Depths for Site 28-1016

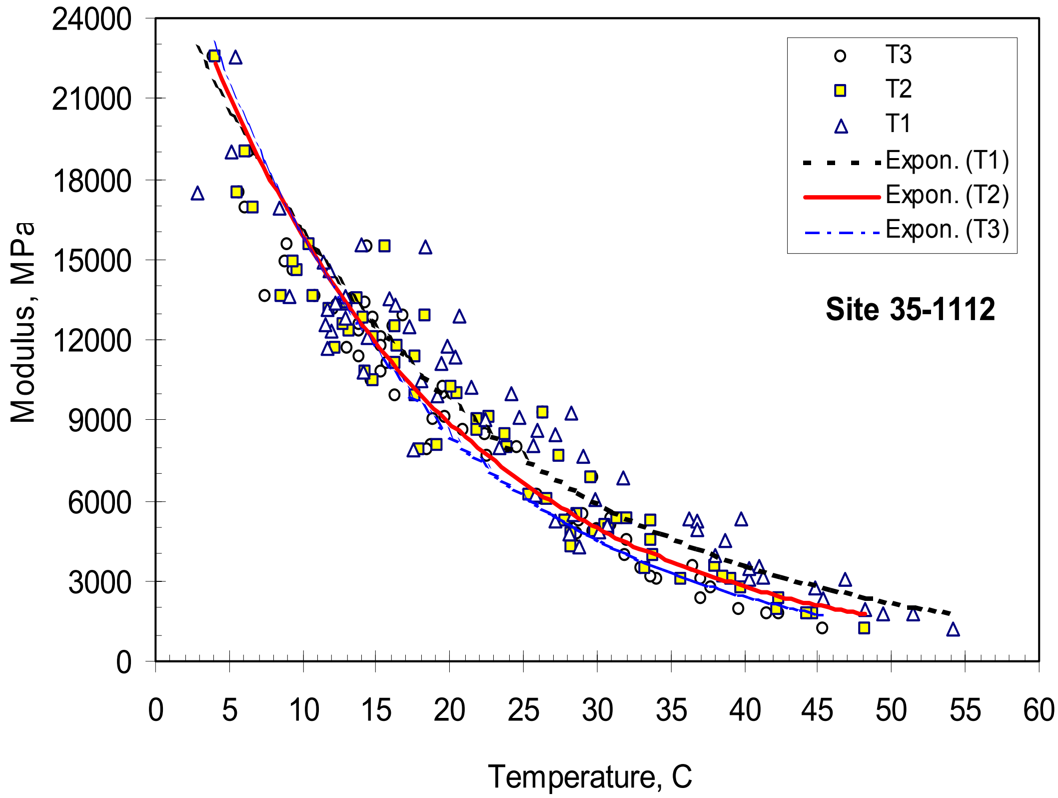

Figure 6.7: AC Modulus versus Temperature at Various Depths for Site 35-1112

6.3.2 AC Modulus versus Mid-Depth Temperature

6.3.2.1 Data from Nonfreezing Zones

The modulus temperature relationships were plotted for five different sites, from nonfreezing zones. The results of the five sites, shown in Figure 6.8, indicate that the AC modulus could be related to the pavement temperature with an exponential function in the form:

$$E = K_o * e^{K2 * Tac} \qquad (6.3)$$

Taking the natural logarithm (log) of Equation 6.3 yields:

$$E_1 = K_1 + K_2 * Tac \qquad (6.4)$$

where,

E = AC elastic modulus

E_1 = Log (E)

Tac = AC pavement temperature

K_1 = Log (k_o)

The values of the model coefficients, K_o, K_1 and K_2 are presented in Table 6.4. The table indicates that this model has a good coefficient of determination, where R^2 ranges from 0.85 to 0.98. The model exponent (K_2) ranges from -0.051 to -0.058, while the intercept (K_1) ranges from 9.86 to 10.42. The model fitted to different nonfreezing sites is shown in Figure 6.8. The figure indicates that the curves for all sites are almost parallel; they have nearly the same slope but different intercepts. The difference in intercepts could be related to the difference in the AC layer properties such as binder grade, binder content, mix specific gravity, aggregate type and /or degree of compaction during construction.

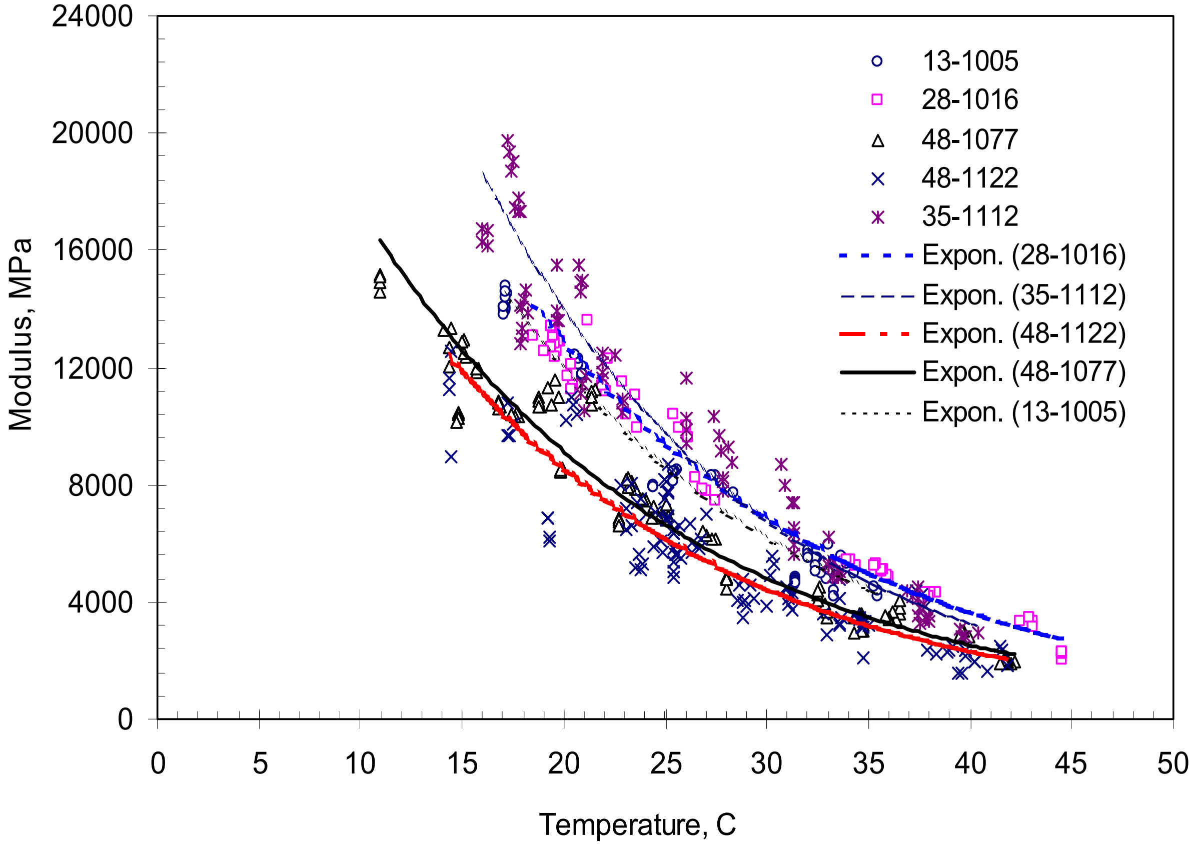

Figure 6.8 AC Modulus - Temperature Relationship for 5 Sites from Nonfreezing Zones

Table 6.4 Estimated Coefficients of the Exponential Function for Nonfreezing Sites

Site	**K_o**	**K_1 = Ln (k_o)**	**K_2**	**R^2**
13-1005	26740	10.19	-0.053	0.96
28-1016	28471	10.26	-0.051	0.98
48-1077	20090	9.91	-0.052	0.96
48-1122	19163	9.86	-0.053	0.85
35-1112	33525	10.42	-0.058	0.95
All Sites	23850	10.13	-0.053	0.83

Comparing the results of Figure 6.8 to the AC layer properties shown on Table 6.1, the data show that the site having the higher intercept (site 35-1112) also has the higher binder grade (AC-30). On the other hand, the site having the lower intercept (site 48-1122) also has the lower binder grade (AC-10). Therefore, the intercept increases with increasing binder grade. This observation makes sense, because higher binder grades are more viscous and less affected by temperature. The effect of binder grade and the other AC layer properties, shown in Table 6.1, will be discussed later in detail, through statistical analysis using the SAS program.

Figure 6.9 shows the model fitted to all five sites. The model coefficients are shown on the last row of Table 6.4. The results indicate that a good R^2 value of 0.83 still could be achieved when applying the model to the data from all sites.

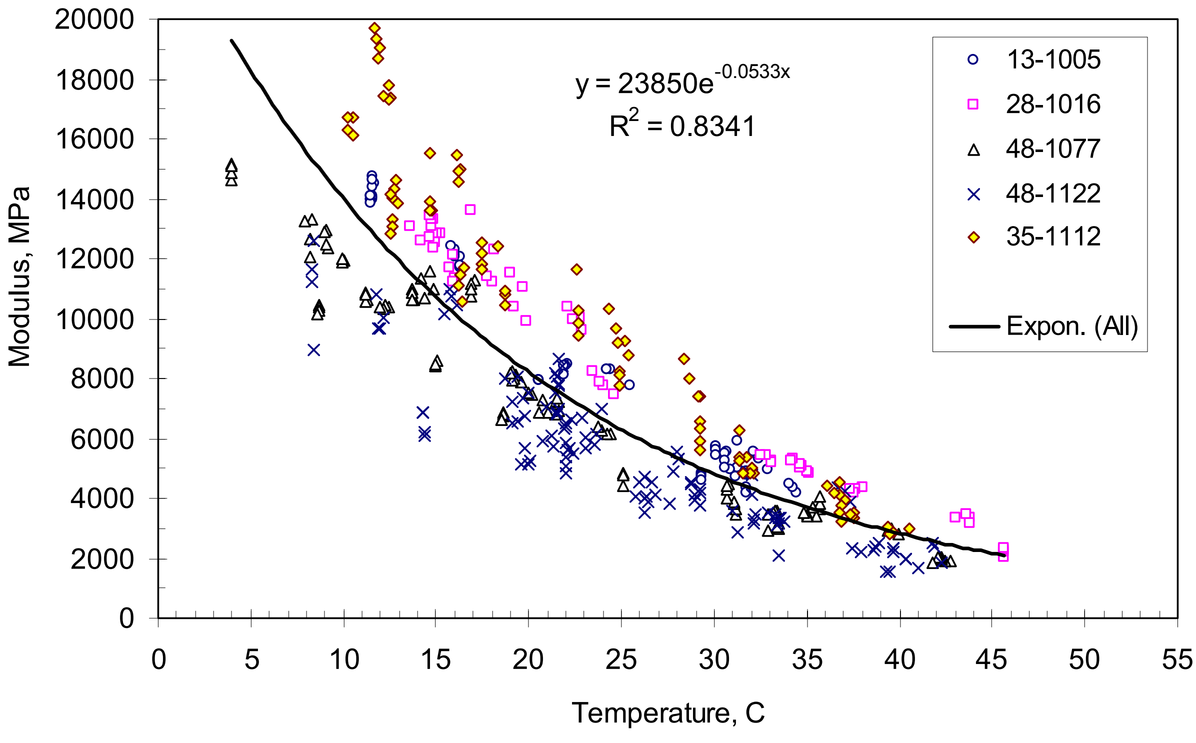

Figure 6.9 AC Modulus - Temperature Relationship (Average of 5 Sites from Nonfreezing Zones)

6.3.2.2 Data from Freezing Zones

It is important to note that "freezing zones" are those classified by LTPP. The term refers to regions where the temperature may fall below zero degrees Celsius. The temperature data reported in the sites in these zones showed temperature ranges well above zero degrees (refer to Figure 6.10). The apparent reason is the fact that it is practically impossible to test the pavements at these low temperatures.

Therefore, the author considered the use of Equation 6.4 to compare the data of the six different sites from freezing zones. The values of the model coefficients, K_o, K_1 and K_2 are shown in Table 6.5. The table shows that this model also achieved a good coefficient of determination, where R^2 ranges from 0.67 to 0.96. The exponent of the power function (K_2) ranges from -0.037 to -0.059 while the intercept (K_1) ranges from 9.24 to 9.76. The model fitted to the data of different freezing sites is shown in Figure 6.10. The figure indicates the curves for the different sites are not as parallel as the sites of nonfreezing zones. The main reason for this difference maybe related to the freezing effect of the AC pavement. When the pavement temperature reaches freezing, higher modulus values are achieved. The modulus variation with temperature below the freezing point is not the same as its variation above the freezing point. It may behave in a different way and at a different rate. Since the minimum temperature that was recorded at these sites is about –3.5 ^oC, there are not enough data available to show this modulus variation with temperature when the temperature falls below the freezing point, simply because the data are not available. Thus, it is important to re-iterate that the freezing effect on the modulus is not quantified in this study, simply because the data are not available or very scarce in the LTPP database.

The model fitted to all six sites is shown in Figure 6.11. The model coefficients are presented on the last row of Table 6.5. The results indicate that R^2 value is 0.77 when applying the model to the data from all freezing sites, which is lower than the corresponding value of the nonfreezing sites (0.83).

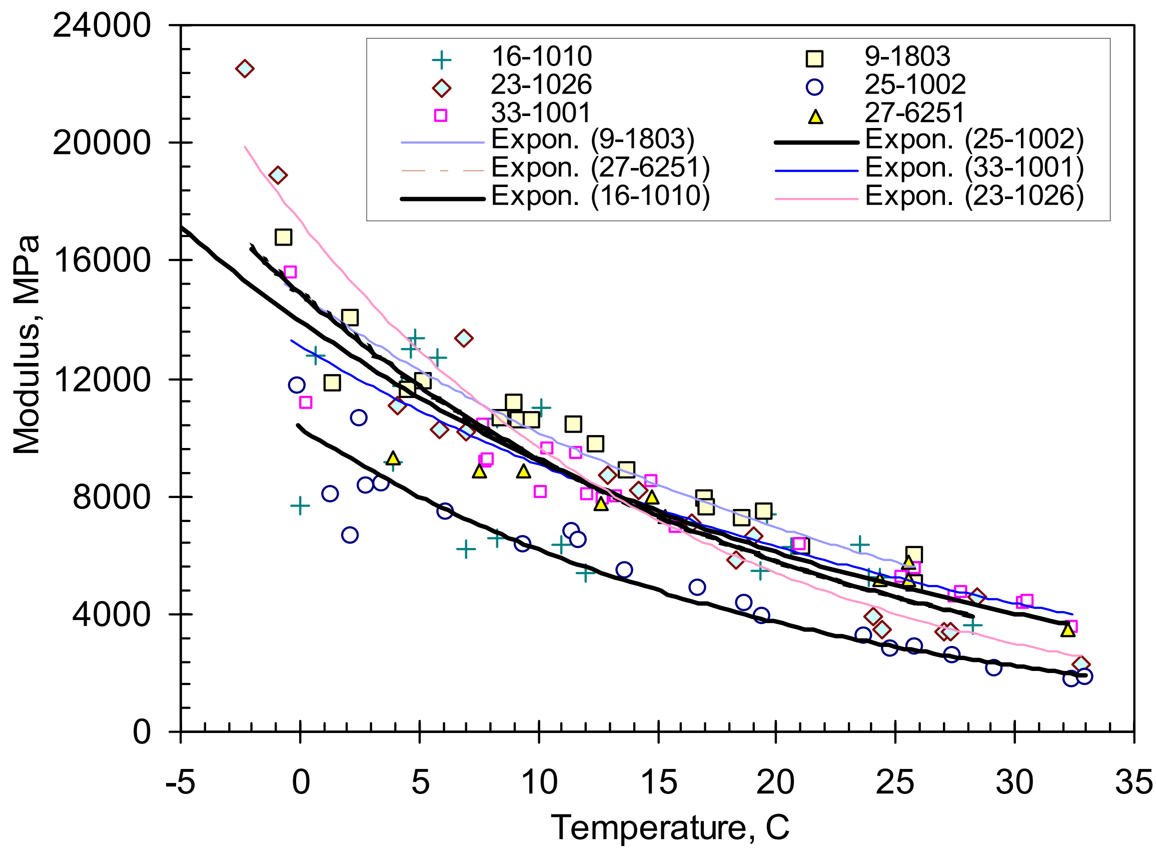

Figure 6.10 AC Modulus - Temperature Relationship for 6 Sites from Freezing Zones

Table 6.5 Estimated Coefficients of The Exponential Function for Freezing Sites

Site	**K_o**	**K_1**	**K_2**	**R^2**
9-1803	14852	9.61	-0.038	0.95
23-1026	17337	9.76	-0.059	0.95
25-1002	10322	9.24	-0.051	0.96
33-1001	13104	9.48	-0.037	0.95
16-1010	14888	9.61	-0.047	0.67
27-6251	13960	9.54	-0.042	0.91
All Sites	14077	9.54	-0.048	0.77

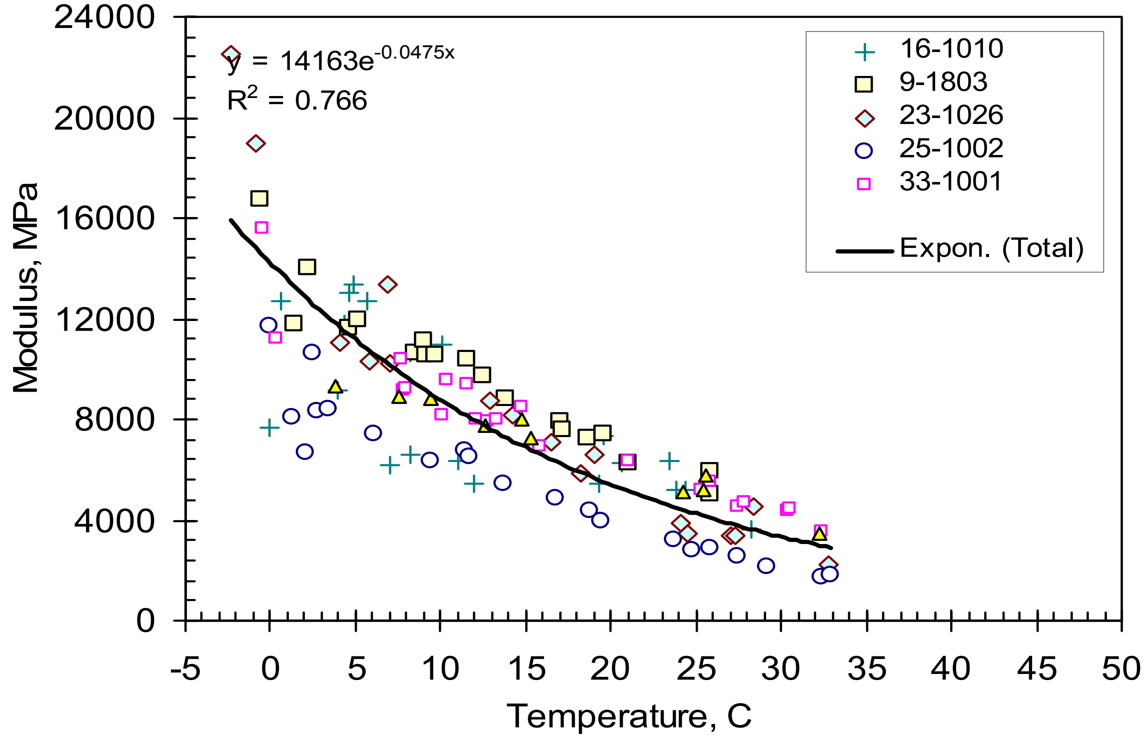

Figure 6.11 Modulus - Temperature Relationship (Average 6 Sites, Freezing Zone)

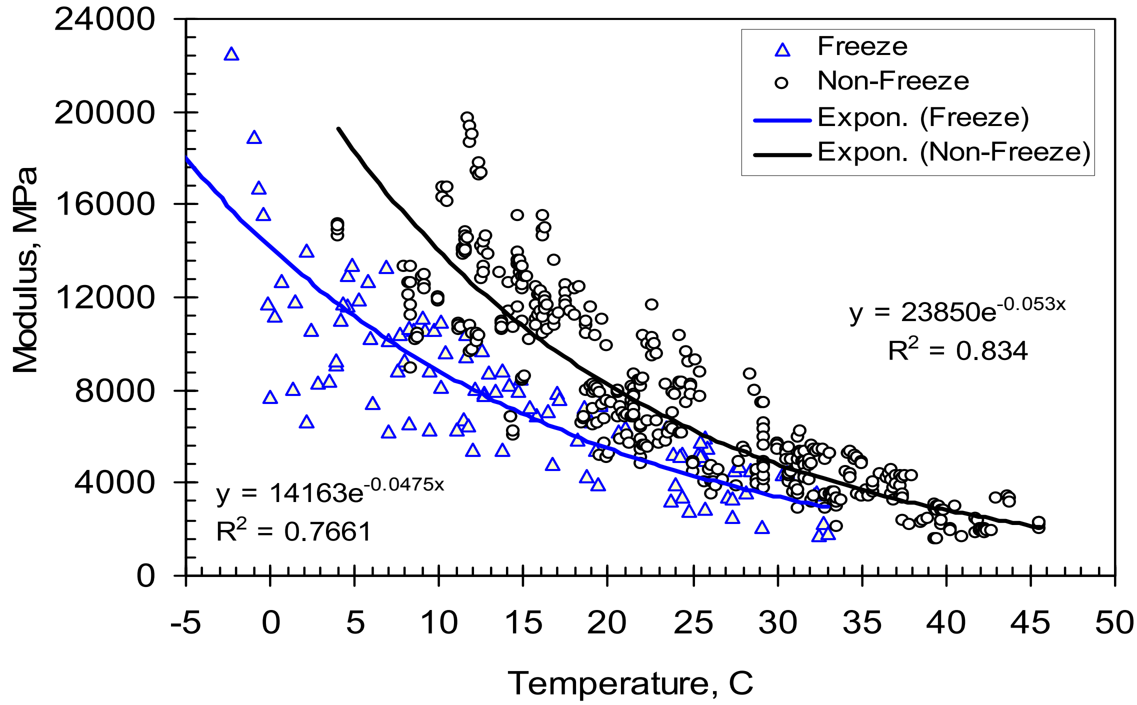

Figure 6.12 Modulus-Temperature Relationship for Freezing & Nonfreezing Zones

6.3.3 Comparing Both Freezing & Nonfreezing Sites

Figure 6.12 shows the exponential model when fitted to both nonfreezing and freezing sites together. The model parameters, shown in the last row of Table 6.4 and Table 6.5 indicate that the intercept and R^2 values in case of nonfreezing sites are greater than those of the freezing sites (K_1= 10.13 & 9.6 respectively, R^2 = 0.83& 0.77 respectively). The exponent coefficient (K_2) values are –0.053 and –0.048 for both nonfreezing and freezing sites respectively. The data shown in Figure 6.12 were reported from eleven different sites (5 from nonfreezing and 6 from freezing zones). The figure indicates that at the same pavement temperature the nonfreezing sites have a greater AC modulus value than the freezing sites. This phenomenon could be related to the freezing and thawing effects that weaken the layer modulus. It could also be related to the properties of the material used in the different sites and/or compaction and construction methods. Additionally, the figure represents a range of the modulus temperature relationship with the nonfreezing sites in its upper limit and the freezing sites in its lower limit. Therefore, this figure could be used to capture the modulus temperature relationship if there is no information about the properties of the AC layer materials.

6.4 AC LAYER MODULUS PREDICTION MODELS

Although the previous analysis showed that the AC modulus has a strong correlation with AC pavement temperature, the temperature alone could not be used to accurately predict the modulus. The AC layer properties surely affect the value of the elastic modulus. Marshal et al. (2001) indicated that the asphalt concrete modulus is a function of the asphalt binder properties; mix volumetrics, and compacted density. This section is devoted to the discussion of the prediction of the AC modulus from the mid-depth pavement temperature and various layer properties.

6.4.1 Nonfreezing sites

As described previously, the AC layer modulus could be related to the asphalt pavement temperature with an exponential function. It was also mentioned above that the different sites of nonfreezing zones followed almost the same exponential function but with different intercepts. The difference in intercepts could be related to the difference in AC layer properties such as layer thickness, mix specific gravity, mix air voids, asphalt binder content and binder grade. Therefore, an attempt was made using the statistical package SAS software to predict the AC layer modulus from the mid-depth pavement temperature and the AC layer properties presented in Table 6.1. The statistical analysis revealed the general model given by Equation 6.6.

$$\text{Log}(E) = C_o + C_1 * \text{Tac} + C_2 * H + C_3 * \text{BSG} + C_4 * \text{AV} + C_5 * \text{GRD} \qquad (6.6)$$

where,

E	= AC elastic modulus, MPa
Log (E)	= Natural logarithm of E
Tac	= AC mid-depth temperature, ^{o}C
H	= AC layer thickness, mm
BSG	= Bulk specific gravity of AC mix
AV	= % of air voids in the mix

GRD = Code representing the binder grade; equals to 1 for AC-10, 2 for AC-20 and 3 for AC-30.

C_o, C_1, C_2, C_3, C_4 & C_5 = Model coefficients equal 7.215, -0.053, 0.001, 1.095, -0.0495 and 0.146, respectively.

The model given by Equation 6.6 could be achieved through the SAS regression results presented in Table 6.6. After substituting the estimated values of model coefficients, the model takes the form shown in Equation 6.7:

$$\text{Log (E)} = 7.215 - 0.053\ \text{Tac} + 0.001\ \text{H} + 1.095\ \text{BSG} - 0.049\ \text{AV} + 0.146\ \text{GRD} \quad (6.7)$$

As shown in Table 6.6, the model given by Equation 6.7 is based on 386 data points from 5 different sites (LTPP sites 13-1005, 28-1016, 35-1112, 48-1077and 48-1122). The coefficient of determination (R^2) for this model is 0.956 and the value of root MSE is 0.123. The positive sign of the coefficients C_2, C_3 and C_5 indicates that the modulus increases with increasing the AC layer thickness, the bulk specific gravity of AC mix and the binder grade. The negative sign of coefficients C_1 and C_4 indicates that the modulus decreases with increasing both the pavement temperature and the air voids in the asphalt mix. The statistical analysis also revealed that adding the binder percentage, binder penetration and binder specific gravity to the model is not significant, so these are not included in the model.

Figure 6.13 shows the model when fitted to the data from five different sites. The figure indicates that the data points in all sites are almost symmetrical around the equity line (45^o line), which indicates that the model fits the data very well.

.

Table 6.6: Regression Analysis for Predicting the AC Modulus for Nonfreezing Zone

Dependent Variable: E1

R-Square Selection Method

Number in Model	R-Square	C(p)	BIC	Root MSE	Variables in Model
1	0.8436	970.9192	-1135.4151	0.23059	Tac
1	0.0917	7479.205	-456.3919	0.55568	Zt
1	0.0911	7484.438	-456.1346	0.55586	Grd
1	0.0789	7589.857	-450.9886	0.55958	BSG
2	0.9483	66.9131	-1558.4751	0.13280	Tac Grd
2	0.9346	185.3512	-1468.9268	0.14933	Tac Zt
2	0.8836	626.3375	-1248.4249	0.19916	Tac BSG
3	0.9516	39.8510	-1582.2036	0.12859	Tac BSG Grd
3	0.9497	56.6429	-1567.2899	0.13114	Tac AV Grd
3	0.9496	57.2448	-1566.7658	0.13123	Tac Zt Grd
4	0.9550	12.1352	-1608.1173	0.12411	Tac BSG AV Grd
4	0.9543	18.2349	-1602.2524	0.12508	Tac Zt BSG Grd
5	0.9560	6.0000	-1614.0502	0.12297	Tac Zt BSG AV Grd

Analysis of Variance

Source	DF	Sum of Squares	Mean Square	F Value	Pr > F
Model	5	125.11478	25.02296	1654.91	<.0001
Error	381	5.76088	0.01512		
Corrected Total	386	130.87566			

Root MSE	0.12297	R-Square	0.9560
Dependent Mean	8.79699	Adj R-Sq	0.9554
Coeff Var	1.39781		

Parameter Estimates

Variable	DF	Parameter Estimate	Standard Error	t Value	Pr > |t|	Variance Inflation
Intercept	1	7.21465	0.35946	20.07	<.0001	0
Tac	1	-0.05330	0.00063214	-84.32	<.0001	1.03034
Zt	1	0.00101	0.00035361	2.85	0.0046	5.60312
BSG	1	1.09529	0.15414	7.11	<.0001	1.43412
AV	1	-0.04948	0.01311	-3.77	0.0002	1.99650
Grd	1	0.14585	0.01738	8.39	<.0001	7.72589

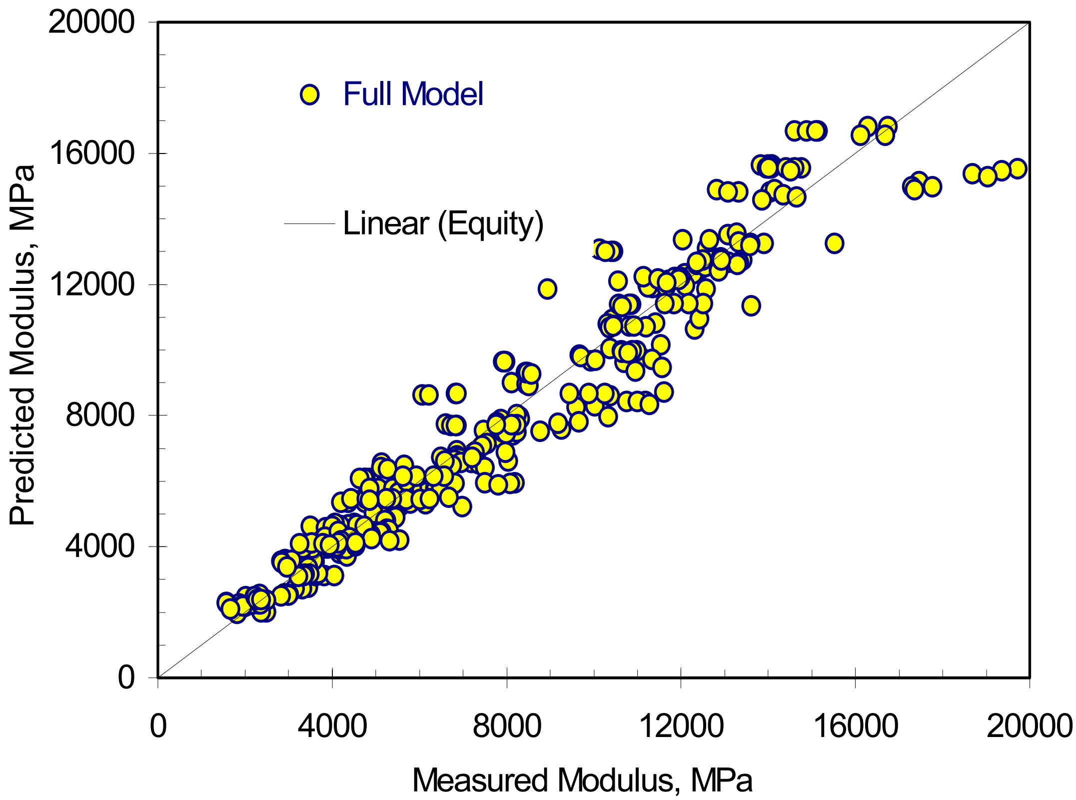

Figure 6.13: Fitting the Model to the Data from 5 Different Nonfreezing Sites

6.4.2 Freezing Sites

Five LTPP sites (9-1803, 23-1026, 25-1002,33-1001, 16-1010) were considered in this analysis; the sixth site (27-6251) was excluded because there is no information available for the properties of the asphalt binder used in it, as it appears in Table 6.1. The same regression procedures used before in the nonfreezing sites were also followed in these sites. The regression results, presented in Table 6.7, indicate that all the variables included in the model are significant. The table shows also that the predicted model takes the general form of the nonfreezing sites, given by Equation 6.6, but with different coefficients. The model coefficients C_o, C_1, C_2, C_3, C_4 and C_5 were found to be 5.398, -0.047, 0.007, 1.753, -0.420 and 0.469 respectively. The model was based on 406 data points from five different sites with R^2 value of 0.897, which is less than that of the nonfreezing zone model, and root MSE of 0.171. Equation 6.8 could represent the developed model.

$$\text{Log (E)} = 5.398 - 0.047\ \text{Tac} + 0.007\ \text{H} + 1.753\ \text{BSG} - 0.420\ \text{AV} + 0.469\ \text{GRD} \quad (6.8)$$

As it appears in the previous equation, the model coefficients C_o, C_1, C_2, C_3, C_4 and C_5 have also the same signs like the nonfreezing zone model, given by Equation 6.7, with slight difference in their numeric values. This agreement between the two models could be considered validation for both of them. The lower R^2 values for the Equation 6.8, compared to Equation 6.7, could be related to the freezing and thawing effect that may cause aging and pavement distress in some of the sites in the freezing zone. This pavement surface distress could make the AC layer behave non-homogenously compared to the nonfreezing sites. The data presented in Figure 6.8 and Figure 6.10 explains this behavior. While the curves are almost parallel for all the nonfreezing sites (Figure 6.8), they are not for the freezing sites (6.10) due to the dissimilarity in the pavement surface condition.

Table 6.7: Regression Analysis for Predicting the AC Modulus in the Freezing Zone

Dependent Variable: E1

R-Square Selection Method

Number in Model	R-Square	C(p)	BIC	Root MSE	Variables in Model
1	0.7619	526.7564	-1097.1391	0.25945	Tac
1	0.0465	3319.781	-534.7746	0.51915	AV
1	0.0308	3381.147	-528.1337	0.52342	Zt
1	0.0261	3399.544	-526.1638	0.52469	BSG
2	0.8127	330.3868	-1192.9843	0.23040	Tac AV
2	0.7763	472.3202	-1121.5184	0.25176	Tac BSG
2	0.7715	491.1850	-1112.9007	0.25446	Tac Grd
3	0.8284	271.0643	-1227.0193	0.22080	Tac Zt AV
3	0.8204	302.1541	-1208.8194	0.22586	Tac AV Grd
3	0.8130	331.0230	-1192.6209	0.23047	Tac BSG AV
4	0.8955	11.0665	-1423.4455	0.17252	Tac Zt AV Grd
4	0.8798	72.4081	-1367.7869	0.18503	Tac Zt BSG AV
4	0.8614	144.1134	-1311.1658	0.19867	Tac BSG AV Grd
5	0.8973	6.0000	-1428.3500	0.17123	Tac Zt BSG AV Grd

Analysis of Variance

Source	DF	Sum of Squares	Mean Square	F Value	Pr > F
Model	5	102.72090	20.54418	700.66	<.0001
Error	401	11.75779	0.02932		
Corrected Total	406	114.47868			

Root MSE	0.17123	R-Square	0.8973
Dependent Mean	8.87885	Adj R-Sq	0.8960
Coeff Var	1.92856		

Parameter Estimates

Variable	DF	Parameter Estimate	Standard Error	t Value	Pr > |t|	Variance Inflation
Intercept	1	5.39834	1.57485	3.43	0.0007	0
Tac	1	-0.04709	0.00091151	-51.66	<.0001	1.04884
Zt	1	0.00735	0.00062079	11.84	<.0001	7.13298
BSG	1	1.75291	0.65941	2.66	0.0082	17.77705
AV	1	-0.41989	0.01949	-21.54	<.0001	4.49315
Grd	1	0.46912	0.05672	8.27	<.0001	10.44904

The model, given by Equation 6.8, was applied to compare data from five different sites of freezing zones; the results are shown in Figure 6.14. The figure indicates that the data are well centered around the equity line except a few data points (13 out of 406) having higher modulus values, which were reported during the freezing season. Figure 6.14 indicates that some of the modulus values reported during freezing season are much higher than usual, where the modulus values exceeded 30, 000 MPa, while the highest modulus value reported in the nonfreezing sites is 20,000 MPa. These higher values maybe related to the freezing effect, which occurs for a limited time period, or to an error in the backcalculation process. Therefore, ignoring these values will not affect the model accuracy. The figures shows also that the model underestimates the modulus during the freezing season, which is considered safe and more conservative because of the high variability in measuring the modulus during freezing season.

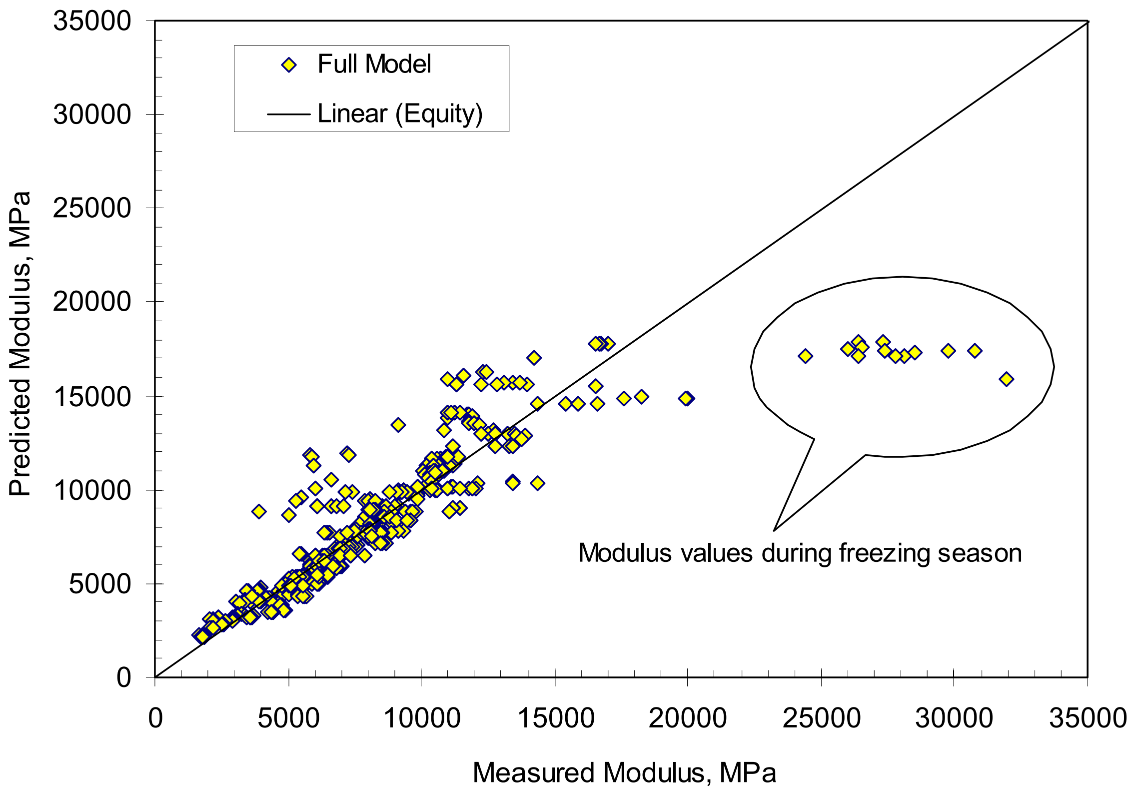

Figure 6.14: Fitting the Model to the Data from 5 Different Freezing Sites

6.5 ESTIMATING THE AC SEASONAL ADJUSTMENT FACTOR

The previous analysis allows for prediction of the absolute value of the AC modulus at a given temperature for the included sites. Although many variables were included in the models given by Equations 6.7 and 6.8 that could accurately estimate the elastic AC modulus from pavement temperature and other layer properties, there maybe some concern that certain other variables may affect the modulus values. These other variables, which could not be included in the model, may include the construction method, pavement surface condition and pavement age. Therefore, another effort was made to make the model applicable for any site. Instead of using the absolute AC modulus values that may be site specific, a relative value called seasonal adjustment factor (SAF_{ac}) was used. The SAF_{ac} is defined as the AC modulus for a certain site at any season divided by the AC modulus during a reference season, summer. The asphalt pavement temperature was also replaced by the temperature ratio (T_r). This is the ratio of the temperature at the season for which one needs to calculate the AC modulus shift factor divided by the temperature of the selected reference season, summer.

Regression analysis was employed to predict the AC modulus shift factor based on pavement temperature and the previously stated layer properties. The regression results for non-freezing sites indicated that the modulus shift factor could be determined only from the temperature ratio (T_r) with R^2 value of 0.90. The statistical analysis also showed that adding the other AC layer properties such as viscosity, thickness, or MSG did not contribute statistically significantly to the model. Therefore the model takes the form shown in Equation 6.9.

$$SAF_{ac} = C_1 \, EXP\,(C_2 \, T_r) \qquad (6.9)$$

where,

SAF_{ac} = AC modulus at any season divided by AC modulus during summer = (E_{season} / E_{summer})

T_r = Temperature ratio = Pavement temperature at any season divided by the summer temperature.

C_1 and C_2 are model coefficients for nonfreezing zones. Thus C_1= 10.44 and C_2 = -2.18. For freezing zones the coefficients C_1 and C_2 were found to be 4.64 and -1.47, respectively. The R^2 value was found to be 0.69, which is smaller than that of the nonfreezing zones but could be considered acceptable due to the fact that the data used here are actual field data, which have been collected under the vast variability in environmental conditions.

The model was compared to data from both nonfreezing and freezing sites; the results are shown in Figure 6.15. The figure shows higher variability of the data from freezing sites while much less variability with nonfreezing sites. The two curves of nonfreezing and freezing sites, shown in Figure 6.15, could be used as upper and lower limits for estimating the seasonal adjustment factor. The figure indicates that if the temperature ratio reduces from 1.0 (during summer) to 0.1 (during winter), the modulus value would increase to more than 8 times of its summer value for nonfreezing sites and about 4 times its summer value for freezing sites.

The model shown in Equation 6.9 is simple, dimensionless and does not need many input parameters. Once the user determines the reference modulus and temperature, Equation 6.9 can be used to determine the modulus at any season by multiplying the reference modulus value by the SAF_{ac} value of that season. In this analysis, the authors used the summer temperature as the reference point, which is the construction season and is generally associated with the lowest AC modulus.

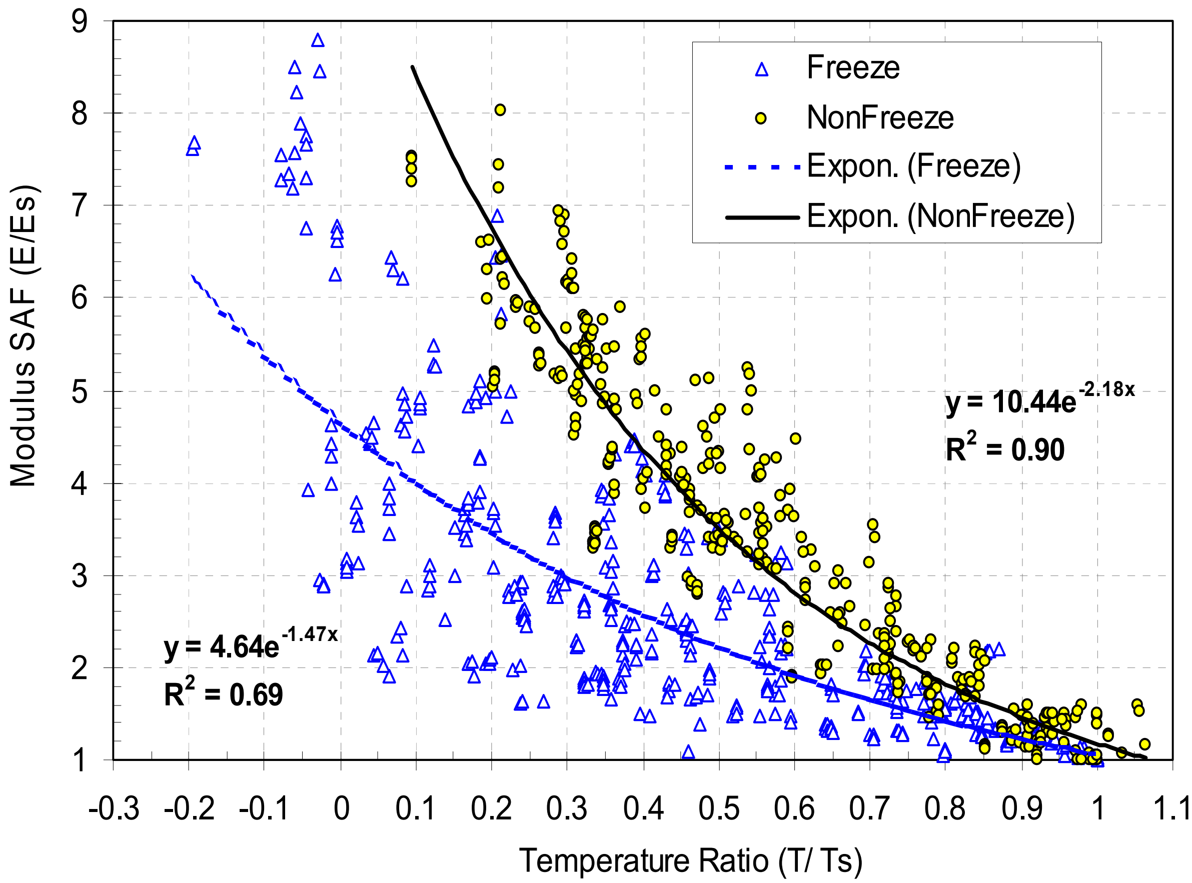

Figure 6.15: Estimated SAF for AC Layer, Nonfreezing & Freezing Zones

6.6 PREDICTION OF ASPHALT PAVEMENT TEMPERATURE

Since the asphalt pavement temperature was found in all the previous models to be related to the AC layer modulus, there is a need to relate the asphalt pavement temperature to the air temperature. Lukanen et al. (2000) and Abo-Hashima and Bayomy (2002) developed regression models to predict the asphalt pavement temperature based on air temperature. Both model are given by Equations 2.35 and 2.36, Chapter 2, respectively. However, these models require much input data that might not be available to the ordinary site engineer, such as the average temperature for the day or for five days before testing.

Therefore, an effort was made to relate the asphalt pavement temperature to the air temperature for different LTPP sites. Data from eight different sites were included in this analysis; five from non-freezing zones and three from freezing zone. The nonfreezing sites were the same as used before in the modulus- moisture relationship. These sites are 13-1005, 28-1016, 48-1077, 48-1122 and 35-1112. The freezing sites were chosen within and surrounding the state of Idaho so that the model could be validated using the data measured from the installed sites in Idaho. These three sites are 16-1010 in Idaho, 30-8129 in Montana and 49-1010 in Utah. The parameters incorporated in the prediction of the AC temperature were the air temperature at the time of testing, the month and the depth at which it is required to predict the AC temperature, and the site latitude. The site latitude was included to represent the solar radiation based on a study by Mohseni and Symons (1998), discussed in Chapter 2. The month number was included in a sinusoidal function because the difference between air and pavement temperatures is greatest during summer and winter while during spring and fall the temperature difference is small.

Regression analysis was employed to predict the asphalt pavement temperature from the previously stated parameters using the SAS program, and the result is shown in Table 6.8. The table indicates that the air temperature is a better predictor of the asphalt pavement temperature than the asphalt surface temperature. In other words, the asphalt pavement temperature could be predicted only from the air temperature with R^2 value of 0.894 and root MSE of 3.96 while it could be predicted only from the asphalt surface temperature with R^2

value of 0.869 with root MSE of 4.4. When the other parameters were added to the model the R^2 value is increased to 0.954 and the root MSE decreased to 2.6.

The analysis of variance (ANOVA) table and the parameter estimates for the model are shown in

Table 6.9 based on 570 data points from eight different sites. Based on

Table 6.9 the full regression model, given by Equation 6.10, was achieved.

$$Tac = 8.956 + 0.398\ Ts + 0.6075\ Tair + 0.16\ T - 0.2709\ T2 - 0.00396\ Lat1 \qquad (6.10)$$

where,

Lat1	$= (Lat)^2$	(6.11a)
M1	$= COS ((M- 7)* \pi/6)$	(6.11b)
Z1	$= Log10 (Z) - 1.25$	(6.11c)
T	$= Tair * M1$	(6.11d)
T2	$= Tair * Z1$	(6.11e)

Tac	= Asphalt pavement temperature, ^oC
Ts	= Asphalt surface temperature recorded during FWD test, ^oC
Tair	= Air temperature, ^oC
Z	= Depth at which it is intended to predict the AC temperature, mm
M	= Month number (1, 2,……..,12)
Lat	= Latitude, Degree

Equation 6.10 can also take the form shown in Equation 6.12, after submitting the variables with their corresponding basic elements.

$$Tac = Tair\ \{0.6075 + 0.16 * COS\ [(M- 7)* \pi/6] - 0.2709\ [Log10\ (Z) - 1.25]\} + 0.398\ Ts - 0.00396\ Lat^2 + 8.956 \qquad (6.12)$$

Although all the model parameters used to predict the AC pavement temperature in Equation 6.12 are significant, there may be a concern that the asphalt surface temperature might not be available in some sites. Therefore, it is excluded from the model to simplify the model input parameters and make it applicable to all sites.

Table 6.8 Regression Analysis for Predicting Pavement Temperature

Dependent Variable: Tac
R-Square Selection Method

Number in Model	R-Square	C(p)	BIC	Root MSE	Variables in Model
1	0.8936	749.8649	1570.6523	3.96225	Tair
1	0.8687	1057.364	1689.8283	4.40093	Ts
1	0.4860	5788.932	2465.8637	8.70746	T
1	0.2607	8574.401	2672.8330	10.44284	T2
2	0.9143	496.0376	1449.1328	3.55942	Ts Tair
2	0.9088	562.9556	1483.7730	3.67005	Tair T2
2	0.9028	637.6704	1520.1100	3.78976	Tair T
2	0.8971	708.0679	1552.3468	3.89919	Tair Lat1
3	0.9309	292.0929	1328.3205	3.19783	Ts Tair T2
3	0.9211	412.9736	1402.9859	3.41663	Ts Tair Lat1
3	0.9199	428.8233	1412.0870	3.44429	Ts Tair T
3	0.9198	429.3338	1412.3778	3.44518	Tair T T2
4	0.9381	204.6769	1267.4929	3.02848	Ts Tair T2 Lat1
4	0.9378	208.7057	1270.4451	3.03645	Ts Tair T T2
4	0.9349	245.1558	1296.4792	3.10761	Ts Tair T Lat1
4	0.9328	270.6037	1313.9726	3.15633	Tair T T2 Lat1
5	0.9544	6.0000	1098.7883	2.60322	Ts Tair T T2 Lat1

Model Parameters

Tac = Asphalt pavement temperature, ^oC

Ts = Asphalt surface temperature recorded during FWD test, oC

Tair = Air temperature, ^oC

Z = Depth at which it is intended to predict the AC temperature, mm

M = Month number (1, 2,…….,12)

Lat = Latitude, Degree

Lat1 = $(Lat)^2$

M1 = COS ((M- 7)* π/6)

Z1 = -1.25 + Log (Z)/ Log (10)

T = Tair * M1

T2 = Tair * Z1

Table 6.9 ANOVA Table & Estimated Model Parameters for Predicting Asphalt Pavement Temperature (Full Model)

Dependent Variable: Tac

Analysis of Variance

Source	DF	Sum of Squares	Mean Square	F Value	Pr > F
Model	5	79959	15992	2359.82	<.0001
Error	564	3822.08053	6.77674		
Corrected Total	569	83781			

Root MSE	2.60322	R-Square	0.9544
Dependent Mean	20.86719	Adj R-Sq	0.9540
Coeff Var	12.47517		

Parameter Estimates

Variable	DF	Parameter Estimate	Standard Error	t Value	Pr > |t|	Variance Inflation
Intercept	1	8.95623	0.58281	15.37	<.0001	0
Ts	1	0.39773	0.02436	16.33	<.0001	7.67947
Tair	1	0.60745	0.03254	18.67	<.0001	9.18587
T	1	0.15997	0.01129	14.17	<.0001	2.17010
T2	1	-0.27087	0.01744	-15.53	<.0001	1.70825
Lat1	1	-0.00396	0.00027690	-14.31	<.0001	1.37288

Table 6.10 ANOVA Table & Estimated Model Parameters for Predicting Asphalt Pavement Temperature (Reduced Model)

Dependent Variable: Tac

Analysis of Variance

Source	DF	Sum of Squares	Mean Square	F Value	Pr > F
Model	4	78153	19538	1961.18	<.0001
Error	565	5628.78377	9.96245		
Corrected Total	569	83781			

Root MSE	3.15633	R-Square	0.9328
Dependent Mean	20.86719	Adj R-Sq	0.9323
Coeff Var	15.12582		

Parameter Estimates

Variable	DF	Parameter Estimate	Standard Error	t Value	Pr > |t|	Variance Inflation
Intercept	1	8.62712	0.70622	12.22	<.0001	0
Tair	1	1.04513	0.02236	46.74	<.0001	2.95110
T	1	0.17794	0.01363	13.06	<.0001	2.14948
T2	1	-0.26184	0.02114	-12.39	<.0001	1.70654
Lat1	1	-0.00349	0.00033391	-10.46	<.0001	1.35803

The analysis of variance (ANOVA) and the parameter estimates for the reduced model are presented in Table 6.10. The table shows that the reduced model, given by Equation 6.13 could be achieved. The table indicates that the reduced model has R^2 value of 0.932 and root MSE of 3.156. The parameters included in Equations 6.12 and 6.13 are the same as stated before in Equation 6.11.

$$\text{Tac} = 8.627 + 1.045\ \text{Tair} + 0.1779\ \text{T} - 0.2618\ \text{T2} - 0.0035\ \text{Lat1} \qquad (6.13)$$

As previously stated, Equation 6.13 can be transformed to the form shown in Equation 6.14.

$$\text{Tac} = \text{Tair}\ \{1.045 + 0.1779 * \text{COS}\ [(\text{M- }7)*\ \pi/6] - 0.2618\ [\text{Log}_{10}\ (\text{Z}) - 1.25]\}$$

$$- 0.0035\ \text{Lat}^2 + 8.627 \qquad (6.14)$$

The general model given by Equation 6.12 was fitted to the data collected from eight different sites (13-1005, 28-1016, 48-1077, 48-1122, 35-1112, 16-1010, 30-8129 and 49-1010), and the results are shown in Figure 6.16. The figure shows that the data are well centered around the equity line, which indicates that the model fits the data very well. Three different models (AI, BELLS and IPAT), which were previously described in Chapter 2 by Equations 2.34, 2.35 and 2.36 were used to fit the data from six different LTPP sites. These sites are 13-1005, 28-1016, 35-1112, 16-1010, 30-8129 and 49-1010. The results are shown Figure 6.17. The figure indicates that the model developed in this study, Equation 6.14, is the best to fit the data (R^2 = 0.96).

Although the BELLS model, by Lukanenet et al. (2000), was developed based on more LTPP sites than this study, it achieved lower correlation (R^2 = 0.935). The reason is simply because the model should be applied on a certain time through the day not on an average daily basis as we did in this figure. The R^2 value for the IPAT model was found to be 0.93 while that for the AI model was 0.89.

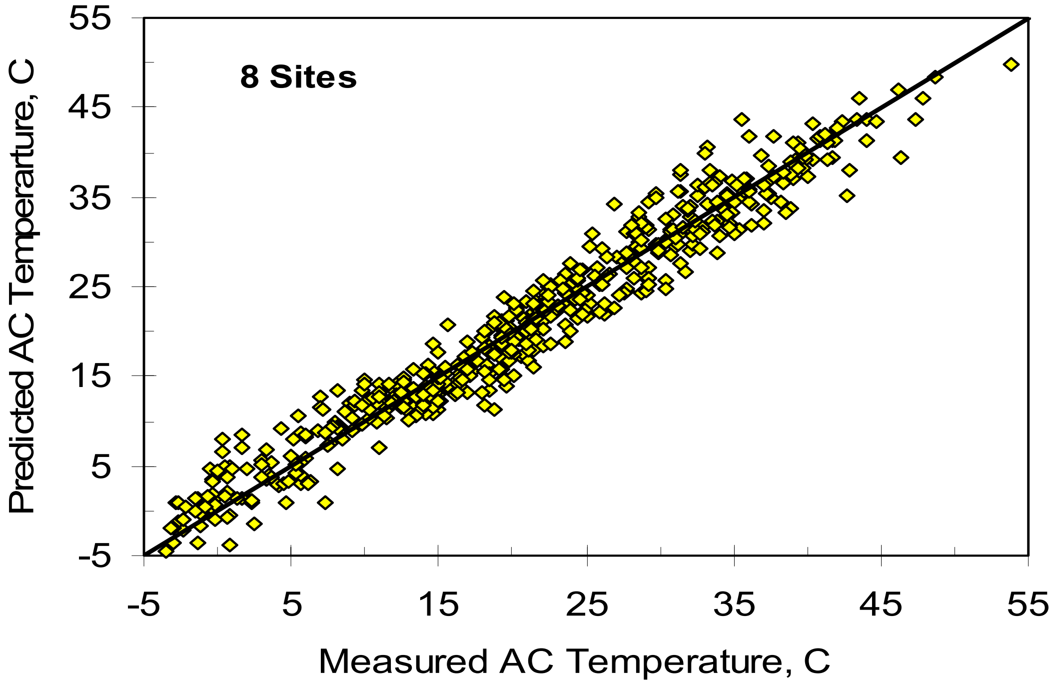

Figure 6.16: Measured vs. Predicted Asphalt Pavement Temperature Using the Model

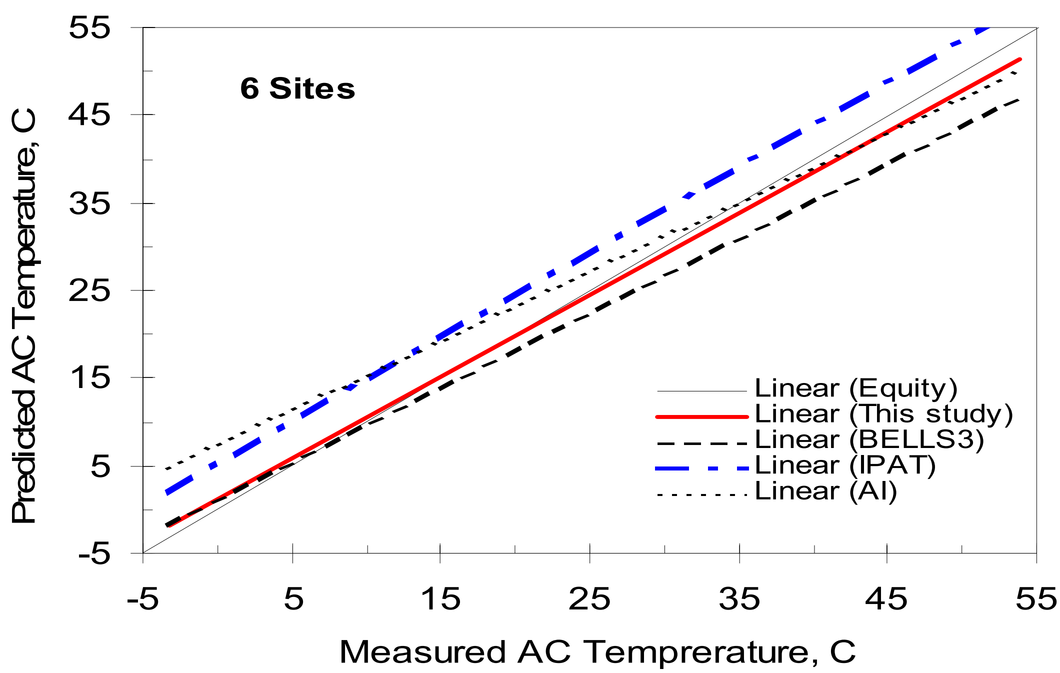

Figure 6.17: Measured versus Predicted Asphalt Pavement Temperature Using the Models and Different Previous Models

6.7 SUMMARY

Based on the analysis of the AC temperature and modulus data described in this chapter, the following main points are summarized:

- The variation of AC modulus and pavement temperature with time followed an inverse function, where the modulus decreases with temperature increase. This result was valid for all sites from freezing and nonfreezing zones.

- The mid-depth pavement temperature was found to be the best temperature to represent AC layer rather than the temperature at 25 mm depth and/or the pavement surface temperature.

- A relationship between AC modulus and pavement temperature was determined for different sites in both freezing and nonfreezing zones. Models relating AC modulus to mid-depth pavement temperature and other AC layer properties were developed and applied for both freezing and nonfreezing zones as given by Equations 6.7 and 6.8.

- A model for calculating the modulus seasonal adjustment factor (SAF_{ac}) of the AC layer was developed. The SAF_{ac}, Equation 6.9, adjusts the AC layer modulus from one reference season to another. The analysis also showed that the AC modulus could increase in winter to more than 8 times its summer value if the temperature ratio reduced from 1.0 to 0.1. This would increase the damage occurring to the pavement during summer, as will be explained later.

- A simple model for estimating the asphalt pavement temperature from the air temperature (refer to Equation 6.14) was also developed.

- It should be noted that the models mentioned above in this summary would be validated in the next chapter, using Idaho data, to be implemented in the pavement performance analysis.

7. VALIDATION OF THE DEVELOPED MODELS USING IDAHO DATA

This chapter describes the backcalculation of the pavement moduli based on the FWD tests that were conducted at the Idaho sites. The chapter also addresses using these data to check the validity of applying the previously developed models, described in Chapters 5 and 6, for the prediction of the subgrade and AC layer moduli at the Idaho sites.

7.1 BACKCALCULATION OF THE LAYERS MODULI

As previously stated in Chapter 3, the FWD testing was conducted at the different Idaho sites to evaluate the pavement structure capacity. The test was conducted once a year for four years (1999, 2000, 2001 and 2002). For each site the test was conducted at five different stations using two different loads 8,000 lb and 12,000 lb (35.6 kN and 53.4 kN). The radial distance between the centerline of the applied load and each of the seven sensors were 0, 8, 12, 18, 24, 36 and 60 inches (0, 20, 30, 45, 60, 90, 150 centimeters). The plate radius on which the load was applied was 5.91 inches. The pavement temperature was recorded during the test, and the resulting pavement deflections recorded at the seven different sensors were used for backcalculating the layers moduli using MODULUS 5.1 software, which was developed by the Texas Transportation Institute.

The general backcalculation procedures are briefly summarized below (Lytton, 1989):

1- Seed moduli: These are the assumed or the starting values of the layer moduli.
2- Deflection calculations: This is usually done using the multi-layer elastic analysis theory. This involves knowledge of the layer thickness, load, latest set of layer moduli, and the radii to the deflection sensors to calculate the surface deflection at each sensor.
3- Error check: Several types of error checks can be used to check the difference between the measured and calculated deflections. The program keeps searching for

the next possible set of moduli and the error checks indicate convergence within acceptable levels of tolerance. One of the available error checks is shown in the following equation:

$$\text{Error, \%} = 100\sqrt{\frac{\sum_{1}^{N}\left(\frac{d_m - d_c}{d_m}\right)}{N}} \tag{7.1}$$

where,

d_m = Measured deflection.

d_c = Calculated deflection

N = Number of sensors.

4- Result: This usually includes the measured deflections, the absolute error, and the final set of the layer moduli.

Several runs of the MODULUS software were performed for each site until the absolute error between the measured and predicted deflection at each station became almost 2% or less. For the few stations at which the calculated absolute error was higher than 2%, the back-calculated modulus values were discarded due to expected bias.

The results of the MODULUS program showing the deflections at each sensor, the backcalculated moduli values and the absolute error at each station for each site are presented in Appendix B.

7.2 VALIDATION OF THE SUBGRADE MODULUS PREDICTION MODEL

The FWD testing was conducted each year for all sites during August, September or October. In Idaho, there is no great variation in the subgrade moisture content during that time period. The subgrade backcalculated elastic moduli of the different sites at each station didn't not show great variation, so the average value for each site was considered. The average value was calculated based on the outputs of the MODULUS software, shown in Appendix B.

The general model for subgrade modulus prediction, given by Equation 5.8, was considered for validation using the Idaho backcalculated data. The subgrade soil properties required as input parameters are present in Table 7.1 for all Idaho sites. Those properties, together with the average subgrade moisture content during the month at which the FWD testing was conducted, were incorporated into the subgrade modulus prediction model (Equation 5.8). Among the subgrade properties required for Equation 5.8 is the subgrade in-situ dry density. This value was not available for Idaho sites. Therefore, the EICM default values were considered based on the soil classification at each site.

The month during which the FWD test was conducted and the corresponding average subgrade moisture content used for modulus prediction is shown in Table 7.1. Both the predicted and backcalculated subgrade moduli values were recorded in the last two rows of the table. Figure 7.1 shows the measured versus predicted subgrade moduli values for Idaho sites. The figure indicates that the predicted moduli values are very close to the measured values at almost all sites except Worley and Weiser (5A). Better correlations might be expected if more data points were available.

Table 7.1 Subgrade Properties Used for Modulus Prediction at Idaho Sites

No	Site	Lewiston	Moscow		Worley	Pack River		Weiser	
		1	2A	2B	3	4A	4B	5A	5B
1	AASHTO classif.	A-4	A-4	A-4	A-6	A-2-4	A-4	A-4	A-4
2	Unified classif.	ML	CL	CL	CL	SM	ML	ML	ML
3	% Pass # 200	62	98	98	82	29.5	92	70	70
4	Dry density, gm/cm^3	1.68	1.62	1.62	1.55	1.70	1.62	1.62	1.62
5	H above, cm	66.0	82.3	82.3	71.1	76.2	30.5	45.7	45.7
6	Stress, gm/cm^2	140.2	174.0	174.0	151.1	161.5	67.1	97.5	97.5
7	FWD month	9	9	9	9	9	9	10	10
8	VMC, %	23.9	31.7	21.3	54.2	41.1	34.6	12.0	15.0
9	GMC, %	14.2	19.6	13.1	35.0	24.2	21.3	7.4	9.3
10	**E predicted, MPa**	**106.7**	**51.5**	**66.9**	**16.9**	**72.6**	**70.1**	**103.3**	**95.8**
11	**E measured, MPa**	**110.3**	**62.7**	**93.8**	**72.4**	**65.5**	**65.5**	**146.2**	**93.1**

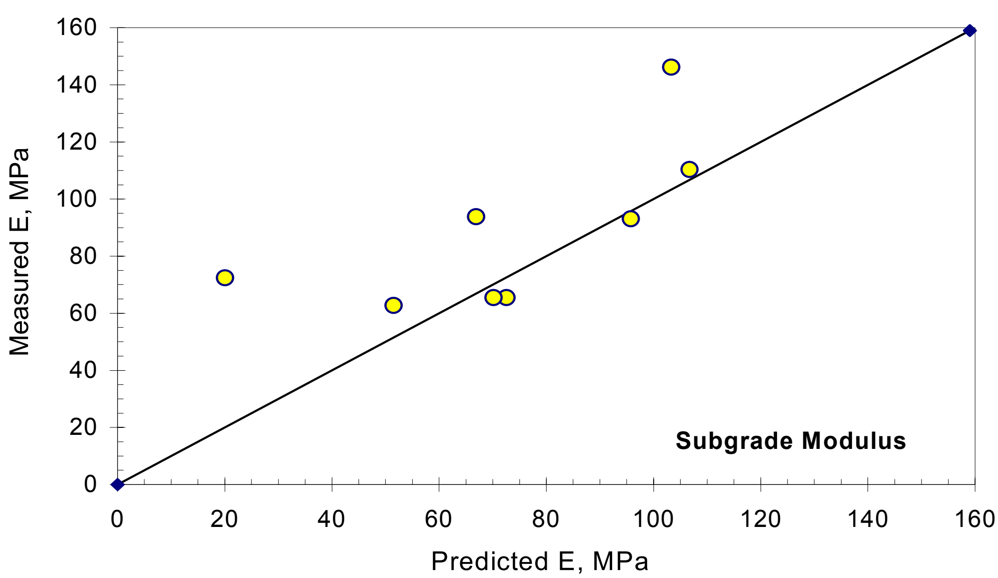

Figure 7.1 Measured versus Predicted Subgrade Modulus for Idaho sites

7.3 VALIDATION OF THE AC LAYER MODULUS PREDICTION MODELS

Unlike the subgrade modulus moisture data in Idaho, there were more data points available for the validation of the modulus - temperature relationship, because the pavement temperature was recorded during the FWD testing. There are ten FWD measurements conducted at the same temperature for each site. The average backcalculated modulus value for each temperature was considered to validate the AC prediction models described in Chapter 6. Both models for nonfreezing and freezing zones can be given by Equations 6.7 and 6.8, respectively.

Table 7.2 presents the AC mix properties of all the Idaho sites. Those mix properties together with the AC pavement temperatures were incorporated into the modulus prediction models (Equations 6.7 and 6.8) for modulus prediction. Figure 7.2 shows the measured versus AC predicted modulus values when applying the models, represented by Equations 6.7 and 6.8, to four different Idaho sites. Those sites are Lewiston (1), Moscow (2A), Moscow (2B) and Worley (3). The figure shows that the data from the nonfreezing zone model (Equation 6.7) are closer to the equity line (45 degree line) than the freezing zone model (Equation 6.8). This indicates that Equation 6.7 is the best to represent the majority of the Idaho sites. That may be because the FWD test was conducted in Idaho sites mainly during August, September and October, which represent the hot weather (nonfreezing). Another reason could be that the Idaho sites are relatively new and did not have surface distress, which makes them to behave like the nonfreezing zone sites.

Figure 7.3-a shows the measured versus predicted moduli for all sites when using Equation 6.7 (Nonfreezing). The figure shows that the data for all sites are almost centered around the equity except Pack River and Weiser, where the model underestimated the modulus in the first case and overestimated it in the second. The reason, as discussed in Chapter 6, could be related to the difference in the mix properties, construction and compaction methods and some other environmental factors. Also, the binder grade at the Weiser site is different from

the other sites, as shown in Table 7.2. In general, the model is considered the average for all sites.

To calibrate the model to be correctly used for those two sites, the model was multiplied by a shift factor for each site. This shift factor was considered as the average value of the ratio between the measured and predicted modulus at each station. The calculated shift factors were found to be 0.97, 1.00, 0.82, 1.93, and 0.50 for Lewiston, Moscow, Worley, Pack River and Weiser. Figure 7.3-b presents the measured versus predicted modulus data after calibration, which indicates very good correlation.

Table 7.2 AC Layer Properties Used for Model Inputs

Site	Lewiston	Moscow		Worley	Pack River		Weiser	
	1	2A	2B	3	4A	4B	5A	5B
Hac, mm	152.4	121.9	121.9	177.8	152.4	304.8	152.4	152.4
Binder Grade	AC10	AC10	AC10	AC10	AC10	AC10	PG 64-34	PG 64-34
BSG	2.423	2.446	2.446	2.343	2.316	2.394	2.431	2.431
AV, %	4.3	4.2	4.2	4.7	4.9	4.6	3.8	3.8

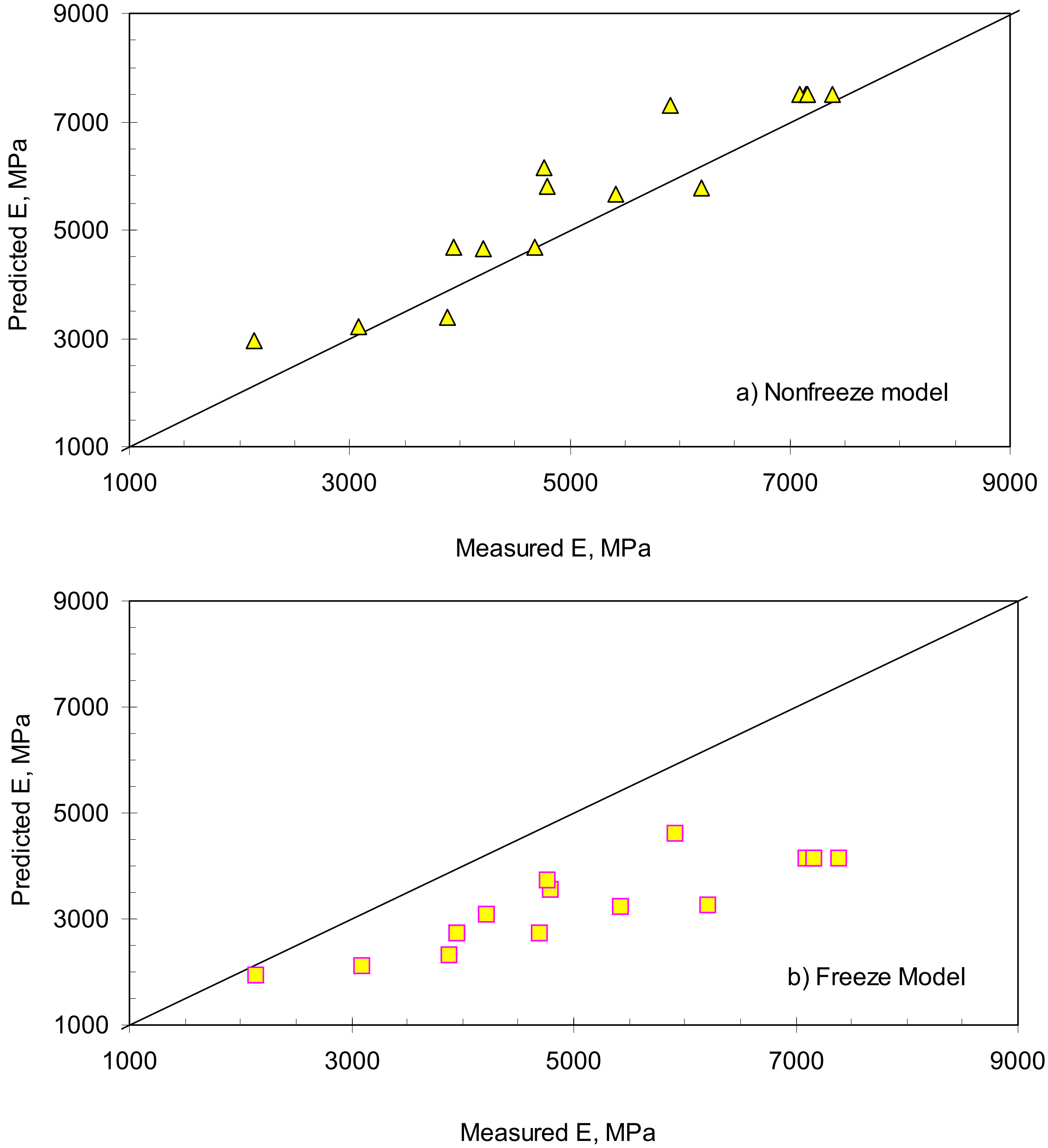

Figure 7.2 Measured versus Predicted AC Modulus when Applying both Models of Freezing and Nonfreezing Zones

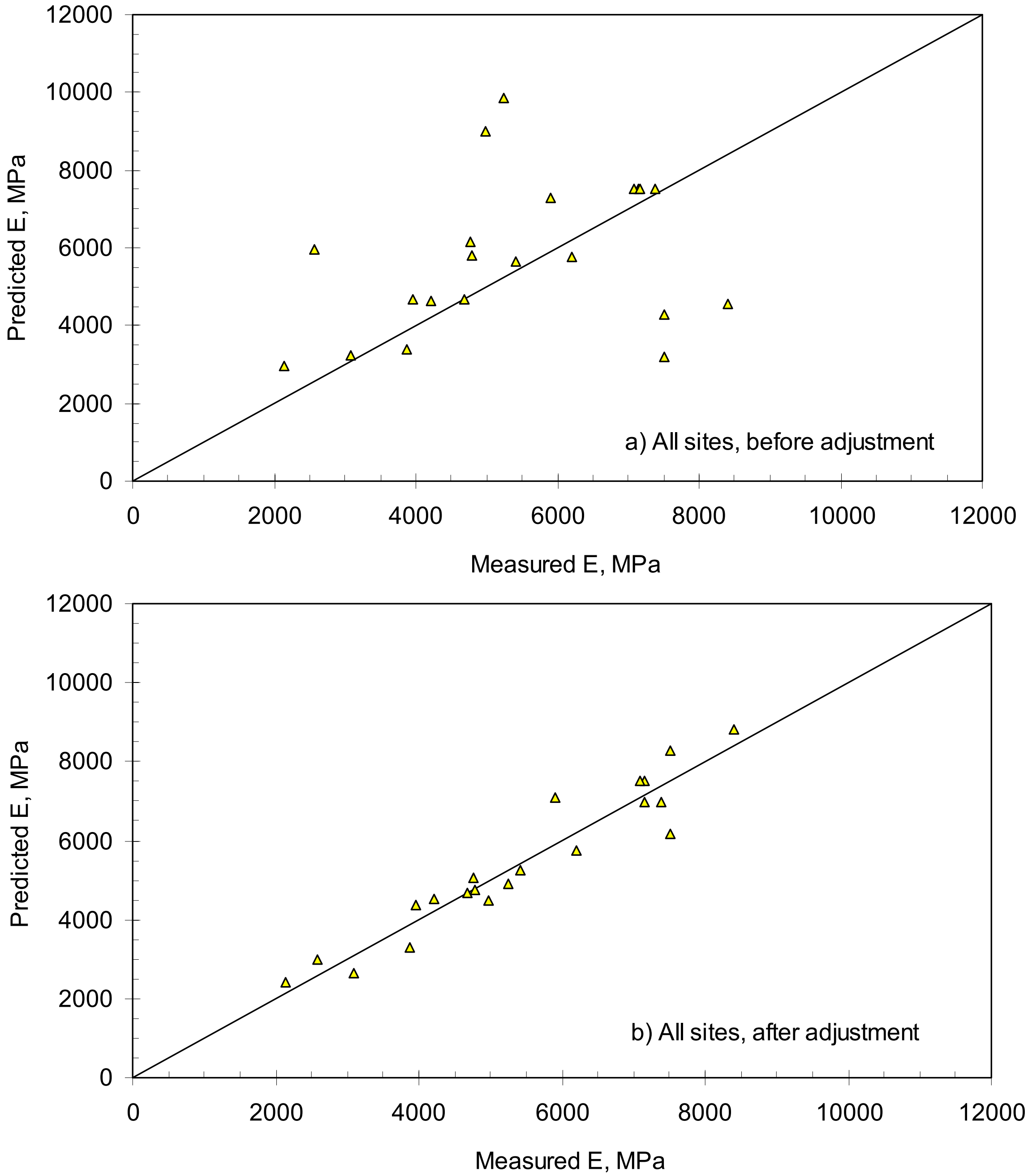

Figure 7.3 Measured versus Predicted Modulus Using the Nonfreeze Zone Model

7.4 VALIDATION OF THE PAVEMENT TEMPERATURE PREDICTION MODEL

The collected data for air and pavement temperatures from sites installed in the state of Idaho were used to check the validity of the pavement temperature prediction model given by Equation 6.14 and to compare it to the asphalt institute (AI) model. The full model (Equation 6.12), the IPAT model, and the BELLS model could not be applied to these data because of the lack of the input data required to apply those models such as the asphalt surface temperature and the average daily air temperature the day before testing.

Figure 7.4 shows the application of the model given by Equation 6.14 on the collected data. The figure shows that the data nearly centered around the equity line, which indicates that the model fits the data very well. Figure 7.5 shows same data when used to fit the AI model. It indicates that the model highly overestimates the pavement temperature.

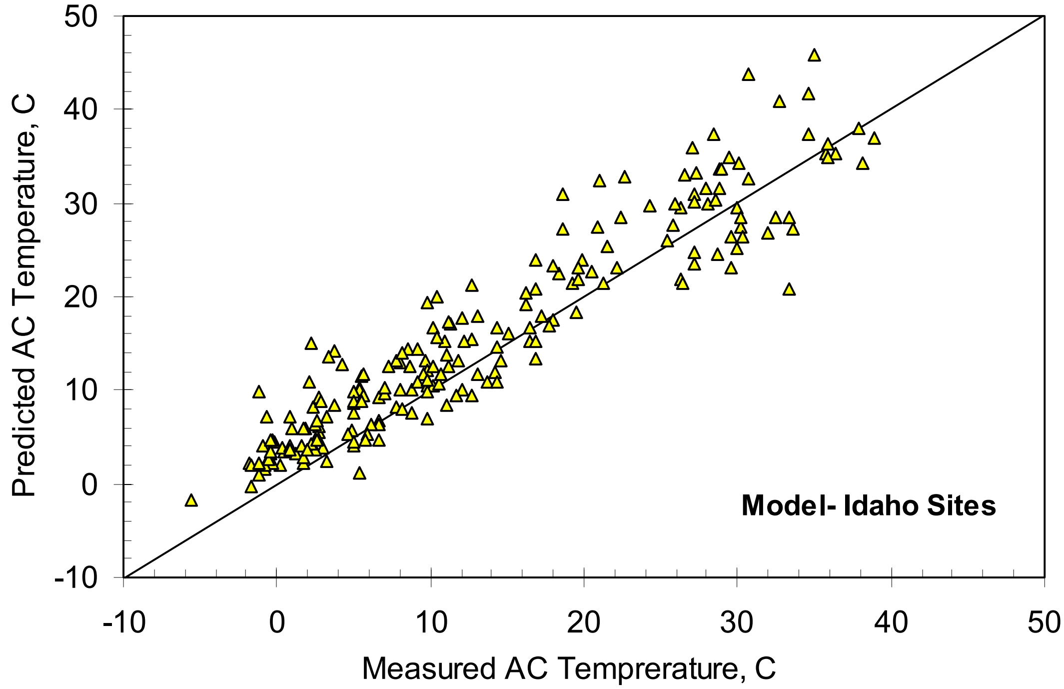

Figure 7.4 Applying the Model to Collected Data from Idaho Sites

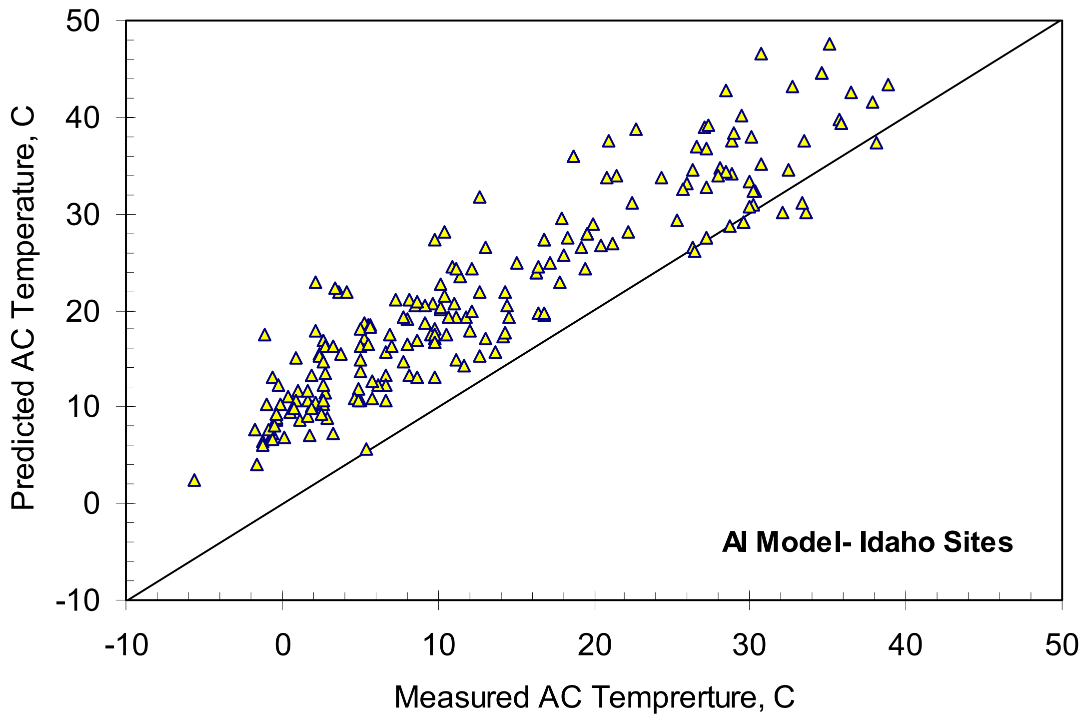

Figure 7.5 Applying AI Model to Collected Data from Idaho Sites

8. IMPLEMENTATION OF THE DEVELEOPED MODELS IN PAVEMENT DESIGN AND PERFORMANCE PREDICTION

This chapter discusses the impact of the seasonal variations on the pavement performance prediction. The chapter illustrates the determination of the suitable timing for the four different seasons; winter, spring, summer and fall at the different Idaho sites. It also explains the determination of the seasonal adjustment factor (SAF) for each season and the impact of these variations in the predicted pavement life. Finally it discusses the impact of rockcap base layer on the pavement structural capacity

8.1 DETERMINATION OF THE SAF FOR IDAHO SITES

8.1.1 Season Determination

The average monthly rainfall and air temperature data were used to determine the suitable months for each season. The data were sorted by month, and each group of months having similar values of rainfall and temperature were assigned to one season. Figure 8.1 through 8.5 show the season assignment for the Lewiston, Moscow, Worley, Pack River and Weiser sites respectively, based on the average monthly rainfall and temperature.

Table 8.1 shows the assigned seasons for each site and the corresponding months, based on the data presented in Figure 8.1 to 8.5. The table shows that the winter season in all sites includes the months of November, December and January. The spring season includes February and March, and could last until May at some sites. The summer season includes July and August, and could last until September. The fall season, for the purpose of this study, includes the months before and after summer that have similar climatic conditions. It includes June and October at all sites and may also include April, May and/or September at some sites.

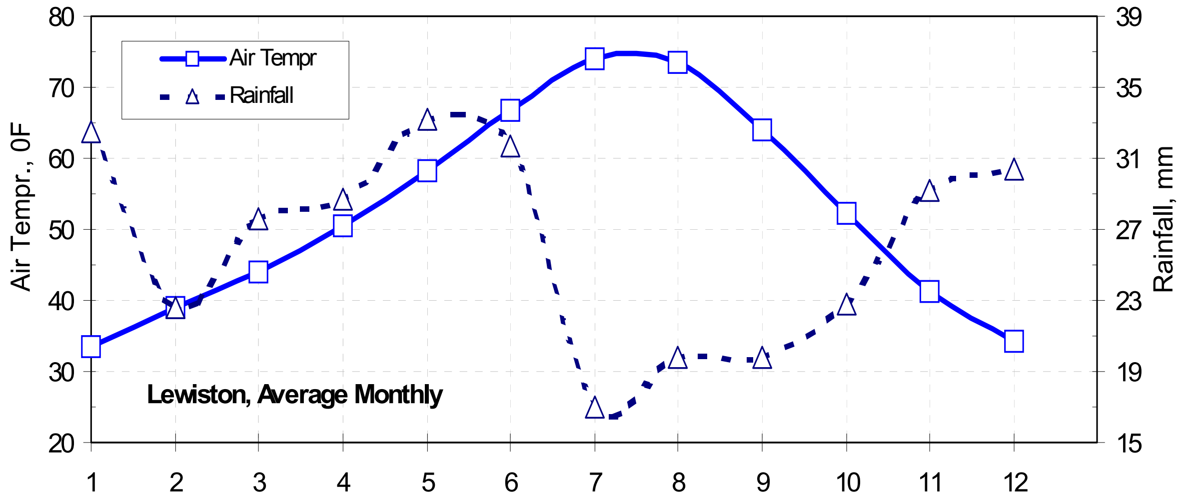

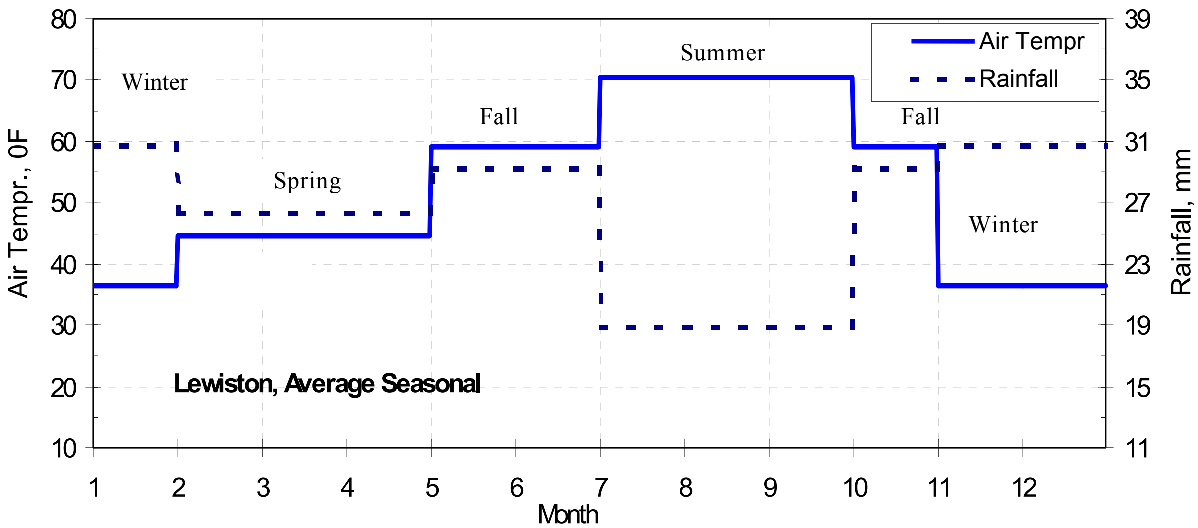

Figure 8.1 Seasons Selection Based on Rainfall and Temperature Data, for the Lewiston Site

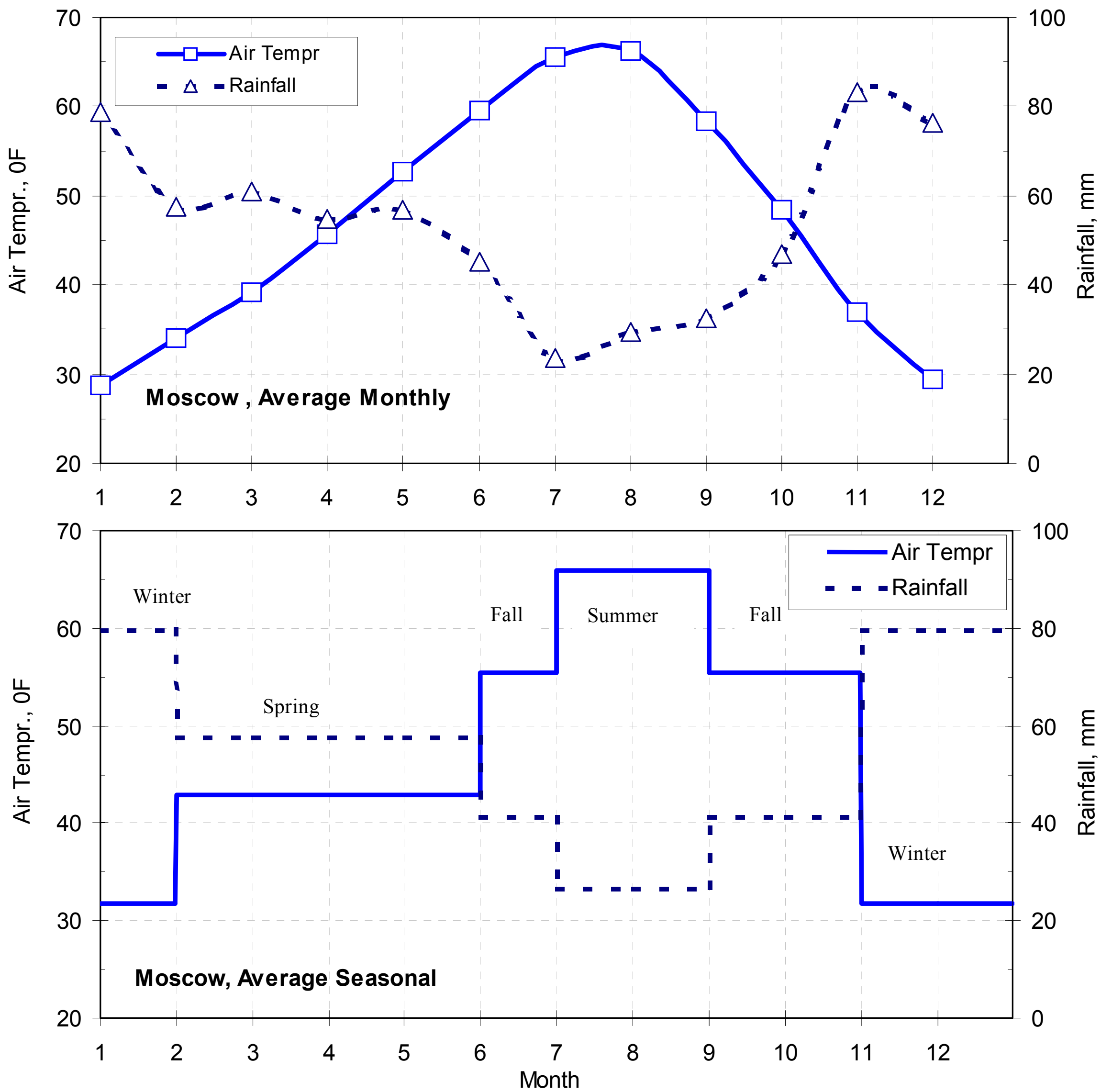

Figure 8.2 Seasons Selection Based on Rainfall and Temperature Data, for the Moscow Site

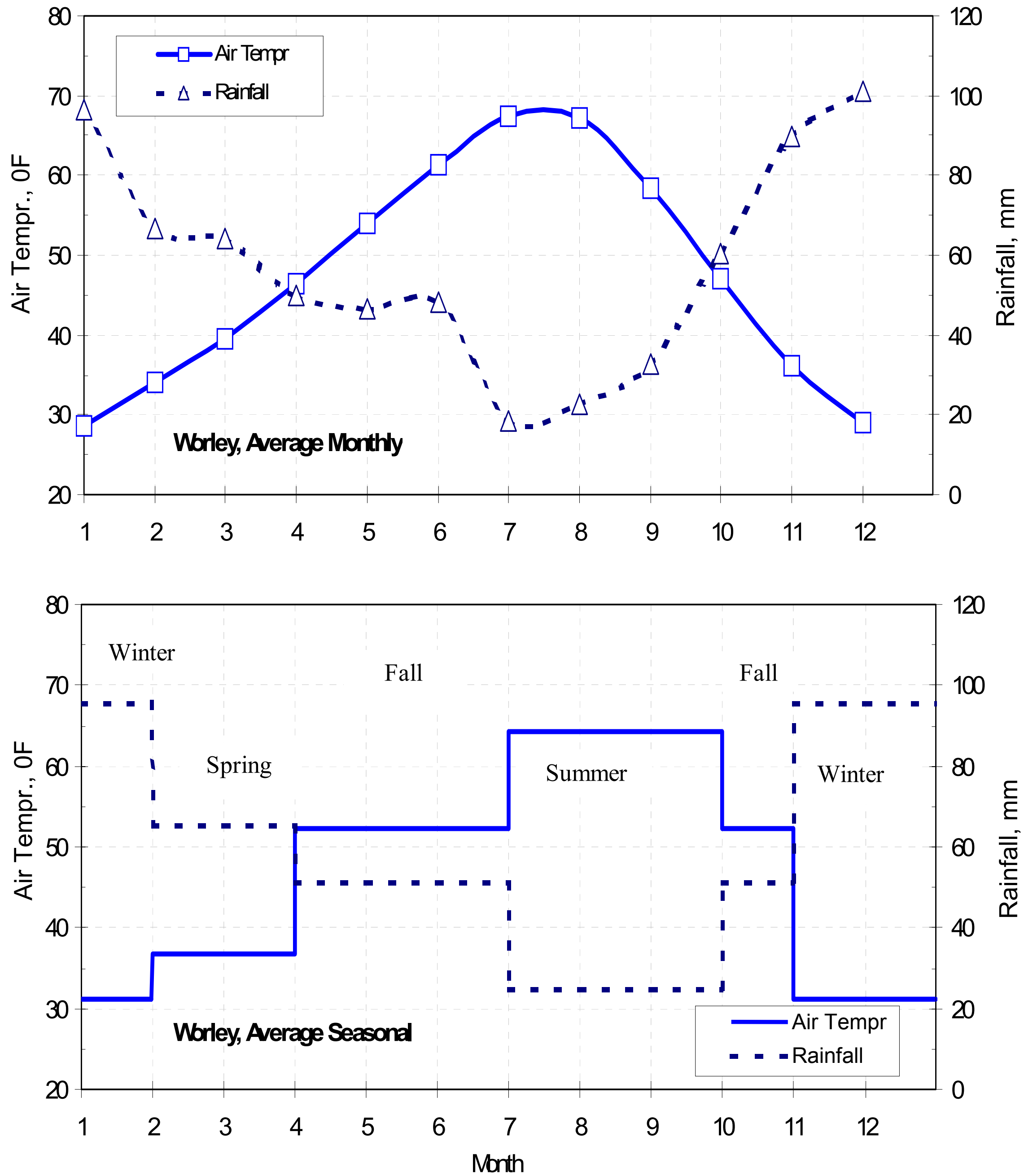

Figure 8.3 Seasons Selection Based on Rainfall and Temperature Data, for the Worley Site

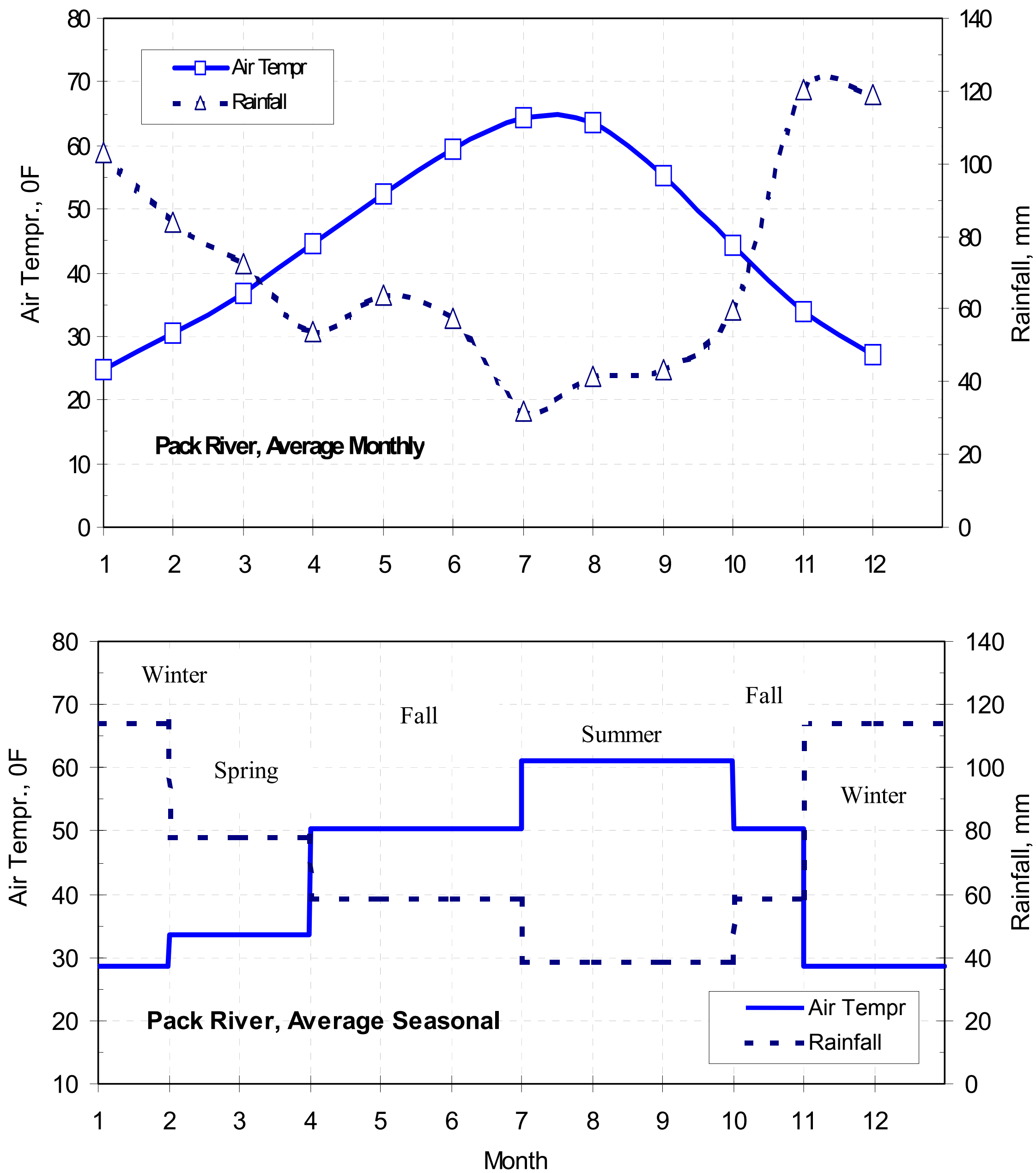

Figure 8.4 Seasons Selection Based on Rainfall and Temperature Data, for the Pack River Site

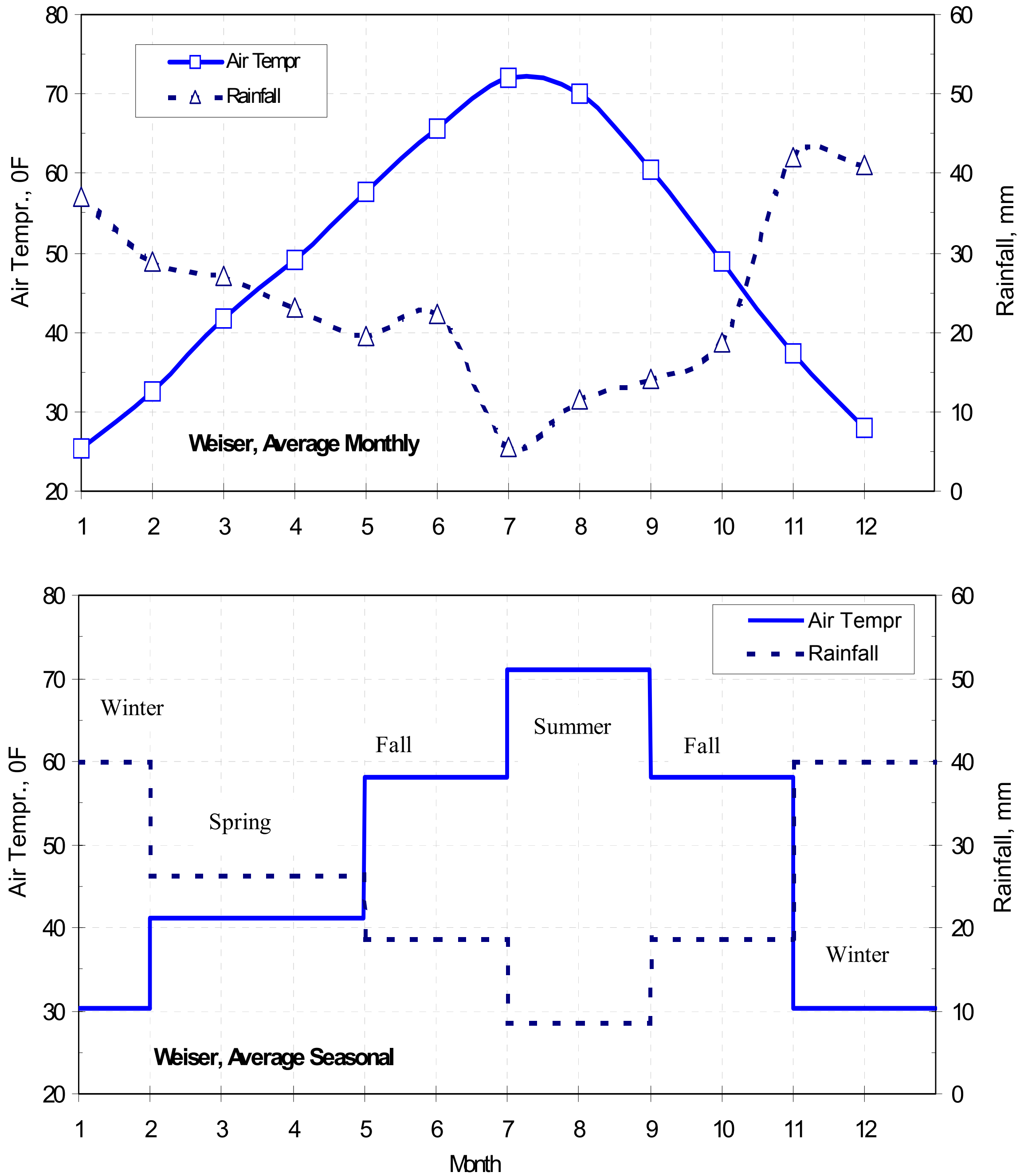

Figure 8.5 Seasons Selection Based on Rainfall and Temperature Data, for the Weiser Site

Table 8.1 Different Seasons and Corresponding Months for Idaho Sites

Season / Site	Months			
	Winter	Spring	Summer	Fall
Lewiston	11, 12, 1	2, 3, 4	7, 8, 9	5, 6, 10
Moscow	11, 12, 1	2, 3, 4, 5	7, 8	6, 9, 10
Worley	11, 12, 1	2, 3	7, 8, 9	4, 5, 6, 10
Pack River	11, 12, 1	2, 3	7, 8, 9	4, 5, 6, 10
Weiser	11, 12, 1	2, 3, 4	7, 8	5, 6, 9, 10

8.1.2 Estimation of the Subgrade SAF

To estimate the seasonal and/ or monthly variation in the subgrade elastic modulus and calculate the corresponding SAF for each of the different Idaho sites, the following steps were followed:

1- The measured volumetric moisture contents, previously presented in Chapter 4 by Figure 4.3, were averaged for each season and are presented in the table below:

Table 8.2 Average Seasonal Subgrade Moisture Content

Site	Volumetric Moisture Content, %			
	Summer	Fall	Winter	Spring
Lewiston	24.3	24.9	22.4	24.3
Moscow (2A)	29.0	34.5	33.7	33.2
Moscow (2B)	21.7	22.9	22.3	23.2
Worley	64.6	61.8	52.7	51.7
Pack River (4A)	40.7	39.9	40.5	41.1
Pack River (4A)	35.1	35.7	34.5	34.2
Weiser (5A)	13.8	12.3	13.3	12.7
Weiser (5B)	18.7	15.9	15.6	18.1

2- The summer season was selected as the reference season, and the moisture ratios for the other seasons were then calculated by dividing the moisture content at each season by the summer moisture content. When there were two adjacent sites in the same location (such as Moscow, Pack River and Weiser), the site having the greater moisture variation was considered to represent that location, as shown in the following table.

Table 8.3 Moisture Ratio at Each Season

Site	Moisture Increase, Ratio			
	Summer	Fall	Winter	Spring
Lewiston	1	1.03	0.93	1.00
Moscow (A)	1	1.19	1.16	1.15
Worley	1	0.96	0.82	0.80
Pack River (B)	1	1.02	0.98	0.97
Weiser (B)	1	0.85	0.83	0.97

3- Equation 5.8 in Chapter 5, which was validated in Chapter 7, can be used to estimate the modulus at each season, and then the SAF_s. However, since the subgrade moduli at Idaho sites were measured using FWD testing, it would be more accurate to use the SAF_s algorithm, given by Equation 5.9, and then multiply these values by the measured summer modulus from the FWD testing. For convenience, Equation 5.9 is presented again below:

$$SAF_s = K_1 (W_r)^{k2} \qquad (5.9)$$

where W_r is the modulus ratio, while K_1 and K_2 are model parameters depending on soil types.

4- According to the data previously presented in Table 5.6, Chapter 5, and based on the soil type, the model parameters K_1 and K_2 could be estimated, as shown in the following table.

Table 8.4 Model Parameters for Subgrade SAF Algorithm

Site	Soil Properties				Model Parameters	
	Soil	Unified	Ps# 200	PI, %	K_1	K_2
Lewiston	Granular Fill	ML	62	NP	1	-1.32
Moscow (A)	CL	CL	98	8	1	-1.07
Worley	Silt & Clayey silt	CL	82	18.4	1	-1.07
Pack River (B)	Lacustrine silt	ML	92	NP	1	-1.32
Weiser (B)	ML	ML	70	9.6	1	-1.32

5- The model, shown in Step 3 above, could then be applied to calculate the seasonal adjustment factors for the different sites, as shown below.

Table 8.5 Subgrade SAF for Idaho Sites

Site	$SAF_s = K_1 * W^{k2}$			
	Summer	Fall	Winter	Spring
Lewiston	1.00	0.96	1.11	1.00
Moscow (A)	1.00	0.83	0.85	0.86
Worley	1.00	1.05	1.24	1.27
Pack River (B)	1.00	0.98	1.02	1.03
Weiser (B)	1.00	1.23	1.27	1.05

6- Applying the previous steps (1 to 5) to the monthly data gives the following monthly adjustment factors. September was considered the reference month because the layer moduli were known from the FWD test during that month, as explained above.

Table 8.6 Subgrade Monthly Adjustment Factors Idaho Sites

Month	1	2	3	4	5	6	7	8	9	10	11	12
Lewiston	1.05	1.06	0.95	0.93	0.86	0.90	0.95	0.99	1.00	1.10	1.07	1.14
Moscow (A)	0.89	0.97	0.95	0.92	0.97	0.82	1.04	1.17	1.00	0.94	0.92	1.00
Worley	1.01	1.03	1.07	0.88	0.99	0.77	0.75	0.77	1.00	1.03	1.07	1.02
P. River (B)	1.06	1.06	0.96	0.95	0.91	0.90	0.96	0.98	1.00	1.11	0.96	1.00
Weiser (B)	1.11	0.77	0.91	0.96	0.98	0.87	0.78	0.90	1.00	1.12	1.07	1.02

7. The subgrade modulus at each month and/ or season can then be calculated by multiplying the SAF (Step 6), by the measured backcalculated moduli from Table 7.1. Those values will be used later in this chapter for the seasonal performance analysis.

Table 8.7 Idaho Subgrade Moduli at Different Months and Seasons

	Subgrade Modulus, MPa				
Season	Lewiston	Moscow (A)	Worley	Pack River (B)	Weiser (B)
Jan	116	56	73	69	103
Feb	117	61	75	70	71
Mar	105	60	78	63	85
Apr	102	58	64	62	89
May	95	61	72	59	91
Jun	99	51	56	59	81
Jul	105	65	54	63	72
Aug	109	73	56	64	84
Sep	110	63	72	66	93
Oct	121	59	74	72	104
Nov	118	58	77	63	99
Dec	125	63	74	65	95
Summer	110	63	72	66	93
Fall	106	52	76	64	115
Winter	122	53	90	67	119
Spring	110	54	92	68	97

8.1.3 Estimation of the AC SAF

The seasonal and monthly variations in the AC elastic moduli and their corresponding SAF were estimated for five different Idaho sites in the following steps:

1- The average monthly air temperatures for all sites, previously presented in Figure 4.15, Chapter 4, were first averaged and compiled in the table below.

Table 8.8 Average Seasonal Air Temperature in Degree Celsius

Site	Average Air Temp, °C			
	Winter	Spring	Summer	Fall
Lewiston	2.39	6.96	21.39	15.04
Moscow	-0.15	6.06	18.81	13.00
Worley	-0.41	2.67	17.94	14.15
Pack River	-1.93	0.86	16.17	10.14
Pack River	-1.00	5.06	21.69	14.53

2- The air temperatures were then converted to pavement temperatures using the model given by Equation 6.14, where,

$$T_{ac} = T_{air} \{1.045 + 0.1779 * COS [(M- 7)* \pi/6] – 0.2618 [Log_{10} (Z) – 1.25]\} – 0.0035 Lat^2 + 8.627 \quad (6.14)$$

The above model requires the month number as an entry value, so the middle month for each season was considered to represent that season. The winter, spring, summer, and fall were represented by December, March, July and October, respectively. The calculated pavement temperatures for all sites are included in Table 8.9.

Table 8.9 Average Seasonal Pavement Temperature in Degrees Celsius

Site	Depth, mm	Latitude, Deg	Average Pavement Temperature, °C			
			Winter	Spring	Summer	Fall
			12	3	7	10
Lewiston	25	46.41	3.1	7.5	26.4	16.2
Moscow	20	46.73	0.8	8.3	17.9	14.7
Worley	29	47.31	0.5	3.8	21.2	13.2
Pack River	25	48.3	-1.1	1.3	17.8	8.9
Weiser	25	44.23	0.9	6.0	26.8	17.8

3- Incorporating the average pavement temperature (Step 3) and the AC layer properties (Table 7.2) into Equation 6.7; the AC modulus at each season and/or month can be calculated.

$$\text{Log}(E) = 7.215 - 0.053\,Tac + 0.001\,H + 1.095\,BSG - 0.049\,AV + 0.146\,GRD \quad (6.7)$$

The above equation was validated in Chapter 7. It was multiplied by the site calibration factor discussed in Chapter 7, which was 0.97, 1.00, 0.82, 1.93 and 0.5 for Lewiston, Moscow, Worley, Pack River and Weiser sites respectively. The values of the AC layer modulus for all Idaho sites at all seasons and months are presented in Table 8.10, shown below.

4- Dividing the monthly moduli by the modulus value in July, and the seasonal moduli by the modulus value in summer, gives the shift factor for each month and/or season. It should be noted that Equation 6.9, Chapter 6, could also be used to estimate the SAF_{ac} with almost the same accuracy. The calculated seasonal adjustment factors for all sites are presented in Table 8.11, shown below.

Table 8.10 Idaho AC Moduli at Different Months and Seasons, in MPa

Season	AC Modulus, MPa				
	Lewiston	Moscow	Worley	Pack River	Weiser
Jan	18650	21698	16654	41533	12335
Feb	16189	18777	14529	35667	9788
Mar	13918	15479	11847	29289	7549
Apr	11155	13850	9388	23578	5480
May	8264	10056	8900	19683	4944
Jun	5897	9581	7086	16005	4041
Jul	4477	6815	5076	12642	2455
Aug	4659	7139	4796	14158	2873
Sep	6876	8185	6338	15907	4619
Oct	10607	13182	9403	23693	5512
Nov	15052	16880	13523	32643	8685
Dec	18215	21345	16416	39054	11194
Summer	5041	8150	5166	13645	2635
Fall	8654	9686	7923	21957	4232
Winter	17324	20147	15539	37333	10414
Spring	13756	13587	13017	32770	7935

Table 8.11 Idaho AC SAF at Different Months and Seasons

Season	AC SAF				
	Lewiston	Moscow	Worley	Pack River	Weiser
Jan	4.17	3.18	3.28	3.29	5.02
Feb	3.62	2.76	2.86	2.82	3.99
Mar	3.11	2.27	2.33	2.32	3.08
Apr	2.49	2.03	1.85	1.87	2.23
May	1.85	1.48	1.75	1.56	2.01
Jun	1.32	1.41	1.40	1.27	1.65
Jul	1.00	1.00	1.00	1.00	1.00
Aug	1.04	1.05	0.94	1.12	1.17
Sep	1.54	1.20	1.25	1.26	1.88
Oct	2.37	1.93	1.85	1.87	2.25
Nov	3.36	2.48	2.66	2.58	3.54
Dec	4.07	3.13	3.23	3.09	4.56
Summer	1.00	1.00	1.00	1.00	1.00
Fall	1.72	1.19	1.53	1.61	1.61
Winter	3.44	2.47	3.01	2.74	3.95
Spring	2.73	1.67	2.52	2.40	3.01

8.2 SEASONAL IMPACTS ON PAVEMENT PERFORMANCE

8.2.1 Performance Prediction Models

Mechanistic-empirical design methods for flexible pavements were based on the assumption that the pavement life is inversely proportional to the magnitude of the traffic-induced pavement strains. Two competing failure mechanisms were typically assumed related to the pavement design. These two failure mechanisms are the cracking due to fatigue of the asphalt bound pavement layers and the rutting due to accumulated permanent deformations at the top of subgrade soil.

There are several models available in the literature to predict the pavement performance based on the predicted rutting and/ or fatigue failures. The performance models considered in this analysis were those included in the Asphalt Institute (1982) design manual. For fatigue cracking, the manual suggested the following performance model for standard AC mixes with an asphalt volume of 11% and air void volume of 5%:

$$N_f = 0.414\ \varepsilon_t^{-3.291}\ E^{-0.854} \tag{8.1}$$

where,

N_f = The allowable number of load applications

ε_t = The tensile strain at the bottom of AC layer

E = The elastic modulus of the asphalt mixture, kPa

For other cases in which the AC modulus is available in psi units, the multiplier coefficient in the previous equation will be 0.0796 instead of the 0.414.

The rutting model incorporated in the Asphalt Institute design manual is given by the following equation:

$$N_{f2} = 1.365 \times 10^{-9}\ \varepsilon_c^{-4.477} \tag{8.2}$$

where,

N_{f2} = Number of load repetitions to failure

ε_c = Compressive strain at the top of the subgrade

The number of repetitions to the pavement failure is considered the lower of the number of repetitions to failure obtained from either the fatigue or the rutting models.

8.2.2 Multi-Layers Elastic Analysis

The KENLAYER computer program (Huang, 2004) was used to calculate the tensile strain at the bottom of the asphalt layer and the compressive strain at the top of the subgrade soil under the application of a standard 80 kN (18 kip) axle load. The axle load is applied over two sets of dual tires having 551.6 kPa (80 psi) tire pressure and 34.3 cm (13.5 inches) dual spacing. This was done with and without considering the seasonal changes in the AC layer modulus, the subgrade modulus and the applied traffic.

8.2.2.1 Seasonal Variation in the Material Properties

The seasonal variation in the material properties was considered based on the estimated seasonal and monthly layers' moduli, described in Chapter 7.

Subgrade and AC Layers

The seasonal and monthly subgrade and AC layers' moduli were considered based on the calculated values in Table 8.7 and Table 8.10, respectively.

Base Layer

The base layer modulus was assumed constant throughout the year in this analysis. This would be a valid assumption since the granular non-plastic base layer is much less affected by moisture variation compared to subgrade fine-grained soils. Also, the data of Table 8.7 and Table 8.10 indicate that the seasonal variation in subgrade moduli is very small compared to that of the AC Layer. The base layer modulus was considered the average value that was backcalculated using Idaho FWD data, Appendix B.

8.2.2.2 Seasonal Variation in the Traffic

The performance prediction of pavement is significantly affected by traffic distribution during the year. The monthly distribution of the traffic at the different Idaho sites was obtained from the automatic traffic recorders (ATR) data available at the Idaho Transportation Department website (ITD, 2004). The traffic data were obtained from the state counters numbered 125, 15, 119 and 88 for Moscow, Worley, Pack River and Weiser sites, respectively. The data were available as average daily traffic (ADT) count for every month through several years.

To include the traffic seasonal distribution in the multi-layer elastic analysis, the average monthly traffic was divided by the total yearly traffic to obtain the percentage of traffic at each month and/ or season. The monthly traffic distribution (in percentage of the yearly traffic) was calculated for different Idaho sites and presented in Table 8.12. Figure 8.7 show the graphical plot of these values. The figure indicates that the traffic percentage is generally higher during the hot months (summer), in which the AC layer modulus is less than other months. This would result in increasing the total damage occurring during the summer season, as will be explained later in this chapter. It should be noted that the previously stated traffic distribution was observed at the rural sites located at the US-95 highway (Pack River, Worley and Weiser). For the urban site at Moscow, the traffic distribution was different due to the effect of local trips.

.

Table 8.12: Percentage of Seasonal Traffic of the Total Yearly Value

Season	% age of Yearly Traffic			
	Moscow	Worley	Pack River	Weiser
Jan	7.7	5.7	6.4	5.6
Feb	8.6	6.5	6.8	6.3
Mar	8.3	7.3	7.2	6.9
Apr	9.2	8.1	7.9	7.5
May	8.4	9.2	8.6	8.7
Jun	7.8	9.5	9.1	9.7
Jul	7.7	10.4	10.5	11.2
Aug	8.6	10.9	10.3	10.7
Sep	8.7	9.8	9.9	9.9
Oct	9.2	9.0	8.8	9.9
Nov	8.3	7.5	7.7	7.5
Dec	7.8	6.1	6.9	6.1
Summer	16.2	31.2	30.7	21.9
Fall	25.7	37.5	34.4	38.2
Winter	23.8	19.3	21.1	19.2
Spring	34.5	13.8	14.0	20.6
Total Yearly	100	100	100	100

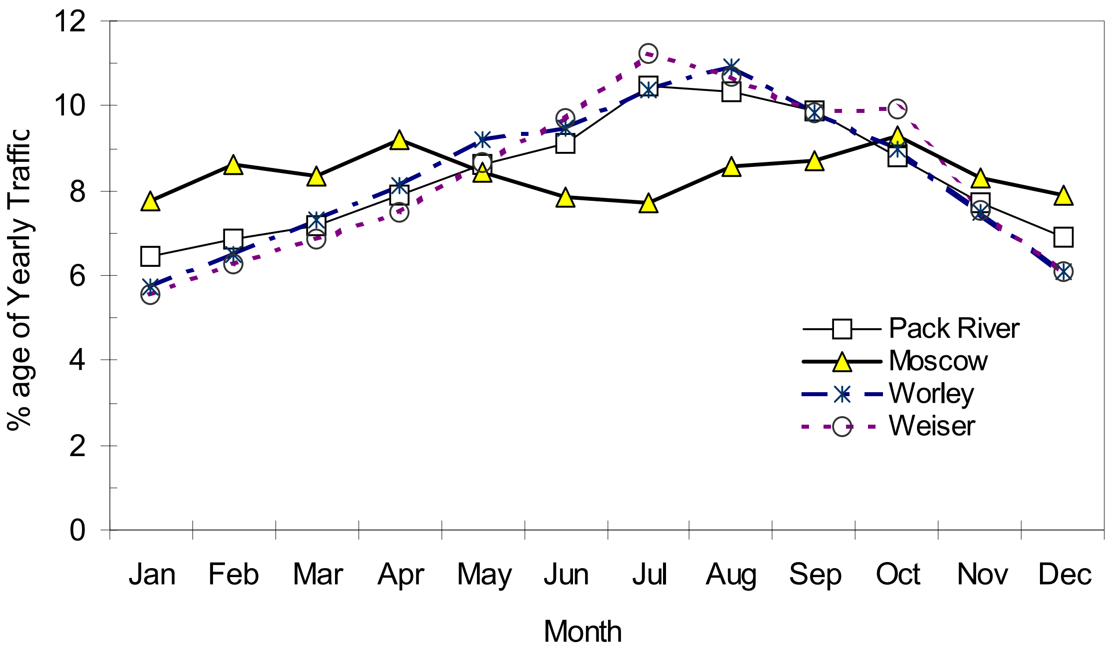

Figure 8.7: Monthly Traffic Distribution for Some Idaho Sites

8.2.3 Prediction of the Pavement Life

The prediction of pavement life is based on the cumulative damage concept in which a damage factor is defined as the damage per pass caused to a specific pavement system by the load in question. The damage (D_i) caused by each application of the 80 kN (18 kip) equivalent single axle load (ESAL) at any season (i) can be given by:

$$D_i = \frac{1}{N_i} \tag{8.3}$$

where N_i is the minimum number of load repetitions required to cause either fatigue or rutting failure, as given by Equations 8.1 and 8.2.

The pavement damage is linearly cumulative according to Miner's hypothesis (1945). Therefore, the total cumulative damage (D_t) occurring to the pavement over its lifetime can then be given by:

$$D_t = \sum_{i=1}^{n} \left(P_i \cdot ESAL\right) \cdot \ D_i = ESAL \sum_{i=1}^{n} \left(\frac{P_i}{N_i}\right) \tag{8.4}$$

where,

n = Number of seasons per year

P_i = Percentage of ESALs occurring during each season

ESAL = Total allowable number of ESALs over the lifetime of pavement.

The total number of load repetitions (ESALs) that are allowed over the pavement lifetime can be determined when total cumulative damage (D_t) reaches one. Therefore, Equation 8.4 can then be solved for the total allowable number of ESALs required to cause either fatigue or rutting failures over the pavement lifetime.

8.2.4 Performance Analysis

The performance analysis was conducted for the Worley and Moscow sites. The analysis considered the monthly (12 seasons/ year) and seasonal (4 seasons/ year) variation in the AC layer modulus, subgrade modulus and traffic. The analysis was also performed without considering any seasonal variation (1 season / year).

To determine which variable (among the AC modulus, subgrade modulus, and traffic) has more seasonal impact on the pavement performance, four different seasonal configurations were considered for the Worley site. The first configuration considered the seasonal variation in all of the layers moduli and the traffic. The second considered the seasonal variation in the layers' moduli with uniform traffic. The third considered the seasonal variation in the traffic and AC modulus with constant subgrade modulus. The fourth configuration considered the seasonal variation in the traffic and subgrade modulus with constant AC modulus.

8.2.4.1 Seasonal Effects on the Computed strains

The tensile stain at the bottom of the AC layer and the compressive strain at the top of subgrade due to the previously stated different seasonal configurations were calculated and are presented in Figure 8.8. The figure shows that the tensile strain at the bottom of the AC layer is mainly affected by the change in the AC layer modulus, while the other two variables (subgrade modulus and traffic) have insignifcant change on the tensile strain values. The figure also shows that the compressive strain at the top of subgarde is affected by the change in both AC layer and subgrade moduli, while the traffic distribution does not have any effect on the compressive strain values. The reason is simply because the strain calculations are not based on the number of load repetions. They are based on the layers' moduli, layers' thicknessés and the value of the wheel load and tire pressure. However, the seasonal traffic distribution or the number of repetations per season affects the damage ratio occuring at each season according to Equations 8.3 and 8.4.

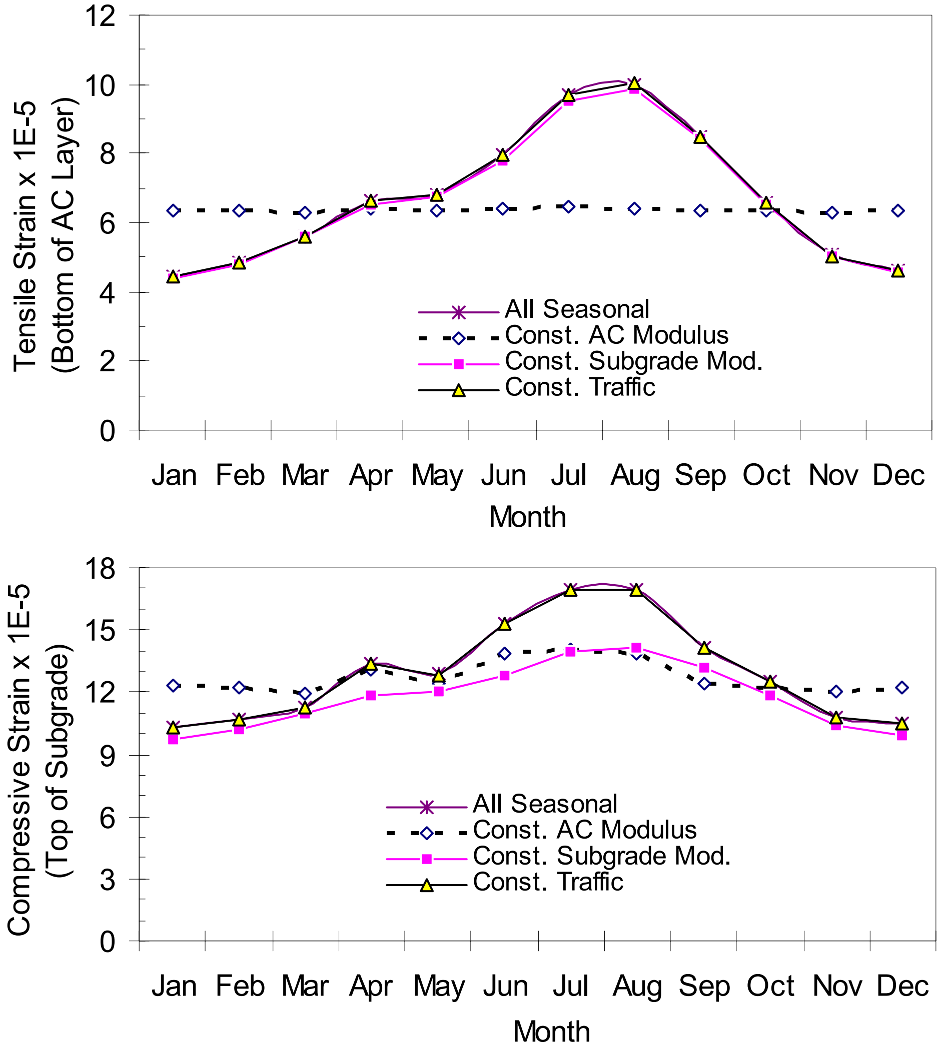

Figure 8.8 AC Tensile Stain and Subgrade Compressive Strain Due to Different Seasonal Configurations

8.2.4.2 Seasonal Damage Analysis and Pavement Life Prediction

As explained above, the total number of load repetitions (ESALs) that are allowed over the pavement lifetime can be determined from Equation 8.4 when total cumulative damage (D_t) equals one. The total allowable number of ESALs over the pavement life time will be considered as the minimum number causing either fatigue or rutting failures.

Figure 8.9 and Figure 8.10 show the total monthly damage ratio to the Worley site during the pavement life when considering the different seasonal configurations, described above, due to both fatigue and rutting failures respectively. Both figures show that the damage ratio, in general, greatly increases during the summer months due to the higher traffic volume and the less pavement moduli. The figures also show that the fatigue damage is much greater than the damage occurring due to rutting.

The data presented in Figure 8.9 indicate that the fatigue damage ratio is greatly reduced when considering constant yearly AC modulus. It is also reduced when constant traffic distribution is considered. The figure also shows that the seasonal changes in the subgrade modulus have a little effect on the estimated fatigue damage. On the other hand, the rutting damage ratio is also reduced when disregarding the seasonal variation in the AC modulus, subgrade modulus, or traffic, as shown in Figure 8.10. The figure also indicates that the more sensitive variable affecting the seasonal rutting damage is the AC modulus, and then subgrade modulus while the traffic is less sensitive.

The total estimated pavement life (in ESALs) due to fatigue and rutting failures, when considering the different seasonal configurations, is presented in Figure 8.11 and Figure 8.12, respectively. The figures generally indicate that the allowable fatigue life in this site (Worley) is much less than the corresponding rutting life. Therefore, the pavement performance in this site is controlled by fatigue not rutting. The figures also show that both fatigue and rutting lives are minimum when considering the seasonal variations in all of the AC modulus, subgrade modulus and traffic, while ignoring the seasonal variation in any of them overestimates the pavement life.

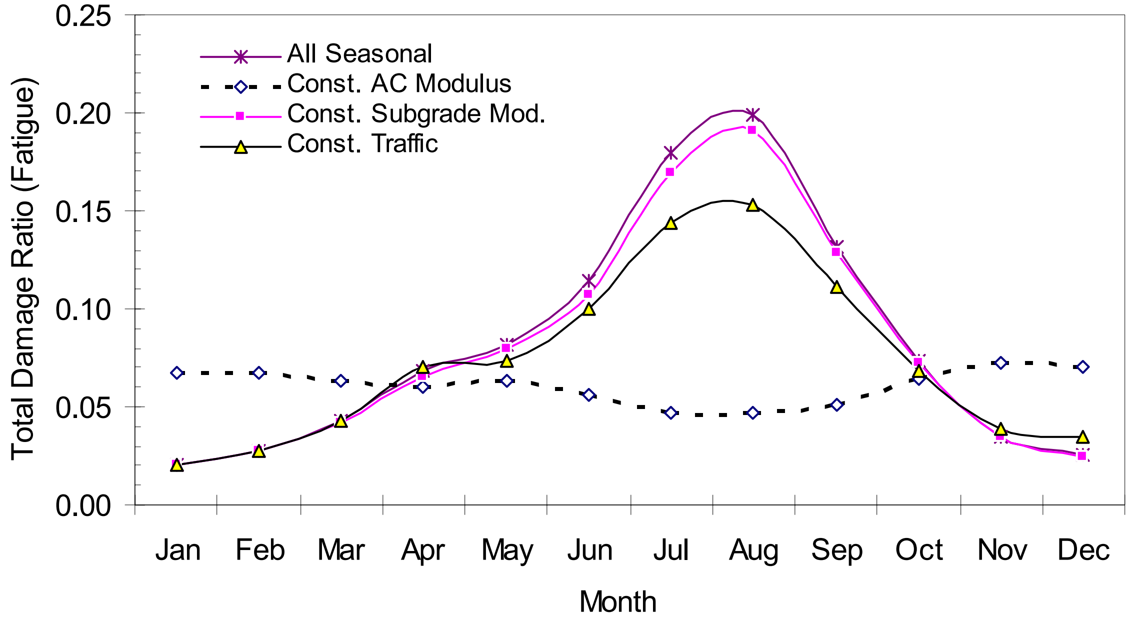

Figure 8.9 Total Monthly Fatigue Damage Ration Due to Different Seasonal Configurations

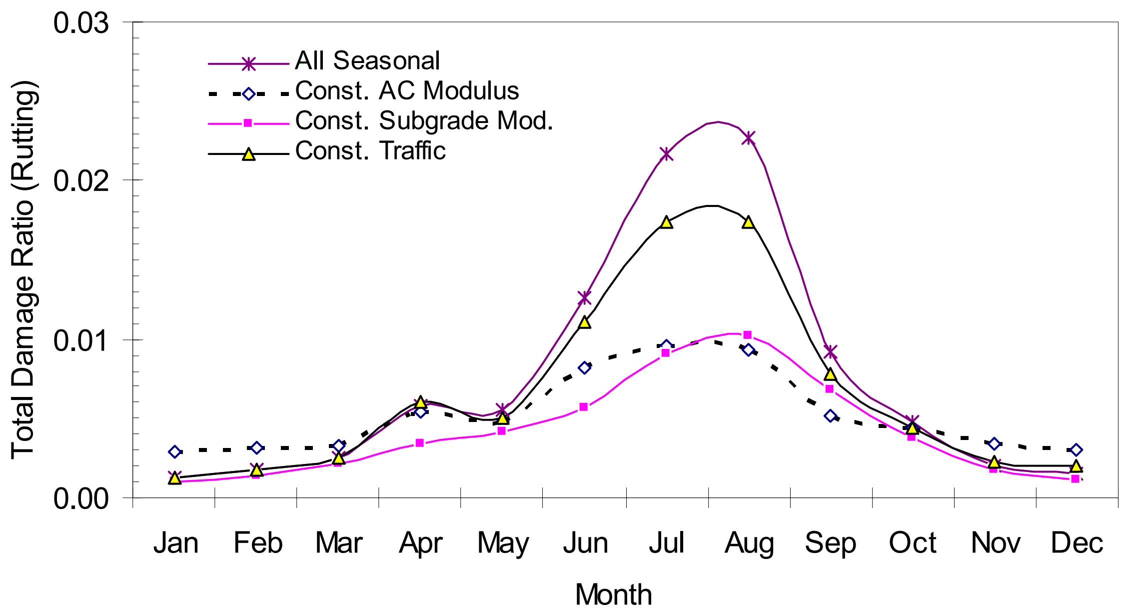

Figure 8.10 Total Monthly Rutting Damage Ratio Due to Different Seasonal Configurations

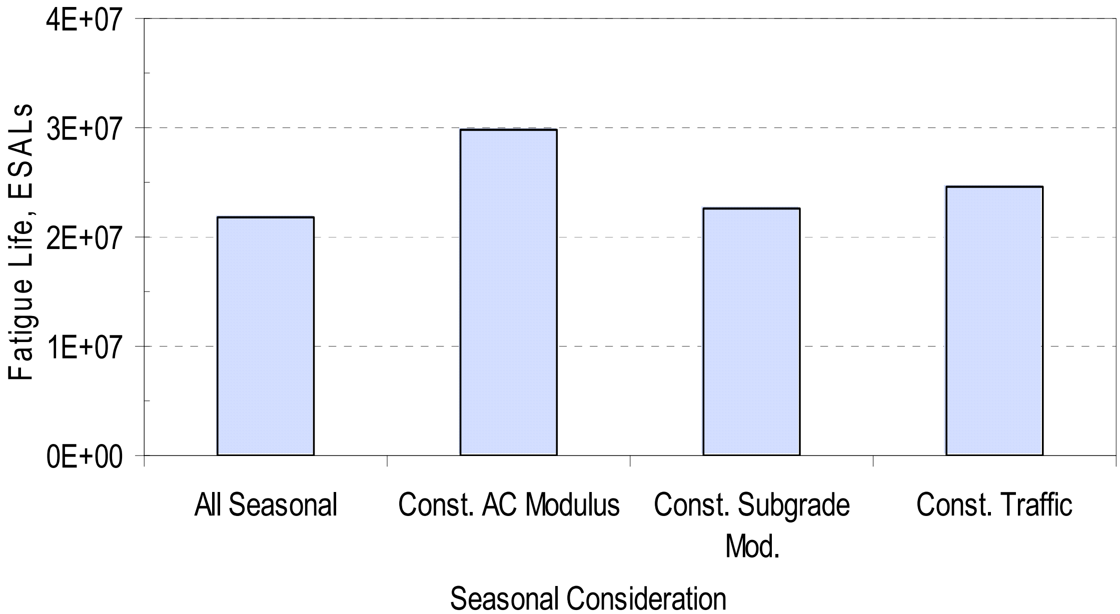

Figure 8.11 Total Fatigue Life (in ESALs) Due to Different Seasonal Configurations

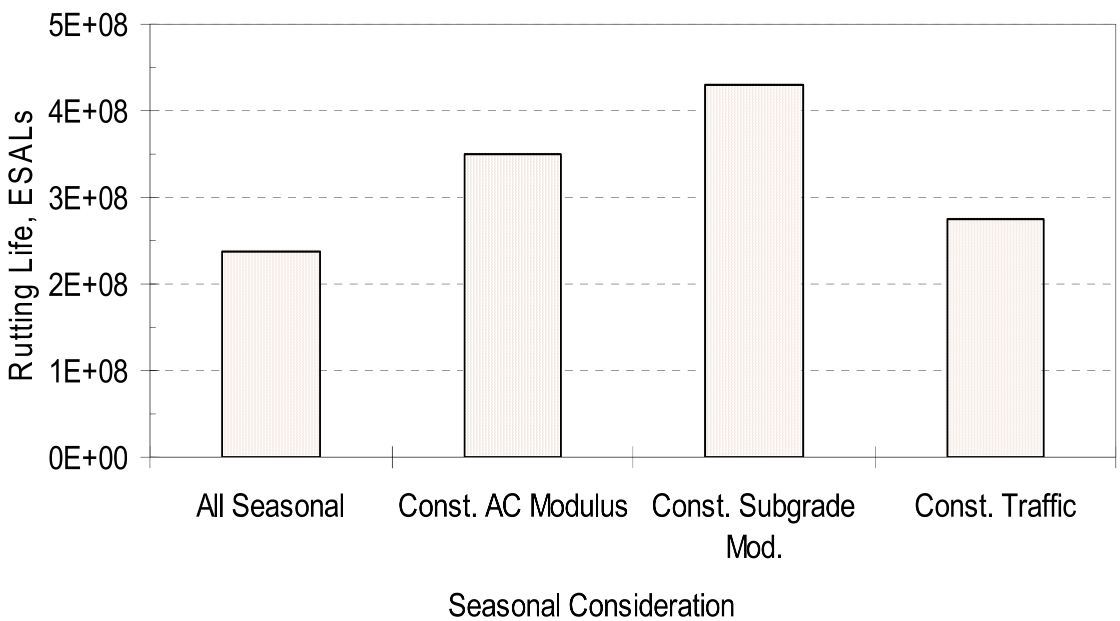

Figure 8.12 Total Rutting Life (in ESALs) Due to Different Seasonal Configurations

8.2.4.3 Effect of Seasonal Approximation on the Predicted Pavement Life

This analysis was performed for the Moscow, Worley and Weiser sites to show the impact of seasonal approximation on the predicted pavement life. The analysis considered the monthly (12 seasons/ year) and seasonal (4 seasons/ year) variations in the AC layer modulus, subgrade modulus and traffic. The analysis was also performed without considering any seasonal variation (1 season/year).

Figure 8.13 and 8.14 show the predicted fatigue and rutting lives, respectively, for all sites when considering different seasons per year. The figure shows that the fatigue life is less than the rutting life for all sites and therefore it controls the pavement life. Figure 8.13 also shows that the allowable fatigue life at Weiser is greater than Moscow, because the Weiser site has greater thickness of AC layer (6'') than Moscow (4.8''). The figure also indicates that the there is no significant difference in the predicted fatigue life when considering twelve or four seasons per year, while considering only one season overestimates the pavement life. On the other hand, the predicted rutting life could be overestimated when the number of seasons per year is reduced, as shown in Figure 8.14

While the Moscow sites showed smaller fatigue life (Figure 8.13) because of its smaller AC thickness as explained in the previous figure, it showed greater rutting life than Weiser because it has a thicker rockcap layer as shown in. The figure also shows that rutting life in Weiser and Worley sites greatly decreases with increasing the number of seasons per year because the effect of both traffic and AC modulus are greater during summer months. However the Moscow site has less traffic during summer, weak AC modulus, this caused the rutting life based on 12 seasons to be greater.

Since the pavement life at both Idaho sites was controlled by fatigue, then considering four seasons could be considered a good indication for capturing the seasonal variations if not possible to consider twelve seasons. It should be noted that the rutting failure was not critical at those Idaho sites because of the presence of a strong base layer, which reduces the compressive strain on the surface of subgrade preventing the occurrence of rutting failure. In some other sites in which weak base or no base layer was used, the rutting failure might be the critical one. Therefore, it is recommended that this analysis be performed at more different sites with different or no base thickness to confirm this conclusion.

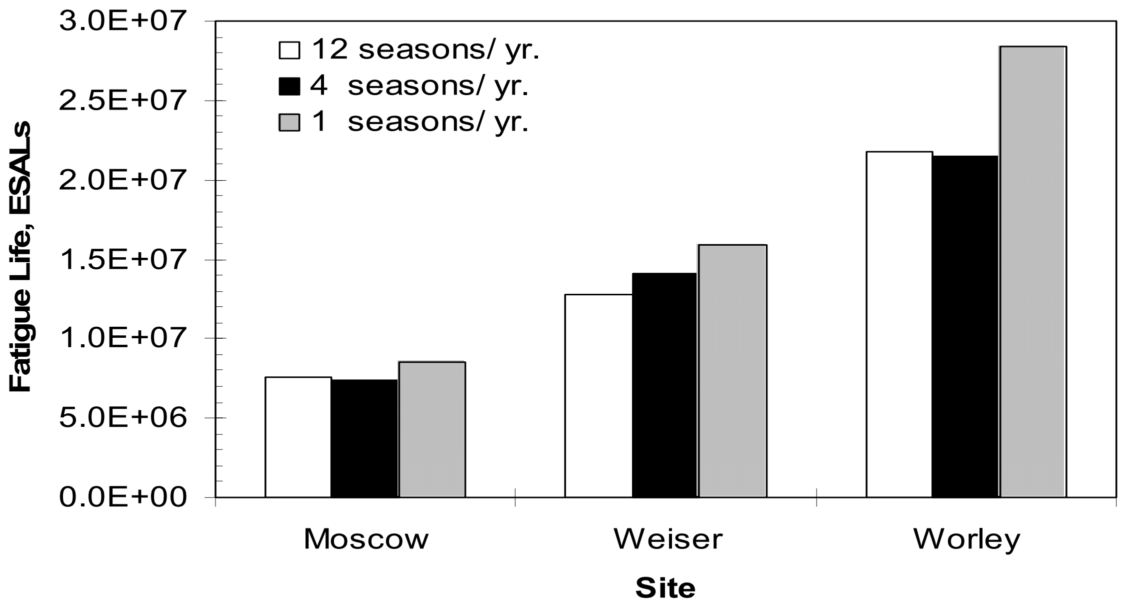

Figure 8.13 Total Fatigue Life Due to Different Seasons/ Year for the Moscow and Worley Sites

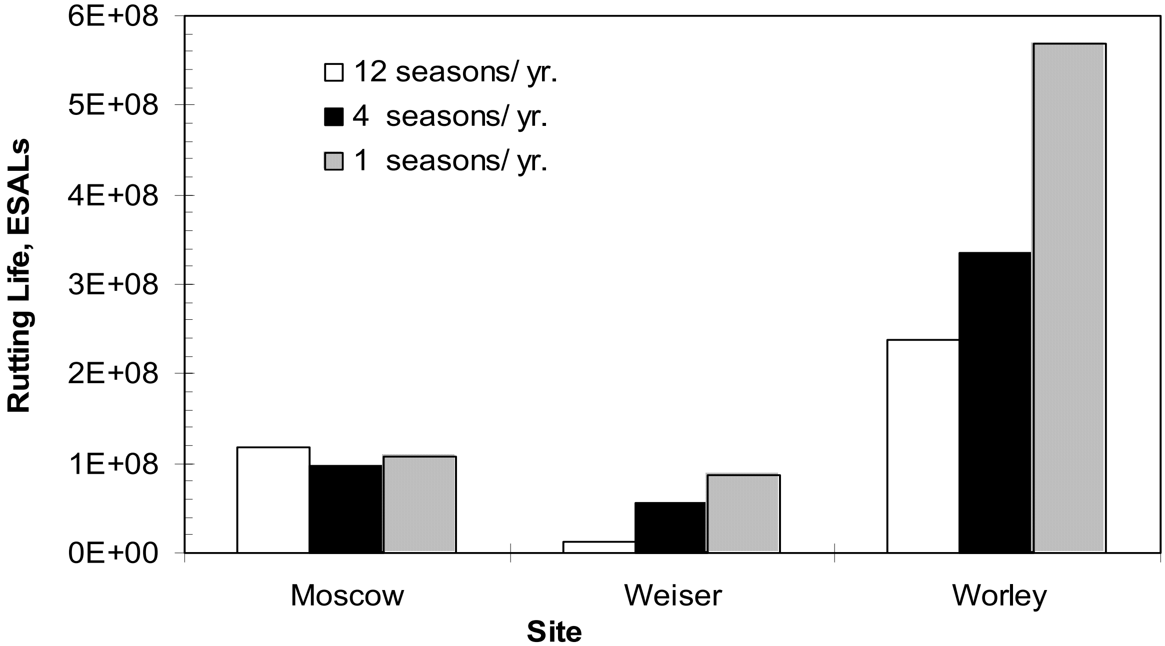

Figure 8.14 Total Rutting Life Due to Different Seasons/ Year for the Moscow and Worley Sites

8.3 IMPACT OF ROCKCAP BASE LAYER ON THE PAVEMENT STRUCTUAL CAPACITY

The analysis presented in Chapter 4 showed that the subgrade moisture content under the rockcap base layer might be greater than the corresponding one in case of using aggregate base. This observation was found in the closed system, like the one in Moscow, in which the rockcap layer was not connected to a daylight drainage layer (open to a side ditch). On the other hand, the rockcap layer has a greater modulus of elasticity than the aggregate base layer. This greater modulus value of the rockcap layer could compensate or exceed the subgrade modulus reduction due to moisture increase, as discussed below.

Figure 8.15 shows the FWD vertical deflection at the Moscow sections having rockcap and aggregate bases during four different years. The figure presents the vertical deflections measured at various distances from the applied load. The figure shows that the recorded deflections at the pavement section having rockcap layer are less than the other section having aggregate base for the four years. This indicate that the pavement section having rockcap layer is always stronger than the section having aggregate base even though the subgrade moisture content under rockcap layer was greater.

Figure 8.16 shows the computed tensile strain at the bottom of the AC layer and the compressive strain at the top of the subgrade soil, for both sections, using the KENLAYER program. The strains were computed based on the backcalculated layers' moduli, shown in Appendix B, and assuming the standard 18 kips axle load with 13.5 inch dual spacing and 80 psi tire pressure. The figure shows that there is no significant difference in the tensile stains when using rockcap or aggregate base layers because the tensile strains are mainly affected by the AC modulus. On the other hand, the figure shows that the compressive strain at the top of subgrade layer is highly reduced when using the rockcap layer.

Figure 8.17 shows the predicted pavement life, in ESALs, for both sections. The upper part of the figure indicates that there is no great difference in the predicted allowable fatigue life when using rockcap or aggregate bases since the fatigue life is mainly affected by the AC modulus. However, the bottom part of the figure indicates that the rutting life is greatly increased (about 5 times) when using the rockcap layer.

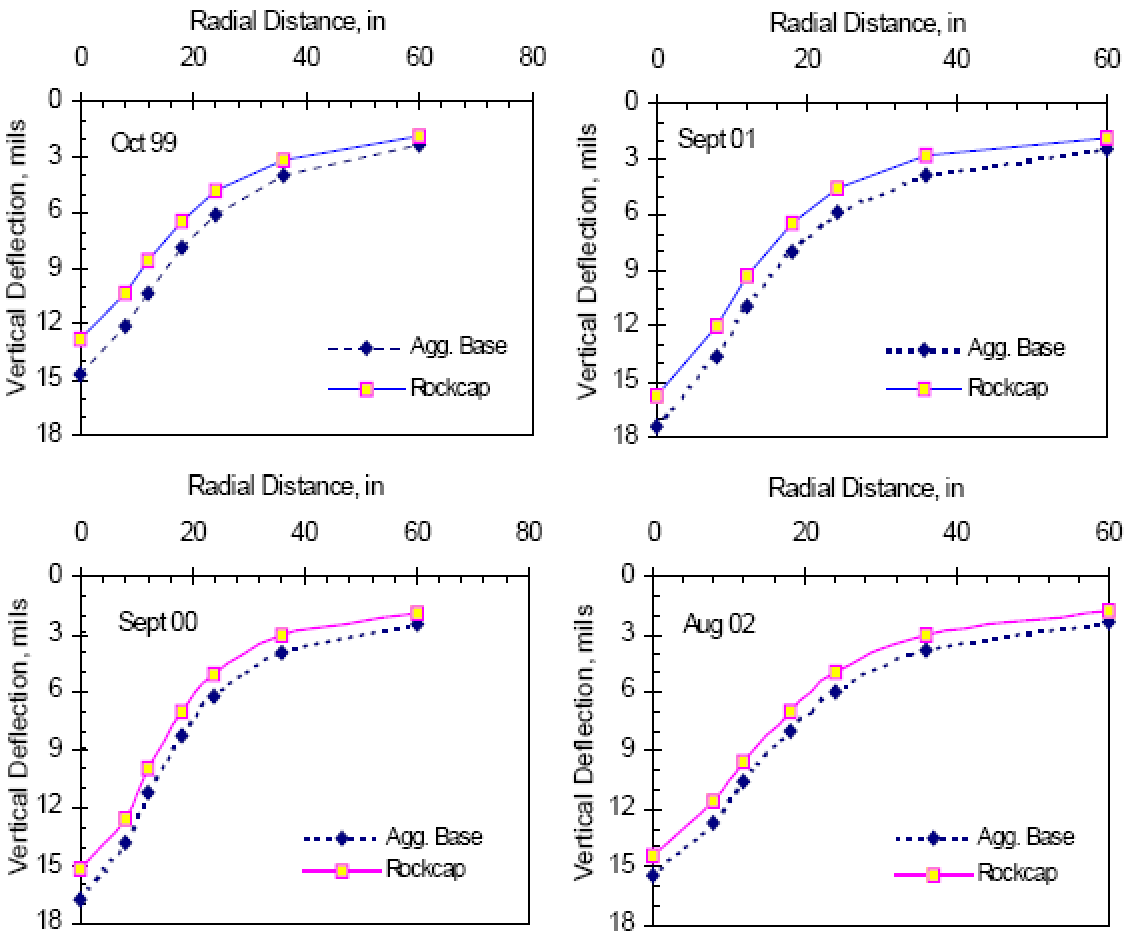

Figure 8.15 Vertical FWD Deflection for Moscow Sections Having Rockcap and Aggregate Bases

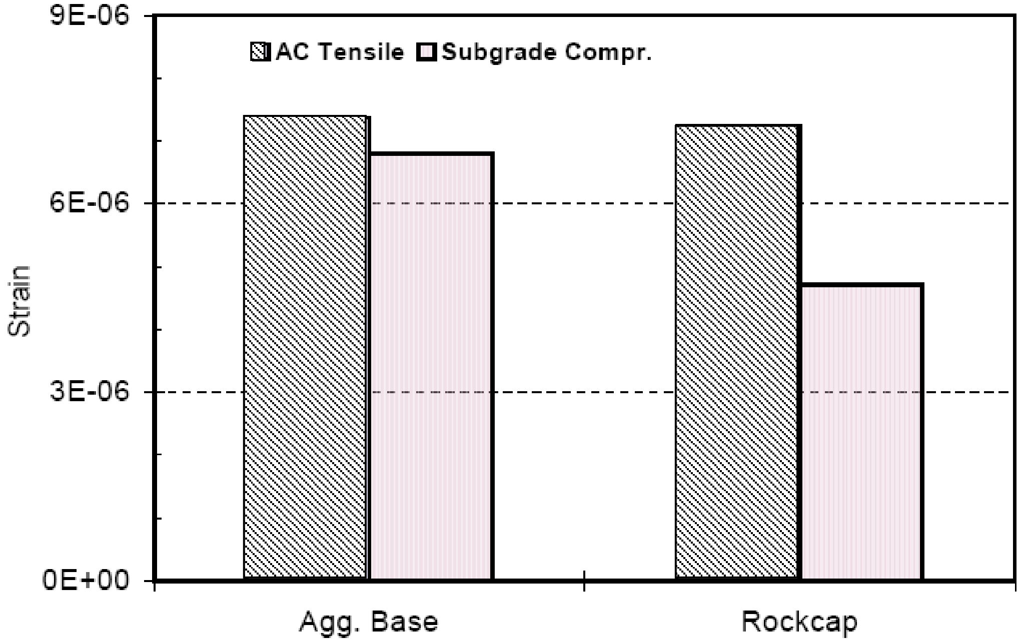

Figure 8.16 Computed Tensile and Compressive Strains for Moscow Sections Having Rockcap and Aggregate Bases

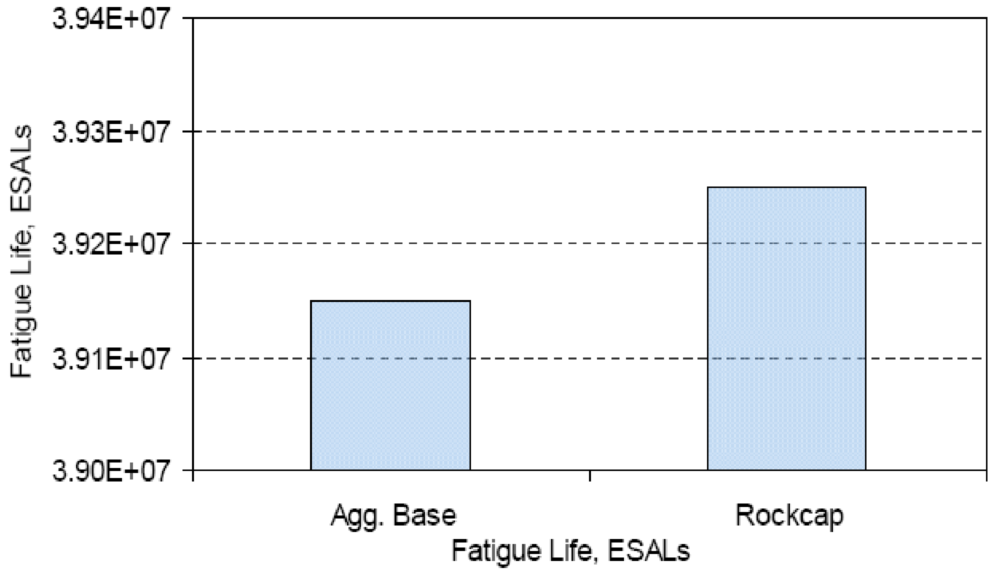

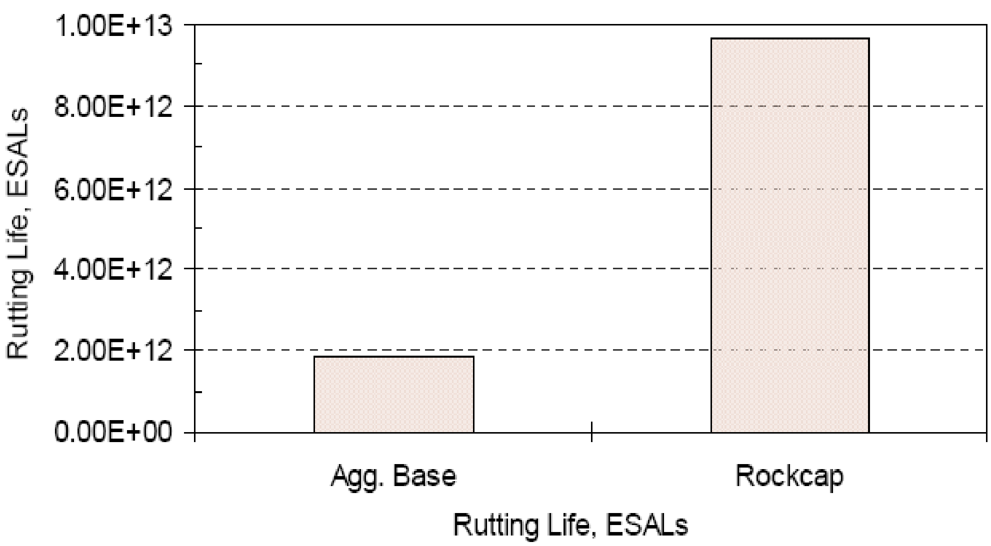

Figure 8.17 Predicted Pavement Life in ESALs for Moscow Sections Having Rockcap and Aggregate Bases

8.4 SUMMARY

In this chapter, the suitable timing for the four different seasons; winter, spring, summer and fall was determined based on the rainfall and temperature data for the different Idaho sites. The chapter also explained the procedures and the necessary equations to determine the seasonal adjustment factors (SAF) for both subgrade and asphalt concrete (AC) layers at the various sites. The chapter discussed the implementation of the developed equations in the pavement design process to reflect the impact of seasonal variation in the pavement performance.

A performance analysis was conducted for Worley and Moscow sites. The analysis showed that the damage ratio was greatly increased during the summer months due to the higher traffic volume and the less pavement moduli. It also showed the predicted pavement life was overestimated when disregarding the seasonal variations in any of the AC modulus, subgrade modulus and traffic. In general, the seasonal variations in the AC modulus showed more severe impacts on the estimated pavement life.

The chapter also illustrated that the pavement life at both sites was controlled by fatigue damage not rutting, and discussed the possible reason behind that. It also showed that there was no significant difference in the predicted fatigue life when considering twelve or four seasons per year, while considering only one season overestimates the pavement life. On the other hand, the predicted rutting life was overestimated when the number of seasons per year was reduced but it did not affect the pavement design since the fatigue life was the critical.

The performance analysis for the two pavement sections, at Moscow, having rockcap and base course layers showed that the section with rockcap layer was always stronger than the other section with aggregate base even though the subgrade moisture content under rockcap layer was greater. The predicted rutting life, for the pavement section with rockcap layer, was about 5 times greater than the other section with aggregate base.

9. SUMMARY, CONCLUSIONS AND RECOMENDATIONS

9.1 SUMMARY

The main objective of this research is to quantify the environmental changes in pavement layers and their impacts on the overall pavement performance. To achieve this objective, five pavement sites in northern and southern Idaho were instrumented to monitor the moisture and temperature changes in the pavement layers over the year. The data were collected on a monthly basis to reflect the seasonal variations over the entire year. In addition to moisture and temperature data, pavement structural capacity was assessed by Falling Weight Deflectometer (FWD), which was conducted annually. Weather and various climatic data such as precipitation and air temperature were obtained from weather stations at or near to the instrumented sites. Soil and aggregate layers parameters relevant to the pavement design, such as Atterberg limits, grain size distribution and classification were determined using routine laboratory tests on representative samples.

The FWD testing was performed by the Idaho Transportation Department (ITD) materials section as part for their normal FWD testing schedule, which was done once a year. It was not possible for ITD to perform FWD testing at each season, and therefore, the study relied on the FHWA Long-Term Pavement Performance Seasonal Monitoring Program (LTPP-SMP) database to acquire the data necessary for model developments. This step was necessary to develop correlation models for the subgrade modulus and moisture and asphalt concrete modulus- temperature relationships. The FWD data measured from the annual FWD testing at the Idaho sites was used to validate the developed models. Further, the data collected at the instrumented Idaho sites were also used to check and validate the use of the Enhanced Climatic Model (EICM) in Idaho conditions.

Analysis of the LTPP and Idaho data resulted in two main models that describe the seasonal variation in the pavement layer moduli. One model is for the soil and unbound materials and the other is for the asphalt concrete layers. To implement the developed models, modulus shift functions which are referred to as Seasonal Adjustment Functions (SAF), were developed to relate the seasonal changes in a layer modulus to an arbitrarily selected reference season. In this study, the reference season was considered to be the “normal” summer conditions. These shift functions were also validated using Idaho data and were used to develop a series of seasonal shift factors for various regions in the state of Idaho. Procedures were outlined to implement the developed seasonal shift functions at the five Idaho sites for estimating the seasonal changes in the layers’ moduli and to calculate the SAF for each layer. The suitable timing for the four different seasons; winter, spring, summer and fall was determined based on the rainfall and temperature data at the instrumented Idaho sites.

To quantify the impact of seasonal variation on pavement performance, mechanistic analysis using multi-layer elastic theory and empirical models of fatigue and rutting was conducted to assess the remaining service lives at the instrumented sites. For this purpose, traffic data were obtained form the ITD traffic section. Through this analysis, the percentage damage occurring each month (and season) was estimated, and the allowable pavement life was predicted with and without considering the seasonal variations in the layers’ moduli and the applied traffic loads.

9.2 CONCLUSIONS

The conclusions of this research are grouped in four sections as presented below:

A. Subgrade Soil Moisture Variation at Idaho sites, and Validation of EICM *Model*

Based on the analysis of the moisture data collected at the instrumented sites in Idaho, the following conclusions are drawn:

- The moisture contents measured at most of the Idaho sites showed long-term equilibrium with only a small seasonal fluctuation. The observed seasonal variation could be related to the rainfall amount, the ground water level (GWL) and the soil type (fine or coarse, plastic or non-plastic).

- The change in subgrade moisture was observed only at shallow depths just below the base or rockcap layer. At deeper depths, there was no significant difference in the moisture content under base or rock cap layers, where the moisture reaches equilibrium.
- The application of the Enhanced Integrated Climatic Model (EICM) to some Idaho sites showed that the model can predict the pavement temperature with good accuracy, but it cannot accurately predict the subgrade water content when using the EICM default values. The analysis showed that the model overestimated the moisture content for plastic soils and underestimated it for nonplastic soils.
- The EICM moisture prediction procedures are highly dependent on the soil water characteristic curve (SWCC) relationships. This study showed that the primary factors affecting the moisture prediction in the EICM are the distance to the GWL and the saturated volumetric moisture content of soil (porosity). Therefore, the model can provide a reasonable estimate of the subgrade water content, but only if the actual values of the saturated volumetric water content and the actual seasonal variation of the GWL are known.

B. Subgrade Modulus-Moisture Relationships

- The variation of the subgrade modulus and moisture with time followed an inverse function, where the modulus decreased with moisture increase. This conclusion was valid for all soils where the field moisture contents were above the optimum. In a few cases, the inverse function was not valid, especially for non-plastic soils and for the moisture condition below the soil's optimum moisture content. It is believed that the increase in modulus with increase in moisture would be reasonable if the existing moisture condition is on the dry side. Thus, an increase in moisture will result in a higher modulus until it reaches the optimum, and then start to decrease. The LTPP database did not have sufficient sites with such conditions to further investigate this observation.
- The modulus-moisture data presented showed that the soils that were more sensitive to moisture variations were the fine silty soils followed by clayey soils. Coarse-grained

soils, like clayey-sand, were less sensitive to moisture variations. This may indicate that the seasonal variation in the granular base or rockcap layers would be minimal.

- A general regression model relating the subgrade modulus to soil moisture and other soil properties was developed based on the LTPP-SMP data and was validated using data from the Idaho sites.

- A model was developed for estimating the modulus seasonal adjustment factor (SAF_s) of subgrade soils. The SAF_s is the ratio of the subgrade soil modulus at a given season to that of a reference season. The moduli ratio is related by power function to the average subgrade moisture content ratio of the given season to the reference season.

C. Asphalt Concrete Modulus-Temperature Relationships

- The variation of AC modulus and pavement temperature with time followed an inverse function, where the modulus decreases with a temperature increase. This result was valid for all sites. The data also showed that the AC modulus might decrease in summer to less than 20% of its winter value.

- The mid-depth pavement temperature was found to be the best temperature to represent the AC layer's condition, rather than the temperature at 25 mm depth, or the pavement surface temperature.

- General regression models relating AC modulus to mid-depth pavement temperature and other AC layer properties were developed for freezing and nonfreezing zones. Those models were also validated using the backcalculated moduli at Idaho sites.

- A model for calculating the modulus seasonal adjustment factor (SAF_{ac}) of the AC layer was developed. The SAF_{ac} is the ratio of the AC modulus at a given season to that of a reference season. The moduli ratio is related by exponential function to the average pavement temperature ratio of the given season to the reference season.

- A model for estimating the asphalt pavement temperature from the air temperature was also developed based on the LTPP data. The model incorporates in addition to the air temperature, the depth, site latitude and the month of the year. The model was also validated using the collected temperature data from the Idaho sites.

D. Effect of Rockcap Layer

- Observations of moisture regime in the subgrade at Moscow and Weiser sites showed opposite results, where at Moscow sites the subgrade under the rockcap base experience higher moisture content than the subgrade under the aggregate. At the Weiser site, the opposite occurred where the subgrade under the rockcap base layer experienced lower moisture content than the one under the aggregate base. The main difference was that the rockcap base layer at Weiser site was extended to the adjacent open ditch drain while at Moscow; the rockcap layer was blocked by the side embankment. This led the researchers to believe that in order for the rockcap layer to be effective in reducing the subgrade moisture, it should be extended to daylight so that it allows for the lateral seepage of the moisture from base to the adjacent open ditch drain, or install edge drains to remove water. Otherwise, the water would seep downward causing higher moisture in the subgrade.
- Analysis of structural support conditions and performance of the two pavement sections at Moscow (rockcap and aggregate base) showed that the section with rockcap layer was stronger than the other section with aggregate base, even though the subgrade moisture content under rockcap layer was greater. The predicted rutting life, (which is more affected by the subgrade layer) for the pavement section with rockcap layer, was about 5 times greater than the other section with aggregate base. Thus, the presence of rockcap base layer would improve pavement performance conditions even though an adverse effect on the subgrade moisture might be observed.

E. Implementation in the Pavement Design and Performance Prediction

The developed models were used to develop series of seasonal shift factors (SAF) for various locations. The developed SAF's were incorporated in mechanistic analysis to asses the impact of seasonal variation on design and performance. The following conclusions are drawn:

- Seasonal adjustment factors for the subgrade soil and the AC layer were estimated for each site based on the collected moisture and temperature data at Idaho and the developed models. Seasonal timing for selected four seasons (summer, fall, winter, and spring) were also determined for the different sites based on the average monthly rainfall and air temperature.
- The mechanistic analysis performed using elastic layer theory in combination with the developed models to predict the pavement fatigue and rutting lives revealed that the inclusion of seasonal variation in pavement layer moduli has resulted in a reduction of pavement service life of about 35% on the average. This indicates if an average modulus for each layer was used, instead of varied seasonal moduli values, it will result in pre-mature failure.

9.3 RECOMMENDATIONS

As mentioned above, the performance prediction was done by theoretical analysis using the elastic layer theory and the empirical models published for fatigue and rutting. Calibration of those models was not possible at the instrumented Idaho sites due to the fact that the pavement conditions at all sites were relatively new. No signs of distress were observed during the study period. Therefore, it is recommended that the instrumented sites in Idaho be monitored continually over the coming years, monitoring shall include pavement surface distress and structural capacity evaluation by FWD. This information would be used to calibrate the developed seasonal adjustment functions and the performance models.

It is also recommended that LTPP sites that have extensive distress data be used to calibrate the performance prediction models using the algorithms developed in this study. The performance prediction validation is an essential step for the implementation of the new AASHTO mechanistic-empirical pavement design guide.

REFERENCES

AASHTO Designation M 147-65. (1990). "Standard Specification for Materials for Aggregate and Soil- Aggregate Subbase, Base and Surface Courses." AASHTO. pp. 157-158.

AASHTO Designation T-274-82 (1982). "Standard Method of Test for Resilient Modulus of Subgrade Soils." Standard Specifications for Transportation Materials and Methods of Sampling and Testing. 13th Edition, American Association of State Highway and Transportation Officials, Washington, D.C., pp. 1157.

AASHTO Guide for Design of Pavement Structures (1986-1993). American Association of State Highway and Transportation Officials, Washington, D.C.

Abo-Hashema, M.A., Bayomy, F.M., Smith, R., and Salem, H.M. (2002). "Environmental Impacts on Subgrade Resilient Modulus for Idaho Pavements." Transportation Research Board, TRB 81st Annual Meeting, Paper Number 02-3247, Washington, D.C.

Abo-Hashema, M., and Bayomy, F. (2002). "Development of Pavement Temperature Prediction Model for Asphalt Concrete Pavements." 6th International Conference on the Bearing Capacity of Roads, Railways and Airfields (BCRA´ 02), Lisbon, Portugal.

Ali, H., and Lopez, A. (1996). "Statistical Analyses of Temperature and Moisture Effects on Pavement Structural Properties Based on Seasonal Monitoring Data." Transportation Research Record No. 1540, Transportation Research Board, Washington, D.C.

Ali, H., and Parker, N. (1996). "Using Time Series to Incorporate Seasonal Variations in Pavement Design." Transportation Research Record No.1539, Transportation Research Board, Washington, D.C., pp 33-43.

Al-Kandari, F. (1994). "Mechanistic Based Overlay Design Procedure for Idaho Flexible Pavements." M.S. Thesis, University of Idaho.

Asphalt Institute, AI (1982)."Research and Development of the Asphalt Institute Thickness Design Manual (MS-1), 9th Ed., Research Report 82-2, Asphalt Institute, Kentucky.

Bayomy, F., Al-Kandari, F., and Nassar, W. (1997). "Computer Aided Overlay Design System for Flexible Pavements," Proceedings of the 8th International Conference on Asphalt Pavements, Seattle, Washington.

Bayomy, F., Al-Kandari, F., and Smith, R. (1996). "Mechanistic-Based Overlay Design System for Idaho." Transportation Research Record, 1543, Transportation Research Board, Washington, D.C., pp. 10-19.

Bayomy, F., and Hardcastle, J. H. (2002). "Monitoring and Modeling Subgrade Soil Moisture for Pavement Design and Maintenance in Idaho." Phase 2: Site Installations and Preliminary Data Collection, Draft Final report of ITD research project SPR-STP-0010 (020) 124, Agreement number FC No. 97-30, UI Budget Number FM-K173, National Institute for Advanced Transportation Technology (NIATT).

Bayomy, F., and Nassar, W. (1997). " WINFLEX 97: A Mechanistic-Empirical Overlay Design System for Flexible Pavements." Final Report of ITD research project RP121-Phase 2, Agreement No. 97-44, UI Budget No. FM-K238, National Center for Advanced Transportation Technology (NCATT), 43 pp.

Bayomy, F., Nassar, W., and Al-Kandari, F. (1996). "Development of Recommendations and Guidelines for Pavement Rehabilitation Design Procedures for the State of Idaho." Phase 2: Development of a Mechanistic-Based Overlay Design System, Volume I: FLEXOLAY Program Documentation, and Volume II: FLEXOLAY Program User Manual, Final Report of ITD research project RP-121, Agreement No. 95-60, Department of Civil Engineering, University of Idaho.

Bayomy, F.M., and Shah, Z.R. (1993). "Development of Recommendations and Guidelines for Pavement Rehabilitation Design Procedure for the State of Idaho; Phase 1 Software Evaluation and Data Analysis." ITD Project No. 92-35 Proj. 112, Final Report.

Bayomy, F.M., Salem, H.M., Smith, R., Santi, M. (2003). "Using LTPP Data to Assess the Impacts of Seasonal Variation of Subgrade Resilient Modulus on Overlay Mechanistic Design." International Conference on Highway Pavement (ICHP) Data, Analysis and Mechanistic Design Applications, Columbus, Ohio, September 7-10.

Berg, R.L. (1988). "Pavement Design for Seasonal Frost Conditions-Current and Future Methods." Federal Aviation Administration, Great Lakes Region, Fourth Annual Airport Engineering/Management Conference.

Bergen, A.T., and Monismith, C.L. (1973). "Characteristics of Subgrade Soils in Cold Regions for Pavement Design Purposes." Highway Research Record 431, Highway Research Board, Washington, D.C., pp. 25-37.

Carmichael, R.F. III, and Stuart, E. (1985). "Predicting Resilient Modulus: A Study to Determine the Mechanical Properties of Subgrade Soils." Transportation Research Record 1043, Transportation Research Board, Washington, D.C., pp. 145-148.

Chamberlain, E.J., Cole, D.M., and Durell, G.F. (1989). "Resilient Modulus Determination for Frost Conditions." State of the Art Pavement Response Monitoring Systems for Roads and Air Fields, Special Report 89-23, V. Jenson and R. Eaton, editors, U.S. Army Cold Regions Research and Engineering Laboratory (CRREL), Hanover, NH, pp. 320-333.

Chamberlain, E.J., Cole, D.M., and Johnson, T.C. (1979). "Resilient Response of Two Frozen and Thawed Soils." Journal of the Geotechnical Engineering Division, American Society of Civil Engineers, Vol. 105, No. GT2, pp. 257-271.

Climate Database (2002). "http://www.worldclimate.com," Accessed on May 20, 2002.

Cumberledge, G., Hoffman, G.L., Bhajandas, A.C., and Cominsky, R.J. (1974). "Moisture Variation in Highway Subgrades and the Associated Change in Surface Deflections." Transportation Research Record 497, Transportation Research Board, Washington, D.C., pp. 40- 49.

DataPave 3.0 (2002). Federal Highway Administration Document No. FHWA-RD-01-148, U.S. Department of Transportation, Washington, D.C.

DataPave online (2003). "http://www.datapave.com,"Accessed on July 30, 2003.

Dempsey, B. J., Herlach, W.A., and Patel, A. J. (1985). " The Climatic- Materials – Structural Pavement Analysis Program." Final Report, FHWA/RD-84/115, Vol 3, Federal Highway Administration, Washington, D. C.

Dore, G., and Savard, Y. (1998). "Analysis of Seasonal Pavement Deterioration." Transportation Research Record, Transportation Research Board, Washington, D.C.

Drumm, E., and Meier, R. (2003). "Daily and Seasonal Variations in Insitu Material Properties." NCHRP Web Document 60 (Project 20-50[7/12]): Contractor's Final Report, National Cooperative Highway Research Program, Transportation Research Board, Washington, D.C, 707 pp.

Edris, E.V., and Lytton, R.L. (1977). "Climatic Materials Characterization of Fine-Grained Soils". Transportation Research Record 642, Transportation Research Board, Washington, D.C., pp. 39-44.

Elliott, R.P., and Thornton, S.I. (1988). "Simplification of Subgrade Resilient Modulus Testing." Transportation Research Record 1192, Transportation Research Board, Washington, D.C., pp. 1-7.

Fredlund, D. G. (1995). "Prediction of Unsaturated Soil Functions Using the Soil-Water Characteristic Curve." Proceedings of the Bength B. Broms Symposium on Geotechnical Engineering, Singapore, 13-15 December, pp. 113-133.

Fredlund, D. G., and Xing, A. (1994). "Equations for the Soil-Water Characteristic Curve." Canadian Geotechnical Journal, Vol. 31, No. 4, pp. 521 - 532.

Guymon, G. L., Berg, R. L., and Johnston, T. C. (1986). "Mathematical Model of Frost Heave and Thaw Settlement in Pavements." Report by U. S. Army Cold Regions Research and Engineering Laboratory.

Hadley, W., Anderson, V., Groeger, J., and Copeland, C. (1994). "SHRP-LTPP Data Analysis Studies: Five Year Report." SHRP-P-688, Strategic Highway Research Program, National Research Council, Washington, D.C.

Halliburton, T.A. (1970). "Subgrade Moisture Variations". Final Report, Research Project 64-01-3, School of Civil Engineering, Oklahoma State University, Stillwater, Oklahoma, 86 pp.

Hardcastle, J., and Bayomy, F. (1996). "Monitoring and Modeling Subgrade Soil Moisture for Pavement Design and Maintenance in Idaho, Phase 1: Development of Scope of

Work." Final report of ITD project RP 124, Agreement No. 96-48, UI Budget No. FM-K428, National Center for Advanced Transportation Technology (NCATT), 35 pp.

Hardcastle, J.H. (1992). "Subgrade Resilient Modulus for Idaho Pavements." Idaho Transportation Department, Boise, ID.

Hardcastle, J.H. (2000). "Engineering Properties of Soils- Some Suction Concepts". University of Idaho, Department of Civil Engineering, CE 561 Class Handouts, Fall semester, Lecture 22.

Hardcastle, J.H., Lottman, R.P., and Buu, T. (1983). "Fatigue Based Criteria for Seasonal Load Limit Selection." Transportation Research Record 918, Washington, D.C., pp. 22-30.

Hicks, R.G., and Monismith C.L. (1971). "Factors Influencing the Resilient Responses of Granular Materials." Highway Research Record 345, Highway Research Board, Washington, D.C., pp. 15- 31.

Huang, Y. H. (2004). "Pavement Analysis and Design." Pearson & Prentice Hall, Upper Saddle River, NJ 07458.

Hudson, J.M., Drumm, E. C., and Madgett, M. (1994). "Design Handbook for the Estimation of Resilient Response of Fine Grained Subgrades." Proc. 4th Int. Conf. on the Bearing Capacity of Roads and Airfields (BCRA), Vol. 2., pp 917-928.

Hwang, D., and Witczak, M. (1979). "Program DAMA (Chevron), User's Manual", Department of Civil Engineering, University of Maryland.

Idaho Department of Transportation, ITD (2004). "State Traffic Counters, http://www.itd.idaho.gov/planning/reports/atr_wim/atr_state.html," Accessed on Jan 10, 2004

Janoo, V.C., and Berg, R.L. (1990). "Thaw Weakening of Pavement Structures in Seasonal Frost Areas." Transportation Research Record # 1286, TRB, Washington, D.C., pp. 217-233.

Jones, M.P. and Witczak, M.W. (1977). "Subgrade Modulus on the San Diego Test Road." Transportation Research Record 641, Transportation Research Board, Washington, D.C., pp. 1-6.

Klute, A. (1986). "Water Retention Laboratory Methods." In Agronomy No. 9, Soil Sci. Soc. Amer. Madison, pp. 635-662.

Larson, G., and Dempsey, B. J. (1997). "Enhanced Integrated Climatic Model Version 2.0." University of Illinois at Urbana-Champaign and Newmark Civil Engineering Laboratory, Report No. DTFA MN/DOT 72114.

Larson, G., and Dempsey, B. J. (2003). "Enhanced Integrated Climatic Model Version 3.0." Applied Research Associates/ ERES Division Staff, for upgrade with results from NCHRP 1-37 A, the 2002 Guide Development.

Lary, J.A., and Mahoney, J.P. (1984). “Seasonal Effects on the Strength of Pavement Structures.” Transportation Research Record No. 954, Transportation Research Board, Washington, D.C., pp. 88-94.

Liang, H. S., and Lytton, R.L. (1989). “Rainfall Estimation for Pavement Analysis and Design.” Presented at 88th Annual Meeting, Transportation Research Board, Washington, D.C.

Liu, S. J., and Lytton, R. L. (1985). “Environmental Effects on Pavement-Drainage.” Report FHWA-DTFH-61-87-C-00057, Vol. IV, Federal Highway Administration, Washington, D. C.

Lukanen, E.O., Stubstad, R., and Robert Briggs, C. (2000). “Temperature Predictions and Adjustment Factors for Asphalt Pavements.” Report FHWA-RD-98-085, Federal Highway Administration, Washington, D. C.

Lytton, R. L. (1989). “Backcalculation of Pavement Layer Properties.” Nondestructive Testing of Pavements and Backcalculation of Moduli, ASTM STP 1026, A. J. Bush II and G.Y. Baladi, Eds., ASTM, Philadelphia, pp 7-38.

Lytton, R.L., Pufahl, D.E., Michalak, C.H., Liang, H.S., and Dempsey, B.J. (1989).”An Integrated Model of Climatic Effects on Pavements.” Final Report, FHWA-RD-90-033, Federal Highway Administration Washington, D. C.

Marks, B.D., and Haliburton, T.A. (1969). “Subgrade Moisture Variations Studied with Nuclear Gages.” Highway Research Record 276, Highway Research Board, Washington, D.C., pp. 14-24.

Marshall, C., Meier, R. and Welsh, M. (2001).”Seasonal Temperature Effects on Flexible Pavements in Tennessee.” TRB 80th meeting, Paper # 02-3642, January 8-11, Washington, DC.

Miner, M. A. (1945). “Comulative Damage in Fatigue.” Tansactions of the ASME, Vol. 67, pp. A159- A164.

Mohseni, A., and Symons, M. (1998)."Improved AC Pavement Temperature Models from LTPP Seasonal Data." TRB 77th Annual meeting, Washington D.C.

MP-917 Technical Brief (2004). “http://www.esica.com/support/tech/pdf/tb01.pdf”, Acessed on Dec 30, 2000.

Nassar, W. (1997). “Analysis and Validation of the Mechanistic- Empirical Overlay Design Procedure Incorporated in FLEXWIN Computer Program.” M.S. Thesis, University of Idaho.

Naval Facilities Command (NAVFAC, 1986). “ Soil Mechanics Design Manual 7.01.” Alexandria, Virginia.

Pavement Systems, LLC (1999). “LTPPBIND Version 2.1, A SUPERPAVE Binder Selection Program.” Developed for the Federal Highway Administration, Washington, D.C.

Picornell, M., and Rahim, M.A.B. (1991). "Simulation of Climatic and Vegetation Effects on Pavements on Expansive Clays." Presented at 70th Annual Meeting, Transportation Research Board, Washington, D.C.

Rada, G., and Witczak, M.W. (1981). "Comprehensive Evaluation of Laboratory Resilient Moduli Results for Granular Materials." Transportation Research Record 810, Transportation Research Board, Washington, D.C., pp. 23-33.

Rada, G., Elkins, G., Henderson, B., Van Sambeek, R., and Lopez, A. (1994). "LTPP Seasonal Monitoring Program: Instrumentation Installation and Data Collection Guidelines." Report FHWA-RD-94-110, Federal Highway Administration, Washington, D.C.

Rada, G.R., Richter, C.A, Stephanos, P.J., (1991). "Layer Moduli from Deflection Measurements." Software Selection and Development of SHRP's Procedure for Flexible Pavements, Beltsville, MD.

Richter, C. A., and Witczak, M. W. (2001). " Application of LTPP Seasonal Monitoring Data to Evaluate Volumetric Moisture Predictions from the Integrated Climatic Model." Transportation Research Board (TRB), 80th Annual Meeting, Washington, D.C.

Salem, H. (2004). "Quantification of Environmental Impacts on the Performance of Asphalt Pavements." Ph.D. Desertation, University of Idaho, Moscow, Idaho.

Salem, H.M, and Bayomy, F.M. (2004). "Prediction of Seasonal Variation of the Asphalt Concrete Modulus Using LTPP Data." Transportation Research Board, TRB 83rd Annual Meeting, Paper # 04-2863, Washington, D.C.

Salem, H.M., Bayomy, F.M., Al-Taher, M.G. (2003). "Prediction of Seasonal Variation of Subgrade Resilient Modulus Using LTPP Data." Transportation Research Board, TRB 82nd Annual Meeting, Paper # 02-3642, Washington, D.C.

SAS Software (2001). Release 8.2, Copyright (c) 2001 by SAS Institute Inc., Cary, NC, USA.

Scrivner, F.H., Peohl, R., Moore, W.M., and Phillips, M.B. (1969). "Detecting Seasonal Changes in Load-Carrying Capabilities of Flexible Pavements." NCHRP Report 7 Highway Research Board, Washington, D.C., 37 pp.

Seed, H. B., Mitry, F. G., Monismith, C. L., and Chan, C. K. (1967). "Factors Influencing the Resilient Deformation of Untreated Aggregate Base in Two-Layer Pavements Subjected to Repeated Loading." Highway Research Record 1, Highway Research Board, Washington, D.C., pp. 19-57.

Seed, H.B., Chan, C.K. and Lee, C.E. (1962). "Resilience Characteristics of Subgrade Soils and Their Relation to Fatigue Failures in Asphalt Pavements." Proc. Int. Conference on the Structural Design of Asphalt Pavements, University of Michigan, pp. 611-636.

Stubstad, R. N., Baltzer, S., Erland, O., Lukanen and Ertman-Larsen, H.J. (1994). "Prediction of AC Mat Temperatures for Routine Load/ Deflection Measurements." Proceedings, 4th International Conference on the Bearing Capacity of Roads and Airfields, Trondheim, Norway, pp. 401-412.

Stubstad, R. N., Erland, O., Lukanen, Richter, C. A., and Baltzer, S. (1998). "Calculation of AC Layer Temperatures from FWD Field Data." Proc. 5th Int. Conference on the Bearing Capacity of Roads and Airfields, Trondheim, Norway, pp. 919-928.

Thompson, M.R., and LaGrow, T. (1988). "A Proposed Conventional Flexible Pavement Thickness Design Procedure." Civil Engineering Studies, Transportation Engineering Series No. 55, University of Illinois at Urbana-Champaign.

Thompson, M.R., and Robnett, Q.L. (1979). "Resilient Properties of Subgrade Soils." Transportation Engineering Journal, ASCE, Vol. 105, No. TE1, pp. 71-89.

Von Quintus, H.L., and Simpson, A.L. (2002). "Backcalculation of Layer Parameters for LTPP Test Sections, Vol. II: Layered Elastic Analysis for Flexible and Rigid Pavements." Report FHWA-RD-01-113, Federal Highway Administration.

White, T.D., and Coree, B.J. (1990). "Threshold Pavement Thickness to Survive Spring Thaw." Proceedings of the Third International Conference on Bearing Capacity of Roads and Airfields, Trondheim, Norway, pp. 41-51

Witczak, M.W., Houston, W.N., Zapata, C.E., Richter, C., Larson, G. and Walsh, K. (2000). "Improvement of the Integrated Climatic Model for Moisture Content Predictions." Inter-Team Technical Report (Seasonal 4), NCHRP 1-37 A.

Zapata, C.E., Houston, W.N., Houston, S.L., and Walsh, K.D. (1999). " Soil-Water Characteristic Curve Variability." Geotechnical special publication No. 99, Advances in Unsaturated Geotechnics, Proc. of sessions of Geo-Denver 2000, ASCE, Denver, Colorado.

Zou, G., Meier, R.W., and Drumm, E.C. (2002). "The Effect of Temperature Averaging on Predicted Pavement Life." Transportation Research Record, No. 1809, TRB, Washington D.C., pp. 119-125.

Zubeck, H.K., and Vinson, T.S. (1996). " Prediction of Low Temperature Cracking of Asphalt Concrete Mixtures with Thermal Stress Restrained Specimen Test Results." Transportation Research Record 1545, Washington DC, pp. 50-58.